Immobilization of molecular late transition metal polymerization catalysts on nanomaterials

Liping Zhang

THÈSE

En vue de l'obtention du

DOCTORAT DE L'UNIVERSITÉ DE TOULOUSE

Délivré par :

Institut National Polytechnique de Toulouse (INP Toulouse)

Discipline ou spécialité :

Chimie Organométallique et de Coordination

Présentée et soutenue par :

Mme LIPING ZHANG

le vendredi 24 janvier 2014

Titre :

IMMOBILISATION DE CATALYSEURS MOLECULAIRES DE POLYMERISATION D'OLEFINES SUR NANOMATERIAUX.

Ecole doctorale :

Sciences de la Matière (SM)

Unité de recherche :

Laboratoire de Chimie de Coordination (L.C.C.)

Directeur(s) de Thèse :

M. JEROME DURAND

Rapporteurs :

Mme BARBARA MILANI, UNIVERSITA DEGLI STUDI DI TRIESTE

Mme XIULIAN PAN, ACADEMIE SCES DE CHINE BEIJING

Membre(s) du jury :

Mme MONTSERRAT GOMEZ SIMON, UNIVERSITE TOULOUSE 3, Président

M. JEROME DURAND, INP TOULOUSE, Membre

Mme FRANCOISE SEREIN-SPIRAU, ECOLE NLE SUP DE CHIMIE DE MONTPELLIER, Membre

Acknowledgments

It has been a pleasure working with the Catalysis and Fine Chemicals group of the Laboratoire de Chimie de Coordination over the last three years and I am honored to have been chosen to participate in the co-project between NSFC and ANR.

First and foremost, my utmost thanks go to my supervisor, Dr Jérôme Durand, for giving me the opportunity to carry out this PhD study under his supervision and for his invaluable advice, guidance, patience and encouragement throughout my work. During my PhD program, his endless support and assistance both in research and in daily life cannot be described in any words. I also wish to express my gratitude to my co-supervisor Prof. Philippe Serp. I appreciate his advices, suggestions and his management that makes the warm atmosphere in the lab.

I wish to express my gratitude to Prof. Wen-Hua Sun for giving me the opportunity to join in the co-project, and helping me during the two times I worked in the 'Key laboratory of Engineering Plastics and Beijing National Laboratory for Molecular Science' in Institute of Chemistry, Chinese Academy of Sciences.

Special thanks go to Dr. Revathi bacsa who gave me lots of warmth during the last three years. I really enjoy the daily café time with you and deeply grateful for your useful suggestions in research and in life. I also would like to thank my best friend Li Xiaojian who gave me a lot of information about Toulouse and helped me to adapt faster and easier to life in France.

I am really indebted to everyone who is or was a member in the Catalysis and Fine Chemicals group. I am especially thankful to Prof. Philippe Kalck, Prof. Martine Urrutigoity, Prof. Maryse Gouygou, Dr Odile Dechy-Cabaret, Dr. Jérôme Volkman and Dr. Rosa Axet for their moral support and kindly help during the last three years.

Special thanks to Dr. Eva Castillejos for her practical help and encouragement during the early stages of this project; and also to Dr. Delphine Crozet who was one of my office mates for her endless help and great friendship in the first year. Thanks also given to Dr. Qi Xueqiang, Dr. Kévin Fourmy, Dr. Bruno Machado, Dr. Meltem Tunckol, Ganna Gogolieva and Jamal El Karroumi for the fun time spent together and the help. I also wish to express my gratitude to Dr. Trang Nguyen, Dr. Mustapha Oubenali, Dr. Romain Adcock, Dr. Duc Hanh Nguyen, Dr. Florence Gayet, Dr. Julien Beausoleil, Leng Faqiang, Pierre Lonchambon, Abdelouahd Oukhrib, Anas Benyounes, Carole Leberre, Manon Gennet, Jasmine Duguet, Laurent Ropiquet, Idaline Chanteperdrix, Sakhayna Caristan and Justine Harmel for their friendship and support during the period of my research work.

I would also like to thank all of the staff who work in LCC, ENSIACET and ICCAS who have helped me to complete my research work in different ways. Special thanks to, Vincent Collière for the SEM and TEM measurements; Jean-François Meunier for the TGA measurements; Sonia Ladeira, Liang Tongling and Hao Xiang for the X-ray single crystal diffraction measurements and Maelenn Aufray for the DSC measurements.

To my Chinese friends, Deng Xu, Ma Hang, Zhao Tianming, Zhou Binbin, Liu Jian, Liu Ran, Liu Hong, Zhao qiao and Wang Tianyuan, thanks to all of you for making my spare time colorful during my Ph.D. study in the Toulouse.

Finally, sincere thanks to give my parents, Zhang Wentian, Wu Quandian, and parents in law Li Haixia and Li Xin’an, for their unlimited support and understanding. Finally I wish to thank my beloved husband, Li Cai, for his love, patience and encouragement. Without your support, this thesis would not have been possible.

Abstract

This present thesis deals with the development of active olefin polymerization catalysts based on late transition metal (nickel and iron) imino-pyridine complexes supported on nanomaterial. Chapter I gives a comprehensive literature review of unsupported and supported ethylene polymerization catalyst. In Chapter II we report the ethylene polymerization studies using nickel complexes containing an $–NH_2$ group for covalent immobilization on multi-walled carbon nanotubes (MWCNTs) of the corresponding precatalysts. Comparison of the homogeneous catalysts with their supported counterparts evidenced higher catalytic activity and higher molecular weights for the polymers produced. In Chapter III, iron complexes containing a pyrene group have been synthesized and immobilized on MWCNTs through non-covalent π-π interactions between pyrene group and surface of MWCNTs. Activated by MMAO, both the iron complexes and immobilized catalysts show high activities for ethylene polymerization. It was possible to evidence that MWCNTs have a great influence on the catalytic activity and on the structure of the resulting polyethylenes. Imino-pyridine nickel complexes containing various kinds of aromatic groups have been synthesized in Chapter IV and polymerization conditions in the presence and in the absence of nanocarbon materials, such as MWCNTs or few layer graphene (FLG), are discussed. For those nickel catalysts bearing 1-aryliminoethylpyridine ligands, the presence of MWCNTs in the catalytic mixture allows the formation of waxes of lower molecular weight and polydispersity, whereas the presence of FLG proved to be beneficial for the catalytic activity. In Chapter V, isoprene polymerization catalyzed by iron complexes containing polyaromatic groups and non-covalently supported on nanoparticles and confined into the inner cavity of

MWCNTs (Cat@NPs and Cat@NPs@MWCNTs) are investigated. Iron complexes show excellent activity for the isoprene polymerization and produced high glass temperature polyisoprene with a high *cis*-1,4-polyisoprene selectivity. Polymer nanocomposites are produced by supported catalysts and, transmission electron microscopy (TEM) evidenced efficient coating of the resulting polyisoprene around the oxygen sensitive iron^{0} nanoparticles.

Keywords: ethylene polymerization, isoprene polymerization, late transition metal catalyst, muti-walled carbon nanotubes, muti-walled carbon nanotubes supported catalyst, few layer graphene, iron particles, particles supported catalyst, protective ability, nanocomposites.

Résumé

Le présent travail de thèse décrit le développement de systèmes actifs de polymérisation d'oléfines basés sur des métaux de fin de transition (nickel et fer) supportés sur des nanomatériaux. Le chapitre I décrit l'état de l'art des systèmes catalytiques supportés ou non pour la polymérisation d'oléfines. Dans le chapitre II, nous décrivons la polymérisation de l'éthylène en utilisant des catalyseurs de nickel contenant un groupement $-NH_2$ pour leur immobilisation covalente sur nanotubes de carbone ; montrant l'influence positive de l'immobilisation : les catalyseurs ainsi supportés sont en effet à la fois plus actifs et conduisant à des polymères de plus haut poids moléculaire.

Dans le chapitre III, des complexes de fer contenant un groupement pyrène sont décrits et immobilisés sur nanotubes de carbone par interaction non covalente π-π. Dans ce cas, à la fois les systèmes homogènes et leurs analogues supportés catalysent la réaction de polymérisation de l'éthylène avec des activités particulièrement élevées. Il a également pu être mis en évidence l'importante influence du support carboné sur les performances du système catalytique ainsi que sur la structure des polymères obtenus.

Différents types de complexes de nickel contenant un ligand imino-pyridine et différents groupes polyaromatiques ont été synthétisés et leur utilisation en polymérisation de l'éthylène est décrite dans le chapitre IV. L'influence de l'addition de faibles quantités de matériaux nanocarbonés (nanotubes de carbone ou graphène) au milieu réactionnel a ainsi été étudiée. Le graphène s'est dans ce cas révélé particulièrement bénéfique sur les performances du catalyseur.

Enfin, le chapitre V décrit la polymérisation de l'isoprène à l'aide de catalyseurs

de fer contenant des groupements polyaromatiques permettant leur immobilisation à la surface de nanoparticules de fer. Ces systèmes ont ensuite pu être confinés dans des nanotubes de carbone. Les systèmes catalytiques décrits sont particulièrement actifs produisant des polyisoprènes à température de transition vitreuse élevée et avec une haute sélectivité *cis*-1,4-polyisoprène.

Table of Contents

Acknowledgments i

Abstract iii

Keywords: iv

Résumé v

General introduction 1

Chapter 1: 5

Literature review of ethylene polymerization catalysis 5

1.1 General introduction on olefin polymerization catalysts 7

1.1.1 Background of the homogeneous olefin polymerization catalysts 7

1.1.2 Background of the homogeneous late transition metal olefin polymerization catalysts 10

1.1.2 Immobilization of homogeneous olefin polymerization catalysts 16

1.2 Literature review of carbon nanomaterial supported catalysts 21

1.2.1 General introduction on carbon nanomaterial supported catalysts 21

1.2.2 Covalent and non-covalent functionalization of carbon nanomaterial and applications in catalysis 25

1.2.3. Nanocarbons supported ethylene polymerization catalyst 32

1.3 Conclusions 39

References 40

Chapter 2: Carbon nanotubes supported nickel catalysts *via* covalent bonds for ethylene polymerization 65

2.1 Introduction 67

2.2 Results and discussions 69

2.2.1 Characterization of the nickel complexes Ni1–Ni4 and the supported catalyst 69

2.2.2 Ethylene polymerization catalyzed by the nickel complexes and CNT-supported nickel complexes 74

2.3 Conclusions 86

2.4 Experimental Section 87

2.4.1 Synthesis and characterization of nickel complexes 87

2.4.2 Synthesis and characterization of CNTs supported nickel complexes 88

References 89

Chapter 3: Ethylene polymerization catalyzed by pyrene-tagged iron complexes: positive effect of π-conjugation and immobilization on multi-walled carbon nanotubes 95

3.1 Introduction 97

3.2 Results and discussions 98

3.2.1 Synthesis and characterization of ligands and iron complexes 98

3.2.2 Synthesis and characterization of MWCNTs supported iron complexes 102

3.2.3 Ethylene polymerization 103

3.3 Conclusions 115
3.4 Experimental Section 116
References 118
Chapter 4: Nickel complexes behavior in ethylene polymerization in the presence of nanocarbons (MWCNTs or FLG) 125
4.1 Introduction 127
4.2 Results and discussion 129
4.2.1 Synthesis and characterization of ligands and their nickel complexes 129
4.2.2 Molecular structures 131
4.2.3 Ethylene polymerization 136
4.3 Conclusions 154
4.4 Experimental Section 155
4.4.1 Synthesis of the ligands L6–L13 155
4.4.2 Synthesis of the nickel complexes 159
References 161
Chapter 5: Catalytic isoprene polymerization around iron nanoparticles confined into multi-walled carbon nanotubes 171
5.1 Introduction 173
5.2 Results and discussion 179
5.2.1 Synthesis and characterization of ligands and iron complexes 179
5.2.2 X-ray crystallographic studies 181
5.2.3 Isoprene polymerization with iron complexes Fe6–Fe8 186
5.2.4 Preparation of nanoparticles supported catalysts (Cat@NPs) 191
5.2.5 Confinement of Cat@NPs inside f-MWCNTs 194
5.2.6 Cat@NPs and Cat@NPs@MWCNT behavior in isoprene polymerization 195
5.3 Conclusions 198
5.4 Experimental Section 199
5.4.1 Synthesis of the iron complexes Fe6–Fe8 199
5.4.2 Immobilization on the surface of iron nanoparticles (Cat@NPs) 199
5.4.3 Confinement of Cat@NPs inside MWCNTs (Cat@NPs@MWCNT) 200
References 200
General conclusions and perspectives 211
Conclusions 213
Perspectives 216
Experimental details 219
1. Materials 219

2. Experimental procedures 220
3. Instruments and measurements 222
References 223

General introduction

Polyolefins, in particular polyethylene and polyisoprene, have been used to make different kinds of daily used products, so they are seen as one of the great innovation of the last century. To discover and synthesize an effective catalyst for ethylene polymerization is critical for both the academy and the industry. After several generations, the late transition catalysts have drawn more attention because of their interesting catalytic behaviors towards ethylene and the easily controlled polyethylene produced. However, this kind of catalyst has the same disadvantages as other homogeneous catalysts, such as a short life time of active sites and the limitations of use in large scale processes. In order to pass those challenges and develop suitable systems for most of the industrial processes (slurry or gas-phase reactors), the immobilization of such catalysts is required. Nanomaterials (carbon nanotubes, few layer graphene or nanoparticles), are attractive candidates as support to immobilize homogeneous ethylene polymerization catalysts. Moreover, nanocarbons, due to their outstanding and unique mechanical, thermal and electronic properties, are hoped to have a positive influence on the catalytic activity and produce advanced polymer nanocomposites.

The present manuscript is composed of five chapters. Chapter I gives a comprehensive literature review of unsupported and supported ethylene polymerization catalysts. In Chapter II, a family of nickel complexes containing an $-NH_2$ function and muti-walled carbon nanotubes (MWCNTs)-supported nickel diimine complexes *via* covalent bonds have been synthesized and used in catalytic ethylene polymerization process. For the homogeneous catalysts, the position of the $-NH_2$ group has a strong influence on the catalytic activity. The activities of these

covalently-attached supported catalysts are higher than for the homogeneous catalysts and higher molecular weight polymers are produced. In addition, the kind of the CNTs used as support can affect directly the catalytic activity. In Chapter III, iron complexes containing at least one pyrene group have been synthesized and been immobilized on MWCNTs *via* π-π interactions between the pyrene group and the surface of MWCNTs. Activated by MMAO, the effects of catalyst ligand (pyrene group) and of the support have been investigated in ethylene polymerization. The homogeneous catalysts promote the formation of polyethylene with high activity, evidencing the positive influence of the π-conjugated pyrene substituents on the ligand backbone. Immobilization onto the surface of MWCNTs has a great influence on the catalytic activity and resulting polyethylene. Nickel complexes bearing 1-aryliminoethylpyridine ligands or arylimino-(5,6,7-trihydroquinolin-8-ylidene) ligands, containing a polyaromatic substituent, have been synthesized and polymerization conditions in the presence or not of nanocarbon materials, such as MWCNTs or FLG, are discussed in Chapter IV. When activated by MAO, nickel catalysts bearing 1-aryliminoethylpyridine ligands exhibit high activities for ethylene polymerization producing polyethylene waxes of lower molecular weight and narrow molecular weight distribution. The presence of MWCNTs in the catalytic mixture allows the formation of waxes of lower molecular weight and polydispersity, whereas the presence of FLG proved to be beneficial for the catalytic activity. Compared to these nickel complexes, the ones bearing arylimino-(5,6,7-trihydroquinolin-8-ylidene) ligands displayed lower activity and produced higher molecular weight polyethylene. The presence of MWCNTs did not change significantly the performances in terms of activity and the nature of the resulting polyethylene. FLG is also investigated in catalytic system and had a positive influence on the catalytic activity. Finally, a series

of iron complexes bearing 1-aryliminoethylpyridine ligands have been synthesized and fully characterized in Chapter V. Using triisopropylaluminum as co-catalyst, those iron complexes show excellent activity for isoprene polymerization and produced high glass temperature polyisoprene with a high selectivity towards *cis* 1,4-polyisoprene. Supporting one of the iron complexes onto Fe^0 nanoparticles (NPs) *via* π-π interactions (**Cat@NPs**) to prepare polyisoprene nanocomposites through *in-situ* polymerization is described. Furthermore, **Cat@NPs@MWCNT** is produced by the confinement of **Cat@NPs** into the inner cavity of MWCNTs and then used for isoprene polymerization. The TEM images of **Cat@NPs@PI** samples shown that NPs are surrounded by the resulting polyisoprene and homogeneously dispersed inside. The polyisoprene produced by **Cat@NPs@MWCNT** are located inside the cavities of the MWCNTs and offer effective protection of the particles against air oxidation.

Chapter 1:

Literature review of ethylene polymerization catalysis

1.1 General introduction on olefin polymerization catalysts

Polyolefins are one of the most important discoveries in human life and thus the most produced synthetic polymer today [1-2]. Due to the importance of their broad-ranging material properties, such as mechanical, thermodynamic and crystalline characteristics, and outstanding resistance to oxygen, heat, weathering, chemicals and ozone, polyolefins are indispensable materials in the modern living and impact our daily lives in countless beneficial ways, including food packages, squeeze bottles, containers, plastic shopping bags, storage boxes, gasoline tanks, toys and car bumpers. It is reported that the requirement of the plastic production is increasing every year (see Figure 1.1), and the requirement will be increased to close to 400 million tons in 2050 according to the research from the Plastics Europe Market Research Group.

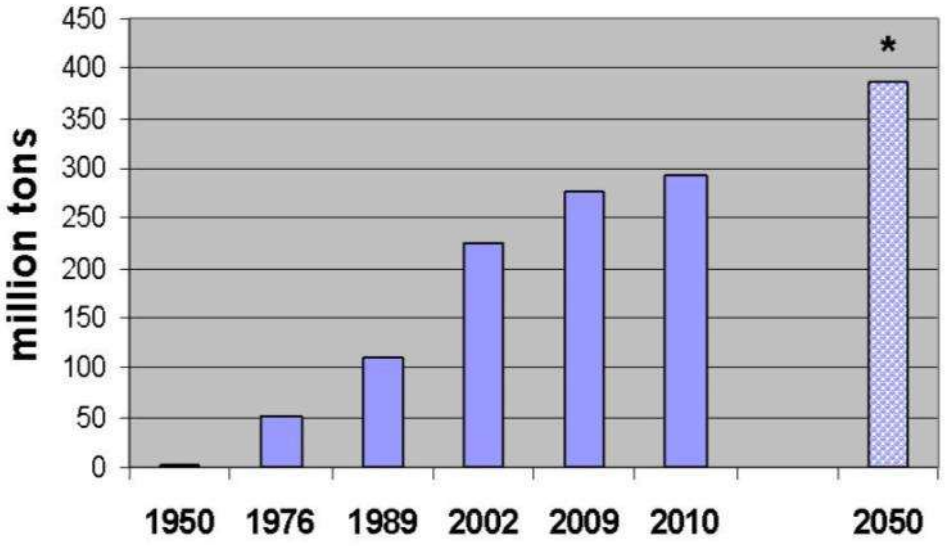

Figure 1.1 Annual world plastic production.

1.1.1 Background of the homogeneous olefin polymerization catalysts

One of the major sources of plastic is polyethylene which is produced by ethylene polymerization. The polymerization of ethylene was firstly discovered in

1933 [3-4], however, the operation was accomplished under harsh conditions with a pressure up to 300 MPa and a temperature of 300 °C. Under these reaction conditions the process could not be used industrially field. Therefore, finding a useful catalyst is the "key" step for the polymerization process, in order to decrease the reaction difficulty and the cost of the production. The stability, activity, selectivity and regeneration ability are the most important properties to be considered in catalyst design. The first key was the combination of $TiCl_4$ and alkylaluminum respectively discovered by Ziegler and Natta [5]. Compared with the high-pressure and high-temperature free-radical polymerization process, the ethylene polymerization conditions using the Ziegler catalyst are milder and activities higher. 20 years later, $MgCl_2$ as a support was introduced for $TiCl_4$-based catalytic systems [6]. These $MgCl_2$-supported $TiCl_4$ exhibited catalysts activities two orders of magnitude greater than Ziegler's original catalysts, and led to continuous significant improvements in the performances of the activity, stereoselectivity, ability to control both the molecular parameters and morphology of the resulting polymers, and they opened the way to its tremendous recent and still ongoing expansion.

The catalysts currently used in industrial processes are still dominated by the multi-sited heterogeneous Ziegler-Natta catalysts represented by $MgCl_2$-supported $TiCl_4$ catalysts. Chromium-based Phillips catalyst [7-8], the group 4 metallocene catalysts [9-13] (see Scheme 1.1, A-C) and constrained-geometry catalysts (CGCs) (see Scheme 1.1, D) [14-18] have also been investigated as ethylene polymerization catalysts and succesfully used in industry process. The firstly discovered group 4 metallocene catalysts are half-sandwich (Scheme1.1, A), which have been seen as derivatives of the Ziegler-Natta catalysts. In the early 1980s, sandwich metallocene Cp_2MCl_2 (M=Ti or Zr) (Scheme1.1, B) catalysts have been discovered by Sinn and

Kaminsky [19]. Due to the high activity of those catalysts, different models of group 4 metallocene catalysts have been developed on the basis of Cp_2MCl_2 (Scheme1.1, C). Using these homogeneous and better-defined metallocenes, products with attractive properties could be obtained, such as well-defined structure, little branching and very narrow molar mass distribution. Another family of ethylene polymerization catalysts, CGCs, has been developed by exchanging one cyclopentadienyl ring by an amido moiety (Scheme 1.1, D) [14-15]. Due to the less crowded coordination sphere, this kind of catalyst is preferred for copolymerization of ethylene and α-olefins. In addition, three major classes of polyethylene are produced by those catalysts: high-density polyethylene (HDPE), linear low-density polyethylene (LLDPE) and low-density polyethylene (LDPE) [20]. Clearly, these different kinds of polymer have their own characteristics and can be used in different fields.

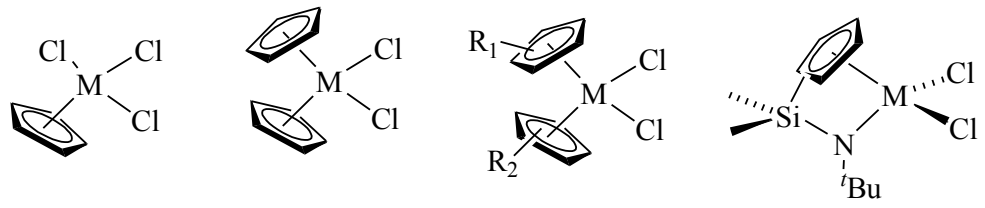

A B C D

M = **Ti** or **Zr**

Scheme 1.1 Group 4 metallocenes catalysts and CGC catalysts.

Late-transition metal complexes were also proved as catalysts for the polymerization in 1978 [21], and attracted the researcher's attention from then on. Those late-transition metal complexes showed some superiorities: 1. The complexes are displaying higher activity for ethylene polymerization, or at least similar activity with the single-site group 4 metallocene catalysts, 2. The synthetic procedure of those

late transition metal complexes is easier, 3. The starting chemical material is cheaper, so the use of those catalysts in industry can reduce the production costs and 4. The lower oxophilicity and the greater functional group tolerance of late transition metals compared to early transition metals, such as Ti, Zr, and Hf, make them likely targets for the development of catalysts for the copolymerization of ethylene with polar comonomers under mild conditions.

1.1.2 Background of the homogeneous late transition metal olefin polymerization catalysts

1.1.2.1 Background of nickel complexes as polymerization catalysts

The first late-transition metal catalysts are the well-known nickel systems used in the Shell Higher Olefin Process (SHOP), bearing monoanionic P^O ligands (Scheme 1.2, A) [22-24]. These catalysts are very selective for the insertion of ethylene *versus* α-olefins, and β-hydride elimination is competitive with olefin insertion, giving high-quality, linear α-olefins (C6–C20) from ethylene.

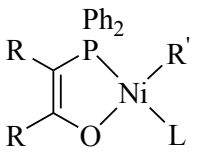

L = PPh_3
R' = o-tolyl, Me, Et, Ph

A

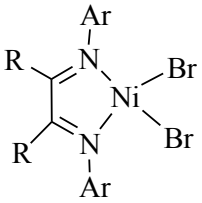

B

Scheme 1.2 Model of the bi-dentate nickel complexes for olefin polymerization.

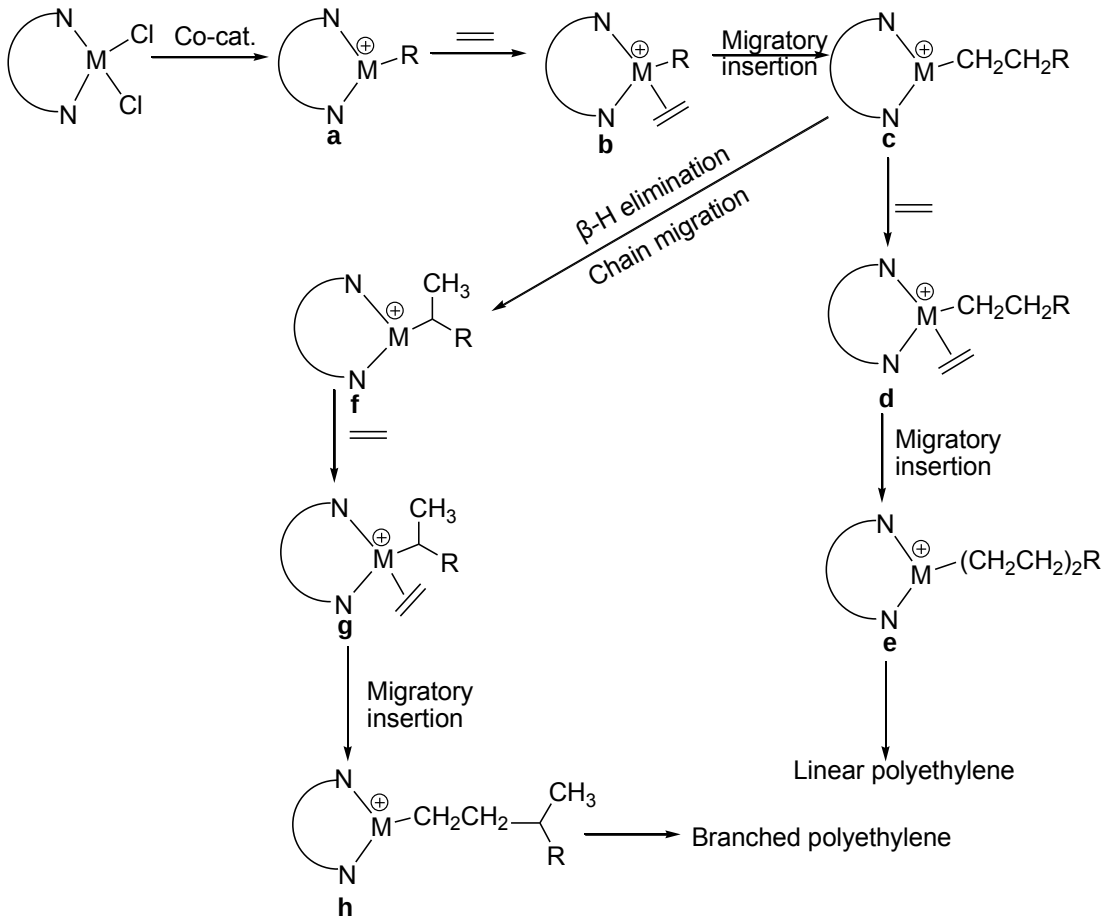

Scheme 1.3 α-diimine nickel complexes catalytic mechanism for ethylene polymerization.

In 1995, a new type of highly active pro-catalysts, a family of new cationic Ni(II) and Pd(II) α-diimine catalysts (Scheme 1.2, B), for ethylene polymerization was reported by Brookhart's group [25]. This kind of Ni(II) complexes display high activity for the ethylene polymerization, which can compete with the metallocene catalysts. In addition, high molecular weight polymer was produced by this kind of complexes. The fact that these complexes produce high molecular weight polymer is a consequence of slow chain transfer relative to chain propagation. Chain transfer is proposed to occur by associative olefin displacement and is hindered by the axial bulkiness provided by the *ortho*-substituents of the aryl rings [20, 26-28]. It is

reasonable that modifying the imino carbon and nitrogen substituents of the α-diimine ligands can adjust the steric and electronic properties of these nickel complexes. A large number of variations have been reported in the academic literature [29–34]. The polymers produced by those catalysts are not only high-molecular-weight polymer but also lower molecular weight polyolefin, e.g. oligomers and waxes. The catalytic mechanism for those α-diimine nickel complexes was also investigated by Brookhart [35] and other researchers [36-37] (Scheme 1.3).

The catalytic mechanism includes 4 steps: 1. Initiation step. The active center should be produced by reaction of the nickel complexes with the proper co-catalyst, like Methylaluminoxane (MAO) and Diethylaluminium chloride ($AlEtCl_2$), and unsaturated cationic species are generated with nickel-alkyl bonds (Scheme 1.3, **a**). Then, a new alkyl nickel complex is produced by the coordination of an ethylene molecule to the active center through a Π-nickel intermediate (Scheme 1.3, **b**). 2. Migratory insertion. The coordinated ethylene can migrate and insert into the nickel-alkyl bond. 3. β-hydride elimination and chain migration. In this process, *β*-hydride elimination first yields a putative hydride olefin Π-nickel complex. Metal migration (*chain walking*) along the alkyl chain can occur in these species *via β*-H elimination and re-insertion reactions (to species **f** and **g**). These migration reactions occur without chain transfer. Successive migratory insertion and ethylene trapping cycle from species **d** leads to linear polymer chains, while insertion following *chain walking* leads to the introduction of short branches in the polymer chain [38]. A high extent of *chain walking* leads to the formation of highly branched polymer. It was also reported that a decrease of the steric bulkiness of the α-diimine ligand results in a lower polymer branching, and formation of high molecular weight polymer [37]. In addition, polymer can be tailored through changes in the reaction parameters like

reaction temperature, ethylene pressure and reaction time. 4. Termination step. In this last step, the polymeric chain is released and the catalytic active species is regenerated. Termination occurs mainly by β-hydride elimination or chain transfer.

Encouragingly, the microstructure of the polyethylene, including the molecular weight and polydispersity, could be finely tuned by employing different substituents on the ligands [20, 24]. This endows those nickel complexes with possibilities of synthesizing new polymers with special microstructures, envisage the (co)polymerization of polar monomers and synthesis of value-added products, such as linear α-olefins, waxes, and polyethylenes.

Additionally, some N^N^N [40–44], N^N^O [45-46], N^P^N [47] tridentate nickel complexes have been synthesized and used as catalyst for polymerization. Those tridentate nickel complexes also displayed high activities for either ethylene oligomerization or polymerization. However, the nickel complexes bearing bi-dentate ligands exhibit better performances for the production of polyethylene. Therefore different kind of bi-dentate N^N nickel complexes were investigated and discussed in this thesis.

1.1.2.2 Background of iron complexes as olefin polymerization catalysts

Some N^N^N iron (II) and cobalt (II) dihalides complexes bearing 2,6-bis(arylimino)pyridyl ligand have been reported independently by Bookhart [48-49] and Gibson [50-51] groups in 1998. Activated by MAO or $EtAlCl_2$, these tri-dentate iron complexes promote ethylene oligomerization or polymerization with high activity. The related publications reported that the nature of the metal center have a great influence on catalytic productivity and the iron complexes show higher activity that their corresponding cobalt analogues. Therefore, publications about the

N^N^N iron(II) catalysts based on this ligand framework for ethylene oligomerization and polymerization have not stopped. Some examples of those iron complexes are shown in Scheme 1.4.

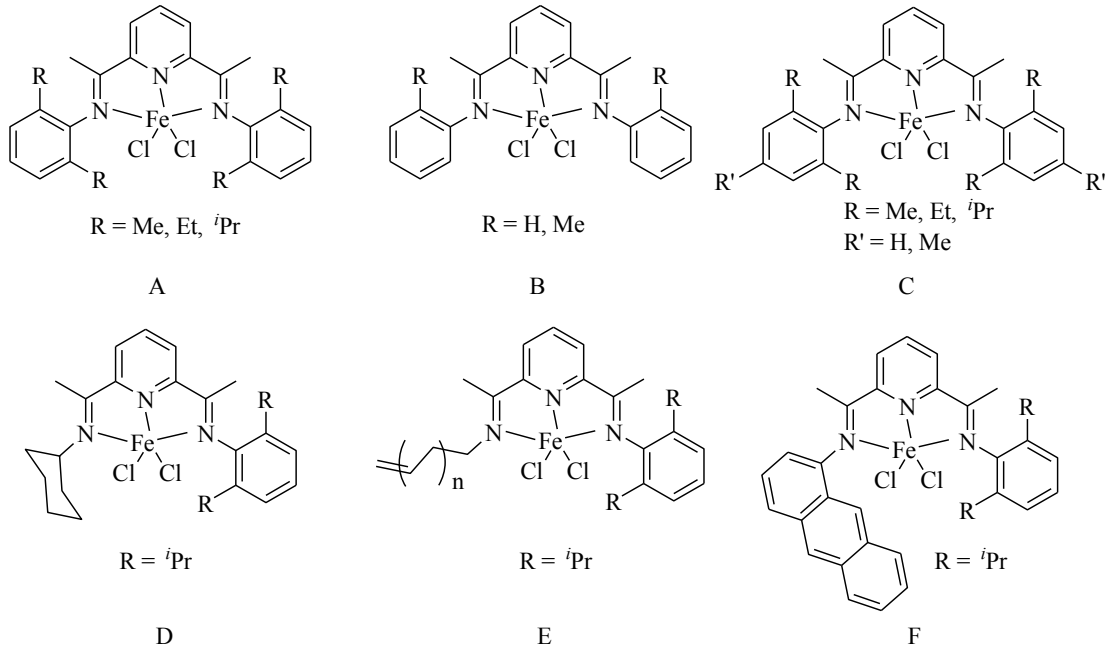

Scheme 1.4 Symmetrical or unsymmetrical bis(imino)pyridine iron(II) complexes.

The catalytic mechanism for those bis(arylimino)pyridyl iron(II) complexes is similar to the above-mentionned nickel complexes based on the α-diimine ligands. However, the polyethylenes produced by those iron complexes are linear unlike the branched polyethylene produced by nickel complexes. The size, nature and regiochemistry of the substituents in the iminoaryl groups are of crucial importance in controlling the polymerization and oligomerization of ethylene. Consequently, changes in the aryl group of the ligand on those iron complexes can affect their catalytic performances. Bookhart group reported [43] that increasing the steric bulkiness of the aryl substituents can increase the molecular weight of the obtained

polymers. In the structures A in Scheme 1.4, if the R = isopropyl not only the catalytic activity but also the molecular weight are higher than that for R = ethyl. Moreover, when one of the *ortho* substituents is replaced by H (Scheme 1.4, B), the activity of the iron complexes decreases immediately, and the products have a broad molecular weight range which can change from olefin to wax to lower molecular weight polymer [48, 52-53]. However, the alkyl group in the *para* position on the aryl ring has little effect on the catalytic performances [52, 54]. On the other side, the electronic density of the ligand surrounding the iron center can also affect products formed. Qian reported a series of iron complexes bearing 2,6-bis(imino)pyridyl ligands with fluoro substituents in different positions on the aryl group [55]. With the modified methylaluminoxane (MMAO) as co-catalyst, all of those iron complexes promoted ethylene oligomerization with high α-olefin selectivity.

Some unsymmetrical bisimino-pyridyl iron(II) complexes were also synthesized, where one of the bulky 2,6-diisopropylphenyl groups was replaced by an alkyl or aryl substituent. The catalysts derived from such iron complexes are still very active but if one of the aryl groups is replaced by an alkyl one (Scheme 1.4, D and E), the catalysts typically gave ethylene oligomers instead of polyethylene [56-57]. When an anthracenyl polyaromatic ring is introduced as substitutuent of the imino nitrogen (Scheme 1.4, E), oligomers are produced with molecular weight from 300-600 g/mol [52, 58]. Because all of these unsymmetrical bisimino-pyridyl iron(II) complexes have a lower degree of steric hindrance at the axial position, the chain transfer reaction is more favored, which results in low-molecular-weight polymers or oligomers.

1.1.2 Immobilization of homogeneous olefin polymerization catalysts

After decades of domination by the classic Ziegler-Natta and Phillips catalysts in catalytic production of polyolefin, metallocenes and other homogeneous catalysts, based on transition metals are now presenting new opportunities for the polyolefin industry. Moreover, due to their superiority, like easy synthetic procedure, cheaper starting materials and high catalytic activity, some people believe that the homogeneous catalysts will replace the established catalyst systems in the near future. However, these new polymerization catalysts are soluble systems [59]. The biggest problem concerning the homogeneous systems is that during polymerization, uncontrollable polymer growth takes place, which causes undesired depositions of polymer on the walls and other components of the reactor [60-61]. This is a large disadvantage that limits their use in large scale processes.

A gas phase process is lower in cost and energy consumption in comparison with a solution process. As most of the existing polymerization plants run a slurry- and gas-phase process with heterogeneous catalysts, the homogeneous catalysts must be heterogenized on a support in order to be applied in those processes. In addition, the heterogenization of the polymerization catalysts is necessary to avoid reactor fouling with finely dispersed polymer crystals, to prevent excessive swelling of polymers, and to produce polymer particles of a desired regular morphology. Therefore, various inorganic materials, such as silica gel [62-64], $MgCl_2$ [65-67], Al_2O_3 [68-70], MgO [70], carbon nanotubes (CNTs) [71-74] etc. have been used as support to immobilize homogeneous polyolefin catalysts.

The immobilization routes reported in the literature for supported catalysts can be described as follow (Figure 1.2): Path 1. Immobilization of the co-catalyst, like methylaluminoxane (MAO), on the support, followed by reaction with the metal

compound [75]; Path 2. Direct impregnation of metal complex on the support [60-61, 70]. This second method is the most widely used; and Path 3. Immobilization of the ligands on the support, then reaction with a metal salt [61, 76]. Moreover, using different preparation routes for supported homogeneous catalysts can have a great influence on catalytic activity and on the polymer properties.

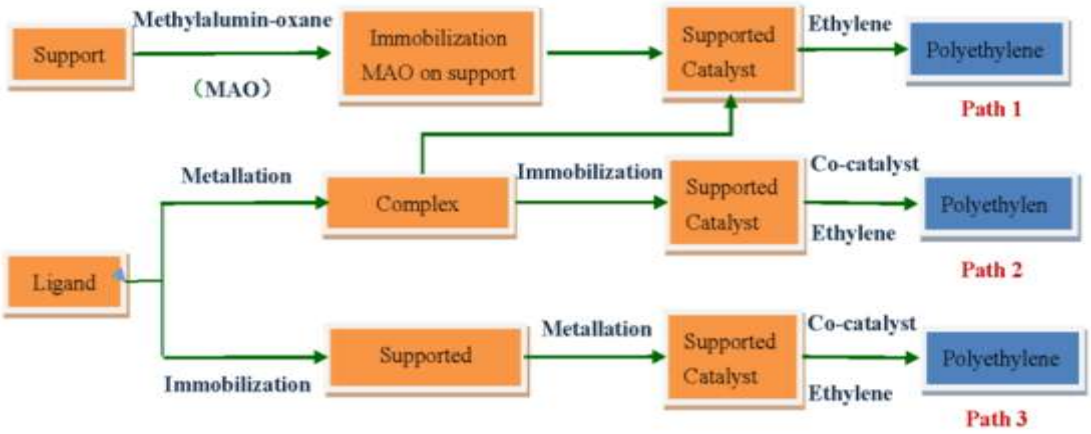

Figure 1.2 Classical methods for immobilization of ethylene polymerization catalysts.

1.1.2.1 Silica supported homogeneous ethylene polymerization catalysts

According to the literature of the heterogeneous polymerization catalysts, silica gel is a support of choice for the immobilization of homogeneous catalysts [63]. One of the major reasons is that it has a large surface area and silanol groups on the silica surface offer a high degree of surface functionality [60], which can be an advantage to immobilize catalyst components. Moreover, other properties like good mechanical properties [77] and stable behavior under reaction conditions made silica a good candidate as support.

Since the end of the last century, group 4 metallocene derivatives have been supported on silica gel and used as catalysts for ethylene polymerization [60, 78].

Later, as the late transition metal complexes display high activity, silica supported nickel (II) [61, 79-80] and iron (II) [81] catalyst have been investigated. However, the catalytic activity of the supported catalysts is always lower than their soluble counterpart [59, 61], with few exceptions reporting that silica has a positive effect on the polymerization activity [82-84]. There are several parameters influencing the activity, such as the type of the silica [85], particle size of silica [86], pore volume [87], pore diameter [85], particle size distribution [88] etc. Moreover, the reaction conditions, which are used to produce the immobilized catalysts are also important for homogeneous catalysis grafted density and catalytic activity, such as: 1) The temperature which is used to activate the silica has a great influence of the –OH group on the surface; and 2) The immobilization route used to prepare the silica supported system is an important parameter for the catalytic activity.

1.1.2.2 Spherical $MgCl_2$-supported homogeneous ethylene polymerization catalyst

After SiO_2, $MgCl_2$ has been used as support to support homogeneous catalysts like group 4 metallocene catalysts [65, 89], non-metallocene group 4 catalysts [65, 67, 90-91] and late transition metal catalysts [67, 92-97]. Unlike SiO_2, there are no hydroxyl groups on the surface of $MgCl_2$, so it is difficult to support the homogeneous catalyst or MAO onto its surface. One useful way reported was the preparation of spherical $MgCl_2 \cdot nEtOH$ adducts by reaction of $MgCl_2$ with ethanol. Before supporting the homogeneous catalyst, formation of the Mg-O-Al active product is the necessary step to immobilize the MAO on the surface of $MgCl_2$ (Figure 1.3).

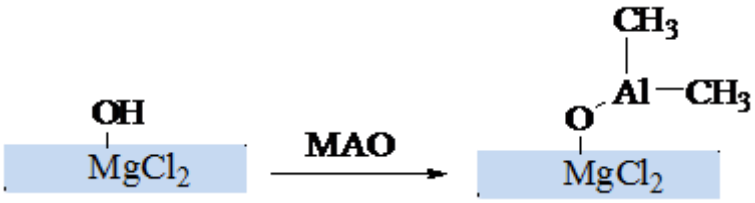

Figure 1.3 $MgCl_2$ supported MAO.

According to literature reports, the spherical $MgCl_2$·nEtOH adducts are a simple and effective support for the immobilization of homogeneous catalysts, facilitating their potential use in industrial process for ethylene polymerization. Chadwick reported that narrow molecular weight distribution polyethylene was obtained by the heterogeneous catalysts supported by $MgCl_2$ [90, 93]. Polymerization activity produced by the $MgCl_2$–supported catalyst at lower grafted homogeneous catalyst content is higher than that of the corresponding homogeneous catalyst. At the same time, the presence of the $MgCl_2$ is relatively extending the lifetime of the catalyst. Similar to SiO_2, the –OH density on the support surface and the method to graft the homogeneous catalyst on the surface of the support are important parameters for the catalytic activity.

1.1.2.3 Other inorganic Supports supported homogeneous ethylene polymerization catalyst

As we know, each support has its own nature and textural properties, immobilization of the homogeneous catalyst onto different support aim to determining the best supports for the development of a supported catalyst for ethylene polymerization. In addition to the above-mentioned SiO_2 and $MgCl_2$, other inorganic supports, like MgO [98-100], Al_2O_3 [98-99, 101], etc., were also used to immobilize ethylene polymerization catalysts. Similar to SiO_2, the temperature has a great influence of the -OH groups on the surface of the MgO and Al_2O_3. It means that the

temperature can affect the basicity of the supports surface as well as the weight percent of the homogeneous catalyst in the immobilized system. Zirconium complexes were supported by MAO-modified MgO and Al_2O_3 and investigated in polymerization process by Basso *et al.* [70]. It was reported that, under the same conditions, MgO and Al_2O_3 supported zirconium complexes show lower catalytic activities compared to their silica analogues. Similar results have been observed for other non-metallocene supported catalysts [98]. The reason for this observation was attributed to the textural properties of the support.

Zeolites, which are characterized by narrow pore size distribution and large surface area, have also been studied as support to support ethylene polymerization catalysts [102-103]. Unlike amorphous silica, zeolites have a more regular structure, pore size and supercages. Metallocene catalysts have been immobilized on various zeolites varying the metal or the groups on their surface [59, 63, 102-105]. These studies evidenced that these supported catalysts show a large decrease in activity but an increase in polymer molecular weight when compared to the corresponding homogeneous systems. Moreover, diffusion effects seem to be a limiting factor of the performance of zeolite-supported polymerization catalysts. Higher amounts of homogeneous catalysts fixed on the support led to lower activity and the accommodation of the homogeneous catalysts can by controlled by pore size and the initial bulk Si/Al ratio of the zeolite [59, 63]. Therefore, other mesoporous materials like molecular sieves, MCM-41, ZSM zeolites and VPI-5, were investigated to reduce the zeolite bulk Si/Al ratio in order to immobilize a various range of homogeneous catalysts and improve their polymerization activity [102, 105-109].

1.2 Literature review of carbon nanomaterial supported catalysts

1.2.1 General introduction on carbon nanomaterial supported catalysts

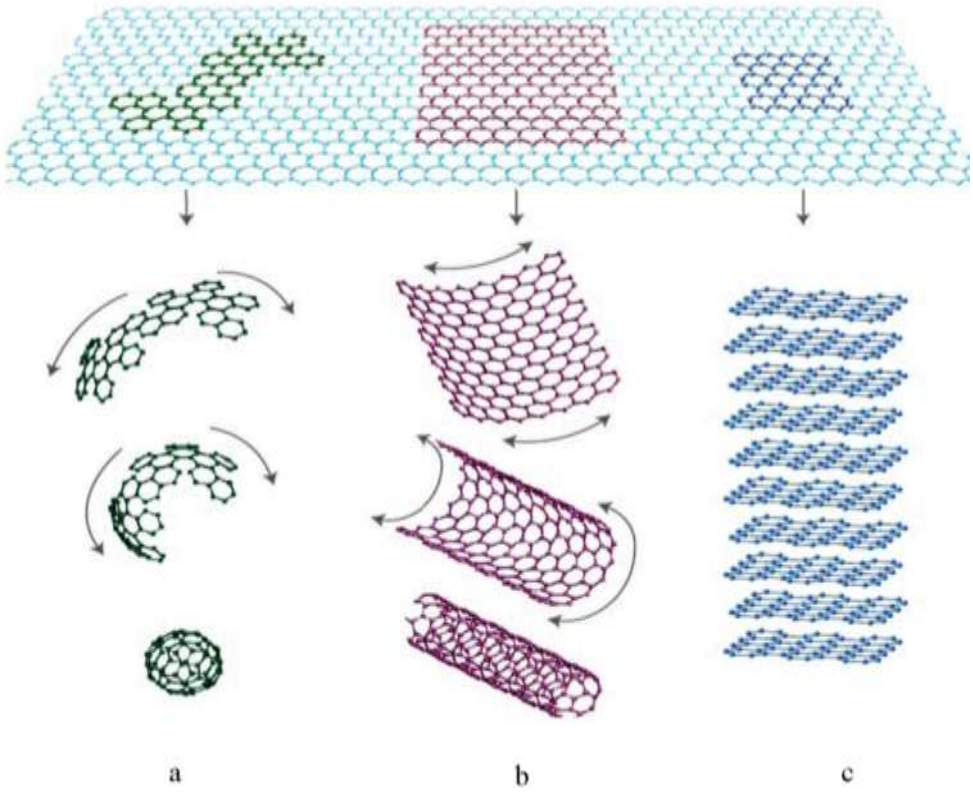

Figure 1.4 Structure of a) fullerenes; b) carbon nanotubes; c) graphene.

Since fullerenes (Figure 1.4, **a**) have been discovered by Smalley *et al.* in the mid-1980s [110], researchers have focused on the area of carbon nanomaterials. A few years later, carbon nanotubes (Figure 1.4, **b**) [111] and graphene (Figure 1.4, c) [112-114] have been synthesized and investigated. It is the chemical genius of carbon that it can bond in different ways to create structures with entirely different properties.

Two kinds of carbon nanomaterials are described and used in this thesis. Few

layer graphene is a layered structure with pure carbon, which is made out of carbon atoms arranged on a honeycomb structure made out of hexagons (Figure 1.4, **c**) and can be thought of as composed of benzene rings stripped out from their hydrogen atoms. Carbon nanotubes can be considered as a rolled-up sheet of graphene. Carbon nanotubes can be divided in two categories. Multi-walled carbon nanotubes (MWCNTs) were the first to be discovered by Iijima in 1991 [111], then single-walled carbon nanotubes (SWCNT) [72, 115] were synthesized two years later (Figure 1.5).

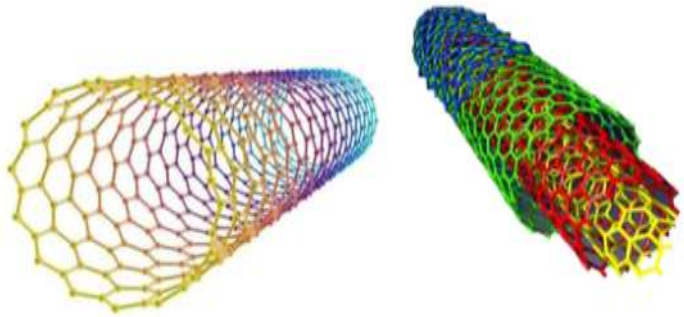

Figure 1.5 Single walled-carbon nanotube (SWCNT, left) and multi walled-carbon nanotube (MWCNT, right).

Due to their unique properties such as extremely high mechanical strength, high electrical, and thermal conductivity [111, 116-119], carbon nanomaterial are expected to have a great impact in a wide range of advanced technological applications [117, 120], including mechanical [117-118], sensors [121], probes [122], automotive [123], aerospace engineering [120], high-strength composites [73, 120, 124-126], gas storage [127-130] and energy storage [131-133]. Moreover, carbon nanomaterials have been attractive as fillers in polymer-based nanocomposites [71, 73-74, 124, 126, 134-136]. The properties of these composites are dependent on the structure, degree of concentration and dispersion of nanocarbons, and interactions between polymer

and nanofiller loads.

Along with the price fall down and derived by the commercial process, carbon nanomaterial instead of the conventional silica or alumina is reported to be a new support to produce supported catalyst. Like inorganic support, carbon nanomaterials have a large surface area, which serves as the support, to form supported catalyst. Moreover, carbon nanomaterials have other exceptional physical and chemical properties, like good thermal conductivity, small size, electron mobility, relatively high temperature, oxidation, basic and acid stability, making them useful support material for heterogeneous catalysis. For those reasons, the presence of carbon nanomaterial can be expected to increase the catalytic activity, enhance the catalytic life time and reduce the reaction time.

Considering these advantages, carbon nanomaterial immobilized molecular catalysts have been prepared. Transition metals complexes, like Co [137], Ni [138], Ru [139-140], Ti [141-142], Zr [143-148], Mn [149-150], Au [151], Cu [152] have been supported on carbon nanomaterial and used in different catalytic reactions. According to the investigations, the presence of the carbon nanomaterial affords the possibility to increase the catalytic activity, improve the reaction selectivity. This is partly since, in a supported catalytic system, the significance of using the carbon nanomaterial as support are to increase the dispersion of the active phases and have an influence on the active center. In addition, carbon materials have also been widely used as support for metallic nanoparticles as catalysts. One example for this is CNTs supported platinum and nickel catalysts used in dehydrogenation reactions [153].

As trends in technological and scientific progress, there is an increasing number of publications dealing with polymerization catalysts immobilized on carbon nanomaterial [143–144]. Smaller particle sizes, more finely dispersed to optimize

yields, decrease in reaction times, possibility to run gas-slurry processes, are reasons why nanomaterial supported catalysts have received attention and they are known to offer the possibility to display higher catalytic activity. In addition they represent a new way to produce polymer nanocomposites [154]. To obtain a carbon nanomaterial supported catalyst, the first step is to load the catalytic materials on the surface of nanocarbon. Similar to the heterogeneized catalysts supported on other inorganic support, like SiO_2 or Al_2O_3, several factors affect the heterogeneous catalysts prepared as well as their activity. 1) The kind of the carbon nanomaterial used to support the homogeneous catalyst; 2) the method to graft the homogeneous catalyst onto nanocarbon; 3) the particle size and the homogeneous catalyst distribution on the surface of nanocarbon. In order to display high activity, well dispersed homogeneous catalysts on the nanomaterial is necessary (Figure 1.6). A variety of synthetic strategies for nanocarbon/metal catalyst can be used and they can be classified into two categories: immobilization through covalent or non-covalent interactions.

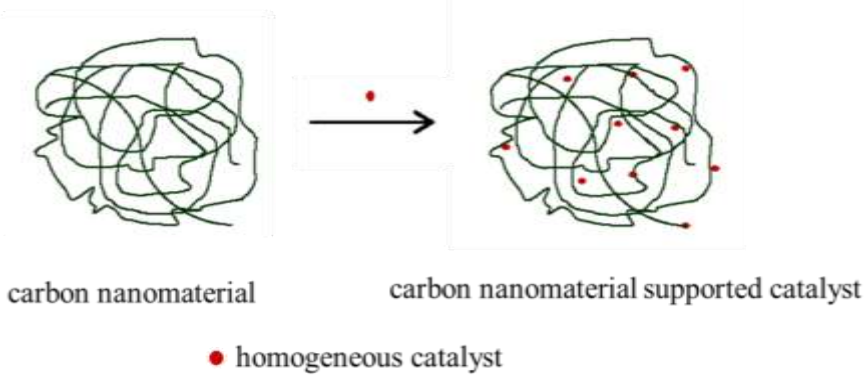

Figure 1.6 Carbon nanomaterial supported catalyst.

1.2.2 Covalent and non-covalent functionalization of carbon nanomaterial and applications in catalysis

1.2.2.1 Covalent functionalization

Covalent functionalization involves formation of covalent bond(s) between various functional groups and the sidewalls or defect sites on tips of carbon nanomaterials. Purified and oxidized nanocarbons bear functional groups such as hydroxyl and carboxyl on their surface [117]. Those groups can react with some complexes with polar groups and the immobilization catalysts are produced through covalent bonding.

1.2.2.1.1 Carbon nanomaterial supported catalyst through an amide linkage

Amide bond is a typical way to covalently attach organic compounds to the functional group of nanocarbons [155-159]. It is reported in the literature that the oxidized nanocarbons are the most promising for the coating process. The important step before "grafting" is to oxidize the purified carbon nanomaterial. As shown in Scheme 1.5, after oxidation by HNO_3, some sp^2 C=C bonds are opened and more carboxylic groups are introduced on the surface. The purpose of this step is to increase the coating sites on the support surface. This treatment can also shorten the length of CNTs. Before reaction of the compound containing the amine group with the oxidized nanocarbon, a necessary step is the reaction of the carboxylic function of the nanocarbon with thionyl chloride (see Scheme 1.6) [157].

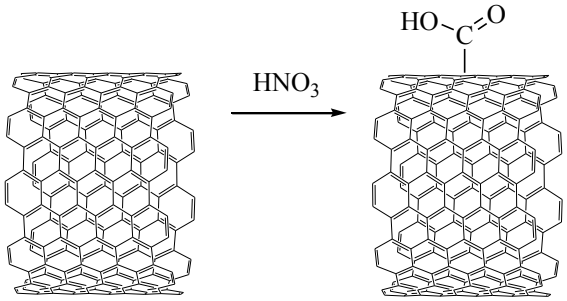

Scheme 1.5 Oxidation of carbon nanomaterial.

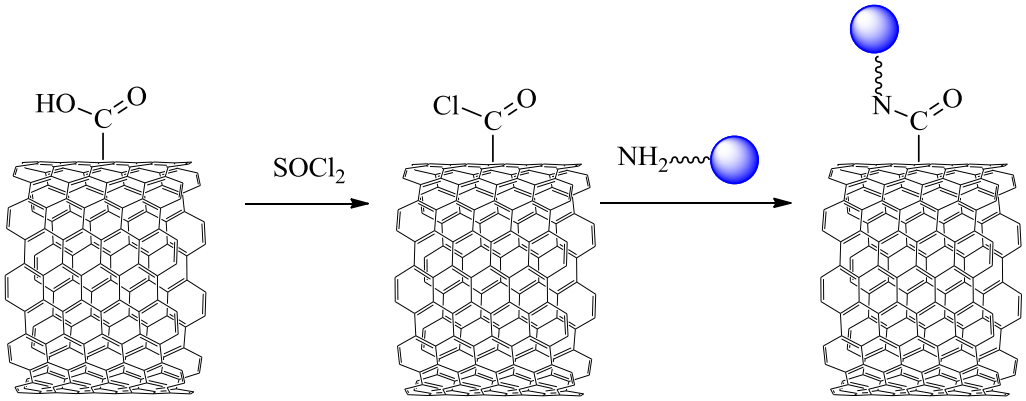

Scheme 1.6 Amide functionalization of oxidized carbon nanomaterial.

Instead of the amine group, compounds containing an alcohol function can link to the nanocarbon sidewalls by carboxylic group [74, 160-161]. According to the above reaction mechanism, some ring-opening polymerization catalytic systems was investigated and nanocarbon composites have been produced [156, 162]. Covalent functionalization is irreversible and the covalent bond is relatively strong, so that the polymer produced can load well around the surface of the carbon nanomaterial.

This grafting-form strategy is the normal way to catch the catalyst on the sidewall of the nanocarbon. The method is also an useful way to prepare ethylene polymerization heterogeneous catalysts. Due to the covalent bond and the nanocarbon's unique physical and chemical properties, the nanocarbon as a support ligand can have a great influence on the polymerization activity.

1.2.2.1.2 Carbon nanomaterial supported catalyst through alkylaluminum

Alkylaluminums such as MAO or modified methylaluminoxane (MMAO) were reported by several groups as the medium to produce heterogeneized catalysts. This approach has been successfully applied for producing CNTs supported ethylene polymerization catalysts [154, 163-167]. Most of the supported catalysts are group IV-based homogeneous catalyst, in particular catalysts containing cyclopentadienyl (Cp) as ligand. The distinct features of this method are: (1) Co-catalysts, MAO, for example, react with well dispersed CNts. This leads to the immobilization of MAO molecules on nanocarbon surface by loose ionic interactions and, to a lesser extent, by virtue of covalent bonding (Scheme 1.7) to −COOH or −OH groups, which are inherent to partially oxidized nanocarbon, and (2) The formation of catalytic active sites is accomplished by means of heterogenization of the metallocene catalyst precursor on nanocarbon surface owing to chemical interaction of metallocene with MAO. Then the active sites formed directly during the initial stage of polymerization at lowered temperature.

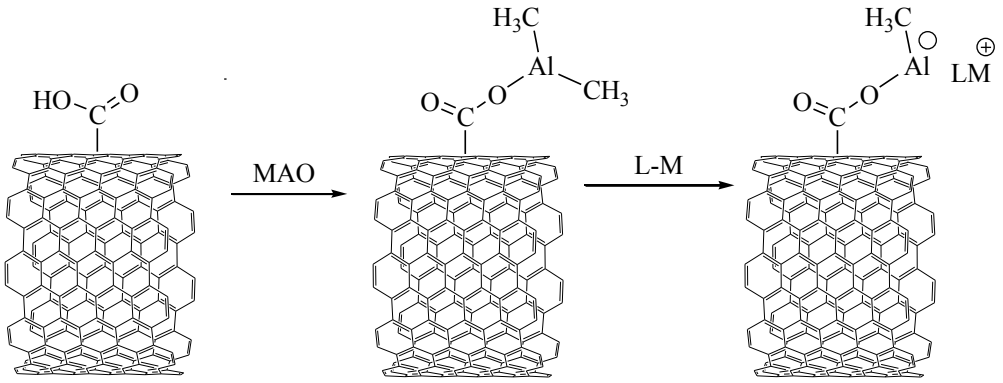

Scheme 1.7 Immobilization of the catalyst on nanocarbon through MAO.

MAO molecules chemically grafted to CNTs surface form catalytic active species, yielding polymer chains attached directly to nanotubes. This represents an excellent way to improve the metallocene/alkylaluminoxane catalytic system and a

new method to cover the carbon nanomaterial by polymer. Moreover, nanocarbons unique physical and chemical properties are hoped to have a positive influence on the activity of the metallocene/alkylaluminoxane catalytic system, due to the covalent bonding between MAO and carbon nanomaterial.

1.2.2.1.3 Carbon nanomaterial supported catalyst through other methods

Similar to the above-mentionned MAO, some other inorganic oxides were used to functionalize the sidewall of the carbon nanomaterial. About ten years ago, it was reported that the nanocarbon could support the Ziegler-Natta catalyst though $MgCl_2$/nOH [168]. Even though, the mechanism of this supported catalyst is not clear, the polymerization process have successfully been accomplished. Later, inorganic support Fe_3O_4/nOH was used to functional the sidewall of the nanocarbon and support $[Sn(Oct)_2]$ (Oct = octanoate) for the ring-opening polymerization [169].

It is well known that the nanocarbons contain many deviations from pure hexagonal structure, which are potentially reactive and can be attacked by nucleophiles such as lithium metal and its alkyls. The lithium is a good leaving group, so, the lithium-functionalized nanocarbon can link to an halogenated compound through a chemically bond (Scheme 1.8, top). Fluorination is a new method for the functionalization of nanocarbons, and an excellent way to locate the compound onto the sidewall of nanocarbons [170]. During the grafting, HF is easy to produce in defluorination and the sp^3 carbon-carbon bonds are created between carbon nanomaterial and the organic compound (Scheme 1.8, bottom). Until now, those methods have not been used to form ethylene polymerization heterogeneous catalysts. However, it can't be denied that those methods are worth being considered in the polymerization field.

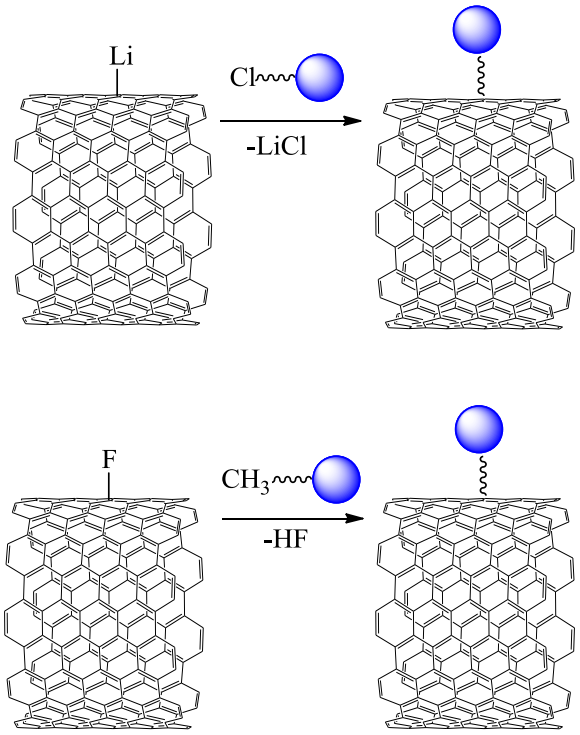

Scheme 1.8 Catalyst covalent immobilization on Li-nanocarbon (up) and F-nanocarbon (bottom).

1.2.2.2 Non-covalent functionalization

Non-covalent functionalization is based on attraction between the hydrophobic end of an adsorbed molecule and the sidewalls of nanocarbon *via* van der Waals forces or π–π interactions. Non covalent functionalization can also be performed using cation- π electrostatic interactions. This type of functionalization does not interfere with the electronic structure of nanocarbons, as it does not involve covalent bonds. The technique is useful for the production of surfactant to exfoliate bundles of CNTs. The main drawback of non-covalent bonding is that it is difficult to control the functionalized system and to characterize the product.

1.2.2.2.1 Carbon nanomaterial supported catalysts via van der Waals forces or π–π interactions

Carbon materials differ in their structure, which results in the variation of surface free energy characteristics and ultimately in altered adsorption profiles. Moreover, to functionalize without damaging the π-electronic structure of nanocarbons, non-covalent attachments seem to be more promising than the covalent attachments. Among the available non-covalent functionalization approaches, the simplest method involves direct π-π stacking of compounds containing aromatic groups. This method has been successfully reported in lots of publications about the π–π interaction between the sidewalls of the nanocarbons and the aromatic moieties of various compounds [138, 140, 151-152, 171-179]. Different polycyclic aromatics rings were investigated in those publications and the most used aromatic moieties are Cp ring [174], benzene ring [179], naphthalene ring [171, 179], anthracene ring [152, 178] and pyrene ring [138-140, 151-152, 171-172]. It is reported that those aromatic moieties can locate very well on the surface of the nanocarbon through π–π interactions, which are possible since those aromatic moieties are electron-rich groups and have similar structures than the one of nanocarbons (Figure 1.7, up). However, compared to a covalent bond, the π–π interaction is weaker. Therefore the incorporation procedure will be greatly influenced by the reaction conditions, like the solvent used and the reaction temperature.

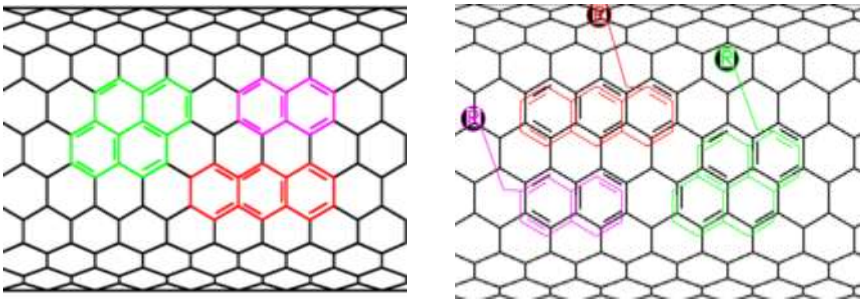

Figure 1.7 Schematic representation of the interaction between a nanotube surface and polycyclic aromatic compounds.

Pyrene moiety is the mostly used to interact with carbon supports through π–π interactions. These reversible interactions have already been used for various applications: 1) Nickel complexes containing a pyrene group have been immobilized through these non-covalent interactions on CNTs and used for catalytic purposes, specifically for H_2 evolution and uptake [138]; 2) Reiser *et al*. have prepared carbon coated cobalt nanoparticles to non-covalently maintain a pyrene-modified palladium complex on the carbon shell to perform the hydroxycarbonylation of aryl halides in water [180]; 3) A pyrene-tagged ruthenium complex was also immobilized *via* π–π stacking on SWCNTs to achieve stable and recyclable catalytic species to promote ring-closing metathesis reactions [139]; and 4) This strategy was also used to produce heterogeneous catalysts for ethylene polymerization by Park *et al*. [144, 181-182], which reported that the intimate interaction of the nanocarbon with the cyclopentadienyl ring catalyst has a great influence on the catalytic nature in their polymerization performances.

1.2.2.2.2 Carbon nanomaterial supported catalyst via π–ionic interaction

Compounds containing an ionic part can locate on the surface of the nanocarbons *via* π–ionic interaction, due to the specific electrical properties of the nanocarbons.

This method, which is used to functionalize the nanocarbons, is easier and greener, most of the reactions can be carried out mixing the nanocarbons with an aqueous salt solution.

Most of the investigations in this field are about nanocarbons functionalized by ionic liquids [183-186]. Usually, the ionic liquids are N-containing cations. The π– ionic interactions between the N-containing cation and the π-electrons of nanocarbons have been certified by the Raman and IR spectrocopy. Subramaniam *et al*. [183] reported that both D and G bands in the Raman spectra are shifted for MWCNTs physically modified by an ionic liquid, which they attributed to π– ionic interactions.

Above all, the nanocarbons have the ability to attach a wide range of chemical species at active sites, such as the sidewall, tubular tips or the defect areas, *via* covalent or non-covalent bonds. Furthermore, the resulting heterogeneous catalysts supported by nanocarbons have been investigated in different areas such as hydrogen evolution and uptake [138], hydrogenation reaction [153] and so on.

1.2.3. Nanocarbons supported ethylene polymerization catalyst

No doubt that how important the catalyst it is for a chemical reaction, the finding of an effective catalyst is also the key step for the polymerization. As already stated, heterogeneous catalysts supported by inorganic support have been reported. Moreover, some of them have been successfully used into industrial processes. It is worth mentioning that nanocarbons have the key properties, similar to the inorganic support used, such as large surface area, high thermal conductivity, porosity, etc. Moreover, nanocarbons are much more stable to the pH, temperature and oxygen. Therefore, nanocarbons have the potential possibility to support the homogeneous catalysts for applications in polymerization processes.

Nanocarbon supported heterogeneous catalysts for the polymerization have been studied. Various publications reported different kinds of polymerization processes for a wide variety of monomers, such as the ethylene polymerization [136, 154-164], propylene polymerization [134, 163], norbornene polymerization [143], styrene polymerization [187] and the caprolactone ring-opening polymerization [169]. Among them, the catalysts for the ethylene polymerization represent the most important part.

As described above, the coordination catalysts, which were used for the ethylene polymerization have been produced using different methods. In the last decade, some of the classic homogeneous catalysts have been anchored to nanocarbons and then investigated in polymerization reactions. It is reported that the presence of the nanocarbons can affect the activity and has a great influence on the produced polymer. During the polymerization reaction, the polymer produced is around these heterogeneous catalysts. In this way, high grafting density can be achieved and the ethylene can be polymerized from the nanocarbon's surface. This represents a new way to produce polymer nanocomposites. Moreover, the nanocarbons are uniformly dispersed and no aggregation is observed in those nanocomposites produced by *in-situ* polymerization (Figure. 1.8).

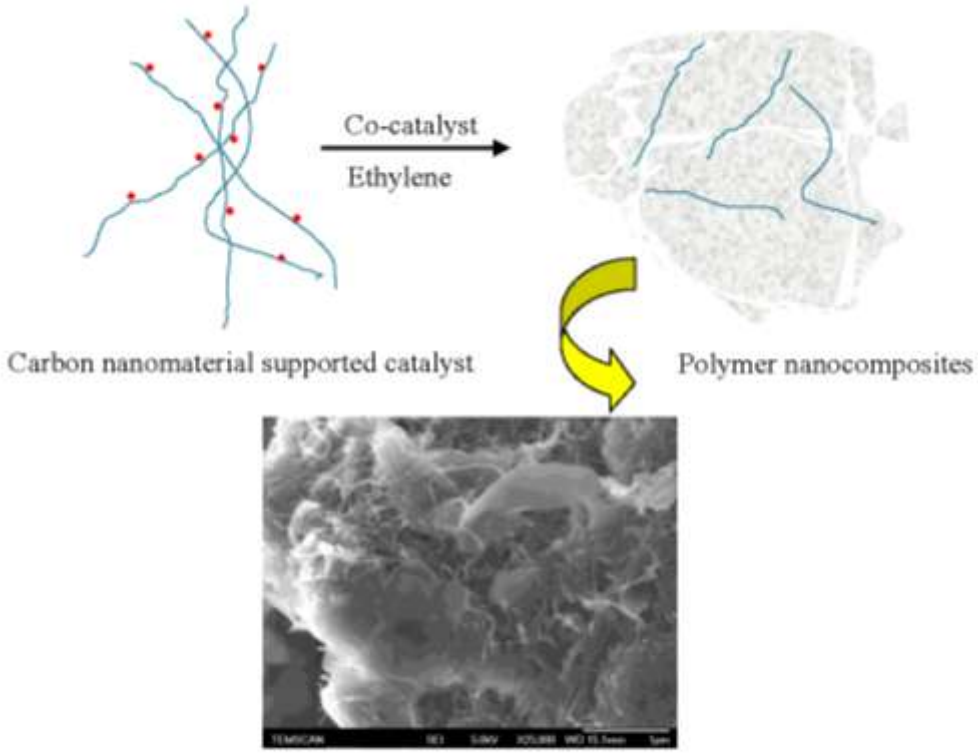

Figure 1.8 Process of the polymerization by nanocarbon immobilized catalyst.

Ziegler-Natta catalyst is well-known as a classic catalyst for the ethylene polymerization. New catalytic systems where CNTs are coated by the Ziegler-Natta catalyst through $MgCl_2$/nOH were synthesized and investigated as polymerization catalysts [134, 168]. It is reported that the polymer is effectively coating the CNTs, and that the presence of the CNTs can increase the polymer's mechanical properties and its melting point or glass temperature. Half-sandwich catalysts ($CpMCl_3$, M = Ti, Zr and Sc) [71, 182], the sandwich catalysts (Cp_2MCl_2, M = Ti, Zr and Sc) [143-144, 163] and their derivatives are reported to be supported on CNTs and graphene [181]. Two different methods are used to anchor these catalysts to nanocarbons: 1. Simple mixing of the nanocarbon and the catalyst, the latter is then is absorbed on the nanocarbon's surface *via* Cp ring; and 2. Anchoring of the catalyst on the sidewall of

the nanocarbon through co-catalyst by covalent bonds. Whatever the method used to support the catalyst, the presence of the nanocarbon was reported to have an influence on the polymer properties, such as high molecular weight and melting point. Results concerning data obtained using nanocarbon-supported Cp_2MCl_2 (M = Ti or Zr) catalysts are summarized in Table 1.1 [143-144, 163]. In addition, few reports mentionned the effect of the nanocarbons on the ethylene polymerization and showed that the presence of the CNTs or graphene can be beneficial to the catalytic activity (Table 1.1). It is necessary to mention that if those supported catalysts not only polymerize ethylene, some of them have been successfully used to co-polymerize ethylene with other monomers, such as norbornene [143] and α-olefin [164].

Table 1.1 Activity and properties of resulting polymer obtained by nanocarbon-suported **Cp_2MCl_2**, M= Ti or Zr catalysts

Entry	Support	Cat.	Activity [a] 10^6	M_w [b] (kg·mol^{-1})	T_m [c] (°C)
1	MWCNTs	Cp_2ZrCl_2	1.0	314-538	132-135
2	MWCNTs	Cp_2TiCl_2	-	266-2270	131-136
3	MWCNTs	$Cp^*_2TiCl_2$	-	229-1060	133-136
4	graphene	Cp_2ZrCl_2	3.5	700-1070	132-133
5	graphene	Cp_2TiCl_2	2.4	520-1490	128-131

[a] g/(mol (metal) h·atm)$^{-1}$; [b] determined by GPC; [c] determined by DSC.

In addition to the catalysts based on group IV metals, late transition metal catalysts can also be grafted on nanocarbons and be investigated in the ethylene polymerization reaction. These catalysts can be supported by nanocarbons through non-covalent or covalent, approaches depending on which kind of group is used to

anchor on to the nanocarbon. A series of nickel complex with the amino group have been synthesized and grafted on carbon nanotubes by Kemp *at al*. [155]. Both the supported catalysts and unsupported catalysts showed good activity, with the supported catalysts being more active.

Due to their extraordinary properties, nanocarbons can provide excellent advantages in polymerization catalytic system, such as, increase the catalytic activity, boost the reaction selectivity and change the produced polymer and nanocomposite's properties. One question must come to our mind is how the nanocarbon affect the reaction activity? Before answering this question, one must remember that the great factors which influence the catalytic activity of the homogeneous systems are the electronic density and the bulkiness around metal center provided by the ligand. Therefore, how the nanocarbon affects the catalytic activity as well as the properties of the nano/polymer composites are discussed as follow.

1.2.3.1 Electronic properties affecting the polymerization

Whether one considers SWCNTs, MWCNTs or graphene, the arrangement of the carbon atoms determines the surface and the electronic properties of those nanocarbons. When the homogeneous catalyst anchored on these nanocarbons through non-covalent or covalent interaction, there should be a strong interaction between the homogeneous compound and the nanocarbons. This naturally has an effect on the electron properties of the metal loaded onto the support [154] and therefore will have a further influence on the catalytic activity.

Moreover, the π-electron of the support has an effect on the produced nano/polymer composites. As mentioned above, after the polymerization, the polymer produced by the supported catalyst coats the surface of the nanocarbon. The

interaction that emerged between them can affect the properties of polymer.

1.2.3.2 The large bulkiness affects the polymerization

As mentioned before, the steric hindrance around of the metal center is one of the important factors influencing the catalytic reaction. The heterogeneous catalysts have a direct interaction between the active center and the nanocarbons support. The nanocarbon is a huge group compared to the organic species. Nanocarbon supports, which can be considered as macro-ligands, are then introduced into the polymerization process. The large bulkiness of this macro-ligand has a great influence of the chain walking and the monomer insertion during the polymerization reaction. By this way, the presence of the nanocarbon plays an important role in the catalytic activity and the branching of the polyethylene as well as their molecular weight.

1.2.3.3 Thermal conductivity affects the polymerization

The productivity of the catalysts is intimately tied to the temperature, which can affect the life time of the active species as well as the feature of the resulting polyolefin, like molecular weights, molecular weight distributions, and degree of branching [20, 28]. Olefin polymerization is a highly exothermic reaction and the formation of hot spot in the reaction mixture is generally not beneficial to the stability of the supported catalytic active species. This is particularly true for the oxide supports. This means that the reaction temperature could locally increase during the reaction and then accelerate the active species decay. Nanocarbon supported catalysts can slow down the decay of catalysts and increase the lifetime of the catalytic active species due to the high thermal conductivity property of nanocarbon materials (between 200 and 600 w/m·K). Moreover, the presence of the nanocarbons can

enhance the thermal conductivity of resulting nanocomposites, then, improve their industrial applicability

1.2.3.4 Other unique properties affecting the polymerization

One reason to consider nanocarbons as suitable supports for metal catalyst is the high surface to volume ratio. High surface areas and a well-developed porosity are essential for achieving large metal dispersions, which usually result in a high catalytic activity. On the other hand, the surface areas and porosity offer the possibility to adsorb the ethylene gas *via* π-π interaction. The *in-situ* polymerization is carried out in gas-slurry processes. So the unique property of the nanocarbon can increase the rate of monomer insertion. In another word, ethylene monomer adsorption on the surface of the nanocarbon can increase the effectiveness of the catalyst.

The nanocarbons are reported to be harder than iron, at the same time nanocarbons are flexible and can be bent several times at 90° without undergoing structural changes. The covalent sp^2 bond and the porosity of the material result in the high strength of the nanocarbon (Figure 1.9), which is not only positive for the vigorously stirred liquid phase reaction, but favorable in producing polymer nanocomposites. The presence of the nanocarbon has a great influence in the polymer's properties, and can increase the polymer technical property, raise the polymer thermal conductivity, enhance the polymer resistance to the stress, and so on. Therefore polymer nanocomposites are seen as a material for future that can be used in some high-tech fields.

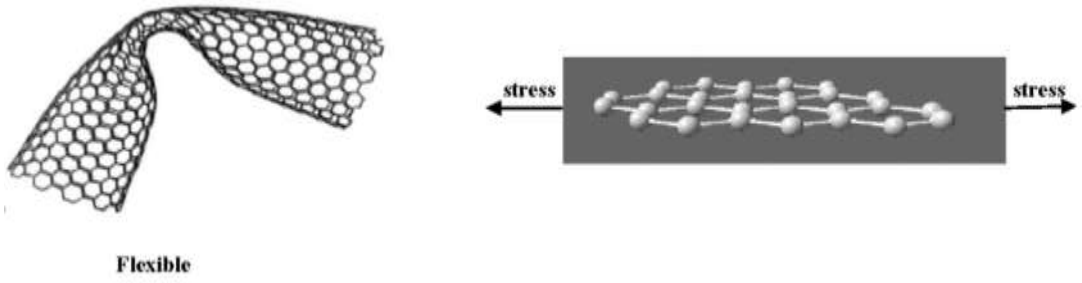

Figure 1.9 Mechanical properties of nanocarbons.

1.3 Conclusions

Polyethylene has been used to make different kinds of daily used products, so it is seen as one of the great innovation of the last century. To discover and synthesize an effective catalyst for ethylene polymerization is critical for both the academy and the industry. After several generations, the late transition catalysts have drawn more attention because of their interesting catalytic behaviors towards ethylene and the easily controlled polyethylene produced. However, this kind of catalyst has the same disadvantages as other homogeneous catalysts, such as a short life time of active sites and the limitations of use in large scale processes. In order to pass those challenges and develop suitable systems for most of the industrial processes (slurry or gas-phase reactors), the immobilization of such catalysts is required.

In the last decade, due to their high surface area, dispersed functionalized groups on the surface and good mechanical properties, various kinds of the supports, such as silica gel, $MgCl_2$, Al_2O_3 MgO and zeolites, were investigated in the field of olefin polymerization. Catalysts based on both early and late transition metals were supported on those inorganic supports. Detailed studies evidenced a strong correlation between the polymerization activity of those supported catalysts and both the nature of the supporting material and the size, diameter and distribution of the pores.

Nanocarbons (CNTs or FLG) were also used as support in catalysis in recent years, due to the characteristics of nanocarbons, such as interness, stability under reaction and regeneration conditions, high surface area and porosity, *etc*. Moreover, naonocarbons have some of unique properties, *e.g.* high thermal conductiviy, mechanical and electronic properties. Most of the typical homogeneous catalysts have been anchored *via* non-covalent or covalent interactions. As shown in Table 1.1, the best activities are observed for CNTs or graphene supported Cp_2MCl_2 (M= Zr or Ti) catalysts systems producing high molecular weight polymer. In addition, during the polymerization, the olefins can be polymerized from the nanocarbon's surface that can thus be covered by the resulting polymers. In this way, the nanocarbons can be homogeneously dispersed into resulting polymers and non aggregated polymer nanocomposites could be obtained.

References

[1] J. Skupinska, "Oligomerization of .alpha.-olefins to higher oligomers", *Chem. Rev.*, 1991, 91, 613–648.

[2] P. Galli, G. Vecellio, "Polyolefins: The most promising large-volume materials for the 21st century", *J. Polym. Sci. Part Polym. Chem.*, 204, 42, 396–415.

[3] E. W. Fawcett, R. U. Gibson, M. W. perrin, J. Paton, E. G. Williams, *GB 471590*, 1936.

[4] "The Plastics and Rubber Institute," Polyethylenes 1933-1983: Past, Present, Future, London, 1983.

[5] G. Natta, P. Pino, P. Corradini, F. Danusso, E. Mantica, G. Mazzanti, G. Moraglio, "crystalline high polymers of α-olefins", *J. Am. Chem. Soc.*, 1995, 77, 1708–1710.

[6] N. Kashiwa, T. Tokuzumi, H. Fujimura, “Process for the Polymerization and/or Copolymerization of Olefins with the Use of Ziegler-Type Catalysts Supported on Carrier”, 1970, DE1939074 (A1).

[7] F. J. Karol, G. L. Karapinka, C. Wu, A. W. Dow, R. N. Johnson, W. L. Carrick, “Chromocene catalysts for ethylene polymerization: Scope of the polymerization”, *J. Polym. Sci. [A1]*, 1972, 10, 2621–2637.

[8] A. K. Tomov, J. J. Chirinos, D. J. Jones, R. J. Long, V. C. Gibson, “Experimental Evidence for Large Ring Metallacycle Intermediates in Polyethylene Chain Growth Using Homogeneous Chromium Catalysts”, *J. Am. Chem. Soc.*, 2005, 127, 10166–10167.

[9] H. Sinn, W. Kaminsky, H.-J. Vollmer, R. Woldt, “‘Living Polymers’ on Polymerization with Extremely Productive Ziegler Catalysts”, *Angew. Chem. Int. Ed. Engl.*, 1980, 19, 390–392.

[10] R. F. Jordan, “Chemistry of Cationic Dicyclopentadienyl Group 4 Metal-Alky I Complexes”, *Advances in Organometallic Chemistry*, 1991, 32, 325–387.

[11] H. H. Brintzinger, D. Fischer, R. Miilhaupt, B. Rieger, R. M. Waymouth, “Stereospecific Olefin Polymerization with Chiral Metallocene Catalysts”, *Angew Chem Int Ed Engl*, 1995, 34, 1143–1170.

[12] W. Kaminsky, “Highly active metallocene catalysts for olefin polymerization”, *J. Chem. Soc. Dalton Trans.*, 1998, 9, 1413–1418.

[13] H. G. Alt, A. Köppl, “Effect of the Nature of Metallocene Complexes of Group IV Metals on Their Performance in Catalytic Ethylene and Propylene Polymerization”, *Chem. Rev.*, 2000, 100, 1205–1222.

[14] A. L. McKnight, R. M. Waymouth, “Group 4 ansa-Cyclopentadienyl-Amido

Catalysts for Olefin Polymerization", *Chem. Rev.*, 1998, 98, 2587–2598.

[15] H. Braunschweig, F. M. Breitling, "Constrained geometry complexes—Synthesis and applications", *Coord. Chem. Rev.*, 2006, 250, 2691–2720.

[16] R. F. Jordan, R. E. LaPointe, N. Baenziger, G. D. Hinch, "Synthesis and structures of neutral and cationic rac-(ethylenebis(tetrahydroindenyl))zirconium(IV) benzyl complexes", *Organometallics*, 1990, 9, 1539–1545.

[17] R. F. Jordan, P. K. Bradley, N. C. Baenziger, R. E. LaPointe, ".beta.-Agostic interactions in $(C_5H_4Me)_2Zr(CH_2CH_2R)(PMe_3)^+$ complexes", *J. Am. Chem. Soc.*, 1990, 112, 1289–1291.

[18] R. F. Jordan, R. E. LaPointe, P. K. Bradley, N. Baenziger, "Synthesis and chemistry of cationic alkyl, alkenyl, and allyl complexes derived from the soluble, cationic hydride $(C_5H_4Me)_2Zr(H)(THF)^+$", *Organometallics*, 1989, 8, 2892–2903.

[19] W. P. Long, D. S. Breslow, "Polymerization of Ethylene with Bis-(cyclopentadienyl)-titanium Dichloride and Diethylaluminum Chloride", *J. Am. Chem. Soc.*, 1960, 82, 1953–1957.

[20] S. D. Ittel, L. K. Johnson, M. Brookhart, "Late-Metal Catalysts for Ethylene Homo- and Copolymerization", *Chem. Rev.*, 2000, 100, 1169–1204.

[21] W. Keim, F. H. Kowaldt, R. Goddard, C. Krüger, "Novel Coordination of (Benzoylmethylene)triphenylphosphorane in a Nickel Oligomerization Catalyst", *Angew. Chem. Int. Ed. Engl.*, 1978, 17, 466–467.

[22] W. Keim, A. Behr, B. Limbäcker, C. Krüger, "Novel Nickel-Oligomerization Catalysts with Arsenic-Oxygen Chelate Ligands", *Angew. Chem. Int. Ed. Engl.*, 1983, 22, 503–503.

[23] M. Peuckert, W. Keim, "A new nickel complex for the oligomerization of ethylene", *Organometallics*, 1983, 2, 594–597.

[24] W. Keim, “Nickel: An Element with Wide Application in Industrial Homogeneous Catalysis”, *Angew. Chem. Int. Ed. Engl.*, 1990, 29, 235–244.

[25] L. K. Johnson, C. M. Killian, M. Brookhart, “New Pd (II)-and Ni (II)-based catalysts for polymerization of ethylene and. alpha.-olefins”, *J. Am. Chem. Soc.*, 1995, 117, 6414–6415.

[26] G. J. P. Britovsek, V. C. Gibson, D. F. Wass, “The Search for New-Generation Olefin Polymerization Catalysts: Life beyond Metallocenes”, *Angew. Chem. Int. Ed.*, 1999, 38, 428–447.

[27] F. M. Bauers, S. Mecking, “High Molecular Mass Polyethylene Aqueous Latexes by Catalytic Polymerization”, *Angew. Chem. Int. Ed.*, 2001, 40, 3020–3022.

[28] V. C. Gibson, S. K. Spitzmesser, “Advances in Non-Metallocene Olefin Polymerization Catalysis”, 2003, 103, 283–315.

[29] F. Speiser, P. Braunstein, L. Saussine, “Catalytic ethylene dimerization and oligomerization: recent developments with nickel complexes containing P, N-chelating ligands”, *Acc. Chem. Res.*, 2005, 38, 784–793.

[30] C.-Y. Guo, N. Peulecke, K. R. Basvani, M. K. Kindermann, J. Heinicke, “2-Phosphinophenolate Nickel Catalysts: Formation of Ethylene Copolymers with Isolated *sec* -Alkyl, Aryl, and Functionally Substituted Alkyl Groups ”, *Macromolecules*, 2010, 43, 1416–1424.

[31] L. Zhang, X. Hao, W.-H. Sun, C. Redshaw, “Synthesis, Characterization, and Ethylene Polymerization Behavior of 8-(Nitroarylamino)-5,6,7-trihydroquinolylnickel Dichlorides: Influence of the Nitro Group and Impurities on Catalytic Activity”, *ACS Catal.*, 2011, 1, 1213–1220.

[32] H. Liu, W. Zhao, X. Hao, C. Redshaw, W. Huang, W.-H. Sun, “2,6-Dibenzhydryl-N-(2-phenyliminoacenaphthylenylidene)-4-methylbenzenamine

Nickel Dibromides: Synthesis, Characterization, and Ethylene Polymerization", *Organometallics*, 2011, 30, 2418–2424.

[33] X. Hou, Z. Cai, X. Chen, L. Wang, C. Redshaw, W.-H. Sun, "N-(5,6,7-Trihydroquinolin-8-ylidene)-2-benzhydrylbenzenaminonickel halide complexes: synthesis, characterization and catalytic behavior towards ethylene polymerization", *Dalton Trans.*, 2012, 41, 1617–1623.

[34] J. Yu, X. Hu, Y. Zeng, L. Zhang, C. Ni, X. Hao, W.-H. Sun, "Synthesis, characterisation and ethylene oligomerization behaviour of N-(2-substituted-5,6,7-trihydroquinolin-8-ylidene)arylaminonickel dichlorides", *New J. Chem.*, 2011, 35, 178.

[35] S. A. Svejda, M. Brookhart, "Ethylene Oligomerization and Propylene Dimerization Using Cationic (α-Diimine)nickel(II) Catalysts", *Organometallics*, 1999, 18, 65–74.

[36] L. Deng, T. K. Woo, L. Cavallo, P. M. Margl, T. Ziegler, "The Role of Bulky Substituents in Brookhart-Type Ni(II) Diimine Catalyzed Olefin Polymerization: A Combined Density Functional Theory and Molecular Mechanics Study", *J. Am. Chem. Soc.*, 1997, 119, 6177–6186.

[37] D. G. Musaev, R. D. J. Froese, M. Svensson, K. Morokuma, "A Density Functional Study of the Mechanism of the Diimine−Nickel-Catalyzed Ethylene Polymerization Reaction", *J. Am. Chem. Soc.*, 1997, 119, 367–374.

[38] G. Wilke, "Contributions to Organo-Nickel Chemistry", *Angew. Chem. Int. Ed. Engl.*, 1988, 27, 185–206.

[39] C. M. Killian, L. K. Johnson, M. Brookhart, "Preparation of Linear α-Olefins Using Cationic Nickel(II) α-Diimine Catalysts", *Organometallics*, 1997, 16, 2005–2007.

[40] F. A. Kunrath, R. F. de Souza, Casagrande, N. R. Brooks, V. G. Young, "Highly Selective Nickel Ethylene Oligomerization Catalysts Based on Sterically Hindered Tris(pyrazolyl)borate Ligands", *Organometallics*, 2003, 22, 4739–4743.

[41] N. Ajellal, M. C. A. Kuhn, A. D. G. Boff, M. Hörner, C. M. Thomas, J.-F. Carpentie, O. L. Casagrande, "Nickel Complexes Based on Tridentate Pyrazolyl Ligands for Highly Efficient Dimerization of Ethylene to 1-Butene", *Organometallics*, 2006, 25, 1213–1216.

[42] S. Al-Benna, M. J. Sarsfield, M. Thornton-Pett, D. L. Ormsby, P. J. Maddox, P. Brès, M. Bochmann, "Sterically hindered iminophosphorane complexes of vanadium, iron, cobalt and nickel: a synthetic, structural and catalytic study", *J. Chem. Soc. Dalton Trans.*, 2000, 23, 4247–4257.

[43] S. O. Ojwach, I. A. Guzei, L. L. Benade, S. F. Mapolie, J. Darkwa, "(Pyrazol-1-ylmethyl)pyridine Nickel Complexes: Ethylene Oligomerization and Unusual Friedel−Crafts Alkylation Catalysts", *Organometallics*, 2009, 28, 2127–2133.

[44] R. Gao, M. Zhang, T. Liang, F. Wang, W.-H. Sun, "Nickel(II) Complexes Chelated by 2-Arylimino-6-benzoxazolylpyridine: Syntheses, Characterization, and Ethylene Oligomerization", *Organometallics*, 2008, 27, 5641–5648.

[45] B. Su, J. Zhao, Q. Zhang, W. Qin, "Cobalt(II) and nickel(II) complexes bearing mono(imino)pyridyl and bis(imino)pyridyl ligands: preparation, structure and ethylene polymerization/oligomerization behaviors", *Polym. Int.*, 2009, 58, 1051–1057.

[46] X. Tang, W.-H. Sun, T. Gao, J. Hou, J. Chen, W. Chen, "Nickel (II) complexes bearing 2-ethylcarboxylate-6-iminopyridyl ligands: synthesis, structures and their catalytic behavior for ethylene oligomerization and polymerization", *J.*

Organomet. Chem., 2005, 690, 1570–1580.

[47] J. Hou, W.-H. Sun, S. Zhang, H. Ma, Y. Deng, X. Lu, "Synthesis and Characterization of Tridentate Nickel Complexes Bearing P^N^N and P^N^P Ligands and Their Catalytic Property in Ethylene Oligomerization", *Organometallics*, 2006, 25, 236–244.

[48] B. L. Small, M. Brookhart, A. M. A. Bennett, "Highly Active Iron and Cobalt Catalysts for the Polymerization of Ethylene", *J. Am. Chem. Soc.*, 1998, 120, 4049–4050.

[49] B. L. Small, M. Brookhart, "Iron-Based Catalysts with Exceptionally High Activities and Selectivities for Oligomerization of Ethylene to Linear α-Olefins", *J. Am. Chem. Soc.*, 1998, 120, 7143–7144.

[50] G. J. P. Britovsek, M. Bruce, V. C. Gibson, B. S. Kimberley, P. J. Maddox, S. Mastroianni, S. J. McTavish, C. Redshaw, G. A. Solan, S. Strömberg, A. J. P. White, D. J. Williams, "Iron and Cobalt Ethylene Polymerization Catalysts Bearing 2,6-Bis(Imino)Pyridyl Ligands: Synthesis, Structures, and Polymerization Studies", *J. Am. Chem. Soc.*, 1999, 121, 8728–8740.

[51] G. J. P. Britovsek, V. C. Gibson, S. J. McTavish, G. A. Solan, A. J. P. White, D. J. Williams, G. J. P. Britovsek, B. S. Kimberley, P. J. Maddox, "Novel olefin polymerization catalysts based on iron and cobalt", *Chem. Commun.*, 1998, 7, 849–850.

[52] G. J. P. Britovsek, S. Mastroianni, G. A. Solan, S. P. D. Baugh, C. Redshaw, V. C. Gibson, A. J. P. White, D. J. Williams, M. R. J. Elsegood, "Oligomerisation of Ethylene by Bis(imino)pyridyliron and -cobalt Complexes", *Chem. Eur. J.*, 2000, 6, 2221–2231.

[53] C. Bianchini, G. Giambastiani, L. Luconi, A. Meli, "Olefin oligomerization,

homopolymerization and copolymerization by late transition metals supported by (imino)pyridine ligands", *Coord. Chem. Rev.*, 2010, 254, 431–455.

[54] J. Yu, H. Liu, W. Zhang, X. Hao, W.-H. Sun, "Access to highly active and thermally stable iron procatalysts using bulky 2-[1-(2,6-dibenzhydryl-4-methylphenylimino)ethyl]-6-[1-(arylimino)ethyl]pyridine ligands", *Chem. Commun.*, 2011, 47, 3257–3259.

[55] Y. Chen, R. Chen, C. Qian, X. Dong, J. Sun, "Halogen-Substituted 2,6-Bis(imino)pyridyl Iron and Cobalt Complexes: Highly Active Catalysts for Polymerization and Oligomerization of Ethylene", *Organometallics*, 2003, 22, 4312–4321.

[56] C. Bianchini, G. Mantovani, A. Meli, F. Migliacci, F. Zanobini, F. Laschi, A. Sommazzi, "Oligomerisation of Ethylene to Linear α-Olefins by new Cs- and C1-Symmetric [2,6-Bis(imino)pyridyl]iron and -cobalt Dichloride Complexes", *Eur. J. Inorg. Chem.*, 2003, 2003, 1620–1631.

[57] C. Wallenhorst, G. Kehr, H. Luftmann, R. Fröhlich, G. Erker, "Bis(iminoethyl)pyridine Systems with a Pendant Alkenyl Group. Part A: Cobalt and Iron Complexes and Their Catalytic Behavior", *Organometallics*, 2008, 27, 6547–6556.

[58] F. A. R. Kaul, G. T. Puchta, G. D. Frey, E. Herdtweck, W. A. Herrmann, "Iminopyridine Complexes of 3d Metals for Ethylene Polymerization: Comparative Structural Studies and Ligand Size Controlled Chain Termination", *Organometallics*, 2007, 26, 988–999.

[59] G. G. Hlatky, "Heterogeneous Single-Site Catalysts for Olefin Polymerization", *Chem. Rev.*, 2000, 100, 1347–1376.

[60] P. A. Zapata, R. Quijada, I. Lieberwirth, H. Palza, "Synthetic layered and

tube-like silica nanoparticles as novel supports for metallocene catalysts in ethylene polymerization", *Appl. Catal. Gen.*, 2011, 407, 181–187.

[61] B. K. Bahuleyan, J. M. Oh, D. Chandran, J. Y. Ha, A. Y. Hur, D.-W. Park, C. S. Ha, H. Suh, I. Kim, "Highly Efficient Supported Diimine Ni(II) and Iminopyridyl Fe(II) Catalysts for Ethylene Polymerizations", *Top. Catal.*, 2010, 53, 500–509.

[62] Y. Chen, E. Callens, E. Abou-Hamad, N. Merle, A. J. P. White, M. Taoufik, C. Copéret, E. Le Roux, J.-M. Basset, "[(SiO)TaVCl_2Me_2]: A Well-Defined Silica-Supported Tantalum(V) Surface Complex as Catalyst Precursor for the Selective Cocatalyst-Free Trimerization of Ethylene", *Angew. Chem. Int. Ed.*, 2012, 51, 11886–11889.

[63] J. R. Severn, J. C. Chadwick, R. Duchateau, N. Friederichs, "'Bound but Not Gagged'Immobilizing Single-Site α-Olefin Polymerization Catalysts", *Chem. Rev.*, 2005, 105, 4073–4147.

[64] A. A. Vasileiou, G. Z. Papageorgiou, M. Kontopoulou, A. Docoslis, D. Bikiaris, "Covalently bonded poly(ethylene succinate)/SiO_2 nanocomposites prepared by in situ polymerisation", *Polymer*, 2013, 54, 1018–1032.

[65] J. R. Severn, J. C. Chadwick, "Activation of Titanium-Based Single-Site Catalysts for Ethylene Polymerization Using Supports of Type $MgCl_2$/AlRn$(OEt)_{3–n}$", *Macromol. Chem. Phys.*, 2004, 205, 1987–1994.

[66] R. Huang, D. Liu, S. Wang, B. Mao, "Spherical $MgCl_2$ Supported Iron Catalyst for Ethylene Polymerization: Effect of the Preparation Procedure on Catalyst Activity and the Morphology of Polyethylene Particles", *Macromol. Chem. Phys.*, 2004, 205, 966–972.

[67] R. Huang, D. Liu, S. Wang, B. Mao, "Preparation of spherical $MgCl_2$ supported bis(imino)pyridyl iron(II) precatalyst for ethylene polymerization", *J. Mol.*

Catal. Chem., 2005, 233, 91–97.

[68] Q. Lin, Y. Gu, D. Chen, "Attapulgite-supported aluminum oxide hydroxide catalyst for synthesis of poly(ethylene terephthalate)", *J. Appl. Polym. Sci.*, 2013, 129, 2571–2579.

[69] G. Nooijen, V. M. Kessel, H. M. A. Stiphout, "Catalyst Precursor and Catalyst for the Polymerisation of Ethylene", 2013,WO2013060444 (A1).

[70] N. R. de S. Basso, G. B. Galland, J. H. Z. dos Santos, F. Fim, C. Sauer, C. Carone, "Polymerization of ethylene by supported zirconium alkoxide complex", *J. Appl. Polym. Sci.*, 2010, 118, 1561–1566.

[71] A. Ravasio, L. Boggioni, I. Tritto, C. D'arrigo, A. Perico, J. Hitzbleck, J. Okuda, "A non-PFT (polymerization filling technique) approach to poly(ethylene-co-norbornene)/MWNTs nanocomposites by in situ copolymerization with scandium half-sandwich catalyst", *J. Polym. Sci. Part Polym. Chem.*, 2009, 47, 5709–5719.

[72] D. S. Bethune, C. H. Klang, M. S. de Vries, G. Gorman, R. Savoy, J. Vazquez, R. Beyers, "Cobalt-catalysed growth of carbon nanotubes with single-atomic-layer walls", *Nature*, 1993, 363, 605–607.

[73] L. Cui, J. Yu, X. Yu, Y. Lv, G. Li, S. Zhou, "In situ synthesis of polyisoprene/grafted single-walled carbon nanotube composites", *Polym. J.*, 2012, 45, 834–838.

[74] S. Qin, D. Qin, W. T. Ford, D. E. Resasco, J. E. Herrera, "Polymer Brushes on Single-Walled Carbon Nanotubes by Atom Transfer Radical Polymerization of *n* -Butyl Methacrylate", *J. Am. Chem. Soc.*, 2004, 126, 170–176.

[75] J. C. W. Chien, D. He, "Olefin copolymerization with metallocene catalysts. III. Supported metallocene/methylaluminoxane catalyst for olefin copolymerization",

J. Polym. Sci. Part Polym. Chem., 1991, 29, 1603–1607.

[76] E. G. Barrera, F. C. Stedile, M. O. de Souza, M. S. L. Miranda, R. F. de Souza, K. Bernardo-Gusmão, "Ethylene polymerization using metallocene catalyst supported on hybrid indenyl silica produced by sol–gel process", *Appl. Catal. Gen.*, 2013, 462–463, 1–7.

[77] Z. Grof, J. Kosek, M. Marek, "Principles of the Morphogenesis of Polyolefin Particles", *Ind. Eng. Chem. Res.*, 2005, 44, 2389–2404.

[78] N. Popoff, R. M. Gauvin, A. De Mallmann, M. Taoufik, "On the Fate of Silica-Supported Half-Metallocene Cations: Elucidating a Catalyst's Deactivation Pathways", *Organometallics*, 2012, 31, 4763–4768.

[79] M. Dötterl, H. G. Alt, "Silica Based Cocatalysts for Heterogeneous Olefin Dimerization and Ethene Polymerization Reactions with Nickel Complexes", *ChemCatChem*, 2012, 4, 660–667.

[80] Y.-G. Li, L. Pan, Z.-J. Zheng, Y.-S. Li, "Polymerization of ethylene to branched polyethylene with silica and Merrifield resin supported nickel(II) catalysts with α-diimine ligands", *J. Mol. Catal. Chem.*, 208, 287, 57–64.

[81] Z. Zheng, J. Liu, Y. Li, "Ethylene polymerization with silica-supported bis(imino)pyridyl iron(II) catalysts", *J. Catal.*, 2005, 234, 101–110.

[82] B. Jongsomjit, J. Panpranot, P. Praserthdam, "Effect of nanoscale SiO_2 and ZrO_2 as the fillers on the microstructure of LLDPE nanocomposites synthesized *via* in situ polymerization with zirconocene", *Mater. Lett.*, 2007, 61, 1376–1379.

[83] K.-T. Li, Y.-T. Kao, "Nanosized silica-supported metallocene/MAO catalyst for propylene polymerization", *J. Appl. Polym. Sci.*, 2006, 101, 2573–2580.

[84] K.-T. Li, F.-S. Ko, "Dimethylsilylbis(1-indenyl) zirconium dichloride/methylaluminoxane catalyst supported on nanosized silica for propylene

polymerization", *J. Appl. Polym. Sci.*, 208, 107, 1387–1394.

[85] V. F. Tisse, F. Prades, R. Briquel, C. Boisson, T. F. L. McKenna, "Role of Silica Properties in the Polymerisation of Ethylene Using Supported Metallocene Catalysts", *Macromol. Chem. Phys.*, 2010, 211, 91–102.

[86] T. Sano, H. Hagimoto, J. Jin, Y. Oumi, T. Uozumi, K. Soga, "Influences of methylaluminoxane separated by porous inorganic materials on the isospecific polymerization of propylene", *Macromol. Rapid Commun.*, 2000, 21, 1191–1195.

[87] M. P. McDaniel, "Influence of Catalyst Porosity on Ethylene Polymerization", *ACS Catal.*, 2011, 1, 1394–1407.

[88] G. Fink, B. Steinmetz, J. Zechlin, C. Przybyla, B. Tesche, "Propene Polymerization with Silica-Supported Metallocene/MAO Catalysts", *Chem. Rev.*, 2000, 100, 1377–1390.

[89] R. Huang, R. Duchateau, C. E. Koning, J. C. Chadwick, "Zirconocene Immobilization and Activation on $MgCl_2$ -Based Supports: Factors Affecting Ethylene Polymerization Activity", *Macromolecules*, 2008, 41, 579–590.

[90] J. R. Severn, R. Duchateau, J. C. Chadwick, "Immobilization and activation of vanadium(III) and titanium(III) single-site catalysts for ethylene polymerization using MgCl2-based supports", *Polym. Int.*, 2005, 54, 837–841.

[91] M. BiaŁek, A. GarŁowska, O. Liboska, "Chlorotitanium (IV) tetradentate Schiff-base complex immobilized on inorganic supports: Support type and other factors having effect on ethylene polymerization activity", *J. Polym. Sci. Part Polym. Chem.*, 2009, 47, 4811–4821.

[92] R. Huang, D. Liu, S. Wang, B. Mao, "Spherical MgCl2 Supported Iron Catalyst for Ethylene Polymerization: Effect of the Preparation Procedure on Catalyst Activity and the Morphology of Polyethylene Particles", *Macromol. Chem. Phys.*,

2004, 205, 966–972.

[93] J. R. Severn, J. C. Chadwick, V. Van Axel Castelli, "$MgCl_2$-Based Supports for the Immobilization and Activation of Nickel Diimine Catalysts for Polymerization of Ethylene", *Macromolecules*, 2004, 37, 6258–6259.

[94] R. Huang, C. E. Koning, J. C. Chadwick, "Synergetic Effect of a Nickel Diimine in Ethylene Polymerization with Immobilized Fe-, Cr-, and Ti-Based Catalysts on $MgCl_2$ Supports", *Macromolecules*, 2007, 40, 3021–3029.

[95] R. Xu, D. Liu, S. Wang, B. Mao, "Preparation of Spherical $MgCl_2$-Supported Late-Transition Metal Catalysts for Ethylene Polymerization", *Macromol. Chem. Phys.*, 2006, 207, 779–786.

[96] R. Huang, N. Kukalyekar, C. E. Koning, J. C. Chadwick, "Immobilization and activation of 2,6-bis(imino)pyridyl Fe, Cr and V precatalysts using a $MgCl_2/AlRn(OEt)_{3-n}$ support: Effects on polyethylene molecular weight and molecular weight distribution", *J. Mol. Catal. Chem.*, 2006, 260, 135–143.

[97] J. C. Chadwick, R. Huang, N. Kukalyekar, S. Rastogi, "Ethylene Polymerization with Combinations of Early- and Late-Transition Metal Catalysts Immobilized on MgCl2 Supports", *Macromol. Symp.*, 2007, 260, 154–160.

[98] A. C. Casagrande, T. T. da R. Tavares, M. C. A. Kuhn, O. L. Casagrande Jr., J. H. . dos Santos, T. Teranishi, "Tris(pyrazolyl)borate imido vanadium (V) compound immobilized on inorganic supports and its use in ethylene polymerization", *J. Mol. Catal. Chem.*, 204, 212, 267–275.

[99] D. Harrison, I. M. Coulter, S. Wang, S. Nistala, B. A. Kuntz, M. Pigeon, J. Tian, S. Collins, "Olefin polymerization using supported metallocene catalysts: development of high activity catalysts for use in slurry and gas phase ethylene polymerizations", *J. Mol. Catal. Chem.*, 1998, 128, 65–77.

[100] S. J. Kim, W. Y. Lee, Y. Park, W. Huh, Y. G. Ko, “Ethylene polymerization over MgO-supported zirconocene catalysts”, *Polym. Eng. Sci.*, 2003, 43, 1011–1017.

[101] S. Collins, W. M. Kelly, D. A. Holden, “Polymerization of propylene using supported, chiral, ansa-metallocene catalysts: production of polypropylene with narrow molecular weight distributions”, *Macromolecules*, 1992, 25, 1780–1785.

[102] M. de F. V. Marques, S. C. Moreira, “ZSM-5 acid zeolite supported metallocene catalysts for ethylene polymerization”, *J. Mol. Catal. Chem.*, 2003, 192, 93–101.

[103] C. Covarrubias, R. Quijada, R. Rojas, “Ethylene polymerization using dealuminated ZSM-2 zeolite nanocrystals as an active metallocene catalyst support”, *Appl. Catal. Gen.*, 2008, 347, 223–233.

[104] Y. S. Ko, S. I. Woo, “Generation of active site confined inside supercage of NaY zeolite on a nano-scale and its ethylene polymerization”, *Eur. Polym. J.*, 2003, 39, 1553–1557.

[105] V. Costa Vayá, P. Belelli, J. H. dos Santos, M. Ferreira, D. Damiani, “Influence of Acidic Support in Metallocene Catalysts for Ethylene Polymerization”, *J. Catal.*, 2001, 204, 1–10.

[106] M. Michelotti, G. Arribas, S. Bronco, A. Altomare, “Effect of the zeolite HY-support on the monoalkene polymerization by group IV metallocenes”, *J. Mol. Catal. Chem.*, 2000, 152, 167–177.

[107] K.-S. Lee, C.-G. Oh, J.-H. Yim, S.-K. Ihm, “Characteristics of zirconocene catalysts supported on Al-MCM-41 for ethylene polymerization”, *J. Mol. Catal. Chem.*, 2000, 159, 301–308.

[108] L. K. Van Looveren, D. F. Geysen, K. A. Vercruysse, B. H. Wouters, P. J. Grobet, P. A. Jacobs, “Methylalumoxane MCM-41 as Support in the

Co-Oligomerization of Ethene and Propene with [{C_2H_4(1-indenyl)$_2$}Zr(CH_3)$_2$]", *Angew. Chem. Int. Ed.*, 1998, 37, 517–520.

[109] L. Novokshonova, N. Kovaleva, I. Meshkova, T. Ushakova, V. Krasheninnikov, T. Ladygina, I. Leipunskii, A. Zhigach, M. Kuskov, "Heterogenization of metalorganic catalysts of olefin polymerization and evaluation of active site non-uniformity", *Macromol. Symp.*, 2004, 213, 147–156.

[110] H. W. Kroto, J. R. Heath, S. C. O'Brien, R. F. Curl, R. E. Smalley, "C60: Buckminsterfullerene", *Nature*, 1985, 318, 162–163.

[111] S. Iijima, "Helical microtubules of graphitic carbon", *Nature*,1991, 354, 56–58.

[112] A. K. Geim, K. S. Novoselov, "The rise of graphene", *Nat. Mater.*, 2007, 6, 183–191.

[113] K. S. Novoselov, A. K. Geim, S. V. Morozov, D. Jiang, Y. Zhang, S. V. Dubonos, I. V. Grigorieva, A. A. Firsov, "Electric Field Effect in Atomically Thin Carbon Films", *Science*, 204, 306, 666–669.

[114] A. H. Castro Neto, N. M. R. Peres, K. S. Novoselov, A. K. Geim, "The electronic properties of graphene", *Rev. Mod. Phys.*, 2009, 81, 109–162.

[115] S. Iijima, T. Ichihashi, "Single-shell carbon nanotubes of 1-nm diameter", *Nature*, 1993, 363, 603–605.

[116] E. W. McQueen, J. I. Goldsmith, "Electrochemical Analysis of Single-Walled Carbon Nanotubes Functionalized with Pyrene-Pendant Transition Metal Complexes", *J. Am. Chem. Soc.*, 2009, 131, 17554–17556.

[117] P. M. Ajayan, "Nanotubes from Carbon", *Chem. Rev.*, 1999, 99, 1787–1800.

[118] J. Carlsson, M. Scheffler, "Structural, Electronic, and Chemical Properties of Nanoporous Carbon", *Phys. Rev. Lett.*, 2006, PRL 96, 046806.

[119] H. Dai, “Carbon Nanotubes: Synthesis, Integration, and Properties”, *Acc. Chem. Res.*, 2002, 35, 1035–1044.

[120] E. T. Thostenson, Z. Ren, T.-W. Chou, “Advances in the science and technology of carbon nanotubes and their composites: a review”, *Compos. Sci. Technol.*, 2001, 61, 1899–1912.

[121] J. Kong, N. R. Franklin, C. Zhou, M. G. Chapline, S. Peng, K. Cho, H. Dai, “Nanotube Molecular Wires as Chemical Sensors”, *Science*, 2000, 287, 622–625.

[122] P. Kim, C. M. Lieber, “Nanotube Nanotweezers”, *Science*, 1999, 286, 2148–2150.

[123] R. H. Baughman, “Carbon Nanotubes--the Route Toward Applications”, *Science*, 2002, 297, 787–792.

[124] L. Cui, J. Yu, Y. Lv, G. Li, S. Zhou, “Doped polyaniline/multiwalled carbon nanotube composites: Preparation and characterization”, *Polym. Compos.*, 2013, 34, 1119–1125.

[125] Y. Zeng, P. Liu, L. Zhao, J. Du, C. Liu, “High electrical sensitivity of polyurethane/carbon nanotube composites to tensile strain”, *Carbon*, 2013, 60, 562.

[126] D. Qian, E. C. Dickey, R. Andrews, T. Rantell, “Load transfer and deformation mechanisms in carbon nanotube-polystyrene composites”, *Appl. Phys. Lett.*, 2000, 76, 2868.

[127] R. Rosen, W. Simendinger, C. Debbault, H. Shimoda, L. Fleming, B. Stoner, O. Zhou, “Application of carbon nanotubes as electrodes in gas discharge tubes”, *Appl. Phys. Lett.*, 2000, 76, 1668.

[128] Y. Ye, C. C. Ahn, C. Witham, B. Fultz, J. Liu, A. G. Rinzler, D. Colbert, K. A. Smith, R. E. Smalley, “Hydrogen adsorption and cohesive energy of single-walled carbon nanotubes”, *Appl. Phys. Lett.*, 1999, 74, 2307.

[129] Y. Chen, D. T. Shaw, X. D. Bai, E. G. Wang, C. Lund, W. M. Lu, D. D. L. Chung, “Hydrogen storage in aligned carbon nanotubes”, *Appl. Phys. Lett.*, 2001, 78, 2128.

[130] A. C. Dillon, M. J. Heben, “Hydrogen storage using carbon adsorbents: past, present and future”, *Appl. Phys. A*, 2001, 72, 133–142.

[131] H. Sugie, M. Tanemura, V. Filip, K. Iwata, K. Takahashi, F. Okuyama, “Carbon nanotubes as electron source in an x-ray tube”, *Appl. Phys. Lett.*, 2001, 78, 2578.

[132] Y. Saito, S. Uemura, “Field emission from carbon nanotubes and its application to electron sources”, *Carbon*, 2000, 38, 169–182.

[133] K. Shakesheff “Nanotechnology for electronic materials and devices”, *Mater. Today*, 2006, 9, 63.

[134] N. Jafariesfad, S. A. Ramazani, B. Azinfar, “Property investigation of polypropylene/multiwall carbon nanotube nanocomposites prepared *via* in situ polymerization”, *Polym. Int.*, 2013, n/a–n/a. DOI: 10.1002/pi.4570

[135] M. Moniruzzaman, K. I. Winey, “Polymer Nanocomposites Containing Carbon Nanotubes”, *Macromolecules*, 2006, 39, 5194–5205.

[136] M. Alexandre, E. Martin, P. Dubois, M. G. Marti, R. Jérôme, “Polymerization-Filling Technique: An Efficient Way To Improve the Mechanical Properties of Polyethylene Composites”, *Chem. Mater.*, 2001, 13, 236–237.

[137] W. Lu, N. Li, W. Chen, Y. Yao, “The role of multiwalled carbon nanotubes in enhancing the catalytic activity of cobalt tetraaminophthalocyanine for oxidation of conjugated dyes”, *Carbon*, 2009, 47, 3337–3345.

[138] P. D. Tran, A. Le Goff, J. Heidkamp, B. Jousselme, N. Guillet, S. Palacin, H. Dau, M. Fontecave, V. Artero, “Noncovalent Modification of Carbon Nanotubes with

Pyrene-Functionalized Nickel Complexes: Carbon Monoxide Tolerant Catalysts for Hydrogen Evolution and Uptake", *Angew. Chem. Int. Ed.*, 2011, 50, 1371–1374.

[139] G. Liu, B. Wu, J. Zhang, X. Wang, M. Shao, J. Wang, "Controlled Reversible Immobilization of Ru Carbene on Single-Walled Carbon Nanotubes: A New Strategy for Green Catalytic Systems Based on a Solvent Effect on π–π Interaction", *Inorg. Chem.*, 2009, 48, 2383–2390.

[140] F. J. Gómez, R. J. Chen, D. Wang, R. M. Waymouth, H. Dai, "Ring opening metathesis polymerization on non-covalently functionalized single-walled carbon nanotubes", *Chem. Commun.*, 2003, 2, 190–191.

[141] Y. Sánchez, C. Albano, A. Karam, R. Perera, E. Casas, "In situ Polymerization of Nanocomposites by $TpTiCl_2(Et)$ System: UHMWPE Filled with Carbon Nanotubes", *Macromol. Symp.*, 2009, 282, 185–191.

[142] M. J. Go, S. H. Kim, K. M. Lee, H. H. Lee, H.-R. Park, J. Lee, S. Park, I. S. Choi, Y. Kim, "*In-situ* generation of a well-dispersed multiwall carbon nanotube/syndiotactic polystyrene composite using pentamethylcyclopentadienyltitanium trimethoxide anchored to multiwall carbon nanotubes", *Polymer*, 2012, 53, 933–938.

[143] S. Bredeau, L. Boggioni, F. Bertini, I. Tritto, F. Monteverde, M. Alexandre, P. Dubois, "Ethylene–Norbornene Copolymerization by Carbon Nanotube-Supported Metallocene Catalysis: Generation of High-Performance Polyolefinic Nanocomposites", *Macromol. Rapid Commun.*, 2007, 28, 822–827.

[144] S. Park, S. W. Yoon, H. Choi, J. S. Lee, W. K. Cho, J. Kim, H. J. Park, W. S. Yun, C. H. Choi, Y. Do, I. S. Choi, "Pristine Multiwalled Carbon Nanotube/Polyethylene Nanocomposites by Immobilized Catalysts", *Chem. Mater.*, 2008, 20, 4588–4594.

[145] S. Li, H. Chen, D. Cui, J. Li, Z. Zhang, Y. Wang, T. Tang, “Structure and properties of multi-walled carbon nanotubes/polyethylene nanocomposites synthesized by in situ polymerization with supported Cp_2ZrCl_2 catalyst”, *Polym. Compos.*, 2010, 31, 507–515.

[146] D. Bonduel, M. Mainil, M. Alexandre, F. Monteverde, P. Dubois, “Supported coordination polymerization: a unique way to potent polyolefin carbon nanotube nanocomposites”, *Chem. Commun.*, 205, 6, 781–783.

[147] K. Wiemann, W. Kaminsky, F. H. Gojny, K. Schulte, “Synthesis and Properties of Syndiotactic Poly(propylene)/Carbon Nanofiber and Nanotube Composites Prepared by in situ Polymerization with Metallocene/MAO Catalysts”, *Macromol. Chem. Phys.*, 2005, 206, 1472–1478.

[148] W. Kaminsky, A. Funck, H. Hähnsen, “New application for metallocene catalysts in olefin polymerization”, *Dalton Trans.*, 2009, 41, 8803.

[149] S. Tangestaninejad, M. Moghadam, V. Mirkhani, I. Mohammadpoor-Baltork, M. S. Saeedi, “Efficient epoxidation of alkenes with sodium periodate catalyzed by reusable manganese(III) salophen supported on multi-wall carbon nanotubes”, *Appl. Catal. Gen.*, 2010, 381, 233–241.

[150] G. S. Machado, K. A. D. de Freitas Castro, F. Wypych, S. Nakagaki, “Immobilization of metalloporphyrins into nanotubes of natural halloysite toward selective catalysts for oxidation reactions”, *J. Mol. Catal. Chem.*, 2008, 283, 99–107.

[151] C. Vriamont, M. Devillers, O. Riant, S. Hermans, “Catalysis with Gold Complexes Immobilised on Carbon Nanotubes by π–π Stacking Interactions: Heterogeneous Catalysis versus the Boomerang Effect”, *Chem. Eur. J.*, 2013, 19, 12009–12017.

[152] D. Didier, E. Schulz, “π-Stacking interactions at the service of

[Cu]-bis(oxazoline) recycling", *Tetrahedron Asymmetry*, 2013, 24, 769–775.

[153] L. M. Ombaka, P. Ndungu, V. O. Nyamori, "Usage of carbon nanotubes as platinum and nickel catalyst support in dehydrogenation reactions", *Catal. Today,* 2013, 217, 65–75.

[154] S. Park, S. W. Yoon, K.-B. Lee, D. J. Kim, Y. H. Jung, Y. Do, H. Paik, I. S. Choi, "Carbon Nanotubes as a Ligand in Cp_2ZrCl_2-Based Ethylene Polymerization", *Macromol. Rapid Commun.*, 2006, 27, 47–50.

[155] Z. Yinghuai, S. L. P. Sia, K. Carpenter, F. Kooli, R. A. Kemp, "Syntheses and catalytic activities of single-wall carbon nanotubes-supported nickel (II) metallacarboranes for olefin polymerization", *J. Phys. Chem. Solids*, 2006, 67, 1218–1222.

[156] L. Qu, L. M. Veca, Y. Lin, A. Kitaygorodskiy, B. Chen, A. M. McCall, J. W. Connell, Y.-P. Sun, "Soluble Nylon-Functionalized Carbon Nanotubes from Anionic Ring-Opening Polymerization from Nanotube Surface", *Macromolecules*, 2005, 38, 10328–10331.

[157] J. Chen, M. A. Hamon, H. Hu, Y. Chen, A. M. Rao, P. C. Eklund, R. C. Haddon, "Solution Properties of Single-Walled Carbon Nanotubes", *Science*, 1998 282, 95–98.

[158] S. Banerjee, S. S. Wong, "Synthesis and Characterization of Carbon Nanotube−Nanocrystal Heterostructures", *Nano Lett.*, 2002, 2, 195–200.

[159] H. Kargar, M. Moghadam, V. Mirkhani, S. Tangestaninejad, I. Mohammadpoor-Baltork, S. Rezaei, "Multi-wall carbon nanotube supported manganese(III) porphyrin: an efficient and reusable catalyst for oxidation of 2-imidazolines with sodium periodate", *Transit. Met. Chem.*, 2013, 38, 1–5.

[160] X. Wang, H. Liu, L. Qiu, "Cationic polymerization of tetrahydrofuran from

multiple-walled carbon nanotubes: Preparation and glass transition kinetics", *Mater. Lett.*, 2007, 61, 2350–2353.

[161] M. Salavati-Niasari, M. Bazarganipour, "Synthesis, characterization and catalytic oxidation properties of multi-wall carbon nanotubes with a covalently attached copper(II) salen complex", *Appl. Surf. Sci.*, 2009, 255, 7610–7617.

[162] Y. Liu, A. Adronov, "Preparation and Utilization of Catalyst-Functionalized Single-Walled Carbon Nanotubes for Ring-Opening Metathesis Polymerization", *Macromolecules*, 2004, 37, 4755–4760.

[163] A. A. Koval'chuk, A. N. Shchegolikhin, V. G. Shevchenko, P. M. Nedorezova, A. N. Klyamkina, A. M. Aladyshev, "Synthesis and Properties of Polypropylene/Multiwall Carbon Nanotube Composites", *Macromolecules*, 2008, 41, 3149–3156.

[164] A. Toti, G. Giambastiani, C. Bianchini, A. Meli, S. Bredeau, P. Dubois, D. Bonduel, M. Claes, "Tandem Action of Early−Late Transition Metal Catalysts for the Surface Coating of Multiwalled Carbon Nanotubes with Linear Low-Density Polyethylene", *Chem. Mater.*, 2008, 20, 3092–3098.

[165] X. Dong, L. Wang, L. Deng, J. Li, J. Huo, "Preparation of nano-polyethylene fibres using Cp_2ZrCl_2/carbon nanotube catalytic system", *Mater. Lett.*, 2007, 61, 3111–3115.

[166] A. Funck, W. Kaminsky, "Polypropylene carbon nanotube composites by in situ polymerization", *Compos. Sci. Technol.*, 2007, 67, 906–915.

[167] X. Dong, L. Wang, T. Sun, J. Zhou, Q. Yang, "Study on ethylene polymerization catalyzed by Cp_2ZrCl_2/carbon nanotube system", *J. Mol. Catal. Chem.*, 2006, 255, 10–15.

[168] X. Tong, C. Liu, H.-M. Cheng, H. Zhao, F. Yang, X. Zhang, "Surface

modification of single-walled carbon nanotubes with polyethylene *via* in situ Ziegler–Natta polymerization", *J. Appl. Polym. Sci.*, 2004, 92, 3697–3700.

[169] J. Feng, W. Cai, J. Sui, Z. Li, J. Wan, A. N. Chakoli, "Poly(l-lactide) brushes on magnetic multiwalled carbon nanotubes by *in-situ* ring-opening polymerization", *Polymer*, 2008, 49, 4989–4994.

[170] M. L. Shofner, V. N. Khabashesku, E. V. Barrera, "Processing and Mechanical Properties of Fluorinated Single-Wall Carbon Nanotube−Polyethylene Composites", *Chem. Mater.*, 2006, 18, 906–913.

[171] A. Schaetz, M. Zeltner, W. J. Stark, "Carbon Modifications and Surfaces for Catalytic Organic Transformations", *ACS Catal.*, 2012, 2, 1267–1284.

[172] F. D'Souza, A. S. D. Sandanayaka, O. Ito, "SWNT-Based Supramolecular Nanoarchitectures with Photosensitizing Donor and Acceptor Molecules", *J. Phys. Chem. Lett.*, 2010, 1, 2586–2593.

[173] F. Li, B. Zhang, X. Li, Y. Jiang, L. Chen, Y. Li, L. Sun, "Highly Efficient Oxidation of Water by a Molecular Catalyst Immobilized on Carbon Nanotubes", *Angew. Chem. Int. Ed.*, 2011, 50, 12276–12279.

[174] Z. Zhang, C. H. Turner, "Structural and Electronic Properties of Carbon Nanotubes and Graphenes Functionalized with Cyclopentadienyl–Transition Metal Complexes: A DFT Study", *J. Phys. Chem. C*, 2013, 117, 8758–8766.

[175] K. Elouarzaki, A. Le Goff, M. Holzinger, J. Thery, S. Cosnier, "Electrocatalytic Oxidation of Glucose by Rhodium Porphyrin-Functionalized MWCNT Electrodes: Application to a Fully Molecular Catalyst-Based Glucose/O_2 Fuel Cell", *J. Am. Chem. Soc.*, 2012, 134, 14078–14085.

[176] S. Banerjee, S. S. Wong, "Functionalization of Carbon Nanotubes with a Metal-Containing Molecular Complex", *Nano Lett.*, 2002, 2, 49–53.

[177] M. V. Escárcega-Bobadilla, L. Rodríguez-Pérez, E. Teuma, P. Serp, A. M. Masdeu-Bultó, M. Gómez, “Rhodium complexes containing chiral P-donor ligands as catalysts for asymmetric hydrogenation in non conventional media”, *Catal. Lett.*, 2011, 141, 808–816.

[178] F. Giroud, S. D. Minteer, “Anthracene-modified pyrenes immobilized on carbon nanotubes for direct electroreduction of O_2 by laccase”, *Electrochem. Commun.*, 2013, 34, 157–160,.

[179] N. Nakashima, “Solubilization of single-walled carbon nanotubes with condensed aromatic compounds”, *Sci. Technol. Adv. Mater.*, 2006, 7, 609.

[180] S. Wittmann, A. Schätz, R. N. Grass, W. J. Stark, O. Reiser, “A Recyclable Nanoparticle-Supported Palladium Catalyst for the Hydroxycarbonylation of Aryl Halides in Water”, *Angew. Chem. Int. Ed.*, 2010, 49, 1867–1870.

[181] B. Choi, J. Lee, S. Lee, J.-H. Ko, K.-S. Lee, J. Oh, J. Han, Y.-H. Kim, I. S. Choi, S. Park, “Generation of Ultra-High-Molecular-Weight Polyethylene from Metallocenes Immobilized onto N-Doped Graphene Nanoplatelets”, *Macromol. Rapid Commun.*, 2013, 34, 533–538.

[182] S. Park, I. S. Choi, “Production of Ultrahigh-Molecular-Weight Polyethylene/Pristine MWCNT Composites by Half-Titanocene Catalysts”, *Adv. Mater.*, 2009, 21, 902–905.

[183] K. Subramaniam, A. Das, D. Steinhauser, M. Klüppel, G. Heinrich, “Effect of ionic liquid on dielectric, mechanical and dynamic mechanical properties of multi-walled carbon nanotubes/polychloroprene rubber composites”, *Eur. Polym. J.*, 2011, 47, 2234–2243.

[184] K. Subramaniam, A. Das, G. Heinrich, “Development of conducting polychloroprene rubber using imidazolium based ionic liquid modified multi-walled

carbon nanotubes", *Compos. Sci. Technol.*, 2011, 71, 1441–1449.

[185] S. Bellayer, J. W. Gilman, N. Eidelman, S. Bourbigot, X. Flambard, D. M. Fox, H. C. De Long, P. C. Trulove, "Preparation of Homogeneously Dispersed Multiwalled Carbon Nanotube/Polystyrene Nanocomposites *via* Melt Extrusion Using Trialkyl Imidazolium Compatibilizer", *Adv. Funct. Mater.*, 20005, 15, 910–916.

[186] J. Wang, H. Chu, Y. Li, "Why Single-Walled Carbon Nanotubes Can Be Dispersed in Imidazolium-Based Ionic Liquids", *ACS Nano*, 2008, 2, 2540–2546.

[187] X.-F. Guo, J.-H. Kim, G.-J. Kim, "Dehydrogenation of ethylbenzene to styrene on a direct synthesized Co, Ni/carbon nanotubes catalysts", *Catal. Today*, 2011, 164, 336–340.

Chapter 2: Carbon nanotubes supported nickel catalysts *via* covalent bonds for ethylene polymerization

2.1 Introduction

In addition to the non-covalent approaches, functionalization of carbon nanotubes *via* covalent bond formation is a useful strategy. Due to their unique chemical and physical properties, the chemical modification of the carbon nanotubes *via* covalent bonds has been the subject of intense recent interest. Covalent functionalization can be realized by chemical modification of carboxylic acid group introduced on the carbon nanotubes by acidic treatment, typically using nitric acid. For instance, amide or ester linkage between the compound and the defect-derived carboxylic acid moiety on the carbon nanotube surface can be used to perform covalent anchoring [1-5]. Besides that, direct addition of reagents to the sidewalls of carbon nanotubes is also a possible alternative [6-8]. Polymeric nanocomposites were reported to be prepared by simply reacting butyllithium-functionalized carbon nanotubes with halogenated polymers [7].

Carboxylic groups are introduced by nitric acid oxidation that occurs first on the CH_n groups [9]. This means that the carboxylic groups are more easily produced at the sidewall, defected areas and the open ends of the carbon nanotubes [10]. Therefore, in order to get more coating sites, mechanical cutting of purified carbon nanotubes by ball-milling is necessary. In rational functionalization strategies used to modify carbon nanotubes using surface chemistry, oxygen containing functional groups are often subjected to chemical transformations; for example, -COOH groups are transformed to acid chlorides as a route to create aminated carbon nanotubes [4, 11]. Hence, organic compounds [1, 4], metal complexes [12], or particles [13] containing an NH_2 group can be covalently anchored to carbon nanotubes. In addition, the surface of carbon nanotubes used in reinforced polymer composites is often modified

covalently by the addition of polar functional groups, not only to improve dispersion properties but also to enhance chemical interactions with the resin matrix [2-4].

The covalent bond formed is irreversible and stronger than non-covalent interactions. The presence of the carbon nanotubes has a great effect on the electronic density of complexes. Carbon nanotubes which have an important steric bulkiness can act as a macro-ligand for the catalyst. In other words, the presence of the carbon nanotubes offers the possibility to tune, electronically and sterically, the reactivity of the grafted metal catalytic species.

Nickel complexes as olefin polymerization catalysts were firstly investigated in the 1980s [14-15], and were sublimated by Brookhart and Gibson in the 1990s [16-17]. From then on, nickel-based ethylene polymerization catalysts have been synthesized by varying the ligand surrounding the nickel center [18-19]. Recently, a series of nickel catalysts have been supported on carbon nanotubes *via* covalent bond (C–N) and were investigated in catalytic polymerization [20]. To the best of our knowledge, this example is the only report up to date of late transition metal complex supported on CNTs for ethylene polymerization.

In this chapter, we describe the synthesis of a series of task-specific nickel(II) complexes containing an amino group. Those nickel complexes were immobilized on the surface of the MWCNTs *via* covalent amide bonds. It is clear that for those nickel complexes, both the steric and electronic environment are modified by the carbon nanotubes through direct interaction between the complexes and the CNTs surface. Our research focus is to explore the effect of the CNTs as macro-ligand in ethylene polymerization. The detailed catalytic results and the influence of CNTs on the activity are discussed below.

2.2 Results and discussions

2.2.1 Characterization of the nickel complexes Ni1–Ni4 and the supported catalyst

Nickel complexes (**Ni1**–**Ni4**) were synthesized in a one-step procedure with 5,6,7-trihydroquinolin-8-one, the corresponding anilines and $NiCl_2 \cdot 6H_2O$ in ethanol with a catalytic amount of acetic acid (Scheme 2.1). All complexes are obtained as yellow and stable solids. **Ni1**–**Ni4** show in the IR spectra, strong bands in the range 1593−1599 cm^{-1} region, that can be ascribed to the stretching vibration of C=N. An amino group is introduced into those nickel complexes, in order to carry out their covalent immobilization on the MWCNTs surface.

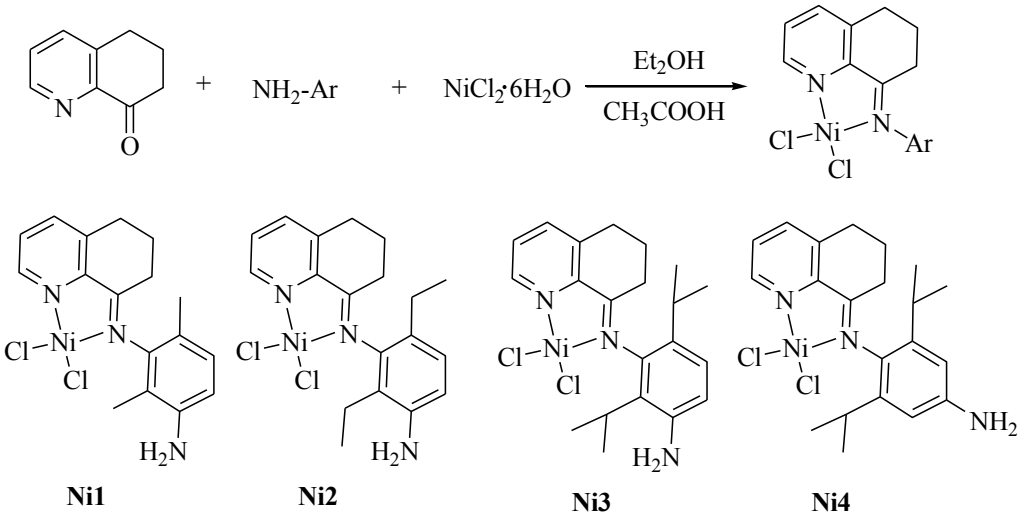

Scheme 2.1 Synthetic procedure of **Ni1**–**Ni4.**

Two kinds of MWCNTs (Figure 2.1) have been used in this study in order to compare their effect on the polymerization activity. The pristine multi-walled carbon nanotubes CNT_C were obtained from Cnano (97% purity) and multi-walled nanotubes

CNT_F (98% purity, 2% iron catalyst) were synthesized in our laboratory by chemical vapor deposition according to previously reported procedures [21].

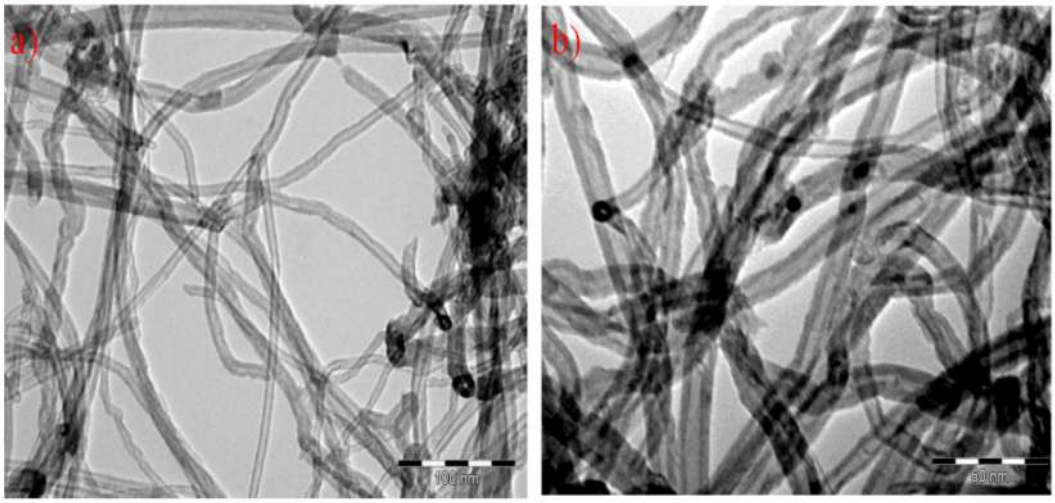

Figure 2.1 TEM micrographs of pristine (a) CNT_F and (b) CNT_C.

The textural properties of those MWCNTs are summarized in Table 2.1.

Table 2.1 Textural properties of CNTs.

Samples	BET (m^2/g)	Mean pore diameter (nm)	I_D/I_G [a]	d_{ex} (nm) [b]	d_{in} (nm) [c]
CNT_C	200	-	1.57	10	5
CNT_F	180	13	1.27	14	7

[a] Determined by Raman spectroscopy; [b] external diameter from TEM; [c] inner diameter from TEM.

Before grafting the nickel complexes on the surface of CNTs through an amide link, it is necessary to fonctionalize the CNT surface with nitric acid at 120 °C for 3h to produce carboxylic acid functions (Scheme 2.2). The functionalized samples were named CNT_{C1} and CNT_{F1}.

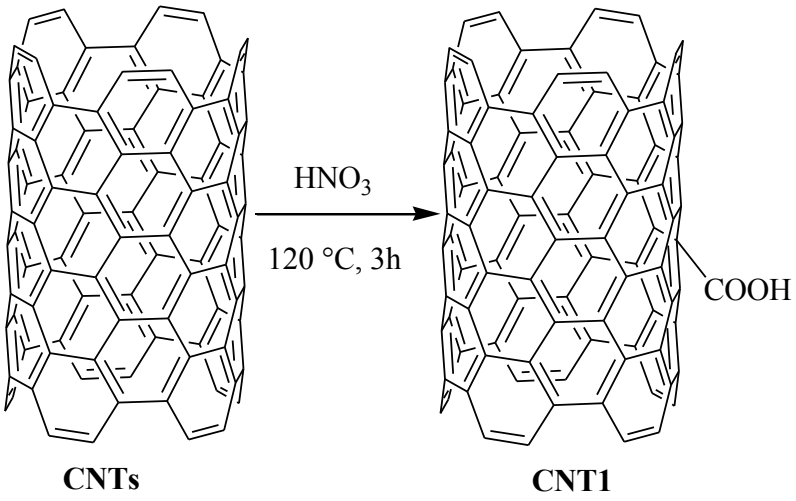

Scheme 2.2 Functionalization the MWCNTs.

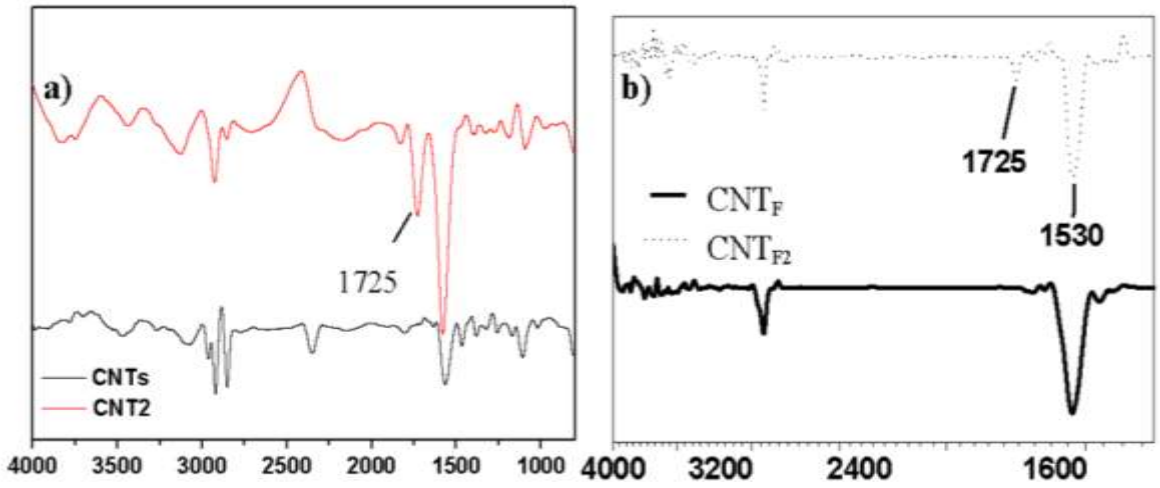

Figure 2.2 IR spectra of the pristine CNTs and the functionalized CNT2: a) CNT_C and b) CNT_F.

Pristine and functionalized CNTs were characterized by infrared spectroscopy. Compared with the pristine nanotubes, an additional peak at 1725 cm^{-1} is observed in the spectra of functionalized samples, which was assigned to the asymmetric CO stretching (ν_{asym}(C=O)) of the carboxylic groups (Figure 2.2). The functionalization was also confirmed by Raman spectroscopy. Due to the presence of sp^3 and sp^2 carbon on the carbon nanotube, the ratio I_D/I_G of the two kinds of CNTs changed from

1.57 (CNT_C) to 2.03 (CNT_{C1}) and 1.27 (CNT_F) to 1.58 (CNT_{F1}). The presence of a higher concentration of defects on CNT_C compared to CNT_F allows a higher degree of functionalization. This was confirmed by chemical titration of surface –COOH groups [22]. CNT_{C1} contains 0.1 mol COOH/g_C, while CNT_{F1} contain 0.01 mol COOH/g_C.

An additional functionalization was performed using thionyl chloride in order to produce the acetyl chloride groups on the surface of the CNTs (Scheme 2.3). Acetyl chloride groups being easily hydrolyzed, acylation of the CNTs must be accomplished under inert atmosphere. The supported catalysts **Ni1**–**Ni4/CNT** were produced by mixing the nickel complexes with the above functionalizated CNTs containing the acetyl chloride groups. The weight percent of those anchored homogeneous nickel complexes were determined by ICP-MS and the results are collected in Table 2.2. 0.08%- 0.26% nickel complexes have been respectively grafted onto the CNT surface. Moreover, the Ni weight percent of the CNT_C supported catalysts are slightly higher than CNT_F supported catalysts, in accordance with a higher concentration defects.

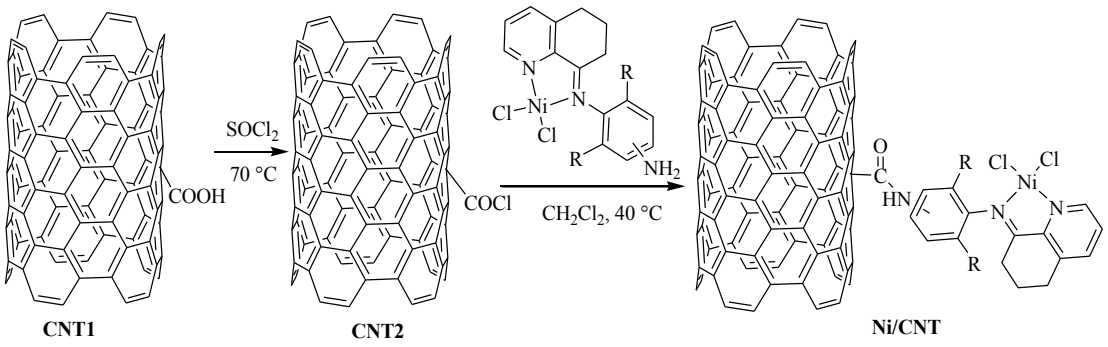

Scheme 2.3 Synthetic procedure for CNT-supported nickel complexes.

These supported catalysts have also been analyzed by X-ray photoelectron spectroscopy (XPS). Results obtained for **Ni1/CNT_C** as a typical example are shown in Figure 2.3. The peak around 400.1 eV can be attributed to the N (1s). Moreover,

peaks at 199.5 and 855.7 eV are observed as signals characteristics of the Cl (2p) and Ni (2p) respectively. The peak observed at 855.7 eV corresponds to the typical Ni^{2+} (2p) binding energy signal. This means that the ligand as well as the $NiCl_2$ fragment are present on the surface of CNTs. In other words, XPS analysis shows the presence of the nickel$^{(II)}$ complexes on the surface of the CNTs and no Ni^0 is observed, evidencing that efficient anchoring of the complexes was achieved without precatalyst decomposition.

Table 2.2 ICP-MS results for CNT_F and CNT_C supported Ni catalysts

Support	Complex	Sample	Ni (mg/kg)	Ni[a] (μmol)
CNT_F	**Ni1**	**Ni_1/CNT_F**	828.45	1.41
	Ni2	**Ni_2/CNT_F**	1 367.37	2.33
	Ni3	**Ni_3/CNT_F**	1 366.12	2.32
	Ni4	**Ni_4/CNT_F**	1 642.71	2.80
CNT_C	**Ni1**	**Ni_1/CNT_C**	2 118.10	3.61
	Ni2	**Ni_2/CNT_C**	2 567.07	4.37
	Ni3	**Ni_3/CNT_C**	1 898.58	3.23
	Ni4	**Ni_4/CNT_C**	1 855.79	3.16

[a] μmol of Ni in 100 mg of sample

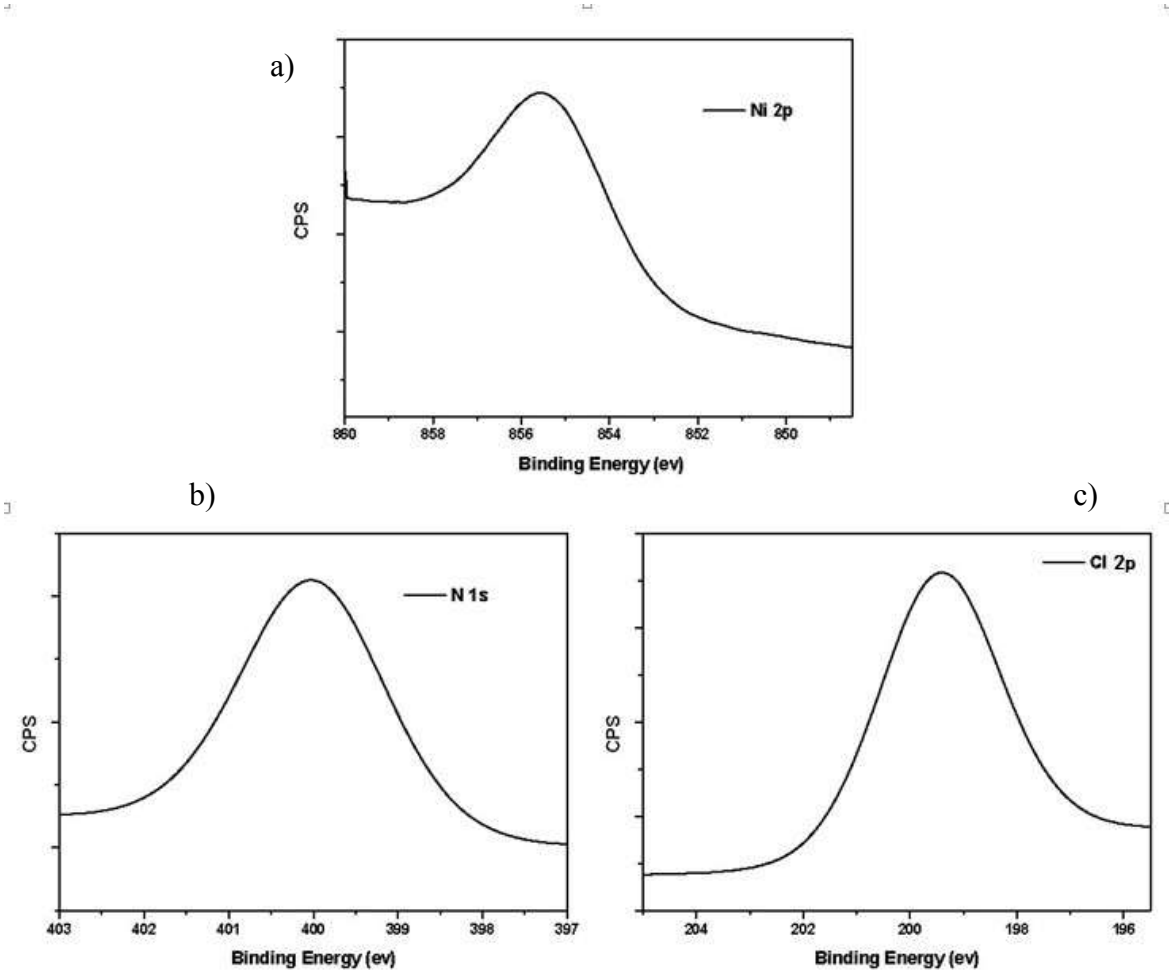

Figure 2.3 XPS spectra of the $\mathbf{Ni_1/CNT_C}$: a) Ni 2p, b) N 1s and c) Cl 2p.

2.2.2 Ethylene polymerization catalyzed by the nickel complexes and CNT-supported nickel complexes

2.2.2.1 Polymerization with nickel complexes Ni1–Ni4

Prior to the study of the catalytic behavior of the supported nickel complexes, we carried out an investigation of their behavior under homogeneous conditions and an optimization of the reaction conditions. Under 10 atm ethylene pressure, the influence of various alkylaluminums such as MAO, MMAO, diethylaluminum chloride (Et_2AlCl) and ethylaluminum sesquichloride (EASC) was evaluated on activation of

Ni3 (Table 2.3). This activator screening evidenced MAO as the best choice for this precatalyst (Table 2.3, Entries 1–4).

Table 2.3 Ethylene polymerization with **Ni3** and different co-catalyst [a]

Entry	Co-Cat.	Al/Ni	Prod. (g)	Activity[b]	T_m [c] (ºC)	M_w [d] (g mol^{-1})	M_w/M_n [d]
1	MMAO	1000	Traces	-	-	-	-
2	MAO	1000	1.9	0.8	114.1	8 117	4.0
3	Et_2AlCl	200	Traces	-	-	-	-
4	EASC	200	Traces	-	-	-	-

[a] Reaction conditions: 5 μmol **Ni3**; 10 atm ethylene; 20 ºC; 30 min; 100 mL toluene. [b] 10^6 g (PE)·mol^{-1}(Ni)·h^{-1}. [c] Determined by DSC. [d] Determined by GPC.

The influence of reaction parameters such as Al/Ni molar ratio as well as reaction temperature on ethylene polymerization activity was investigated using MAO as co-catalyst. Detailed data are collected in Table 2.4. Upon increasing of the Al/Ni ratio from 1000 to 1500, the polymerization rate was increased, and then the activity decreases when the ratio Al/Ni > 1500. The optimum condition for the Al/Ni ratio is 1500, for which a maximum activity of 1.3 × 10^6 g (PE)·mol^{-1}(Ni)·h^{-1} is reached (Table 2.4, Entry 3). The reaction temperature is also an important factor for the catalytic reaction. When the reaction temperature is increased from 20 ºC to 30 ºC (Table 2.4, Entries 3 *vs* 6), the catalytic activity shows a slight decrease. Moreover, an incerase of the temperature up to 50 ºC leads to a clear decrease of the catalytic activity (Table 2.4, Entry 7). This is partly because higher reaction temperatures are detrimental to the stability of the active species. At the same time, the molecular

weight of the polymer that are produced at 30 ºC and 50 ºC are lower than that of the polyethylene obtained at 20 ºC. It is known that there is a relationship between the molecular weight and the life time of the active center, that is longer life time of the catalyst prefers to produce higher molecular weight polymer.

Table 2.4 Ethylene polymerization with **Ni3**/MAO system [a]

Entry	Al/Ni	T (ºC)	Prod. (g)	Activity[b]	T_m[c] (ºC)	M_w[d] (g mol^{-1})	M_w/M_n[d]
1	1000	20	1.9	0.8	114.1	8 117	4.0
2	1250	20	2.2	0.9	113.2	9 977	3.6
3	1500	20	3.3	1.3	116.7	9 934	3.8
4	1750	20	2.5	1.0	114.5	12 696	4.0
5	2000	20	1.6	0.6	113.1	11 152	4.1
6	1500	30	2.2	0.9	119.8	4 094	2.8
7	1500	50	0.5	0.2	120.1	5 596	3.9

[a] Reaction conditions: 5 μmol **Ni3**; 10 atm ethylene; MAO; 30 min; 100 mL toluene. [b] 10^6 g (PE)·mol^{-1}(Ni)·h^{-1}. [c] Determined by DSC. [d] Determined by GPC.

In addition, the branch information of two representative polyethylenes (Table 2.4, Entries 3 and 6) were confirmed by ^{13}C NMR (Figure 2.4) using $CDCl_3$ as solvent. The number of branches was calculated according to a literature method [23]. The numbers of branches is 43/1000 C at 20 ºC. Compared to literature reports, the branch number is slightly higher than that obtained with other nickel complexes bearing 5,6,7-dihydroquinoline-based ligand [24], but lower than nickel complexes bearing 2-iminopyridine [25-26]. Generally, an increase of the temperature results in a faster

chain walking, leading to a higher branching [27-30]. The opposite trend is observed with the systems reported here since the branching number decreases to 32/1000 C when the reaction is carried out at 30 ºC.

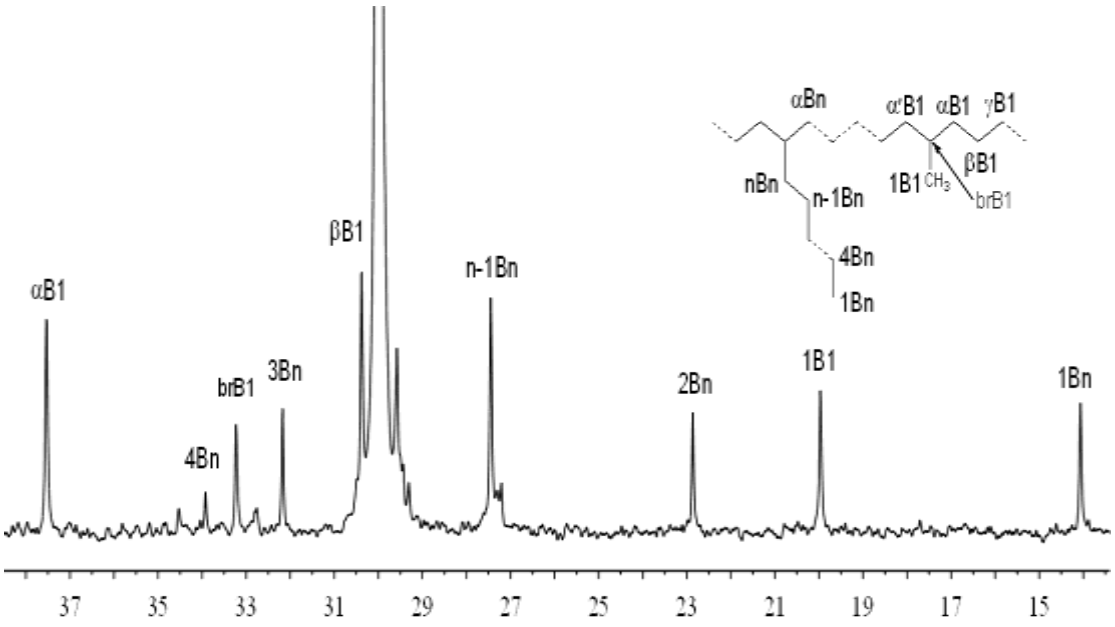

Figure 2.4 ^{13}C-NMR spectrum of polyethylene prepared using **Ni3**/MAO at 20 °C (Table 2.4, Entry 3).

The other nickel complexes were then investigated at 20 ºC in the presence of MAO with an Al/Ni ratio of 1500. As shown in Table 2.5, the activity of those nickel complexes decreases in the order is **Ni3**>**Ni2**>**Ni1**. This means that the larger steric hindrance on the ligand has a slight positive effect on the polymerization activity. Such tendency is similar with that observed for other nickel complexes [18, 24].

Moreover, the molecular weight of the polymer produced by **Ni3** is higher that the polymer produced by **Ni2** and **Ni1**. According to reports from the literature, large bulky alkyl substituents help to solubilize the pre-catalysts thereby enhancing the activity. In addition, bulky substituents group increase catalyst lifetime and yield high molecular weight polyethylene [29]. The additional amino group has also an influence of the catalytic activity. Compared to previously reported nickel complexes [18-19]

also based on the 5,6,7-trihydroquinolin-8-one ligand framework, those title complexes perform ethylene polymerization with lower activity.

A significant influence of the amino-group position is also observed by comparing the activities obtained using complexes **Ni3** (Table 2.5, Entry 3) and **Ni4** (Table 2.5, Entry 4) containing the di-isopropyl group. The catalyst containing the amino-substituent in the *para*-position of the *N*-aryl group showed lower activity than the catalyst bearing the ligand where the $-NH_2$ group occupies the *meta*-position of the *N*-aryl group. Catalyst **Ni4** shows low activity which is just ten percent of the **Ni3**. It is clear that the position of the $-NH_2$ group on the aryl ring affects the activity of ethylene polymerization.

Table 2.5 Ethylene polymerization with **Ni1**–**Ni4**/MAO system [a]

Entry	Cat.	Prod. (g)	Activity[b]	T_m[c] (ºC)	M_w[d] (g mol^{-1})	M_w/M_n[d]
1	**Ni1**	2.1	0.8	121.6	1 662	1.9
2	**Ni2**	2.7	1.1	118.8	2 819	2.5
3	**Ni3**	3.3	1.3	116.7	9 934	3.8
4	**Ni4**	0.2	0.1	120.6	1 086	1.4

[a] Reaction conditions: 5 μmol; 20 ºC; 10 atm ethylene; MAO; Al/Ni = 1500 ; 30 min; 100 mL toluene. [b] 10^6 g (PE)·mol^{-1}(Ni)·h^{-1}. [c] Determined by DSC. [d] Determined by GPC.

2.2.2.2 Heterogeneous ethylene polymerization

As mentioned above, two kinds of MWCNTs have been used as support to support nickel complexes **Ni1**–**Ni4**. Therefore, the polymerization results obtained

using those heterogeneous catalysts are divided two parts, **Ni1–4**/CNT_F and **Ni1–4**/CNT_C. Those complexes being immobilized on the surface of CNTs *via* covalent (C–N) bonds, the following discussion is to explore the effect of CNTs as macro-ligands in polymerization.

2.2.2.2.1 Ethylene activation by the ***Ni1-4/CNT$_F$***

As shown in Table 2.6, all of the **Ni /CNT$_F$** catalysts have been investigated in ethylene polymerization with the MAO as co-catalyst at 20 °C and under an ethylene pressure of 10 atm. Different amounts of MAO were used to activate the **Ni1/CNT$_F$** catalysts (Al/Ni = 3500 and 1500). However, there is no significant change for the polymerization activities using different Al/Ni ratios (Table 2.6, Entry 1 *vs* 2).

Compared to its corresponding homogeneous precatalyst **Ni1**, the **Ni1/CNT$_F$** system displays higher activity, up to 6.52×10^6 g (PE)·mol^{-1}(Ni)·h^{-1}. Therefore, CNT_F have a positive influence on the catalytic performances of **Ni1**. In addition, the molecular weight and the molecular weight distribution of the polymer produced by **Ni1/CNT$_F$** are higher than that produced by **Ni1**. This phenomenon was also reported in some literature articles which are about the early transition metal catalysts immobilized on CNTs [31-34]. One example described by Choi *et al*. that the molecular weight is increased more than ten-fold just because the half-titanocene catalysts are supported on MWCNTs [32]. This can also be attributed to an enhanced stability of the catalytic active species due to the presence of CNTs as macro-ligand.

Table 2.6 Ethylene polymerization by CNT_F supported catalysts[a]

Entry	Sample	Ni (μmol)	Al/Ni	Polymer (g)	Activity[b]	T_m[c] (ºC)	M_w[d] (g mol^{-1})	M_w/M_n[d]
1	**Ni1/CNT$_F$**	1.41	3500	4.4	6.24	121.6	3 669	3.2
2	**Ni1/CNT$_F$**	1.41	1500	4.6	6.52	120.8	4 233	3.7
3	**Ni2/CNT$_F$**	2.33	3500	3.3	2.83	119.4	3 890	3.5
4	**Ni2/CNT$_F$**	2.33	1500	1.8	1.55	120.5	6 135	4.8
5	**Ni3/CNT$_F$**	2.32	3500	7.5	6.47	121.9	15 295	4.2
6	**Ni3/CNT$_F$**	2.32	1500	6.9	5.95	121.0	13 759	3.1
7	**Ni4/CNT$_F$**	2.80	3500	0.1	0.07	125.9	5 651	3.9
8	**Ni4/CNT$_F$**	2.80	1500	0.4	0.29	123.5	4 011	3.1

[a] Reaction conditions: MAO, 10 atm ethylene; 20 °C ; 30 min; 100 mL toluene, 100 mg support catalyst. [b] 10^6 g (PE)·mol^{-1}(Ni)·h^{-1}. [c] Determined by DSC. [d] Determined by GPC.

Concerning the **Ni2/CNT$_F$**/MAO system (Table 2.6, Entries 3 and 4), upon increasing the Al/Ni ratio from 1500 to 3000, and unlike what was observed for **Ni1/CNT$_F$**/MAO, activity was also doubled (form 1.55 to 2.83 × 10^6 g (PE)·mol^{-1}(Ni)·h^{-1}). Compared to the **Ni2** unsupported system, **Ni2/CNT$_F$** shows higher activity. Moreover, the molecular weight of the polymer produced by the **Ni2/CNT$_F$** is higher than its corresponding homogeneous catalyst **Ni2**, evidencing a positive influence of the presence of the CNT_F on the catalytic activity as well as the polymer's molecular weight.

As observed for **Ni1–2/CNT$_F$**, either at Al/Ni = 1500 (Table 2.6, Entry 5) or

Al/Ni = 3500 (Table 2.6, Entry 6), high activities are obtained using the **Ni3/CNT$_F$**/MAO catalytic system. The activity of 6.47×10^6 g (PE)·mol^{-1}(Ni)·h^{-1} is higher than that of its corresponding homogeneous catalyst **Ni3**. Moreover, the molecular weight increased up to 15 295 g mol^{-1} due to the presence of the CNT$_F$. The representative polyethylene obtained using **Ni3/CNT$_F$** (Table 2.6, Entry 5) was characterized by ^{13}C NMR measurements, and showed 44 branches/1000 carbons (Figure 2.5) according to the interpretation reported by Galland *et al* [23]. Compared to its corresponding homogeneous counterpart **Ni3**, 10 branches more for 1000 carbons are shown in ^{13}C NMR spectra of **Ni3/CNT$_F$**.

The polymerization takes place close to the CNTs surface, due to the covalent bond between the nanotubes and the immobilized catalyst. Therefore it is likely that the polymer chain grows directly from the nanotube surface leading to coverage around CNTs during the polymerization process. The polymer samples produced by the **Ni3/CNT$_F$** catalyst have been characterized by scanning electron microscopy (SEM). As shown in Figure 2.6, the CNT$_F$ are homogeneously dispersed inside of the polymer matrix. Moreover, the diameter of the CNT$_F$ is about 14 nm and the diameter of the CNT$_F$ dispersed into the polymer is about 54 nm. So, it is clear that the CNT$_F$ is completely covered by the polymer layer after the coating process.

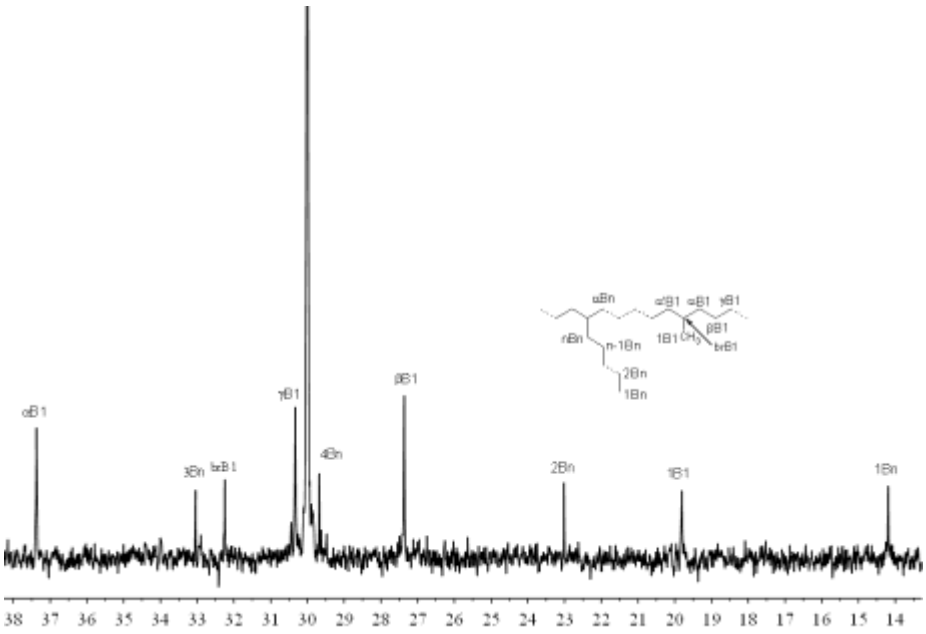

Figure 2.5 ^{13}C NMR spectrum of polyethylene prepared by system **Ni3/CNT$_F$** (Table 2.6, Entry 5).

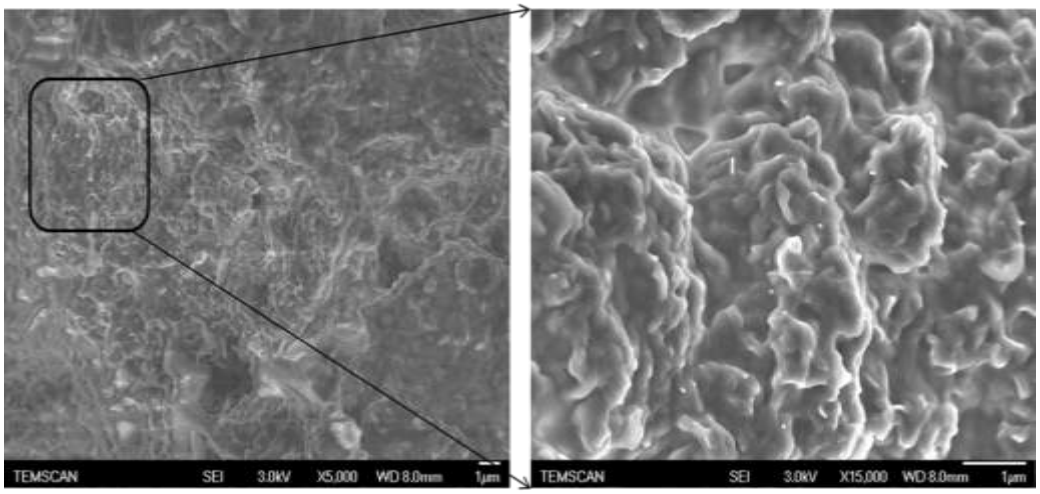

Figure 2.6 SEM micrographs for the CNT/Polymer sample produced by **Ni3/CNT$_F$** (Table 2.6, Entry 6).

Unlike for the other nickel catalysts, comparison of the performances of the **Ni4/CNT$_F$** system (Table 2.6, Entry 7–8) with the **Ni4** (Table 2.5, Entry 4) evidenced that the presence of the CNT$_F$ has a negative influence on the activity. However, the immobilized catalyst produced polymeric chains of higher molecular weight than the

polymer produced by **Ni4**.

*2.2.2.2.2 Ethylene activation by the **Ni1–4/CNT$_C$***

The catalysts **Ni1–4/CNT$_C$** were also investigated in polymerization using the MAO as the co-catalyst. **Ni1/CNT$_C$** and **Ni2/CNT$_C$** shown higher activity at lower Al/Ni ratio (Al/Ni = 1500, Table 2.7, Entries 2, 4) than at higher ratio (Al/Ni = 3500, Table 2.7, Entries 1, 3). Using CNT$_C$ as support, the activities of the immobilized catalysts **Ni1/CNT$_C$** and **Ni2/CNT$_C$** are higher than that of their corresponding homogeneous catalysts (increase respectively from 0.8 to 2.16 × 10^6 g (PE)·mol^{-1}(Ni)·h^{-1} for **Ni1** and **Ni1/CNT$_C$** and 1.1 to 2.61 × 10^6 g (PE)·mol^{-1}(Ni)·h^{-1} for **Ni2** and **Ni2/CNT$_C$**). Moreover, high molecular weight and the high molecular weight distribution polymers are produced by those immobilized catalysts.

Unlike for **Ni1/CNT$_C$** and **Ni2/CNT$_C$**, the activity of the **Ni3/CNT$_C$** is similar to that of the corresponding **Ni3** unsupported catalyst. Moreover, considering the polymer properties, the molecular weight of the polymer produced by **Ni3/CNT$_C$** is lower than that produced by **Ni3** unlike what observed for the other immobilized catalysts described above. Similar with the **Ni4/CNT$_F$** system, the CNT$_C$ supported **Ni4** catalyst shown poor activity for the ethylene polymerization.

In summary, compared to the homogeneous catalysts (**Ni1**–**Ni3**), immobilized catalytic systems **Ni1**–**Ni3/CNT$_{(F\ or\ C)}$** shown higher activity. It is possible that thermal conductivity of the CNTs can be used to manage the exothermicity of the polymerization reaction and hence induce an increased stability of the active species. In addition, the activities increased from 2.16 (Table 2.7, Entry 2) to 6.52 (Table 2.6, Entry 2) (more than three-fold increase) for **Ni1/CNT** by only changing the support from CNT$_C$ to CNT$_F$. This can be also observed for the **Ni3/CNT$_{(F\ or\ C)}$** systems (Table

2.7, Entry 5, 6 and Table 2.6, Entry 5, 6). The reactive mechanism for those supported catalysts is not very clear; however, one can mentioned that the nature of the CNT supports has a great influence in polymerization. This could be due to a lower defect concentration of CNT_F, and thus to the higher electrical and thermal conductivity of those samples.

Table 2.7 Ethylene polymerization by CNT_C supported catalysts[a]

Entry	Sample	Ni (μmol)	Al/Ni	Polymer (g)	Activity[b]	T_m[c] (ºC)	M_w[d] (g mol^{-1})	M_w/M_n[d]
1	**Ni1/CNT$_C$**	3.61	3500	2.5	1.39	121.1	5 631	5.2
2	**Ni1/CNT$_C$**	3.61	1500	3.9	2.16	120.9	5 109	4.3
3	**Ni2/CNT$_C$**	4.37	3500	5.1	2.33	121.1	5 268	4.3
4	**Ni2/CNT$_C$**	4.37	1500	5.7	2.61	122.1	4 384	4.0
5	**Ni3/CNT$_C$**	3.23	3500	1.9	1.18	121.8	4 140	3.1
6	**Ni3/CNT$_C$**	3.23	1500	1.2	0.74	122.1	4 034	2.6
7	**Ni4/CNT$_C$**	3.16	3500	0.1	0.06	-	-	-
8	**Ni4/CNT$_C$**	3.16	1500	0.1	0.06	-	-	-

[a] Reaction conditions: MAO, 10 atm ethylene; 20 °C ; 30 min; 100 mL toluene, 100 mg support catalyst. [b] 10^6 g (PE)·mol^{-1}(Ni)·h^{-1}. [c] Determined by DSC. [d] Determined by GPC.

*2.2.2.2.3 Ethylene activation by the **Ni5***

Above all, the **Ni1–3/CNT$_F$** and **Ni1–3/CNT$_C$** show the highest activity increase compared to their conresponding homogeneous catalysts. An uncertainty should come

in mind concerning the factor responsible for the activity increase: the presence of the CNT or the disappearance of the NH_2 group. In oder to clarify this point, **Ni5** was synthesized by reacting **Ni3** with benzene chloride (Scheme 2.4).

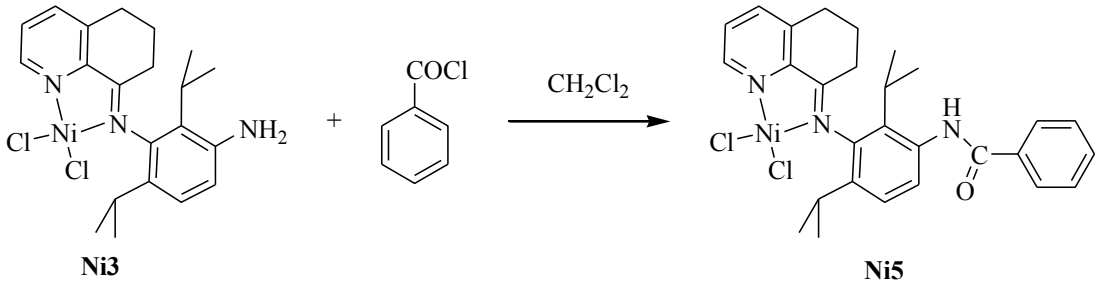

Scheme 2.4 Synthetic procedure of **Ni5**.

Using MAO as co-catalyst, the optimization of the reaction parameters was conducted with pre-catalyst **Ni5**, and the results are shown in Table 2.8. The polymerization reactions were conducted under different conditions by changing the Al/Ni ratio and the reaction temperature. The polymerization activities of **Ni5** are in the range of 0.92 to 6.04×10^5 g (PE)·mol^{-1}(Ni)·h^{-1}, which is lower than the above CNT supported catalyst and even lower than the homogeneous catalysts **Ni1**–**Ni3**. Up to this point, it is clear that the disappearance of the NH_2 group has no positive for the activity of catalyst **Ni3**. In other words, the presence of the CNT (CNT_C and CNT_F) as support for the homogeneous catalysts has a great influence on ethylene polymerization activity.

Table 2.8 Ethylene polymerization catalyzed by **Ni5**[a]

Entry	Al/Ni	T (°C)	Polymer (g)	Activity[b]
1	1500	20	0.77	3.08
2	2000	20	1.44	5.76
3	2500	20	1.51	6.04
4	3000	20	1.03	4.12
5	2500	30	1.20	4.80
6	2500	40	0.88	3.52
7	2500	50	0.23	0.92

[a] Reaction conditions: 5 μmol **Ni5**, 10 atm ethylene, 100 mL toluene, 30 min, MAO. [b] 10^6 g (PE)·mol^{-1}(Ni)·h^{-1}.

2.3 Conclusions

A family of nickel complexes (**Ni1**–**Ni4**) containing an -NH_2 function have been synthesized by a one-step procedure. Two kinds of multi-walled carbon nanotubes, CNT_F and CNT_C, are used to immobilize those homogeneous nickel complexes *via* covalent bonds. According to the ICP-MS results, the weight percent of those anchored homogeneous nickel complexes are in the range of 0.08%- 0.21%. In addition, the nickel complexes grafted on the CNTs have been characterized by XPS, evidencing the presence of Ni^{2+} species and no Ni^0 observed. Using MAO as co-catalyst, those homogeneous catalysts and supported catalysts have been investigated in the ethylene polymerization reaction. All of the homogeneous catalysts show moderate activity. Using CNTs as support, the activities of these immobilized catalysts are higher than those of the homogeneous systems. The activities of

precatalysts (**Ni1** and **Ni3**) increase remarkably with the CNT_F as the support, much more than with CNT_C. Moreover, the presence of the CNTs can also be efficient for increasing the molecular weight of the produced polymer. In addition, according to the SEM analysis, the CNTs are uniformly dispersed into the polymeric matrix, and completely covered by a polymer layer.

2.4 Experimental Section

2.4.1 Synthesis and characterization of nickel complexes

The nickel complexes (**Ni1**–**Ni4**) were prepared using a similar procedure. The typical complex **Ni1** was synthesized as follow: using acetic acid as catalyst, a mixture of 5,6,7-dihydroquinolin-8-one (3.0 mmol), 2,6-dimethylbenzene-1,3-diamine (3.0 mmol) and $NiCl_2·6H_2O$ (3.0 mmol) in ethanol (10 mL) was refluxed for 3 h. Ethanol was evaporated under reduced pressure, and the residue was dissolved in 10 mL of dichloromethane. Unreacted $NiCl_2$ was removed by filtration. 50 mL of diethyl ether was added to precipitate the complex **Ni1**. After filtration and washing with diethyl ether under N_2, the collected solid was dried under vacuum. The yellow powder was obtained in 62.7% yield. IR (KBr; cm^{-1}): 2864, 1597 (υ C=N), 1458, 1422, 1283, 1208, 1130, 1208, 825, 797, 659.

Using the same procedure, **Ni2** was obtained as a green powder in 51.3%. IR (KBr; cm^{-1}): 2832, 1599 (υ C=N), 1481, 1412, 1168, 1107, 1026, 872, 678.

Ni3 (green powder, 59.4%): IR (KBr; cm^{-1}): 2957, 1597 (υ C=N), 1480, 1424, 1338, 1209, 1130, 1047, 826, 796, 678.

Ni4 (green powder, 58.4 %): IR (KBr; cm^{-1}): 2792, 1593 (υ C=N), 1465, 1407, 1281, 1206, 1133, 859, 802, 657.

Ni5 is prepared from **Ni3**. A flask was charged under argon with 0.09 g of **Ni3** (0.2 mmol), 0.03 g benzyl chloride and 10 mL CH_2Cl_2, then stirred 12h at room temperature. The precipitation was completed by addition of 80 mL of diethyl ether and the solid was collected by filtration, washed with diethyl ether until the solvent was colourless, and dried under reduced pressure to afford a brown solid with a yield of 93.1%. IR (KBr; cm^{-1}): 1657 (υ C=O), 1625, 1593(υ C=N), 1578, 1517, 1428, 1356, 1291, 1208, 1106, 915, 797, 647.

2.4.2 Synthesis and characterization of CNTs supported nickel complexes

The pristine multi-walled carbon nanotubes CNT_C were obtained from Cnano (97% purity). Multi-walled carbon nanotubes CNT_F (98% purity, 2% iron catalyst) were synthesized by chemical vapor deposition according to a previously reported procedure [9]. The textural properties of the two kinds of CNTs are collected in Table 2.1. Surface functionalization was performed prior to the chemical anchoring of the complex onto the CNTs. The functionalization of CNT surface with carboxylic groups was achieved by nitric acid oxidation at 120 ºC for 3h, yielding CNT_{C1} and CNT_{F1} respectively.

CNT supported nickel complex **Ni1/CNT** was prepared as followed. Fistly, 1g of dry oxydized CNT (CNT_{C1} and CNT_{F1}) were reacted with thionyl chloride for 24h under inert atmosphere at 70 ºC to produce acetyl chloride species. CNT_{C2} and CNT_{F2} were obtained after $SOCl_2$ evaporation under reduced pressure. Then CNT_{C2} and CNT_{F2} were contacted with a solution of **Ni1** (0.2 g) in 20 mL CH_2Cl_2 and stirred for 6 h at room temperature. The slurry was then filtered through a glass frit. The resulting solids were washed several times with CH_2Cl_2 and toluene and then dried

under vacuum for 24 h at room temperature. All the other CNT supported nickel complexes were prepared according to a similar procedure.

References

[1] J. Chen, M. A. Hamon, H. Hu, Y. Chen, A. M. Rao, P. C. Eklund, R. C. Haddon, "Solution Properties of Single-Walled Carbon Nanotubes", *Science*, 1998, 282, 95–98.

[2] H. Kong, C. Gao, D. Yan, "Controlled Functionalization of Multiwalled Carbon Nanotubes by in Situ Atom Transfer Radical Polymerization", *J. Am. Chem. Soc.*, 2004, 126, 412–413.

[3] S. Qin, D. Qin, W. T. Ford, D. E. Resasco, J. E. Herrera, "Polymer Brushes on Single-Walled Carbon Nanotubes by Atom Transfer Radical Polymerization of *n* -Butyl Methacrylate", *J. Am. Chem. Soc.*, 2004, 126, 170–176.

[4] L. Qu, L. M. Veca, Y. Lin, A. Kitaygorodskiy, B. Chen, A. M. McCall, J. W. Connell, Y.-P. Sun, "Soluble Nylon-Functionalized Carbon Nanotubes from Anionic Ring-Opening Polymerization from Nanotube Surface", *Macromolecules*, 2005, 38, 10328–10331.

[5] X. Wang, H. Liu, L. Qiu, "Cationic polymerization of tetrahydrofuran from multiple-walled carbon nanotubes: Preparation and glass transition kinetics", *Mater. Lett.*, 2007, 61, 2350–2353.

[6] M. Moniruzzaman, J. Chattopadhyay, W. E. Billups, K. I. Winey, "Tuning the Mechanical Properties of SWNT/Nylon 6,10 Composites with Flexible Spacers at the Interface", *Nano Lett.*, 2007, 7, 1178–1185.

[7] R. Blake, Y. K. Gun'ko, J. Coleman, M. Cadek, A. Fonseca, J. B. Nagy, W. J. Blau, "A Generic Organometallic Approach toward Ultra-Strong Carbon Nanotube

Polymer Composites", *J. Am. Chem. Soc.*, 2004, 126, 10226–10227.

[8] J. Feng, W. Cai, J. Sui, Z. Li, J. Wan, A. N. Chakoli, "Poly(l-lactide) brushes on magnetic multiwalled carbon nanotubes by *in-situ* ring-opening polymerization", *Polymer*, 2008, 49, 4989–4994.

[9] A. Solhy, B. F. Machado, J. Beausoleil, Y. Kihn, F. Gonçalves, M. F. R. Pereira, J. J. M. Órfão, J. L. Figueiredo, J. L. Faria, P. Serp, "MWCNT activation and its influence on the catalytic performance of Pt/MWCNT catalysts for selective hydrogenation", *Carbon*, 2008, 46, 1194–1207.

[10] I. Gerber, M. Oubenali, R. Bacsa, J. Durand, A. Gonçalves, M. F. R. Pereira, F. Jolibois, L. Perrin, R. Poteau, P. Serp, "Theoretical and Experimental Studies on the Carbon-Nanotube Surface Oxidation by Nitric Acid: Interplay between Functionalization and Vacancy Enlargement", *Chem. Eur. J.*, 2011, 17, 11467–11477.

[11] K. A. Wepasnick, B. A. Smith, K. E. Schrote, H. K. Wilson, S. R. Diegelmann, D. H. Fairbrother, "Surface and structural characterization of multi-walled carbon nanotubes following different oxidative treatments", *Carbon*, 2011, 49, 24–36.

[12] H. Kargar, M. Moghadam, V. Mirkhani, S. Tangestaninejad, I. Mohammadpoor-Baltork, S. Rezaei, "Multi-wall carbon nanotube supported manganese(III) porphyrin: an efficient and reusable catalyst for oxidation of 2-imidazolines with sodium periodate", *Transit. Met. Chem.*, 2013, 38, 1–5.

[13] S. Banerjee, S. S. Wong, "Synthesis and Characterization of Carbon Nanotube−Nanocrystal Heterostructures", *Nano Lett.*, 2002, 2, 195–200.

[14] W. Keim, A. Behr, B. Limbäcker, C. Krüger, "Novel Nickel-Oligomerization Catalysts with Arsenic-Oxygen Chelate Ligands", *Angew. Chem. Int. Ed. Engl.*, 1983, 22, 503–503.

[15] M. Peuckert, W. Keim, “A new nickel complex for the oligomerization of ethylene”, *Organometallics*, 1983, 2, 594–597.

[16] L. K. Johnson, C. M. Killian, M. Brookhart, “New Pd (II)-and Ni (II)-based catalysts for polymerization of ethylene and. alpha.-olefins”, *J. Am. Chem. Soc.*, 1995, 117, 6414–6415.

[17] G. J. P. Britovsek, V. C. Gibson, D. F. Wass, “The Search for New-Generation Olefin Polymerization Catalysts: Life beyond Metallocenes”, *Angew. Chem. Int. Ed.*, 1999, 38, 428–447.

[18] L. Zhang, X. Hao, W.-H. Sun, and C. Redshaw, “Synthesis, Characterization, and Ethylene Polymerization Behavior of 8-(Nitroarylamino)-5,6,7-trihydroquinolylnickel Dichlorides: Influence of the Nitro Group and Impurities on Catalytic Activity”, *ACS Catal.*, 2011, 1, 1213–1220.

[19] J. Yu, X. Hu, Y. Zeng, L. Zhang, C. Ni, X. Hao, W.-H. Sun, “Synthesis, characterisation and ethylene oligomerization behaviour of N-(2-substituted-5,6,7-trihydroquinolin-8-ylidene)arylaminonickel dichlorides”, *New J. Chem.*, 2011, 35, 178.

[20] Z. Yinghuai, S. L. P. Sia, K. Carpenter, F. Kooli, R. A. Kemp, “Syntheses and catalytic activities of single-wall carbon nanotubes-supported nickel (II) metallacarboranes for olefin polymerization”, *J. Phys. Chem. Solids*, 2006, 67, 1218–1222.

[21] R. Philippe, A. Morançais, M. Corrias, B. Caussat, Y. Kihn, P. Kalck, D. Plee, P. Gaillard, D. Bernard, P. Serp, “Catalytic Production of Carbon Nanotubes by Fluidized-Bed CVD”, *Chem. Vap. Depos.*, 2007, 13, 447–457.

[22] H. Hu, P. Bhowmik, B. Zhao, M. Hamon, M. Itkis, R. Haddon, “Determination of the acidic sites of purified single-walled carbon nanotubes by acid–

base titration", *Chem. Phys. Lett.*, 2001, 345, 25–28.

[23] G. B. Galland, R. F. de Souza, R. S. Mauler, F. F. Nunes, "13C NMR Determination of the Composition of Linear Low-Density Polyethylene Obtained with [η3-Methallyl-nickel-diimine]PF6 Complex", *Macromolecules*, 1999, 32, 1620–1625.

[24] J. Yu, Y. Zeng, W. Huang, X. Hao, W.-H. Sun, "*N*-(5,6,7-Trihydroquinolin-8-ylidene)arylaminonickel dichlorides as highly active single-site pro-catalysts in ethylene polymerization", *Dalton Trans.*, 2011, 40, 8436.

[25] L. Zhang, E. Yue, B. Liu, P. Serp, C. Redshaw, W.-H. Sun, J. Durand, "Beneficial influence of nanocarbon on the aryliminopyridylnickel chloride catalyzed ethylene polymerization", *Catal. Commun.*, 2014, 43, 227–230.

[26] S. Zai, F. Liu, H. Gao, C. Li, G.u Zhou, S. Cheng, L. Guo, L. Zhang, F. Zhua, Q. Wu, "Longstanding living polymerization of ethylene: substituent effect on bridging carbon of 2-pyridinemethanamine nickel catalysts", *Chem. Commun.*, 2010, 46, 4321–4323.

[27] H. Liu, W. Zhao, J. Yu, W. Yang, X. Hao, C. Redshaw, L. Chen, W.-H. Sun, "Synthesis, characterization and ethylene polymerization behavior of nickel dihalide complexes bearing bulky unsymmetrical α-diimine ligands", *Catal. Sci. Technol.*, 2012, 2, 415.

[28] H. Liu, W. Zhao, X. Hao, C. Redshaw, W. Huang, W.-H. Sun, "2,6-Dibenzhydryl-N-(2-phenyliminoacenaphthylenylidene)-4-methylbenzenamine Nickel Dibromides: Synthesis, Characterization, and Ethylene Polymerization", *Organometallics*, 2011, 30, 2418–2424.

[29] S. D. Ittel, L. K. Johnson, M. Brookhart, "Late-Metal Catalysts for Ethylene Homo- and Copolymerization", *Chem. Rev.*, 2000, 100, 1169–1204.

[30] T. V. Laine, K. Lappalainen, J. Liimatta, E. Aitola, B. Löfgren, M. Leskelä, "Polymerization of ethylene with new diimine complexes of late transition metals", *Macromol. Rapid Commun.*, 1999, 20, 487–491.

[31] S. Park, S. W. Yoon, K.-B. Lee, D. J. Kim, Y. H. Jung, Y. Do, H. Paik, and I. S. Choi, "Carbon Nanotubes as a Ligand in Cp_2ZrCl_2-Based Ethylene Polymerization", *Macromol. Rapid Commun.*, 2006, 27, 47–50.

[32] S. Park, I. S. Choi, "Production of Ultrahigh-Molecular-Weight Polyethylene/Pristine MWCNT Composites by Half-Titanocene Catalysts", *Adv. Mater.*, 2009, 21, 902–905.

[33] Y. Sánchez, C. Albano, A. Karam, R. Perer, E. Casas, "In situ Polymerization of Nanocomposites by $TpTiCl_2(Et)$ System: UHMWPE Filled with Carbon Nanotubes", *Macromol. Symp.*, 2009, 282, 185–191.

[34] D. Bonduel, M. Mainil, M. Alexandre, F. Monteverde, P. Dubois, "Supported coordination polymerization: a unique way to potent polyolefin carbon nanotube nanocomposites", *Chem. Commun.*, 2005, 6, 781–783.

Chapter 3: Ethylene polymerization catalyzed by pyrene-tagged iron complexes: positive effect of π-conjugation and immobilization on multi-walled carbon nanotubes

3.1 Introduction

Due to a unique structure and surface free energy characteristics [1], carbon nanotubes ultimately have been used as support in catalytic system [2-3]. A valuable and elegant approach for catalytic systems involves the non-covalent immobilization on CNTs of complexes *via* π-stacking interactions. The benefits are obvious: pristine CNTs can be used without any pretreatment or functionalization, and the grafting proceeds simply by mixing catalyst solution and the CNTs. The non-covalent modification of the CNTs is of growing interest and different types of molecular structures can be immobilized onto the CNTs surface, such as pyrene [4-9], anthracene [10-11], naphthalene [9, 12] and cyclopentadienyl [13].

Recently, CNTs immobilized catalysts through non-covalent interactions have been described in some publications and successfully used for different catalytic applications. Hermans *et al*. reported the immobilization on CNTs of pyrene-tagged gold catalysts as enyne cyclisation catalyst [4]. CNTs modified ruthenium catalyst has been investigated as water oxidation catalyst by Sun *et al*. [6]. Moreover, CNTs can also adsorb polymerization catalysts based on polycyclic aromatic groups *via* π-stacking interactions for norbornene polymerization [5], ethylene polymerization [14-15] and its co-polymerization with norbornene [16].

As already stated before, the catalytic performances of olefin polymerization catalysts depend on the electronic and the steric interactions between the active center [17] and the ligand surrounding the metallic center [18-19]. Carbon nanotubes as support for homogeneous catalysts can affect the electronic properties due to their π-electron structure. Moreover, the CNTs are huge ligands compared to common organic ligands. Through non-covalent immobilization, CNTs can be seen as

macro-ligands to the metal center. Above all, CNTs are potential supports which offer the possibility to improve the performances of homogeneous catalysts. The researches published by Park and Choi showed that CNTs as support, for metallocene catalysts, dramatically changed the catalytic performances [14-15], and those immobilized catalysts prefer to produce polyethylene with the high molecular weight. In addition, this approach would be beneficial in industrial processing and is also seen as a new efficient way to produce polymer nanocomposites.

Since the typical bisiminopyridine structure for iron complexes reported by Brookhart showed excellent performances in ethylene polymerization [19-20], two iron complexes with a ligand containing the 2,6-bisiminopyridyl framework and pyrene group(s) have been synthesized in our work. Simple mixing of the iron complex and the pristine CNTs in an appropriate solvent produced immobilized catalyst thought non-covalent interactions. These homogeneous catalysts and immobilized catalysts show high activity for the ethylene polymerization, providing highly linear polyethylene (PE).

3.2 Results and discussions

3.2.1 Synthesis and characterization of ligands and iron complexes

Pyrene-tagged ligands **L1** and **L2** (Scheme 3.1) were synthesized using a modified published procedure for 2,6-bis(arylimino)pyridine [21]. The synthesis of **L1** was carried out by reaction of **a1** with 1.5 eq. of 1-aminopyrene and a catalytic amount of *p*-TsOH in refluxing toluene for 2 days. Ligand **L2** was synthesized by the condensation reaction of 2,6-diacetylpyridine and 3 eq. of 1-aminopyrene (Scheme 3.1). Iron complexes **Fe1** and **Fe2** were prepared by reacting $FeCl_2$ with one

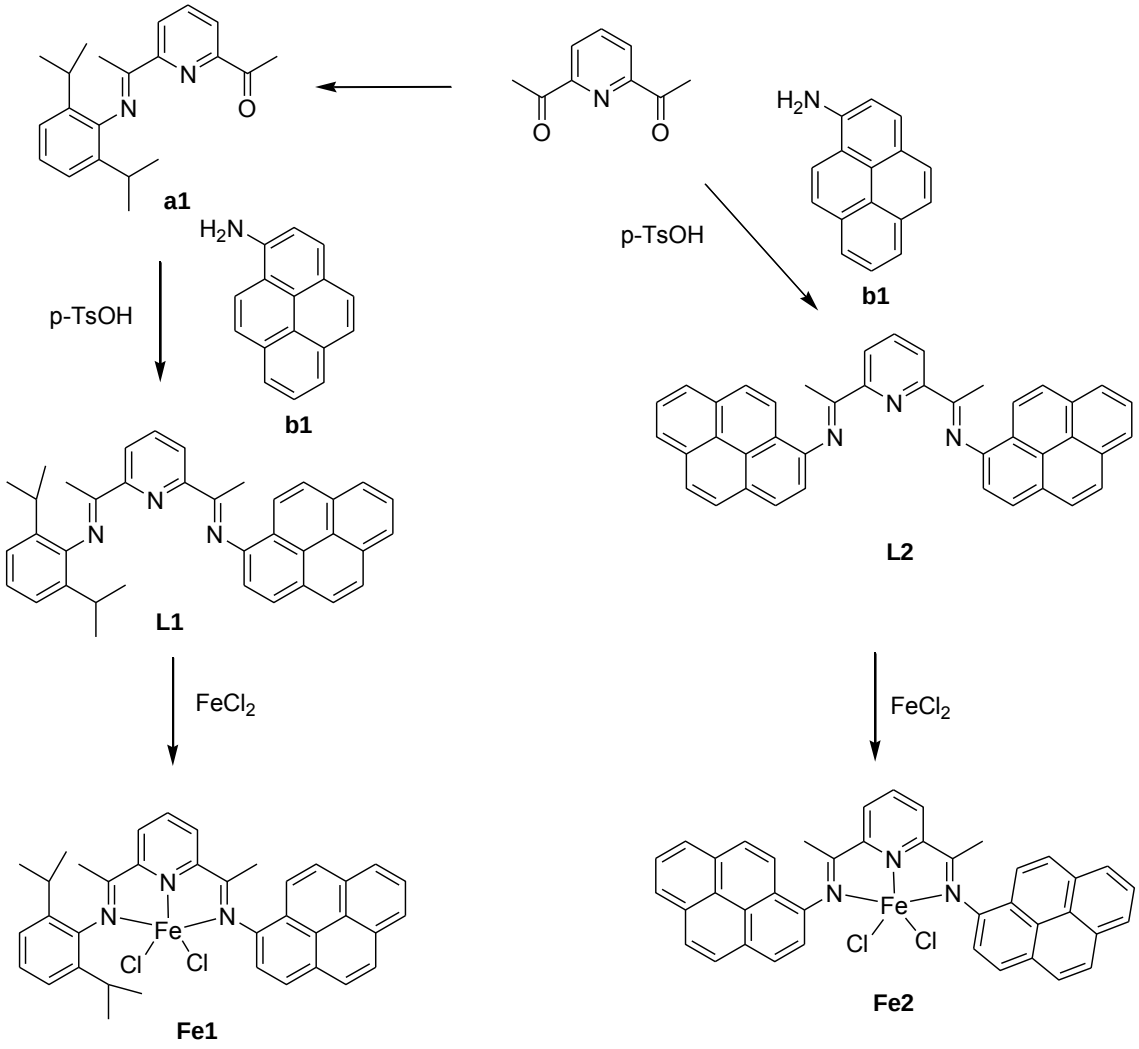

Scheme 3.1 Synthetic procedure for ligands **L1**–**L2** and complexes **Fe1**–**Fe2**.

equivalent of the corresponding ligand in THF (Scheme 3.1). All iron complexes were isolated as air-stable solids but slowly turn from blue to yellow in solution upon air exposure, probably due to oxidation from Fe(II) to Fe(III). Compared to the IR spectra of the free ligands, the C=N stretching vibrations in complexes **Fe1** and **Fe2** are shifted to lower frequencies (1586 cm^{-1} *vs* 1639 and 1638 cm^{-1}), indicating effective coordination between the imino nitrogen atoms and the iron center. The molecular structure of complex **Fe1** was further confirmed by single-crystal X-ray diffraction (Figure 3.1).

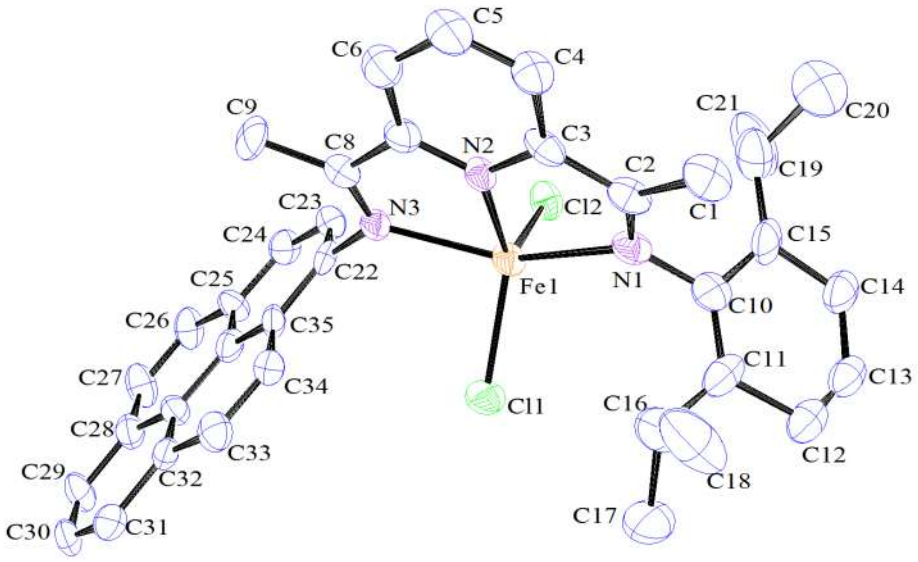

Figure 3.1 ORTEP molecular structure of **Fe1**. Thermal ellipsoids are shown at 30% probability. Hydrogen atoms have been omitted for clarity. Selected bond lengths (Å) and angles (º): Fe1–N1 2.296(5), Fe1–N2 2.083(4), Fe1–N3 2.247(5), Fe1–Cl1 2.2723(18), Fe1–Cl2 2.3000(19), N1–Fe1–N2 73.28(19), N1–Fe1–N3 146.22(19), N2–Fe1–N3 73.05(17), Cl1–Fe1–Cl2 115.82(7).

The coordination geometry around the iron center can be described as distorted square-pyramidal, with the basal plane composed of N1, N2, N3, and Cl1. The iron center deviates from the basal plane by 0.6574 Å, and the Cl2 deviates by 2.9465 Å on the same side. The equatorial plane formed by N1, N2 and N3, is almost perpendicular to the imino-pyrene ring (86.1º) and to the 2,6-diisprolphenyl group (79.1 º). The chlorine atoms are setting on the different sites from the basal plane with distance of 1.6508 Å for Cl1 and 2.1830 Å for Cl2. Concerning the bond lengths around the iron center, Fe1–Cl2 (2.3000(19) Å) is longer than Fe1–Cl1 (2.2723(18) Å); the bond Fe1–N1 is similar to the Fe1–N3 but longer than Fe1–N2 (about 0.2 Å). This is partly due to N1 and N3 belonging to imino groups but N2 belonging to the pyridine ring. A similar geometry was also observed for analogous tridentate iron (II) complexes [22-29]. Details of the X-ray structure determinations and refinements are

provided in Table 3.1.

Table 3.1 Crystal data and structure refinement for **Fe1**

	Fe1
Empirical formula	$C_{37}H_{35}Cl_2FeN_3$
Formula weight	648.43
Temperature [K]	173(2) K
Wavelength [Å]	0.71073
Crystal system	Tetragonal
Space group	I4(1)/a
a [Å]	23.447(3)
b [Å]	23.447(3)
c [Å]	29.697(6)
α [°]	90
β [°]	90
γ [°]	90
V [Å^3]	16326(5)
Z, *D*calcd. [g·cm^{-3}]	16, 1.055
μ [mm^{-1}]	1.345
F(000)	5408
Crystal size [mm]	0.17× 0.03 × 0.03
θ range [°]	1.11–25.32
Limiting indices	-13 ≤ h ≤ 28
	-15 ≤ k ≤ 28
	-35 ≤ l ≤ 24

Reflections collected	15655
Independent reflections	7443, [R(int) = 0.0623]
No. of parameters	416
Completeness to θ [%]	99.8 %
Goodness of fit on F^2	1.012
Final R indices [$I>2\sigma(I)$]	R1 = 0.0933, wR2 = 0.2243
R indices (all data)	R1 = 0.1547, wR2 = 0.2551
Max./min. $\Delta\rho$[a] [eÅ^{-3}]	0.384 and -0.263

3.2.2 Synthesis and characterization of MWCNTs supported iron complexes

Immobilization of the iron complexes **Fe1** and **Fe2** on MWCNTs was carried out under nitrogen atmosphere by stirring a CH_2Cl_2 solution containing the corresponding complex and a suspension of the purified MWCNTs (Scheme 3.2). The suspension was filtrated and washed several times with toluene and CH_2Cl_2 until the filtrate was colourless. XPS analysis confirmed the presence of Fe(II) species on the MWCNTs surface. The absence of peak corresponding to Fe(0) also proved that the iron complexes did not suffered from reduction during the anchoring process. Since the amount of iron complex is too low to allow semi-quantitative analysis by XPS, the exact amount of iron immobilized on the MWCNTs was determined using ICP-MS (2657.83 mg Fe/kg for **Fe1** and 2908.65 mg Fe/kg for **Fe2**).

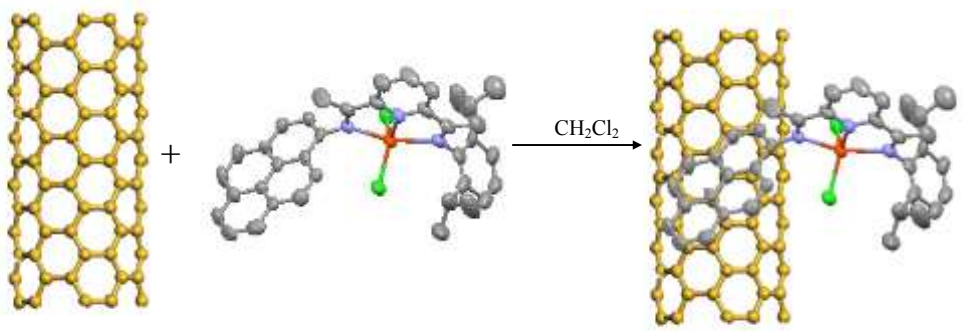

Scheme 3.2 Schematic representation of the immobilization of **Fe1** on MWCNTs.

3.2.3 Ethylene polymerization

3.2.3.1 Ethylene polymerization by iron complexes

Prior studying the catalytic behavior of the MWCNT-supported iron catalysts, we carried out an investigation of the homogeneous behavior of the iron complexes **Fe1** and **Fe2** in the ethylene polymerization reaction in order to both optimize reaction conditions and ensure that the introduction of the pyrene moiety on the ligands was not detrimental to the catalyst performances.

As shown in Table 3.2, pre-catalyst **Fe1** was investigated for determining the optimum reaction conditions under 10 atm of ethylene. In order to find the best co-catalyst for **Fe1**, MAO and MMAO were used with a Al/Fe molar ratio of 1000 (Table 3.2, Entries 1–2). The highest activity was observed employing MMAO as co-catalyst (Table 3.2, Entry 2), which was selected for further investigation. Evaluation of the catalytic behavior of **Fe1** was then carried out varying the Al/Fe molar ratio (Table 3.2, Entries 2–6). When the Al/Fe molar ratio is increased from 1000 to 3000 (Table 3.2, Entries 2–6), the activity of the polymerization is firstly increased and then decreased, the best Al/Fe molar ratio being 2000. Interestingly, the

molecular weight (M_w) and molecular weight distribution (M_w/M_n) values of the PE increased with the molar Al/Fe ratio.

Table 3.2 Ethylene polymerization with **Fe1** pre-catalyst[a]

Entry	Co-Cat.	Al/Fe	PE (g)	Act.[b]	T_m[c] (ºC)	M_w[d] (kg mol^{-1})	M_w/M_n[d]
1	MAO	1000	5.7	2.3	128.7	108	80.3
2	MMAO	1000	10.5	4.2	124.6	21.6	10.2
3	MMAO	1500	15.9	6.4	124.7	16.3	9.30
4	MMAO	2000	19.8	7.9	124.4	30.4	19.8
5	MMAO	2500	17.3	7.0	124.2	39.5	30.9
6	MMAO	3000	15.3	6.1	125.3	145	163

[a] Reaction conditions: 5 μmol of **Fe1**; 30 min; 30 °C; 10 atm ethylene; 100 mL toluene. [b] 10^6 g (PE)·mol^{-1}(Fe)·h^{-1}. [c] Determined by DSC. [d] Determined by GPC.

The influence of reaction temperature (Table 3.3, Entries 1–3) and reaction time (Table 3.3, Entries 1, 4–8) for precatalyst **Fe1** were also investigated under the best Al/Fe ratio. The catalytic activity shows a slight decrease (from 7.9 to 5.5 × 10^6 g (PE)·mol^{-1}(Fe)·h^{-1}) when the reaction temperature is increased form 30 °C to 50 °C (Table 3.3, Entries 1–3). However, the molecular weights and the molecular weight distributions of PE are increased at higher temperatures (M_w ranging from 30.4 to 127.6 kg mol^{-1} and between M_w/M_n 19.8 and 75.6, Figure 3.2). Data concerning the effect of the reaction time on the catalytic activity show that the highest value of 2.74 × 10^7 g (PE)·mol^{-1}(Fe)·h^{-1} was reached within 5 min (Table 3.3, Entry 4) and that the

reaction was almost finished after 30 minutes which can be certified by the ethylene absorption curve (Figure 3.3).

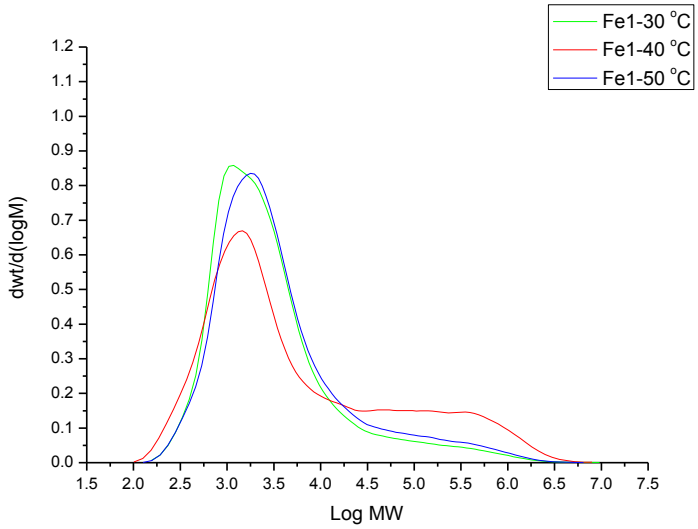

Figure 3.2 GPC traces of polyethylene produced by **Fe1** catalyst at different temperatures (Table 3.3, Entries 1–3).

The pre-catalyst **Fe2** was also evaluated using MMAO as co-catalyst (Table 3.4, Entries 1–5). The best activity is observed with the optimal Al/Fe molar ratio of 2000 at 30 ºC (Table 3.4, Entry 2) and the best activity is 1.15×10^7 g (PE)·mol^{-1}(Fe)·h^{-1}, making **Fe2** *ca.* 1.5 more active than **Fe1** under similar conditions (Table 3.4, Entry 4). It appears therefore that the pyrene ring has a beneficial influence in terms of activity for ethylene polymerization. The ethylene absorption curve showed that the precatalyst **Fe2** has a remarkable activity in the first 15 min and that the reaction is almost finished after 30 min (Figure 3.4). As for **Fe1**, an increase of the reaction temperature from 30 °C to 50 °C led to a remarkable decrease of activity (from 11.5 to 5.4×10^6 g (PE)·mol^{-1}(Fe)·h^{-1} , Table 3.4, Entries 2, 4, 5), however, the M_w and M_w/M_n values of the PE obtained are less sensible to temperature increase (Figure 3.5, M_w ranging from 2.71 to 6.12 kg mol^{-1} and M_w/M_n between 2.9 and 5.1). These

narrower molecular polydispersities of obtained PEs can probably be attributed to the symmetric structure of the **Fe2** pre-catalyst, leading to a lower number of different active species after activation by the co-catalyst.

Table 3.3 Ethylene polymerization with **Fe1** /MMAO system[a]

Entry	T (ºC)	t (min)	PE (g)	Act.[b]	T_m[c] (ºC)	M_w[d] (kg mol^{-1})	M_w/M_n[d]
1	30	30	19.8	7.9	124.4	30.4	19.8
2	40	30	16.7	6.7	122.1	38.1	22.4
3	50	30	13.8	5.5	127.6	112	75.6
4	30	5	11.4	27.4	122.4	4.32	2.40
5	30	10	13.4	16.1	123.8	14.1	7.50
6	30	15	15.2	12.2	124.0	12.4	8.20
7	30	45	21.3	5.7	125.8	71.2	66.5
8	30	60	22.8	4.6	125.1	38.8	32.2

[a] Reaction conditions: 5 μmol of **Fe1**; MMAO; Al/Fe = 2000; 10 atm ethylene; 100 mL toluene. [b] 10^6 g (PE)·mol^{-1}(Fe)·h^{-1}. [c] Determined by DSC. [d] Determined by GPC.

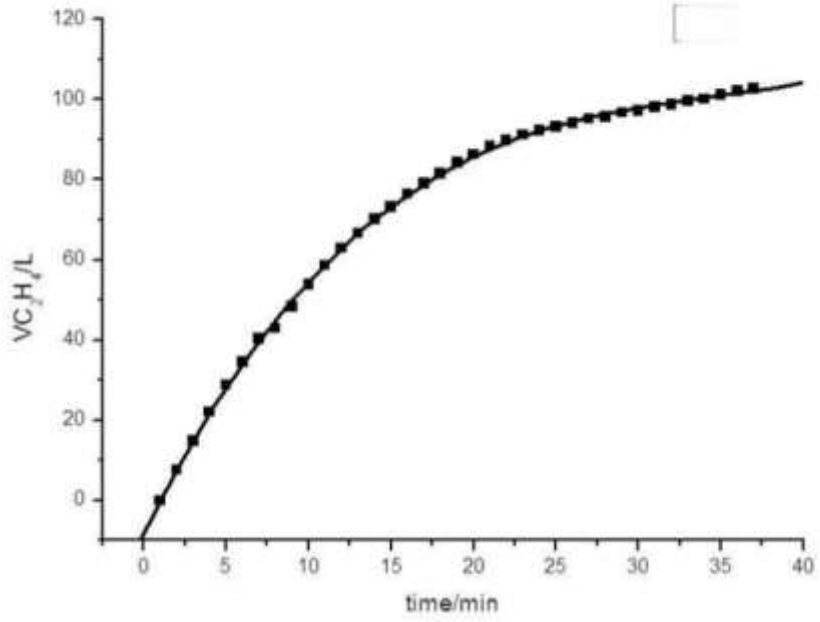

Figure 3.3 Ethylene absorption curve of the catalyst **Fe1** (Table 3.3, Entry 1).

Table 3.4 Ethylene Polymerization with **Fe2** pre-catalyst[a]

Entry	Al/Fe	T (ºC)	t (min)	PE (g)	Act.[b]	T_m[c] (ºC)	M_w[d] (kg mol^{-1})	M_w/M_n[d]
1	1500	30	30	23.7	9.5	120.1	3.57	2.9
2	2000	30	30	28.9	11.5	119.9	2.71	3.0
3	2500	30	30	22.3	8.9	119.5	3.38	4.1
4	2000	40	30	15.5	6.2	122.0	4.39	3.3
5	2000	50	30	13.6	5.4	122.7	6.12	5.1

[a] Reaction conditions: 5 μmol of **Fe2**; MMAO; 10 atm ethylene; 100 mL toluene. [b] 10^6 g (PE)·mol^{-1}(Fe)·h^{-1}. [c] Determined by DSC. [d] Determined by GPC.

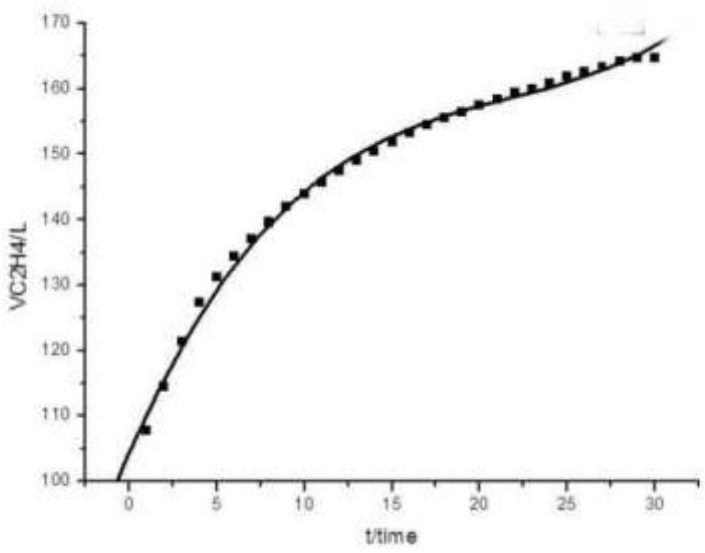

Figure 3.4 Ethylene absorption curve of the catalyst **Fe2** (Table 3.4, Entry 2).

The steric and electronic effects of the aromatic groups on the ligand clearly affect the molecular weight of the obtained polyethylenes. According to the observed data, the current complex pre-catalysts generally showed higher activities than their analogs [30-35], illustrating the positive influences of pyrene-tagged ligands on their iron complexes. Though PEs with lower molecular weights were reported for iron complexes bearing ligands lacking *ortho*-substituted aryl groups [20, 22, 24, 34] and there is no substituent on 1-aminopyrene, the current pre-catalysts produced PEs with higher molecular weights than their analogs [22, 34]. The pyrene played an important role as a bulky aryl group but the lack of substituent in the *ortho* position, which was confirmed by the replacement of the 2,6-diisopropylphenyl fragment forming **Fe1** by the pyrene moiety within **Fe2**, resulting in a higher activity for ethylene polymerization.

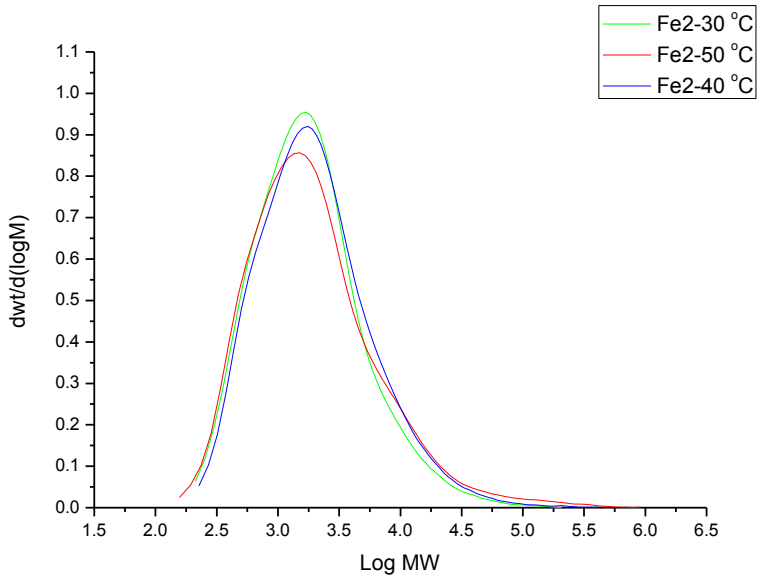

Figure 3.5 GPC traces of polyethylene produced by **Fe2** catalyst at different temperatures (Table 3.4, Entries 2, 4, 5).

3.2.3.2 Polymerization using MWCNT-supported iron pre-catalysts

Subsequently, the polymerization behavior of MWCNT-supported iron catalysts was investigated using MMAO as co-catalyst. The influence of the reaction parameters, including the Al/Fe molar ratio and reaction temperature, was studied using the **MWCNT-Fe1**/MMAO system. Increasing the Al/Fe from 1500 to 4000 (Table 3.5, Entries 1–5), the activities sharply increase to reach a maximum when Al/Fe = 3000. This optimum ratio for the MWCNTs supported iron catalyst is significantly higher than the one of the corresponding homogeneous catalyst. This can be attributed: 1) to the interaction force between the MWCNTs and the iron complex requiring a larger amount of co-catalyst for activation and/or 2) to partial co-catalyst deactivation by adsorption on the MWCNTs surface. On the other side, the best catalytic activity reached by the **MWCNT-Fe1** system after 30 min. (9.11×10^6 g (PE)·mol^{-1}(Fe)·h^{-1}) is higher than of **Fe1** used under homogeneous conditions (Table

3.5, Entry 3 vs Table 3.2, Entry 4) thus evidencing a beneficial influence of the nanocarbon support on the catalyst's performances. Indeed, the immobilization of the catalytic system leads to an increase of the steric hindrance around the active centre due to the presence of the MWCNTs acting as a macro-ligand. Moreover, charge transfer between the CNTs surface and the pyrene group through π-π interaction can also have a significant influence on the electronic environment of the iron. Indeed, charge transfer between CNTs and various adsorbed species has already been reported in the literature [36-38], including for immobilized ethylene polymerization catalysts [14].

Table 3.5 Ethylene polymerization with **MWCNT-Fe1**/MMAO[a]

Entry	Al/Fe	T (ºC)	PE (g)	Act.[b]	T_m[c] (ºC)	M_w[d] (kg mol^{-1})	M_w/M_n[d]
1	1500	30	3.8	3.21	124.4	18.8	12.1
2	2500	30	5.4	4.57	124.0	6.59	3.50
3	3000	30	10.8	9.11	126.4,	27.6	12.6
4	3500	30	6.7	5.65	124.8	5.07	2.20
5	4000	30	5.1	4.30	123.7	18.6	11.2
6	3000	40	6.2	5.23	127.5	55.5	23.6
7	3000	50	2.4	2.03	127.9	67.9	27.2

[a] Reaction conditions: **MWCNT/Fe1** (50 mg); MMAO; 10 atm ethylene; 30 min; 100 mL toluene. [b] 10^6 g (PE)·mol^{-1}(Fe)·h^{-1}. [c] Determined by DSC. [d] Determined by GPC. [e] DSC value of the polymer with MWCNTs.

By changing the Al/Fe molar ratio, the PEs obtained by the **MWCNT-Fe1** system showed adaptable molecular weights (M_w from 5.07 to 27.6 kg mol^{-1}). A narrower molecular polydispersity (M_w/M_n from 2.2 to 12.1) than that of homogeneous system is observed. However, the best activity for the **MWCNT-Fe2** is 8.35 × 10^6 g (PE)·mol^{-1}(Fe)·h^{-1} (Table 3.6, Entry 2), which is lower than for its corresponding homogeneous counterpart (Table 3.6, Entry 2). The two pyrene rings present within the framework of complex **Fe2**, can interact with the MWCNT surface, thus resulting in a too high steric hindrance around the iron center, reducing its accessibility and therefore leading to a lower activity compared to its non-supported counterpart.

Table 3.6 Ethylene polymerization with **MWCNT-Fe2** /MMAO[a]

Entry	Al/Fe	T (ºC)	PE (g)	Act.[b]	T_m[c] (ºC)	M_w[d] (kg mol^{-1})	M_w/M_n[d]
1	2500	30	7.41	5.70	122.4	11.5	8.48
2	3000	30	10.86	8.35	122.4	8.32	5.61
3	4000	30	5.38	4.14	122.9	8.76	6.29
4	3000	40	6.03	4.64	121.0	4.13	2.99
5	3000	50	2.58	1.98	122.2	3.88	2.38

[a] Reaction conditions: **MWCNT-Fe2** (50 mg); MMAO; 10 atm ethylene; 30 min; 100 mL toluene. [b] 10^6 g (PE)·mol^{-1}(Fe)·h^{-1}. [c] Determined by DSC. [d] Determined by GPC. [e] DSC value of the polymer with MWCNTs.

Using the optimum molar ratio of Al/Fe (3000), the influence of reaction

temperature was investigated (Table 3.5, Entries 3, 6 and 7 for **MWCNT-Fe1** and Table 3.6, Entries 2, 4 and 5 for **MWCNT-Fe2**). The elevated reaction temperature resulting in lower catalytic activity is even more pronounced in the case of the supported systems, evidencing that MWCNTs are not able to stabilize the active species when operating at higher temperature. In addition, assuming that at least a part of the MMAO introduced in the catalytic system can be adsorbed on the MWCNTs surface, temperature has an impact on the adsorption process and therefore on the catalytic performances. Moreover, the M_w and M_w/M_n values are also influenced by the temperature: higher molecular weights and broader distributions are observed at elevated reaction temperature for **MWCNT-Fe1** (Figure 3.6).

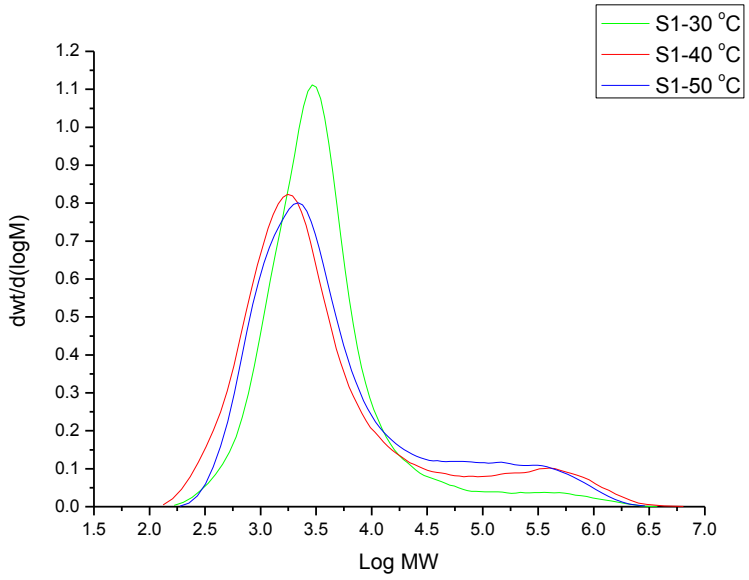

Figure 3.6 GPC traces of polyethylene produced by **MWCNT-Fe1** catalyst at different temperatures (Table 3.5, Entries 3, 6 and 7).

Interestingly, M_w and M_w/M_n values for the PEs obtained employing **MWCNT-Fe2** slightly decrease at higher reaction temperatures because two pyrene groups had interactions with MWCNTs. One advantage was the production of

polyethylenes with narrower polydispersity (Figure 3.7). This phenomenon is just opposite to the trend observed for **MWCNT-Fe1**.

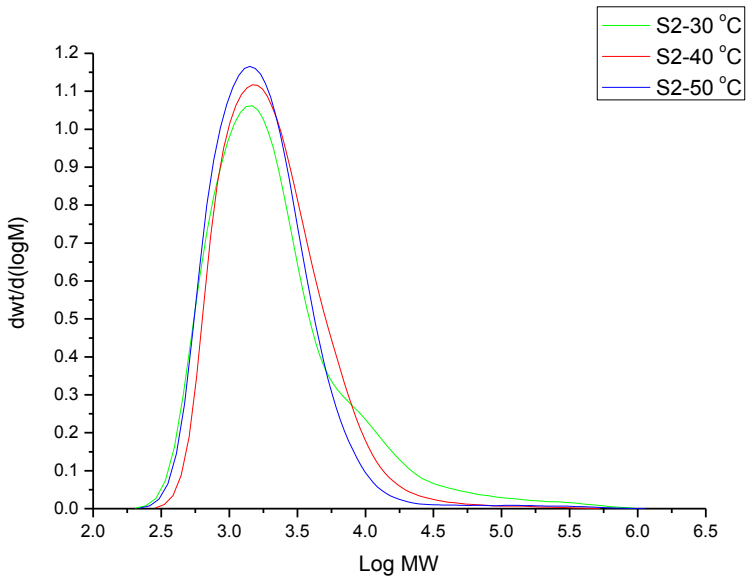

Figure 3.7 GPC traces of polyethylene produced by **MWCNT-Fe2** catalyst at different temperatures (Table 3.6, Entries 2, 4 and 5).

During the polymerization process, polyethylene nanocomposites are produced by direct growth of the polymeric chains from the MWCNT surface due to its interaction with the catalytically active species. Surface-initiated polymerization processes have been reported in some cases as an efficient way to homogeneously disperse CNTs into polyethylene matrices [14-15, 17, 39-44]. Moreover, the presence of the MWCNTs has the possibility to enhance the resulting polyethylene properties. According to the DSC values, under the same condition, the melting point of the polymer without MWCNTs (the MWCNTs were removed from the resulting polyethylene), which is produced by **MWCNT-Fe1** is 126.4 °C (Table 3.5, Entry 3), however, the melting point of polymer with MWCNTs is increased to 131.7 °C. This means that, owing to the effect of 0.46% MWCNTs on the polyethylene, the melting

point of the resulting polymer has increased of 5.3 °C. The same results can be observed with the **MWCNT-Fe2** catalytic system. Compared to the melting point values of polymer without MWCNTs (Table 3.5, Entry 3), in the presence of 0.46% MWCNTs inside of the polymer, an increase of 5.5 °C is measured from the DSC values.

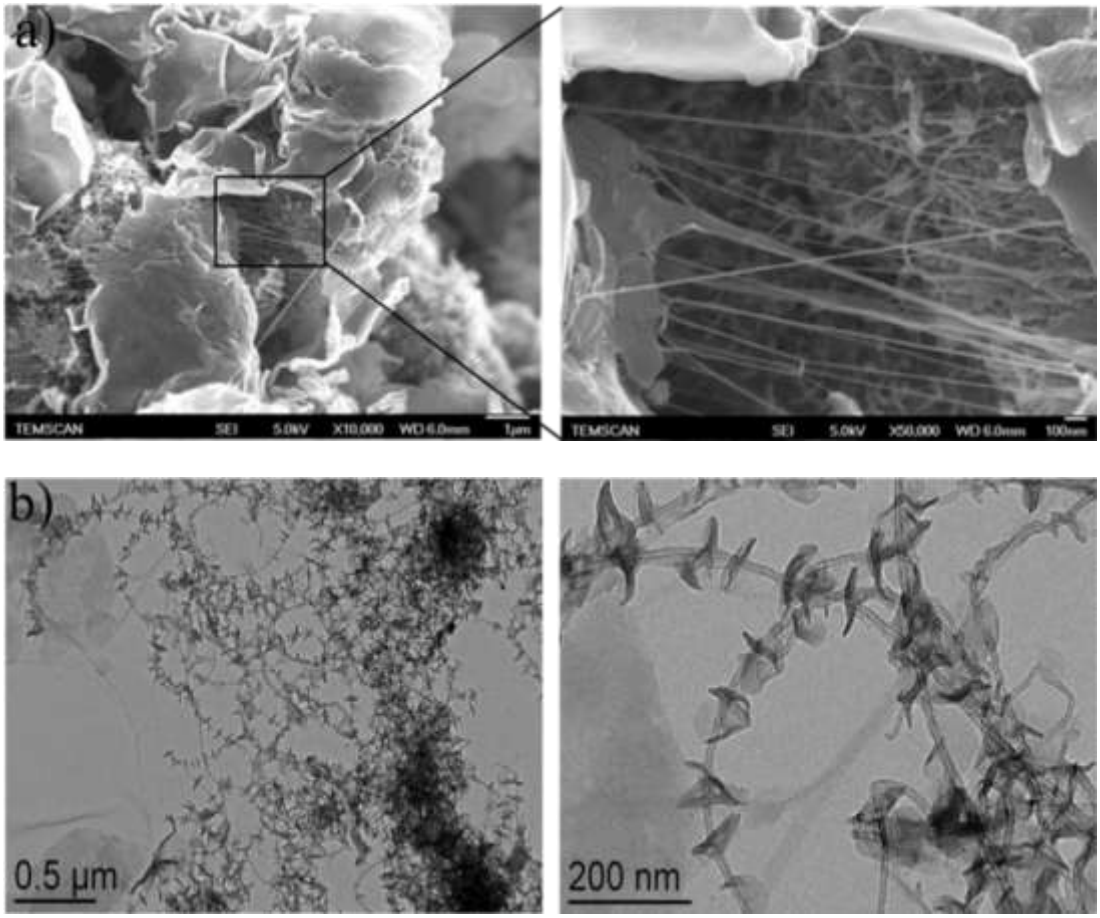

Figure 3.8. a) SEM images of MWCNT/PE composites; and b) TEM images of the MWCNT/PE composites after partial polyethylene removal.

The polymeric materials obtained using MWCNT-supported iron catalysts were analyzed by scanning electron microscopy (SEM) and evidenced a good level of dispersion inside the polyethylene matrix of the MWCNTs, which are individually

separated (Figure 3.8 a). When some of the polymeric material is removed from the samples, a particular lamellar structure is observed, showing regular dispersion of small quantities of polymeric material along the MWCNTs (Figure 3.8 b), similar to that observed for crystallization of polyethylene around CNTs acting as nucleating agents [45].

3.3 Conclusions

Two iron complexes based on the 2,6-bis(imino)pyridyl framework and containing a pyrenyl moiety have been synthesized and characterized. Activated by MMAO, all of the iron pre-catalysts promote ethylene polymerization with high activities, comparable to that of the most efficient systems described in the literature [25, 27-28], evidencing a beneficial influence of the pyrene substituent(s) introduced on the ligands. Using π-π stacking interactions, MWCNT-supported catalysts are efficiently produced by impregnating the iron complexes on MWCNTs in dichloromethane. Efficient anchoring is confirmed by IR, XPS and ICP-MS analysis. The catalytic screening of these heterogenized systems evidenced in one case a significant increase of the productivity compared to the analogous unsupported system. Meanwhile, in another case, the lower production of polyethylene is due to the presence of two pyrene moieties on the iron complex for interaction, but leads to narrower polydispersities; thus evidencing a non-innocent role of CNTs in the polymerization process. Finally, the resulting materials show good dispersion of the MWCNTs into the polyethylene matrix, resulting from the surface initiated polymerization reaction.

3.4 Experimental Section

*Synthesis of ligand **L1**, 2-(2,6-diisopropylphenyliminoethyl)-6-(pyren-1-yliminoethyl) pyridine*

The monoamine compound **a1** was synthesized by the condensation reaction of 2,6-diacetylpyridine with 2,6-diisopropylaniline according to a previously reported procedure [21]. A mixture of **a1** (0.97 g, 3 mmol), 1.5 equivalent of 1-aminopyrene (**b1**, 0.98 g, 4.5 mmol) and a catalytic amount of *p*-toluenesulfonic acid (0.1 g) in toluene (50 mL) was refluxed for 10h. After solvent evaporation, the crude product was purified by column chromatography on silica gel with petroleum ether/ethyl acetate (50/1: v/v) as eluent to afford the product as a yellow powder in 68% yield. IR (KBr, cm^{-1}): 3029 (m), 1639 (s), 1597 (w), 1454 (m), 1362 (m), 1228 (m), 1105 (s), 840 (m), 765 (m).

^{1}H NMR (400 MHz, acetone-d_6, TMS): 8.72 (dd, 1H, ^{3}J = 4.5 Hz, ^{4}J = 0.8 Hz pyridine), 8.59 (dd, 1H, ^{3}J = 4.4 Hz, Py), 8.33 (d, 1H, J = 4.1Hz, pyrene), 8.03- 8.28 (m, 8H, pyrene, Ar), 7.60 (d, 1H, J = 4.1 Hz, Ar), 7.22 (d, 2H, J = 4.1, Ar), 7.11 (t, 1H, J = 4.5 Hz, Ar), 2.83–2.91 (m, 2H, C*H*), 2.48 (s, 3H, CH_3), 2.33(s, 3H, CH_3), 1.16-1.22 (m, 12H, CH(CH_3)$_2$).

^{13}C NMR (100 MHz, acetone-d_6, TMS): 165.4, 164.9, 148.2, 137.9, 137.4, 135.5, 131.8, 127.5, 126.9, 126.3, 125.9, 124.8, 124.6, 123.7, 123.6, 122.9, 122.8, 122.7, 122.6, 122.3, 22.6, 22.1, 16.5, 16.1.

*Synthesis of ligand **L2**, 2,6-di(pyren-1-yliminoethyl)pyridine*

A mixture of 2,6-diacetylpyridine (0.97 g, 2 mmol), 3 equivalent of 1-aminopyrene (**b1**, 1.27 g, 6 mmol) and a catalytic amount of *p*-toluenesulfonic acid (0.1 g) in toluene (50 mL) was refluxed for 3 days. After solvent evaporation, the

crude product was purified by column chromatography on silica gel with petroleum ether/ethyl acetate (50/1: v/v) as eluent to afford the product as a yellow powder.

Yield :52%. IR (KBr, cm^{-1}): 3045 (m), 1638 (s), 1621 (m), 1566 (m), 1449 (w), 1362 (s), 1226 (s), 1119 (m), 848(s), 758 (s), 711 (m).

^1H NMR (400 MHz, $CDCl_3$, TMS): 8.72 (d, 2H, J = 3.8 Hz, Py), 8.20 (d, 2H, J = 4.0 Hz, Py), 8.14–8.17 (m, 4H, Ar), 8.05–8.09 (m, 3H, Py H, Ar H), 8.04–8.07 (m, 6H, Ar), 8.03 (d, 2H, J = 3.8 Hz, Ar), 7.39 (d, 2H, J = 4.0 Hz, Ar), 2.36 (s, 6H, CH_3).

^{13}C NMR (100 MHz, $CDCl_3$, TMS): 168.8, 155.5, 145.6, 137.2, 131.7, 131.5, 127.9, 127.4, 126.9, 126.1, 125.9, 125.4, 124.8, 124.6, 122.9, 122.8, 116.6, 17.0.

*Synthesis of iron complexes **Fe1** and **Fe2**.*

The iron complexes were prepared by reacting $FeCl_2$ with one equivalent of the corresponding ligand (L1 or L2) in THF at room temperature for 12 h (Scheme 3.1). The obtained precipitate was collected by filtration and washed with diethyl ether, followed by drying under reduced pressure. **Fe1**. Yield: 88 %. IR (KBr, cm^{-1}): 1621 (w), 1586 (s), 1463 (m), 1436 (m), 1371 (s), 1104 (m), 845 (s), 799 (m), 713 (m). Anal. Calcd for $C_{37}H_{35}Cl_2FeN_3$ (647.16): C, 68.53; H, 5.44; N, 6.48. Found C: 68.83; H: 5.43 N: 6.38. **Fe2**. Yield: 82 %. IR (KBr, cm^{-1}): 1623 (w), 1586 (s), 1504 (w), 1486 (w), 1369 (m), 1265(m), 1186 (w), 843 (s), 710 (m).

Immobilization of iron complexes on CNT

Prior to use, MWCNTs were purified and mechanical cut 6h by ball-milling. Under N_2 atmosphere, CH_2Cl_2 (100 mL) was added to a mixture of MWCNTs (3 g) and the iron complex (**Fe1** or **Fe2**) (0.15 g). The resulting suspension was stirred for 6 h at room temperature. After filtration, the remaining black powder was fully washed by toluene and CH_2Cl_2, and then dried under vacuum for 2 days. The amount of iron complex anchored on the MWCNTs (2657.83 mg Fe/kg for **Fe1** and 2908.65 mg

Fe/kg for **Fe2**) was determined by ICP-MS taking into account the amount of iron present (residual catalyst) in the unfunctionalized samples.

References

[1] P. M. Ajayan, "Nanotubes from Carbon", *Chem. Rev.*, 1999, 99, 1787–1800.

[2] F. Rodríguez-Reinoso, "The role of carbon materials in heterogeneous catalysis", *Carbon*, 1998, 36, 159–175.

[3] P. Serp, M. Corrias, P. Kalck, "Carbon nanotubes and nanofibers in catalysis", *Appl. Catal. Gen.*, 2003, 253, 337–358.

[4] C. Vriamont, M. Devillers, O. Riant, S. Hermans, "Catalysis with Gold Complexes Immobilised on Carbon Nanotubes by π–π Stacking Interactions: Heterogeneous Catalysis versus the Boomerang Effect", *Chem. Eur. J.*, 2013, 19, 12009–12017.

[5] F. J. Gómez, R. J. Chen, D. Wang, R. M. Waymouth, H. Dai, "Ring opening metathesis polymerization on non-covalently functionalized single-walled carbon nanotubes", *Chem. Commun.*, 2003, 2, 190–191.

[6] F. Li, B. Zhang, X. Li, Y. Jiang, L. Chen, Y. Li, L. Sun, "Highly Efficient Oxidation of Water by a Molecular Catalyst Immobilized on Carbon Nanotubes", *Angew. Chem. Int. Ed.*, 2011, 50, 12276–12279.

[7] P. D. Tran, A. Le Goff, J. Heidkamp, B. Jousselme, N. Guillet, S. Palacin, H. Dau, M. Fontecave, V. Artero, "Noncovalent Modification of Carbon Nanotubes with Pyrene-Functionalized Nickel Complexes: Carbon Monoxide Tolerant Catalysts for Hydrogen Evolution and Uptake", *Angew. Chem. Int. Ed.*, 2011, 50, 1371–1374.

[8] F. D'Souza, A. S. D. Sandanayaka, O. Ito, "SWNT-Based Supramolecular Nanoarchitectures with Photosensitizing Donor and Acceptor Molecules", *J. Phys.*

Chem. Lett., 2010, 1, 2586–2593.

[9] A. Schaetz, M. Zeltner, W. J. Stark, "Carbon Modifications and Surfaces for Catalytic Organic Transformations", *ACS Catal.*, 2012, 2, 1267–1284.

[10] D. Didier, E. Schulz, "π-Stacking interactions at the service of [Cu]-bis(oxazoline) recycling", *Tetrahedron Asymmetry*, 2013, 24, 769–775.

[11] F. Giroud, S. D. Minteer, "Anthracene-modified pyrenes immobilized on carbon nanotubes for direct electroreduction of O_2 by laccase", *Electrochem. Commun.*, 2013, 34, 157–160.

[12] N. Nakashima, "Solubilization of single-walled carbon nanotubes with condensed aromatic compounds", *Sci. Technol. Adv. Mater.*, 2006, 7, 609.

[13] Z. Zhang, C. H. Turner, "Structural and Electronic Properties of Carbon Nanotubes and Graphenes Functionalized with Cyclopentadienyl–Transition Metal Complexes: A DFT Study", *J. Phys. Chem. C*, 2013, 117, 8758–8766.

[14] S. Park, S. W. Yoon, H. Choi, J. S. Lee, W. K. Cho, J. Kim, H. J. Park, W. S. Yun, C. H. Choi, Y. Do, I. S. Choi, "Pristine Multiwalled Carbon Nanotube/Polyethylene Nanocomposites by Immobilized Catalysts", *Chem. Mater.*, 2008, 20, 4588–4594.

[15] S. Park, I. S. Choi, "Production of Ultrahigh-Molecular-Weight Polyethylene/Pristine MWCNT Composites by Half-Titanocene Catalysts", *Adv. Mater.*, 2009, 21, 902–905.

[16] S. Bredeau, L. Boggioni, F. Bertini, I. Tritto, F. Monteverde, M. Alexandre, P. Dubois, "Ethylene–Norbornene Copolymerization by Carbon Nanotube-Supported Metallocene Catalysis: Generation of High-Performance Polyolefinic Nanocomposites", *Macromol. Rapid Commun.*, 2007, 28, 822–827.

[17] W. Kaminsky, A. Funck, H. Hähnsen, "New application for metallocene

catalysts in olefin polymerization", *Dalton Trans.*, 2009, 41, 8803.

[18] L. Deng, T. K. Woo, L. Cavallo, P. M. Margl, T. Ziegler, "The Role of Bulky Substituents in Brookhart-Type Ni(II) Diimine Catalyzed Olefin Polymerization: A Combined Density Functional Theory and Molecular Mechanics Study", *J. Am. Chem. Soc.*, 1997, 119, 6177–6186.

[19] B. L. Small, M. Brookhart, A. M. A. Bennett, "Highly Active Iron and Cobalt Catalysts for the Polymerization of Ethylene", *J. Am. Chem. Soc.*, 1998, 120, 4049–4050.

[20] S. D. Ittel, L. K. Johnson, M. Brookhart, "Late-Metal Catalysts for Ethylene Homo- and Copolymerization", *Chem. Rev.*, 2000, 100, 1169–1204.

[21] C. Wallenhorst, G. Kehr, H. Luftmann, R. Fröhlich, G. Erker, "Bis(iminoethyl)pyridine Systems with a Pendant Alkenyl Group. Part A: Cobalt and Iron Complexes and Their Catalytic Behavior", *Organometallics*, 2008, 27, 6547–6556.

[22] B. L. Small, M. Brookhart, "Polymerization of Propylene by a New Generation of Iron Catalysts: Mechanisms of Chain Initiation, Propagation, and Termination", *Macromolecules*, 1999, 32, 2120–2130.

[23] F. A. R. Kaul, G. T. Puchta, G. D. Frey, E. Herdtweck, W. A. Herrmann, "Iminopyridine Complexes of 3d Metals for Ethylene Polymerization: Comparative Structural Studies and Ligand Size Controlled Chain Termination", *Organometallics*, 2007, 26, 988–999.

[24] L. Guo, H. Gao, L. Zhang, F. Zhu, Q. Wu, "An Unsymmetrical Iron(II) Bis(imino)pyridyl Catalyst for Ethylene Polymerization: Effect of a Bulky Ortho Substituent on the Thermostability and Molecular Weight of Polyethylene", *Organometallics*, 2010, 29, 2118–2125.

[25] J. Yu, H. Liu, W. Zhang, X. Hao, W.-H. Sun, “Access to highly active and thermally stable iron procatalysts using bulky 2-[1-(2,6-dibenzhydryl-4-methylphenylimino)ethyl]-6-[1-(arylimino)ethyl]pyridine ligands”, *Chem. Commun.*, 2011, 47, 3257–3259.

[26] W.-H. Sun, W. Zhao, J. Yu, W. Zhang, X. Hao, C. Redshaw, “Enhancing the Activity and Thermal Stability of Iron Precatalysts Using 2-(1-2,6-bis[bis(4-fluorophenyl)methyl]-4-methylphenyliminoethyl)-6-[1-(arylimino) ethyl]pyridines”, *Macromol. Chem. Phys.*, 20112, 213, 1266–1273.

[27] X. Cao, F. He, W. Zhao, Z. Cai, X. Hao, T. Shiono, C. Redshaw, W.-H. Sun, “2-[1-(2,6-Dibenzhydryl-4-chlorophenylimino)ethyl]-6-[1-(arylimino)ethyl]pyridyliron(II) dichlorides: Synthesis, characterization and ethylene polymerization behavior”, *Polymer*, 2012, 53, 1870–1880.

[28] S. Wang, B. Li, T. Liang, C. Redshaw, Y. Li, W.-H. Sun, “Synthesis, characterization and catalytic behavior toward ethylene of 2-[1-(4,6-dimethyl-2-benzhydrylphenylimino)ethyl]-6-[1-(arylimino)ethyl]pyridylmetal (iron or cobalt) chlorides”, *Dalton Trans.*, 2013, 42, 9188–9197.

[29] W. Zhang, W. Chai, W.-H. Sun, X. Hu, C. Redshaw, X. Hao, “2-(1-(Arylimino)ethyl)-8-arylimino-5,6,7-trihydroquinoline Iron(II) Chloride Complexes: Synthesis, Characterization, and Ethylene Polymerization Behavior”, *Organometallics*, 2012, 31, 5039–5048.

[30] B. L. Small, M. Brookhart, “Iron-Based Catalysts with Exceptionally High Activities and Selectivities for Oligomerization of Ethylene to Linear α-Olefins”, *J. Am. Chem. Soc.*, 1998, 120, 7143–7144.

[31] G. J. P. Britovsek, V. C. Gibson, S. J. McTavish, G. A. Solan, A. J. P. White, D. J. Williams, G. J. P. Britovsek, B. S. Kimberley, P. J. Maddox, “Novel olefin

polymerization catalysts based on iron and cobalt", *Chem. Commun.*, 1998, 7, 849–850.

[32] G. J. P. Britovsek, M. Bruce, V. C. Gibson, B. S. Kimberley, P. J. Maddox, S. Mastroianni, S. J. McTavish, C. Redshaw, G. A. Solan, S. Strömberg, A. J. P. White, D. J. Williams, "Iron and Cobalt Ethylene Polymerization Catalysts Bearing 2,6-Bis(Imino)Pyridyl Ligands: Synthesis, Structures, and Polymerization Studies", *J. Am. Chem. Soc.*, 1999, 121, 8728–8740.

[33] G. J. P. Britovsek, V. C. Gibson, D. F. Wass, "The Search for New-Generation Olefin Polymerization Catalysts: Life beyond Metallocenes", *Angew. Chem. Int. Ed.*, 1999, 38, 428–447.

[34] V. C. Gibson, S. K. Spitzmesser, "Advances in Non-Metallocene Olefin Polymerization Catalysis", 2003, 103, 283–315.

[35] G. J. P. Britovsek, S. Mastroianni, G. A. Solan, S. P. D. Baugh, C. Redshaw, V. C. Gibson, A. J. P. White, D. J. Williams, M. R. J. Elsegood, "Oligomerisation of Ethylene by Bis(imino)pyridyliron and -cobalt Complexes", *Chem. Eur. J.*, 2000, 6, 2221–2231.

[36] K. V. Singh, R. R. Pandey, X. Wang, R. Lake, C. S. Ozkan, K. Wang, M. Ozkan, "Covalent functionalization of single walled carbon nanotubes with peptide nucleic acid: Nanocomponents for molecular level electronics", *Carbon*, 2006, 44, 1730–1739.

[37] O. O. Ogunro, X.-Q. Wang, "Charge transfer in the non-covalent functionalization of carbon nanotubes", *New J. Chem.*, 2010, 34, 1084–1088.

[38] A. K. Manna, S. K. Pati, "Doping single-walled carbon nanotubes through molecular charge-transfer: a theoretical study", *Nanoscale*, 2010, 2, 1190.

[39] L. Zhang, E. Yue, B. Liu, P. Serp, C. Redshaw, W.-H. Sun, J. Durand,

"Beneficial influence of nanocarbon on the aryliminopyridylnickel chloride catalyzed ethylene polymerization", *Catal. Commun.*, 2014, 43, 227–230.

[40] X. Tong, C. Liu, H.-M. Cheng, H. Zhao, F. Yang, X. Zhang, "Surface modification of single-walled carbon nanotubes with polyethylene *via* in situ Ziegler–Natta polymerization", *J. Appl. Polym. Sci.*, 2004, 92, 3697–3700.

[41] B. M. Amoli, S. A. A. Ramazani, H. Izadi, "Preparation of ultrahigh-molecular-weight polyethylene/carbon nanotube nanocomposites with a Ziegler–Natta catalytic system and investigation of their thermal and mechanical properties", *J. Appl. Polym. Sci.*, 2012, 125, E453–E461.

[42] M. Trujillo, M. L. Arnal, A. J. Müller, E. Laredo, S. Bredeau, D. Bonduel, P. Dubois, "Thermal and Morphological Characterization of Nanocomposites Prepared by *in-Situ* Polymerization of High-Density Polyethylene on Carbon Nanotubes", *Macromolecules*, 2007, 40, 6268–6276.

[43] S. Li, H. Chen, D. Cui, J. Li, Z. Zhang, Y. Wang, T. Tang, "Structure and properties of multi-walled carbon nanotubes/polyethylene nanocomposites synthesized by in situ polymerization with supported Cp_2ZrCl_2 catalyst", *Polym. Compos.*, 2010, 31, 507–515.

[44] M. J. Go, S. H. Kim, K. M. Lee, H. H. Lee, H.-R. Park, J. Lee, S. Park, I. S. Choi, Y. Kim, "*In-situ* generation of a well-dispersed multiwall carbon nanotube/syndiotactic polystyrene composite using pentamethylcyclopentadienyltitanium trimethoxide anchored to multiwall carbon nanotubes", *Polymer*, 2012, 53, 933–938.

[45] E. D. Laird, C. Y. Li, "Structure and Morphology Control in Crystalline Polymer–Carbon Nanotube Nanocomposites", *Macromolecules*, 2013, 46, 2877–2891.

Chapter 4: Nickel complexes behavior in ethylene polymerization in the presence of nanocarbons (MWCNTs or FLG)

4.1 Introduction

Carbon nanotubes and graphene are two typical representatives of the carbon nanomaterial family, which offers an unparalleled flexibility for tailoring catalysts repertories to special needs, due to their uniform carbon made surface and porous structure [1-2]. Due to their unique physical and chemical properties, CNTs [3] have widely been used since their emergence in 1991 [4] and shown to exhibit various bonding modes [5-8] and influence the behavior of the resultant complex system [9-16]. Within the family of carbon nanomaterials, graphene is another emerging class of material that has been intensively studied since its direct observation and characterization reported in 2004 [17]. Graphene, a one-atom-thick planar sheet of sp^2 hybridized carbon [17], has similar properties with CNTs and every functionalization and dispersion approach applicable to CNTs can also be applied to graphene. Therefore, graphene has emerged as a promising new nanomaterial for a variety of potential applications, including electronic devices, as energy-storage materials, in chemical-bio-sensors and for bio-medical application [18-22]. Moreover, graphene has been successfully used as catalyst [23-24] or as support in catalytic reaction [25-26]. Similarly to CNTs, excellent electrical and thermal conductivity [27] (~5000 W/(s.m), even higher than CNTs) and mechanical properties made that graphene was used as nanofiller in composites [24, 28]. In addition, single-layer graphene which offer a high surface area [18, 21] (2630 m^2/g) for the dispersion of the catalytic phases has been used as support to immobilize ethylene polymerization catalysts [29-30]. Cr-based single-site catalysts were supported on graphene, and high molecular weight polyethylenes were produced by the graphene immobilization catalysts [29]. Classic ethylene polymerization catalysts (Cp_2MCl_2, M = Zr, Ti) were also supported by

graphene through π-π interactions and successfully used as catalysts in ethylene polymerization process [30].

Since the discovery that α-diiminonickel complexes were found to be highly active pre-catalysts for ethylene polymerization [31], extensive studies have been conducted on such systems [32-38]. It is reported that the modification of existing ligand sets is necessary to finely tune the catalytic behavior of their metal complex pre-catalysts in ethylene polymerization. Moreover, different types of aromatic groups, such as pyrene [10, 12, 39-42], anthracene [43-44], naphthalene [42, 45] and cyclopentadienyl [46], are reported to be immobilized onto the surface of CNTs *via* noncovalent bonds. Therefore, the catalysts having those common aromatic frameworks could be considered to potentially provide the π-π interactions with the CNTs and have a further inference in their activity. In order to extend the properties and to create hybrids of polyethylene, the influence of aryl groups based on naphthalene, anthracene and pyrene in the 2-iminopyridylnickel and *N*-(5,6,7-trihydroquinolin-8-ylidene)arylaminenickel complex pre-catalysts have been considered with particular focus on their slightly different interactions with MWCNTs and FLG. Their influence was reflected by the catalytic behavior of the nickel complexes. All the nickel complexes performed well for ethylene polymerization, and additionally, a positive influence in relation with the presence of MWCNTs or FLG was observed. The catalytic performances and reaction parameters of the nickel complex pre-catalysts during ethylene polymerization were explored and are discussed in detail.

4.2 Results and discussion

4.2.1 Synthesis and characterization of ligands and their nickel complexes

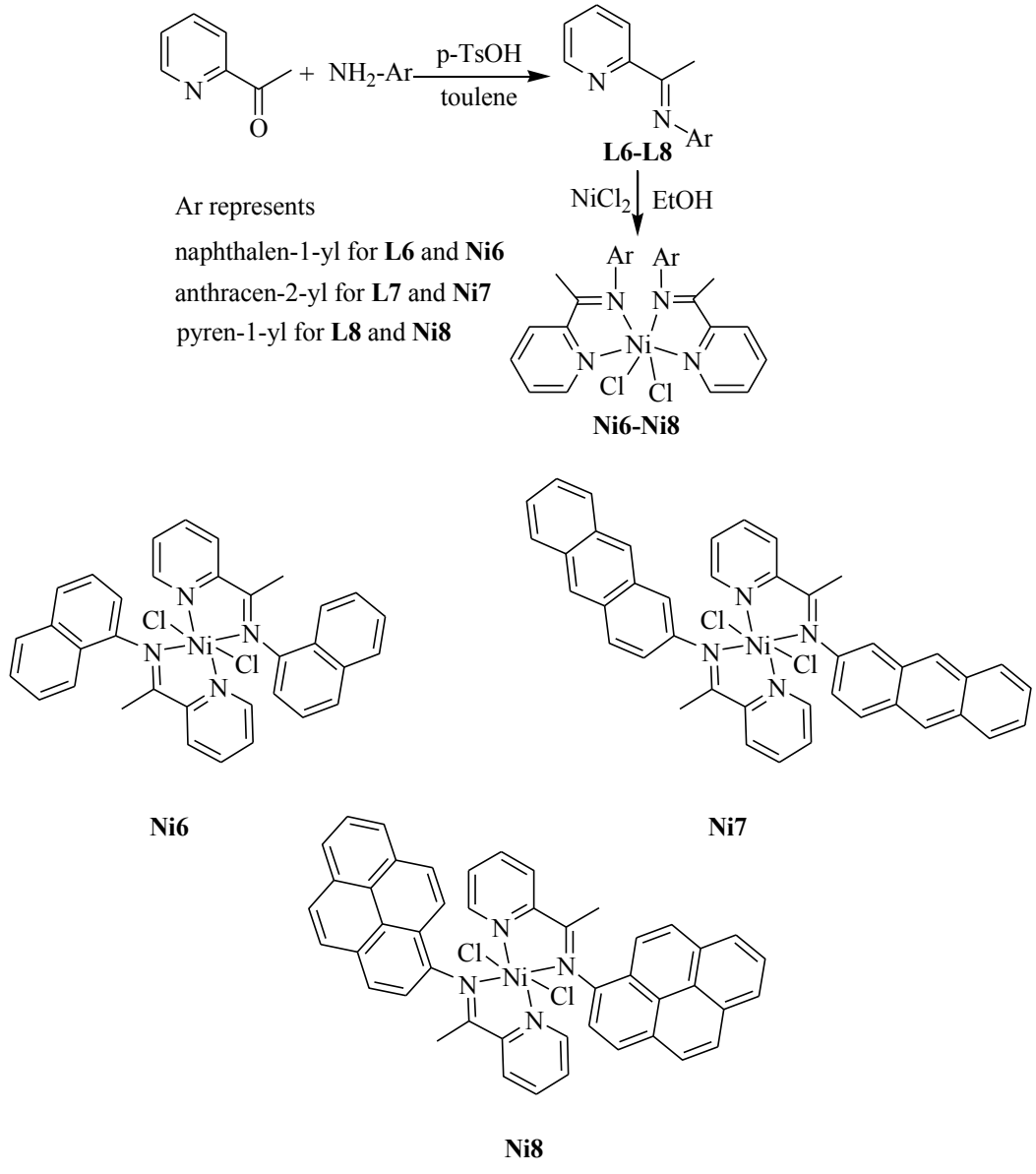

Scheme 4.1 Synthetic procedure of ligands **L6**–**L8** and nickel complexes **Ni6**–**Ni8**.

By employing established synthetic procedures [34, 36-37], the condensation

reaction of 2-acetylpyridine with three different aromatic amines in toluene provided the corresponding 2-imino-ethylpyridines (**L6**–**L8**) (Scheme 4.1). All of the ligands are yellow solids, and were fully characterized by FT-IR, ^{1}H-NMR and ^{13}C-NMR spectroscopy. The nickel complexes (**Ni6**–**Ni8**) were prepared by combining $NiCl_2 \cdot 6H_2O$ with two equivalents of the corresponding ligand in ethanol, and stirring at room temperature for 6 h (Scheme 4.1). Complexes (**Ni6**–**Ni8**) were isolated as air-stable powders in high yield (> 80%). On comparison with the IR spectra of the free ligands, the *v* C=N stretching vibrations in complexes **Ni6**–**Ni8** are shifted to lower frequencies (around 1598–1600 cm^{-1}), indicative of an effective coordination interaction between the amino nitrogen atom and the nickel center. The molecular structures of complexes **Ni6** and **Ni8** were further confirmed by single-crystal X-ray diffraction studies (see Section 4.2.2).

Ligands **L9**–**L13** were synthesized by reaction of 5,6,7-trihydroquinolin-8-one with the corresponding aniline in toluene (Scheme 4.2). As detailed before for analogous ligand sets[34, 37-38], **L9**–**L11** are a mixture of isomers with a ratio of the major and the minor of 5:1. Unlike for **L9**–**L11**, the quinoline group ligands **L12** and **L13** are obtained as a unique isomer due to the electron-withdrawing N atom in the quinoline ring. Similar phenomena were investigated and discussed before [34]. Interestingly, **L12** and **L13** showed a different structure. Due to the different position of the N atom on the quinoline ring, ligand **L12** produced by 5,6,7-trihydroquinolin-8-one and 5-amino-quinoline shows a structure with the enolization of the imine (like the minor structure of the ligands **L9**–**L11**, Scheme 4.2). However, only the sp^2-*N* (imine bond C=N) exists in ligand **L13**. The nickel complexes (**Ni9**–**Ni13**) were obtained by blending $NiCl_2 \cdot 6H_2O$ with one equivalent of the corresponding ligand in ethanol, and stirring at room temperature for 6h (Scheme

4.2). All these complexes were isolated as air-stable powders in high yields.

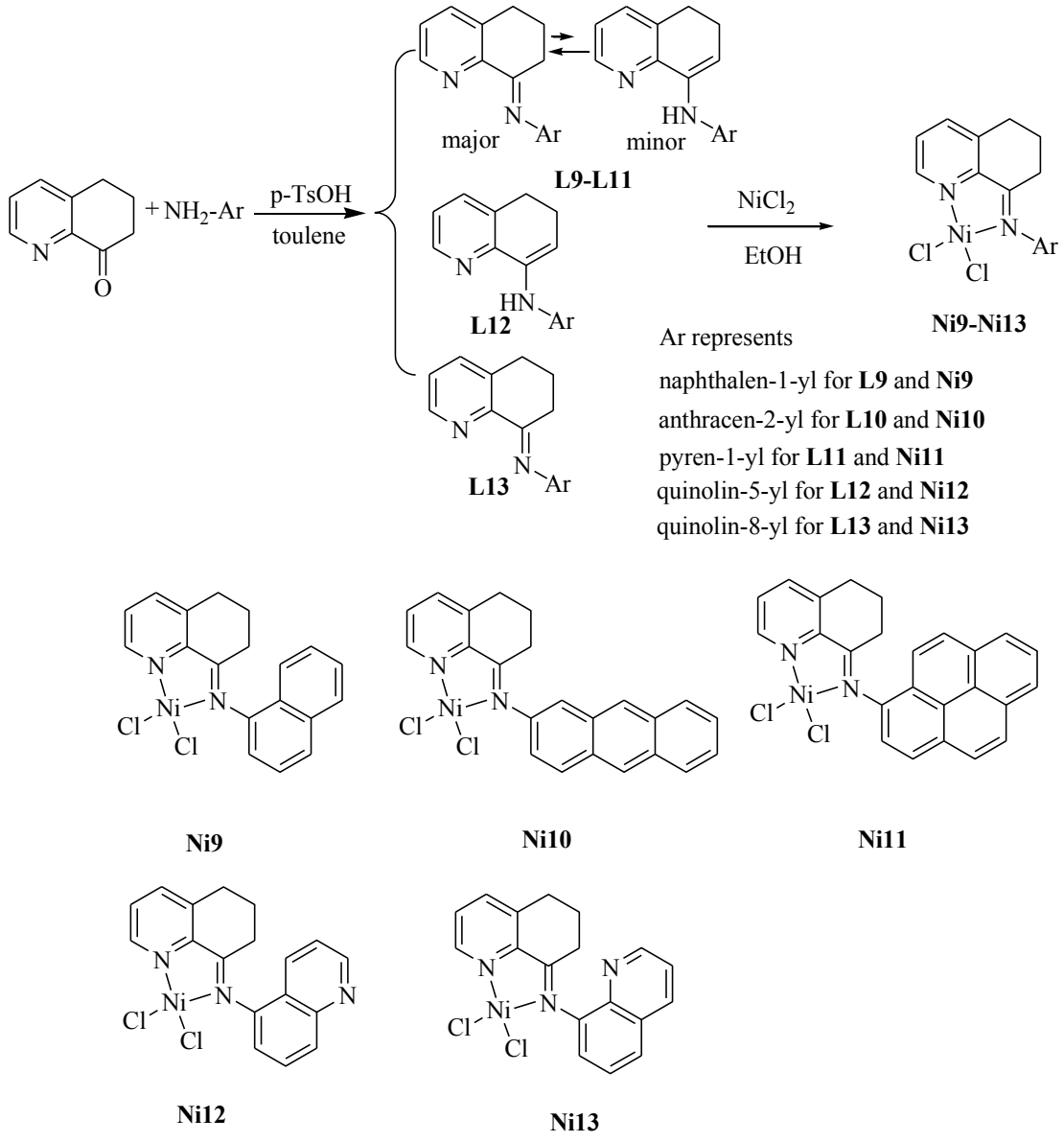

Scheme 4.2 Synthetic procedure of ligands **L9**–**L13** and nickel complexes **Ni9**–**Ni13**.

4.2.2 Molecular structures

Crystals of complexes **Ni6** and **Ni8** suitable for single crystal X-ray analysis were grown by laying diethyl ether onto their methanol solutions at room temperature.

As revealed by the molecular structure of **Ni6** (Figure 4.1), the nickel center was surrounded by two bidentate ligands and two chlorides to afford a distorted octahedral geometry around the metal center. The nickel atom deviates by 0.0182 Å from the equatorial plane, which contains N2, N4, Cl1 and Cl2. This equatorial plane and the plane formed by N1, N3 and Ni1 are almost perpendicular with a dihedral angle of 95.9°. The dihedral angle comprising the pyridine ring of one ligand and the amino-naphthalene ring of another ligand is 24.9°. However, the dihedral angle comprising the pyridine ring of the ligand and the amino-naphthalene ring belonging to the same ligand is 77.9°. Additionally, the distance between the pyridine ring of one ligand and the amino-naphthalene ring of the other ligand is 3.5972 Å, indicating the effective π-π interactions induced by the naphthalene ring. Considering the bond lengths around the nickel center, the Ni1–Cl2 (2.3724(9) Å is shorter than the bond of Ni1–Cl1 (2.4356(9) Å), whilst the bond length of Ni1–N1 (pyridine) is 2.067(2) Å and Ni–N2 (imino) is 2.135(2) Å.

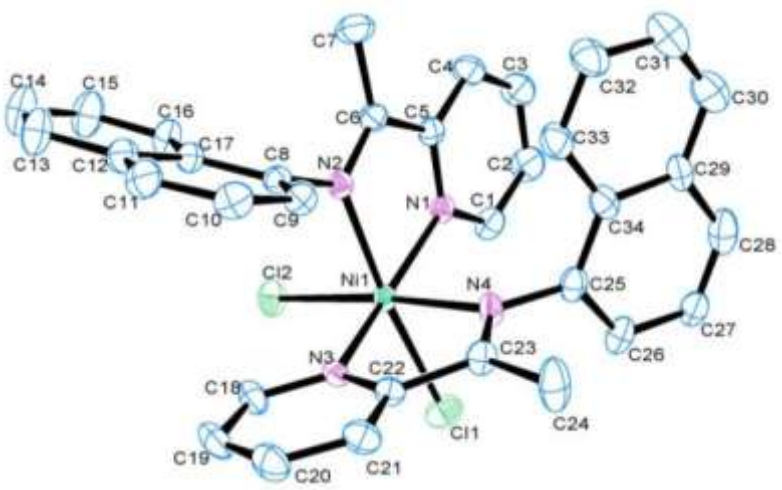

Figure 4.1 ORTEP molecular structure of **Ni6**. Thermal ellipsoids are shown at 30 % probability. Hydrogen atoms and solvent molecules have been omitted for clarity. Selected bond lengths (Å) and angles (°): Ni1−N1 = 2.067(2); Ni1−N2 =

2.135(3); Ni1−N3 = 2.065(2); Ni1−N4 = 2.129(3); Ni1−Cl1 = 2.4356(9); Ni1−Cl2 = 2.3724(9); N2−C6 = 1.293(4); N4−C23 = 1.278(4). N1−Ni1−N2 = 77.50(10); N1−Ni1−N3 = 164.09(10); N1−Ni1−N4 = 91.34(10); N2−Ni1−N3 = 91.80(10); N2−Ni1−N4 = 93.14(10); N3−Ni1−N4 = 77.37(10); N1−Ni1−Cl1 = 96.53(8); N2−Ni1−Cl1 = 173.83(7); N3−Ni1−Cl1 = 93.72(7); N4−Ni1−Cl1 = 85.40(8); N1−Ni1−Cl2 = 93.28(7); N2−Ni1−Cl2 = 90.28(7); N3−Ni1−Cl2 = 98.57(7); N4−Ni1−Cl2 = 174.76(8); Cl1−Ni1−Cl2 = 91.61(3).

The molecular structure of **Ni8** (Figure 4.2) comprises a dimer in which the two nickel centers are linked by two bridging chloride atoms. There is no direct bonding between two nickel atoms, for which the intra-molecular distance is 3.575 Å, which is slightly longer than that observed in other iminopyridylnickel dimers (3.475 Å) [35]. Similar to **Ni6**, the Ni centres of **Ni8** are also bound by two bi-dentate ligands, with Ni–N (belonging to the pyridine ring) bond lengths similar to those of **Ni6**. However, the Ni–N bond lengths (belonging to the amino ring) of the **Ni8** are quite different from **Ni6**. Also, Ni–N2 (2.099(3) Å) and Ni–N4 (2.083(3) Å) are shorter than for **Ni6**. Moreover, the distance between the pyridine ring of one ligand and the amino-pyrene ring of the other ligand is 3.3767 Å, showing that the π-π interactions induced by the pyrene ring in **Ni8** are stronger than that of naphthalene ring in **Ni6**. This could be considered in terms of the increased potential of the **Ni8** for effective immobilization on MWCNTs or FLG through π-π interactions. The X-ray structure detail of complexes **Ni6** and **Ni8** determinations and refinement is provided in Table 4.1.

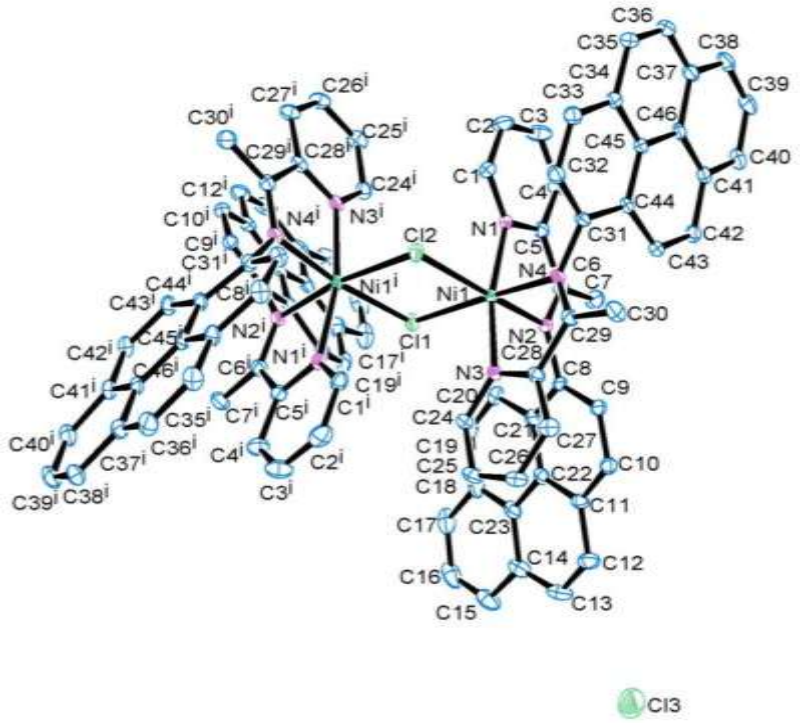

Figure 4.2 ORTEP molecular structure of **Ni8**. Thermal ellipsoids are shown at 30 % probability. Hydrogen atoms and solvent molecules have been omitted for clarity. Selected bond lengths (Å) and angles (°): Ni1−N1 = 2.066(2); Ni1−N2 = 2.099(3); Ni1−N3 = 2.062(2); Ni1−N4 = 2.083(3); Ni1−Cl1 = 2.4093(8); Ni1−Cl2 = 2.4546(8); N2−C6 = 1.282(4); N4−C29 = 1.280(4). N1−Ni1−N2 = 78.43(10); N1−Ni1−N3 = 168.06(9); N1−Ni1−N4 = 93.02(9); N2−Ni1−N3 = 94.52(9); N2−Ni1−N4 = 96.28(10); N3−Ni1−N4 = 78.05(10); N1−Ni1−Cl1 = 92.95(7); N2−Ni1−Cl1 = 88.61(7); N3−Ni1−Cl1 = 96.54(7); N4−Ni1−Cl1 = 172.94(7); N1−Ni1−Cl2 = 95.71(7); N2−Ni1−Cl2 = 171.38(7); N3−Ni1−Cl2 = 92.28(7); N4−Ni1−Cl2 = 90.29(7); Cl1−Ni1−Cl2 = 85.36(3).

Table 4.1 Crystal data and structure refinement for **Ni6** and **Ni8**

	Ni6	**Ni8**
empirical formula	$C_{34}H_{28}Cl_2N_4Ni$	$C_{46}H_{32}Cl_2N_4Ni$
formula weight	622.19	770.37
T (K)	180(2)	110(2)
wavelength (Å)	0.71073	0.71073
cryst syst	Orthorhombic	Monoclinic
space group	p 21 21 21	C2/c
a (Å)	8.2375(3)	29.0288
b (Å)	14.6511(5)	11.6481
c (Å)	28.2388(10)	28.0664
α (°)	90	90
β (°)	90	97.125(2)
γ (°)	90	90
V (Å^3)	3408.1(2)	9416.8(6)
Z	4	8
*D*calcd. (gcm^{-3})	1.213	1.087
μ (mm^{-1})	0.753	0.557
F(000)	1288	3184
cryst size (mm)	0.28 × 0.26 × 0.16	0.42 × 0.30 × 0.18
θ range (°)	2.57–24.27	1.41–28.15
limiting indices	$-9 \le h \le 9$ $-16 \le k \le 16$ $-32 \le l \le 32$	$-34 \le h \le 38$ $-15 \le k \le 15$ $-37 \le l \le 36$
no. of rflns collected	41120	47554

no. unique rflns [R(int)]	5520(0.0407)	11397
completeness to θ (%)	99.7%	98.6%
data/ restraints/ params	5520 / 0 / 373	11397 / 0 / 479
Goodness of fit on F^2	1.081	1.123
Final R indices [$I>2\sigma(I)$]	R1 = 0.0344	R1 = 0.0701
	wR2 = 0.0882	wR2 = 0.2142
R indices (all data)	R1 = 0.0370	R1 = 0.0877
	wR2 = 0.0897	wR2 = 0.2240
largest diff peak and hole (e Å^{-3})	0.406 and −0.296	1.176 and −2.113

4.2.3 Ethylene polymerization

4.2.3.1 Ethylene polymerization from Ni6–Ni8

Ethylene polymerization catalyzed by these nickel complexes has been investigated at 10 atm ethylene. As shown in Table 4.2, **Ni6** was subjected to a study under different reaction parameters by varying the co-catalyst, the molar ratio of Al/Ni, the temperature and the reaction time. Several alkylaluminium reagents (Et_2AlCl, MAO and MMAO) were initially used to activate complex **Ni6** at 30 °C (Table 4.2, Entries 1, 2, 4). Given the highest activity obtained with the **Ni6**/MAO system (Table 4.2, Entry 4), MAO was employed as the co-catalyst in the subsequent screening of the other nickel complexes. The molar ratio of Al/Ni was found to play an important role on the catalytic performances. On increasing the Al/Ni from 500 to 2500 (Table 4.2, Entries 3−7), the optimum ratio for best activity was Al/Ni = 1500 (Table 4.2, Entry 5). Interestingly, when the Al/Ni = 500 and 1000, the M_w and M_w/M_n values of the polyethylene possessed the same values, suggesting that similar

polyethylene was produced (Table 4.2, Entries 3−4). On using an Al/Ni ratio as high as 1500, the M_w and M_w/M_n values of the obtained polyethylene increase; however, on further increasing the Al/Ni ratio to 2000, the resulting polyethylene has slightly smaller values of M_w and M_w/M_n. Such phenomena are different from other nickel complexes derived from the 2-acetylpyridine, for which the resulting polyethylene showed lower molecular weight but higher polydispersity on increasing the Al/Ni ratio [48-49]. To investigate the influence of the Al/Ni ratio on the degree of branching in the polymer, the branch information of some representative polyethylene was confirmed by ^{13}C NMR spectroscopic analysis (shown in Figure 4.3) [50]. As shown in Table 4.2 (Entries 4−6), the branch number is similar at different Al/Ni ratios.

Table 4.2 Ethylene polymerization with **Ni6**[a]

Entry	Co-cat	Al/Ni	PE (g)	Act[b]	T_m[c] (ºC)	M_w[d] (kg mol^{-1})	M_w/M_n[d]	Branches /1000C[e]
1	Et_2AlCl	200	2.51	1.00	59.77	0.60	1.30	nd
2	MMAO	1000	trace	nd	nd	nd	nd	nd
3	MAO	500	4.78	1.91	63.82	0.60	1.38	nd
4	MAO	1000	6.93	2.77	62.78	0.60	1.38	78.7
5	MAO	1500	7.78	3.11	61.07	0.90	1.74	82.0
6	MAO	2000	5.45	2.18	61.49	0.80	1.56	81.4
7	MAO	2500	4.49	1.80	56.92	0.50	1.39	nd

[a] Reaction conditions: 5 μmol **Ni6**; 30 min; 30 ºC; 10 atm ethylene; 100 mL toluene. [b] 10^6 g (PE)·mol^{-1}(Ni)·h^{-1}. [c] Determined by DSC. [d] Determined by GPC. [e] Determined by ^{13}C NMR.

The catalytic system **Ni6**/MAO was then investigated over different reaction temperatures and the life-time of the nickel complexes was evaluated. Similar to other iminopyridine catalytic systems [51-52], the activity for polymerization decreased sharply when the reaction temperature increased from 30 °C to 50°C (Table 4.3, Entries 1–3), partly due to the instability of the active species at higher temperatures. However, the degree of branching in the PE waxes produced at 40 °C increased sharply [32, 53]. As far as the lifetime of **Ni6** is concerned, it was found that the activity decreased on increasing the reaction time. In addition, the M_w and M_w/M_n values of the polyethylene waxes showed only a slight variation on extending the reaction time, whilst the narrow molecular distributions (1.28−1.94) were indicative of single-site active species. Examination of the ^{13}C NMR spectra indicated that the branch number slightly decreased on prolonging the reaction time (Table 4.3, Entries 1, 4–6)

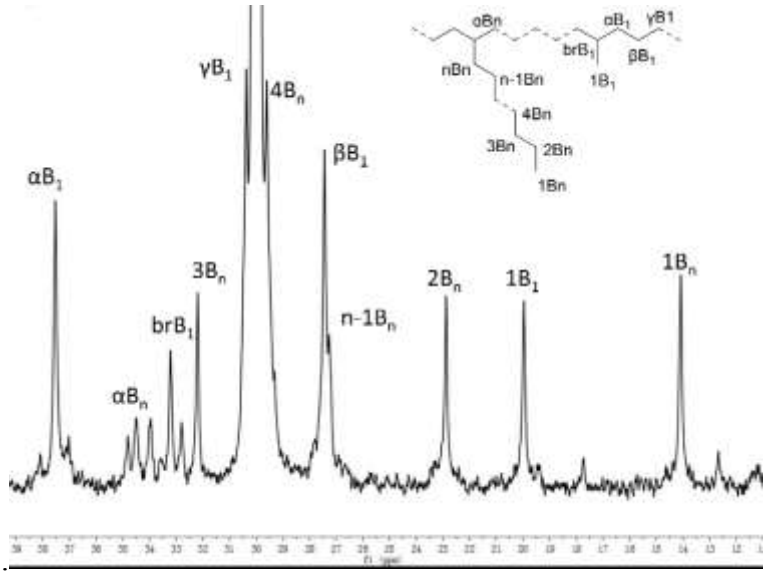

Figure 4.3 ^{13}C-NMR spectrum of the polyethylene prepared using the system **Ni6**/MAO (Table 4.3, Entry 2).

Table 4.3 Ethylene polymerization with **Ni6**/ MAO[a]

Entry	T (ºC)	t (min)	PE (g)	Act[b]	T_m[c] (ºC)	M_w[d] (kg mol^{-1})	M_w/M_n[d]	Branches /1000C[e]
1	30	30	7.78	3.11	61.07	0.90	1.74	82.0
2	40	30	4.72	1.89	60.47	0.60	1.39	191
3	50	30	1.87	0.75	62.04	1.00	1.52	nd
4	30	15	3.91	3.13	57.85	0.50	1.28	87.8
5	30	45	10.13	2.70	60.46	0.80	1.94	76.8
6	30	60	11.64	2.33	62.85	0.80	1.74	62.0

[a] Reaction conditions: 5 μmol **Ni6**; 10 atm ethylene; 100 mL toluene. [b] 10^6 g (PE)·mol^{-1}(Ni)·h^{-1}. [c] Determined by DSC. [d] Determined by GPC. [e] Determined by ^{13}C NMR.

The polymerization behaviour of **Ni7** and **Ni8** were also investigated using MAO as co-catalyst. The optimum Al/Ni ratio for **Ni7** (Table 4.4, Entries 1−3) and **Ni8** (Table 4.4, Entries 5−7) were the same as for **Ni6**. Typically, the higher temperatures also proved to be detrimental to the polymerization activity (Table 4.4, Entry 4 for **Ni7** and Table 4.4, Entry 8 for **Ni8**). Considering the molecular weight and molecular weight distributions, the catalyst system employing **Ni7** was similar to that of **Ni6** with the range of M_w values observed from 0.6 kg mol^{-1} to 0.8 kg mol^{-1} and with M_w/M_n at about 1.4. However, the M_w and M_w/M_n values of the PE waxes obtained *via* the use of **Ni8** were larger than those from the other two catalyst systems.

Table 4.4 Ethylene polymerization with nickel pre-catalysts / MAO[a]

Entry	cat	Al/Ni	T (ºC)	PE (g)	Act[b]	T_m[c] (ºC)	M_w[d] (kg mol^{-1})	M_w/M_n[d]	Branches /1000C[e]
1	**Ni7**	1000	30	0.99	0.40	73.31	0.80	1.49	nd
2	**Ni7**	1500	30	2.29	0.92	71.71	0.70	1.37	76.5
3	**Ni7**	2000	30	1.67	0.67	70.34	0.60	1.37	nd
4	**Ni7**	1500	40	0.93	0.37	67.15	0.70	1.41	87.1
5	**Ni8**	1000	30	6.32	2.53	67.48	1.30	2.03	nd
6	**Ni8**	1500	30	8.54	3.42	64.39	1.50	2.39	55.8
7	**Ni8**	2000	30	7.05	2.82	64.90	1.10	2.10	nd
8	**Ni8**	1500	40	6.03	2.41	65.22	3.10	2.57	64.6

[a] Reaction conditions: 5 μmol; 30 min; 10 atm ethylene; 100 mL toluene. [b] 10^6 g (PE)·mol^{-1}(Ni)·h^{-1}. [c] Determined by DSC. [d] Determined by GPC. [e] Determined by ^{13}C NMR.

4.2.3.2 Ethylene polymerization in the presence of MWCNTs or FLG

The use of either MWCNTs or FLG (Figure 4.4) was studied; each of them was separately added to the reaction mixture. We wanted to evaluate if their good electron conductivity could allow to manage the exothermicity of the reaction, thus providing extended catalyst lifetime.

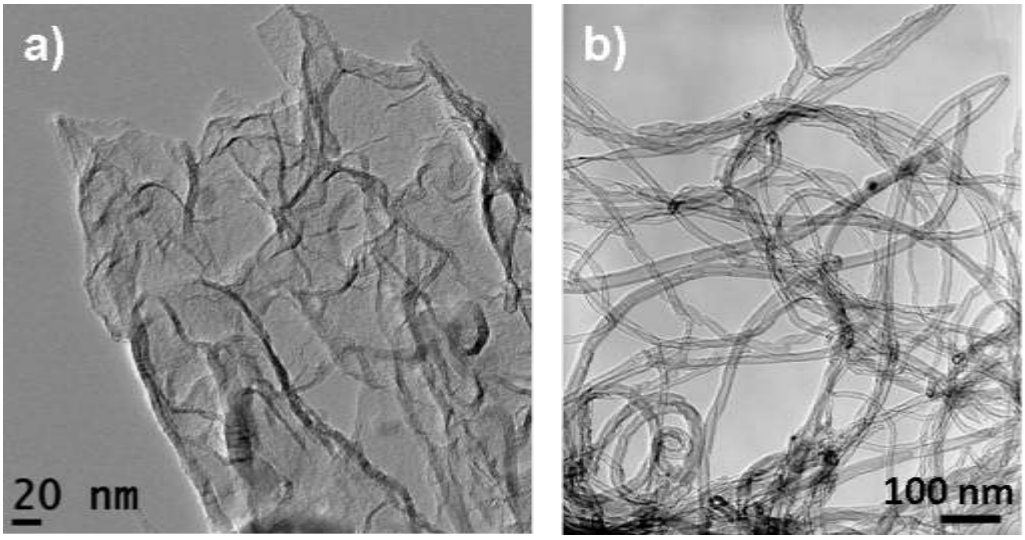

Figure 4.4 TEM micrographs of a) FLG and b) MWCNTs used in this study.

Typically, MAO was used as the co-catalyst to generate the active nickel species. The polymerization reactions were conducted under the conditions Al/Ni = 1500, 30 °C, 30 min and 10 atm ethylene. In the presence of different amounts of MWCNTs, **Ni6** and **Ni8** were studied. As shown in Table 4.5, the MWCNTs produced a contrasted effect on the ethylene polymerization. Indeed, at low MWCNTs content the activity does not change significantly compare to the homogenous catalysts, but the observed activity decreased as the amount of the MWCNTs was raised (Table 4.5, Entries 1−5 for **Ni6** and Entries 6−8 for **Ni8**). However, polyethylene waxes characterization by GPC and ^{13}C NMR spectroscopy analysis indicated that the polyethylene waxes in the presence of the MWCNTs were different from those produced by the nickel systems above. For the **Ni6**/MWCNT/MAO system, the M_w, M_w/M_n and the number of branches were higher than for the polyethylene produced by **Ni6** in the absence of MWCNTs. Similarly, when compared with **Ni8** without MWCNTs, the polyethylene waxes obtained *via* the **Ni8**/MWCNT/MAO system exhibited lower M_w and M_w/M_n values. In general, the catalytic activities of the nickel pre-catalysts decrease in the presence of MWCNTs along with producing

polyethylenes of lower molecular weight and narrower polydispersity, suggesting that there was effective immobilization of the nickel complex on the MWCNTs. These results suggest that the immobilizing support occupied some pathways to slightly decrease the coordination of ethylene on active sites, which will result in the slower propagation reaction for polyethylenes with lower molecular weights. Meanwhile, the immobilized nickel catalysts had a better stability with better controlling active species for the polyethylenes with narrow polydispersity. In addition, the slower propagation reaction with ethylene polymerization favoured its chain transfer reaction, therefore higher branched polyethylenes were obtained.

Table 4.5 Ethylene polymerization with nickel pre-catalysts / MAO in the presence of the MWCNTs [a]

Entry	Cat.	CNT (mg)	PE (g)	Act[b]	T_m[c] (ºC)	M_w[d] (kg mol^{-1})	M_w/M_n[d]	Branches /1000C[e]
1	**Ni6**	-	7.78	3.11	61.07	0.90	1.74	82.0
2	**Ni6**	5	7.96	3.18	58.05	0.90	1.78	86.2
3	**Ni6**	10	6.74	2.70	59.65	0.80	1.65	112
4	**Ni6**	20	5.85	2.34	58.15	0.60	1.45	93
5	**Ni6**	0.04	4.41	1.76	62.85	0.90	1.61	nd
6	**Ni8**	-	8.54	3.42	64.39	1.50	2.39	55.8
7	**Ni8**	5	8.18	3.27	67.78	0.70	1.37	nd
8	**Ni8**	10	7.21	2.88	72.19	1.00	1.78	80.1
9	**Ni8**	20	6.25	2.50	66.91	1.40	2.26	nd

[a] Reaction conditions: 5 μmol Ni; Al/Ni = 1500; 30 min; 30 °C; 10 atm ethylene; 100 mL toluene. [b] 10^6 g (PE)·mol^{-1}(Ni)·h^{-1}. [c] Determined by DSC. [d] Determined by GPC. [e] Determined by ^{13}C

By contrast, the use of FLG was positive in terms of activity for ethylene polymerization. As shown in Table 4.6, using **Ni6**, the best catalyst performance was observed with an amount of graphene at 0.01 g, and the molecular weight observed was 3.00 kg mol^{-1} (Table 4.6, Entry 2). In presence of graphene, the molecular weight of the result PE waxes were in range of 2.40−3.53 kg mol^{-1} (Table 4.6, Entries 1−4), which was higher than that produced by **Ni6** and also **Ni6**/MWCNT. According to the GPC/^{13}C NMR data for the polyethylene waxes, higher branching was produced along

with higher distribution molecular weight. Interestingly, increasing the amount of FLG (from 0.005 g to 0.04 g) led to higher molecular weight and molecular weight distribution. Such phenomenon could probably be interpreted as stabilization of the active sites achieved by the graphene.

Table 4.6 Ethylene polymerization with **Ni6**/ MAO in the presence of FLG [a]

Entry	FLG (g)	PE (g)	Act[b]	T_m[c] (ºC)	M_w[d] (kg mol^{-1})	M_w/M_n[d]	Branches /1000C[e]
1	0.005	9.55	3.82	51.84	3.53	6.95	163.7
2	0.01	10.6	4.22	69.31	3.00	5.41	141.1
3	0.02	8.87	3.55	53.57	2.82	5.02	nd
4	0.04	8.47	3.39	63.39	2.40	4.85	nd

[a] Reaction conditions: 5 μmol **Ni6**; Al/Ni = 1500; 30 min; 30 °C; 10 atm ethylene; 100 mL toluene. [b] 10^6 g (PE)·mol^{-1}(Ni)·h^{-1}. [c] Determined by DSC. [d] Determined by GPC. [e] Determined by ^{13}C NMR.

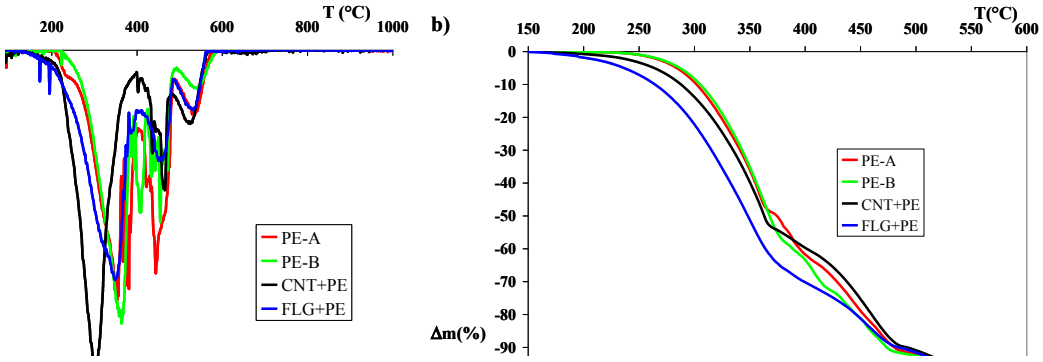

Figure 4.5 TGA curves of PE waxes. a) derivative of the weight loss along with the temperature; b) weight loss along with the temperature.

The quality of the polyethylene waxes produced from the different pre-catalysts can be determined from TGA. As shown in Figure 4.5, the curves for the polyethylene waxes are quite different. The decomposition temperature of the polyethylene waxes made *via* the nickel complexes is around 275 °C. The decomposition temperature of the polyethylene waxes formed in the presence of MWCNTs is around 250 °C, and the polyethylene waxes with FLG start to decompose at 235 °C. However, if MWCNTs are removed from the polyethylene waxes/MWCNT system, the decomposition temperature of the polyethylene waxes returns to 275 °C. This suggests that the presence of nanocarbons can lower the polyethylene wax decomposition temperature. DSC data produced the same results. In order to characterize the polyethylene wax coatings around the nano-carbons, SEM observations have been carried out (Figure 4.6). The polyethylene wax have a regular flower-like shape, as depicted on Figure 4.6-a. The aspect of the PE wax coating on MWCNTs is drastically different (Figure 4.6-b), and it appears that the MWCNTs are well dispersed into the polyethylene waxes. Several MWCNTs make bridges with the polyethylene wax, thus acting as nodes. Since MWCNTs should interact with the nickel pre-catalysts, the ethylene polymerization should operate around the MWCNTs, resulting in an homogeneous dispersion of MWCNTs within the formed polyethylene. For the FLG/ polyethylene wax samples (Figure 4.6-c), it was difficult to visualize the FLG into the polyethylene wax, but no segregation was observed, suggesting there also a homogeneous dispersion. The morphology of the polymer particles is uniform, and different from the previous ones.

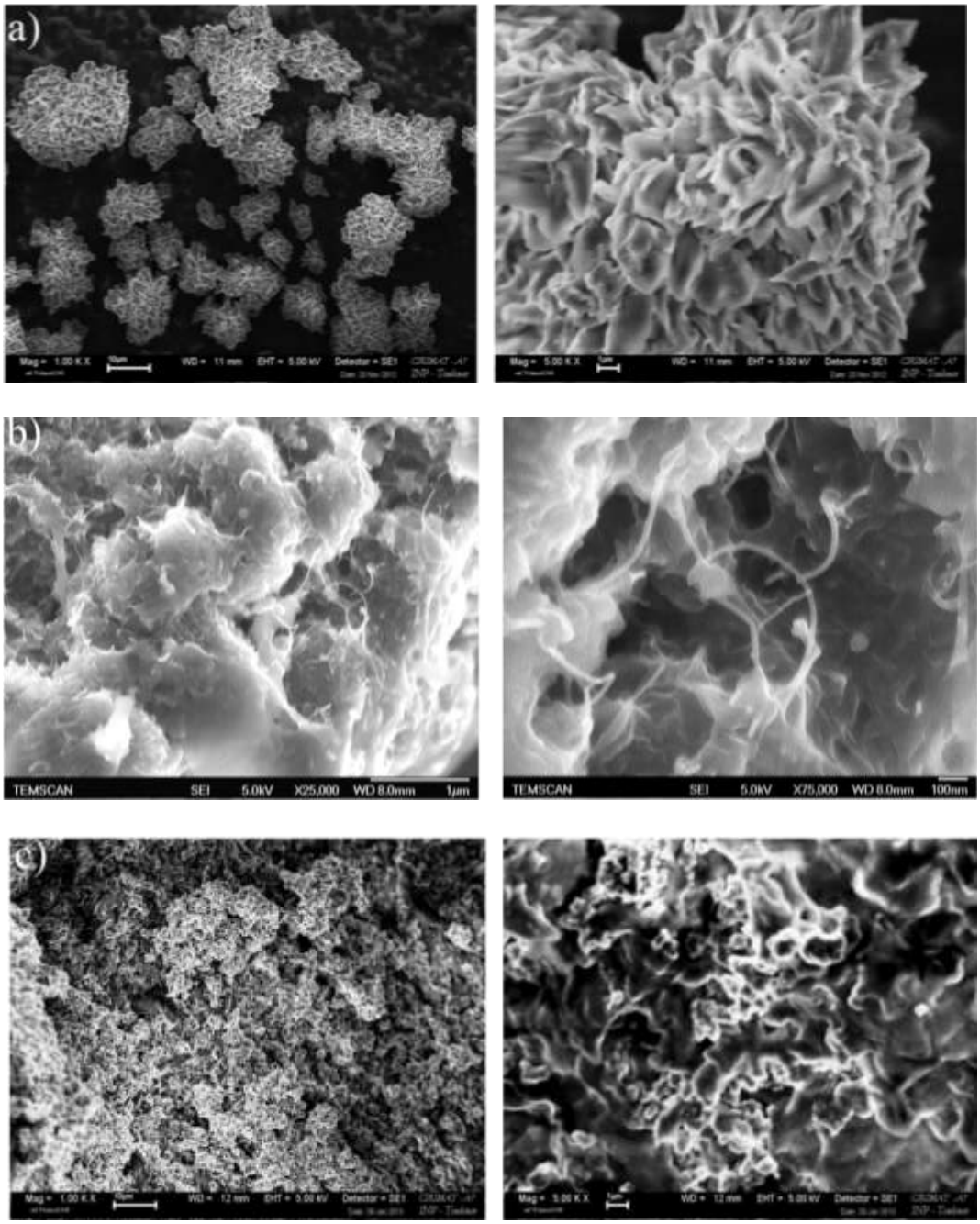

Figure 4.6 SEM images of a) PE wax; b) PE wax with MWCNTs; and c) PE wax with FLG.

4.2.3.3 Ethylene polymerization by Ni9–Ni13

Considering the activity performance of the nickel complexes bearing the 5,6,7-trihydroquinolin-8-imino ligands, we investigated the performances of **Ni9**–**Ni13** with or without nanocarbons for ethylene polymerization process and the detail

of the result are discussed below.

As shown in Table 4.7, pre-catalyst **Ni9** was typically studied using various alkylaluminum reagents such as MAO, MMAO, and Et_2AlCl as co-catalysts in ethylene polymerization (Table 4.7, Entries 1–3). The highest activity was observed by employing MAO as co-catalyst (Table 4.7, Entry 2). So, MAO was selected for further investigation.

Table 4.7 Selection of Suitable Alkylaluminum for activate of **Ni9** [a]

Entry	Co-Cat.	Al/Ni	PE (g)	Act[b]	T_m[c] (ºC)	M_w[d] (kg mol^{-1})	M_w/M_n[d]	Branches /1000C
1	MMAO	1000	1.43	0.57	80.17	1.1	1.63	39[e]
2	MAO	1000	5.12	2.05	78.56	1.1	1.72	54[f]
3	Et_2AlCl	200	0.63	0.25	69.31	0.80	1.48	13[e]

[a] Reaction conditions: 5 μmol; 10 atm ethylene; 30 min; 30 ºC; 100 mL toluene. [b] 10^6 g (PE)·mol^{-1}(Ni)·h^{-1}. [c] Determined by DSC. [d] Determined by GPC. [e] Determined by IR. [f] Determined by ^{13}C NMR.

In order to evaluate the influence of the reaction conditions on the polymerization activity, **Ni9**/MAO system was fully investigated under different reaction conditions, such as Al/Ni ratio, temperature and reaction time. Increasing the Al/Ni from 500 to 2000 (Table 4.8, Entries 1–6), the activities showed the best value with an optimum ratio of 1000 (Table 4.8, Entry 3). The M_w values of the polyethylene formed showed little variation (from 0.8 kg mol^{-1} to 1.2 kg mol^{-1}). Moreover, the M_w/M_n values of the polyethylene which produced under different Al/Ni ratio are closed to 2. This means that catalyst **Ni9** is a single-site active species

catalyst.

Table 4.8 Ethylene polymerization with **Ni9**/MAO system[a]

Entry	Al/Ni	PE (g)	Act[b]	T_m[c] (ºC)	M_w[d] (kg mol^{-1})	M_w/M_n[d]	Branches /1000C
1	500	3.12	1.25	70.78	1.00	1.68	29[e]
2	750	3.43	1.37	70.21	1.10	1.73	26[e]
3	1000	5.12	2.05	78.56	1.10	1.72	54[f]
4	1250	3.87	1.55	78.45	0.80	1.36	20[e]
5	1500	2.83	1.13	67.73	1.20	1.72	25[e]
6	2000	2.52	1.01	63.41	1.00	1.62	-

[a] Reaction conditions: 5 μmol; 30 °C ; 30 min; 10 atm ethylene; 100 mL toluene. [b] 10^6 g (PE)·mol^{-1}(Ni)·h^{-1}. [c] Determined by DSC. [d] Determined by GPC. [e] Determined by IR. [f] Determined by ^{13}C NMR.

Considering the influence of the reaction temperature, the activity decreased sharply with of an increase the temperature from 30 °C to 50 °C (Table 4.9, Entries 1–3). Increasing the reaction temperature, the M_w and M_w/M_n values of the resulting polyethylenes show a slight decrease. The branching of those polyethylenes were also characterized by infrared spectroscopy and ^{13}C NMR and calculated according to the literature methods reported before [50, 54]. As shown in Table 4.9, the branching number of the same polyethylene determined by infrared is lower than by NMR. This is partly because of the quality of the film made for the infrared is an important factor for the calculation. A nice film is difficult to make due to the low molecular weight

polyethylene produced by pre-catalyst **Ni9**. Therefore, the branching number calculated by NMR is more accurate. Moreover, the branching number is highly dependent on the reaction temperature. The highly branched polyethylene is produced at high temperature due to β-hydrogen migration. The same phenomena are also observed for other nickel catalyst system [32, 35, 46, 51, 55]. To understand the lifetime of the active species, trials of **Ni9**/MAO were carried out over different reaction times (Table 4.9, Entries 1, 4–6) under the optimum Ni/Al ratio and temperature. The catalytic activities slowly decreased with prolonged reaction time.

Table 4.9 Selection of other reaction parameters (T and t) for **Ni9**/MAO system[a]

Entry	T (°C)	t (min)	PE (g)	Act[b]	T_m[c] (ºC)	M_w[d] (kg mol^{-1})	M_w/M_n[d]	Branches /1000C
1	30	30	5.12	2.05	78.56	1.10	1.72	54[f]
2	40	30	2.19	0.88	79.12	0.90	1.44	34[e],61[f]
3	50	30	1.23	0.49	87.25	0.90	1.45	-
4	30	15	2.70	2.16	85.60	1.00	1.52	15[e],39[f]
5	30	45	6.61	1.76	91.51	1.00	1.44	20[e],31[f]
6	30	60	6.98	1.40	93.43	1.20	1.59	-
7[g]	30	30	4.37	1.75	75.34	0.90	1.43	7[e],43[f]

[a] Reaction conditions: 5 μmol; 10 atm ethylene; 100 mL toluene. [b] 10^6 g (PE)·mol^{-1}(Ni)·h^{-1}. [c] Determined by DSC. [d] Determined by GPC. [e] Determined by IR. [f] Determined by ^{13}C NMR. [g] 0.01 g MWCNTs.

The influence of MWCNTs on the ethylene polymerization activity of **Ni9** was

investigated by adding 0.01 g of MWCNTs into the polymerization reaction (Table 4.9, Entry 7). MWCNTs were stirred with **Ni9** in toluene before MAO co-catalyst was injected, in order to immobilize the pre-catalyst **Ni9** on the surface of the support. The activity in the presence of MWCNTs is 1.75 × 10^6 g (PE)·mol^{-1}(Ni)·h^{-1}, which is lower than the corresponding reaction without MWCNTs (Table 4.9, Entry 1). The M_w and the M_w/M_n values of the polyethylenes produced in the presence or not of MWCNTs are not changed significantly. However, lower branching number polyethylenes are obtained from the catalytic system with the MWCNTs as support, which are bulky ligands and can increase the barrier of the chain walking [32].

The catalytic performance of the **Ni10** having the anthracene group was studied and showed the same tendency as the **Ni9**/MAO system. Due to the effect of the ligand, the best activity of the **Ni10** (Table 4.10, Entry 3) is higher than that performed by the **Ni9** containing the naphthalene ring (Table 4.8, Entry 3). Lower molecular weight and molecular weight distribution polyethylenes were produced by the Ni10/MAO system. Moreover, the same molecular weight (600 g/mol) polyethylenes were obtained under different Al/Ni ratio and the M_w/M_n values is in the range of 1.30 to 1.47 (Table 4.10, Entries 1–4). Increasing the temperature from 30 °C to 40 °C, the activity decrease from 2.45 to 1.44 × 10^6 g (PE)·mol^{-1}(Ni)·h^{-1} and the M_w value fall down from 600 to 500 g mol^{-1} (Table 4.10, Entries 3, 5).

In the presence of MWCNTs, the activities show a slight increase (Table 4.10, Entries 6–9) and changed with the amount of MWCNTs introduced. The best activity 3.16 × 10^6 g (PE)·mol^{-1}(Ni)·h^{-1} is reached by addition of 10 mg MWCNTs. Similar to the **Ni9**/MAO/MWCNT system, narrow M_w polyethylenes were produced by the **Ni10**/MAO/MWCNT system. However, lower molecular weight polyethylenes were obtained when the MWCNTs were used.

Table 4.10 Ethylene Polymerization with **Ni10** Pre-catalysts / MAO[a]

Entry	Al/Ni	CNT (mg)	T (°C)	PE (g)	Act.[b]	T_m[c] (ºC)	M_w[d] (g mol^{-1})	M_w/M_n[d]	Branches /1000C[e]
1	500	0	30	4.46	1.78	69.23	600	1.41	-
2	750	0	30	4.98	1.99	68.76	600	1.30	-
3	1000	0	30	6.13	2.45	68.97	600	1.47	52
4	1500	0	30	5.17	2.07	66.72	600	1.36	-
5	1000	0	40	3.60	1.44	64.92	500	1.26	-
6	1000	5	30	6.37	2.55	64.09	400	1.34	-
7	1000	10	30	7.89	3.16	71.44	400	1.42	48
8	1000	20	30	6.69	2.67	67.26	400	1.30	51
9	1000	30	30	6.23	2.49	63.78	500	1.46	-

[a] Reaction conditions: 5 μmol; 30 min; 10 atm ethylene; 100 mL toluene. [b] 10^6 g (PE)·mol^{-1}(Ni)·h^{-1}. [c] Determined by DSC. [d] Determined by GPC. [e] Determined by ^{13}C NMR.

Pre-catalyst **Ni11** having the pyrene group has also been investigated in ethylene polymerization. The best activity is shown at the Al/Ni = 1000, which is lower than for **Ni9** and **Ni10**. Upon increasing of the reaction temperature to 40 °C, the catalytic activity decreases from 1.82 (Table 4.11, Entry 2) to 0.63 × 10^6 g (PE)·mol^{-1}(Ni)·h^{-1} (Table 4.11, Entry 4) as well as the M_w/M_n of the polyethylene decreases from 1.1 to 0.8 kg mol^{-1}. Similar phenomena were discussed and attributed to higher reaction temperatures being detrimental to the stability of the active species [38, 53]. However, highly branched polyethylene is produced at 40 °C, due to favoured chain

isomerization at high temperature. This phenomenon was observed in the above mentioned **Ni6**–**Ni8**/MAO systems and other publications [32, 35, 46, 51, 55].

Table 4.11 Ethylene polymerization with **Ni11** Pre-catalysts / MAO[a]

Entry	Al/Ni	T (°C)	PE (g)	Act.[b]	T_m[c] (ºC)	M_w[d] (kg mol^{-1})	M_w/M_n[d]	Branches /1000C[e]
1	500	30	3.89	1.56	91.74	1.10	1.67	-
2	1000	30	4.55	1.82	88.78	1.00	1.46	32.1
3	1500	30	3.01	1.20	102.36	1.30	1.63	32
4	1000	40	1.57	0.63	62.49	0.80	1.34	79.3

[a] Reaction conditions: 5 μmol; 30 min; 10 atm ethylene; 100 mL toluene. [b] 10^6 g (PE)·mol^{-1}(Ni)·h^{-1}. [c] Determined by DSC. [d] Determined by GPC. [e] Determined by ^{13}C NMR.

Two kinds of nanocarbons, MWCNTs and FLG, have been used for the **Ni11**/MAO system. Similar with the **Ni10**/MAO system, the catalytic activity increased in the presence of MWCNTs and the best activity is 2.39 × 10^6 g (PE)·mol^{-1}(Ni)·h^{-1} when 10 mg of MWCNTs were added into the catalytic mixture (Table 4.12, Entry 2). Unlike the **Ni10**/MAO system, **Ni11**/MAO/MWCNT prefers to produce high molecular weight polyethylene. This phenomenon was also reported in some literature articles about group 4 based catalysts immobilized on CNTs [13-14, 16, 56]. At the same time, the melting points and the M_w/M_n values of the polyethylene produced by the **Ni11**/MAO/MWCNT (Table 4.12, Entries 1–4) are higher than that produced by **Ni11**/MAO (Table 4.11).

Under the same conditions, adding 10 mg FLG into the **Ni11**/MAO system, the

activity increased from 1.82 to 3.14 × 10^6 g (PE)·mol^{-1}(Ni)·h^{-1}. Higher amounts of FLG in catalytic system, result in the actvities showing a slight decrease (Table 4.12, Entries 7–8). Unfortunately, the FLG cannot be removed clearly from the resulting polyethylenes. Therfore, the molecular weight and the molecular weight distribution values of the polyethylenes produced by the **Ni11**/MAO/FLG system could not be measured by GPC. However, from the DSC and NMR data, the melting point and the branching number of the results polyethylenes are lower when the support was changed from MWCNTs to FLG.

Table 4.12 Ethylene polymerization with **Ni11**/MAO in the presence of MWCNTs or FLG[a]

Entry	CNT or FLG	(mg)	PE (g)	Act.[b]	T_m[c] (ºC)	M_w[d] (kg mol^{-1})	M_w/M_n[d]	Branches /1000C[e]
1	CNT	5	4.66	1.86	102.90	2.40	2.01	-
2	CNT	10	5.98	2.39	101.24	2.10	2.47	82.1
3	CNT	20	5.37	2.15	104.28	2.80	2.61	-
4	CNT	40	4.74	1.90	103.19	2.70	2.78	-
5	FLG	5	7.15	2.96	102.22	-	-	-
6	FLG	10	7.85	3.14	94.60	-	-	25.9
7	FLG	20	7.54	3.00	99.63	-	-	30.9
8	FLG	40	7.30	2.92	98.17	-	-	-

[a] Reaction conditions: 5 μmol; 30 °C; 30 min; 10 atm ethylene; 100 mL toluene. [b] 10^6 g (PE)·mol^{-1}(Ni)·h^{-1}. [c] Determined by DSC. [d] Determined by GPC. [e] Determined by ^{13}C NMR.

Finally, complexes **Ni12** and **Ni13** with quinoline groups were used as the pre-catalysts for the ethylene polymerization. Using the MAO as the co-catalyst, only traces of polymers were obtained. This suggested that quinoline group is not a good choice to modify the ethylene polymerization catalysts.

4.3 Conclusions

A series of nickel complexes (**Ni6**–**Ni8**) bearing 1-aryliminoethylpyridine ligands have been synthesized and characterized. When activated by MAO, such nickel catalysts exhibit high activities for ethylene polymerization producing polyethylene waxes of low molecular weight and narrow molecular weight distribution. Furthermore, in the presence of either MWCNTs or FLG, the obtained polyethylenes are highly branched. The presence of MWCNTs in the catalytic mixture allows the formation of waxes of lower molecular weight and polydispersity, whereas the presence of FLG proved to be beneficial for the catalytic activity. The SEM observations of the polyethylene waxes produced in the presence of nanocarbons show a homogeneous dispersion of these carbon nanomaterials in the polyethylene matrix.

Complexes **Ni9**–**Ni13** bearing arylimino-(5,6,7-trihydroquinolin-8-ylidene) ligands were efficiently prepared by an optimized and high yield route. These complexes were successfully used as a new catalyst to perform polymerization of ethylene in the presence or not of nanocarbons. The microstructure of the polyethylene and the activities behavior could be controlled and tailor-made by ligand design and the presence of the nanocarbons. The complex **Ni10** bearing the anthracene group shows higher activity than the other complexes **Ni9** and **Ni11**, but produced lower molecular weight polyethylenes. The presence of MWCNTs did not

changed significantly the performances in terms of activity and of resulting polyethylene of the **Ni9** and **Ni10** pre-catalysts. However, the activity of complex **Ni11** is increased and the molecular weight of the resulting polyethylenes is raised when MWCNTs are added into the catalytic mixture. FLG have a positive effect on the catalytic activity of the **Ni11**/MAO system.

4.4 Experimental Section

4.4.1 Synthesis of the ligands L6–L13

2-(1-(1-naphthalenylimino)ethyl)pyridine (**L6**). A mixture of 2-acetylpyridine (2.0 mmol), 1.5 eq. 1-aminonaphtalene (3.0 mmol) and a catalytic amount of *p*-toluenesulfonic acid were refluxed in toluene for 15 h. After the reaction, the black solid was separated by filtration and most of the solvent was removed under reduced pressure, until black–red oil was obtained. Pentane was then added into the solution drop-wise, and the color of the solution changed from black-red to yellow. The yellow solution was transferred to a new flask and kept at 0 ^{o}C for 15 h. 2-(1-(1-naphthalenylimino)ethyl)pyridine (**L6**) was isolated as a yellow precipitate, yield 0.25 g (1.02 mmol, 51 %). FT−IR (KBr, cm^{-1}): 3054, 1642 (C=N), 1585, 1573, 1507, 1466, 1390, 1363, 1300, 1263, 1226, 1104, 1089, 805, 778, 743, 619. ^{1}H NMR (400 MHz, $CDCl_3$, TMS): δ 8.74 (d, *J* = 2.0 Hz, 1H, Py *H*); 8.50 (d, *J* = 4.0 Hz, 1H, Py *H*); 8.87-7.90 (m, 2H, Py *H*); 7.80 (d, *J* = 4.2 Hz, 1H, Ph *H*); 7.65 (d, *J* = 4.2 Hz, 1H, Ph *H*); 7.47-7.52 (m, 3H, Ph *H*); 7.43 (d, *J* = 3.4 Hz, 1H, Ph *H*); 6.84 (d, *J* = 3.2 Hz, 1H, Ph *H*); 2.36 (s, 3H, C*H*$_3$). ^{13}C (100 MHz, $CDCl_3$, TMS): δ 168.4, 156.6, 148.7, 136.5, 128.6, 128.0, 126.4, 126.2, 125.9, 125.5, 125.0, 123.7, 123.5, 121.6, 120.8, 119.0, 16.8. Anal. Calcd for $C_{17}H_{14}N_2$ (246.31): Calcd. C 82.90, H 5.73, N

11.37; Found C 82.58, H 5.85, N 11.56 %.

The yellow solid ligands *2-(1-(2-anthracenylimino)ethyl)pyridine* (**L7**) and *2-(1-(1-pyrenylimino)ethyl)pyridine* (**L8**) were prepared using a similar produce. The yield of the ligand **L7** is 67 %. FT−IR (KBr, cm^{-1}): 3209, 3046, 1624 (C=N), 1584, 1562, 1463, 1430, 1406, 1257, 1140, 1106, 994, 880, 786, 745, 708. ^{1}H NMR (400 MHz, $CDCl_3$, TMS): δ 8.77 (d, *J* = 2.4 Hz, 1H, Py *H*); 8.57 (d, *J* = 2.4 Hz, 1H, Py *H*); 8.20 (s, 1H, Ph *H*); 8.79-7.84 (m, 2H, Py *H*); 7.71 (d, *J* = 3.8 Hz, 1H, Ph *H*); 7.62 (t, *J* = 5.0 Hz, 1H, Ph *H*); 7.51 (t, *J* = 5.0 Hz, 1H, Ph *H*); 7.25-7.30 (m, 2H, Ph *H*); 7.15 (d, *J* = 4.0 Hz, 1H, Ph *H*); 7.05 (d, *J* = 4.0 Hz, 1H, Ph *H*); 6.31 (s, 1H, Ph *H*); 1.79 (s, 3H, C*H*$_3$). ^{13}C (100 MHz, $CDCl_3$, TMS): δ 164.9, 159.8, 149.5, 148.7, 137.7, 135.9, 130.7, 128.9, 128.5, 127.8, 127.7, 126.8, 125.2, 124.0, 123.9, 123.4, 122.0, 121.9, 120.7, 119.4, 29.2. Anal. Calcd for $C_{21}H_{16}N_2$ (296.37): Calcd. C 85.11, H 5.44, N 9.45; Found C 84.83, H 5.57, N 9.60 %.

For the ligand **L8**, the yield is 40 %. FT−IR (KBr, cm^{-1}): 3039, 2963, 1638 (C=N), 1597, 1564, 1512, 1485, 1464, 1433, 1362, 1262, 1226, 1180, 1102, 1019, 880, 857, 710, 678. ^{1}H NMR (400 MHz, $CDCl_3$, TMS): δ 8.77 (d, *J* = 2.4 Hz, 1H, Py *H*); 8.58 (d, *J* = 4.0 Hz, 1H, Ph *H*); 8.14-8.21 (m, 2H, Py *H*); 8.06-8.09 (m, 2H, Ph *H*); 7.99-8.03 (m, 3H, Ph *H*); 7.92 (t, *J* = 1.8 Hz, 1H, Ph *H*); 7.46-7.49 (m, 2H, Ph *H*); 7.41 (d, *J* = 4.0 Hz, 1H, Ph *H*); 2.39 (s, 3H, C*H*$_3$). ^{13}C (100 MHz, $CDCl_3$, TMS): δ 168.9, 156.6, 147.3, 134.9, 126.9, 126.4, 125.4, 124.5, 124.2, 123.8, 123.3, 122.0, 121.9, 119.1, 117.3, 15.1. Anal. Calcd for $C_{23}H_{16}N_2$ (320.39): Calcd. C 86.22, H 5.03, N 8.74; Found 85.92, H, 5.01; N 9.07%.

8-(1-naphthalenylimino)-5,6,7-trihydroquinoline (**L9**). A solution of 5,6,7-trihydroquinolin-8-one (0.45 g, 3 mmol), 1-aminonaphthalene (0.87 g, 4.5 mmol), and a catalytic amount of *p*-toluenesulfonic acid in toluene (50 mL) was

refluxed for 1 h. The colour of the solution was changed from colourless to orange. Most of the solvent was removed under reduced pressure and pentane was added into the solution drop by drop. The yellow solution was transferred to a clean flask and keeps at -20 °C for one night, then the yellow solid was obtained. The yield of the ligand **L9** is 62 %. For combined isomers: FT−IR (KBr, cm^{-1}): 3048, 1697, 1632 (C=N), 1574, 1527, 1496, 1406, 1384, 1283, 1195, 1088, 789, 771, 697. For the major ligand: ^{1}H NMR (400 MHz, $CDCl_3$, TMS): δ 8.81 (d, 1H, *J* = 2.2 Hz, Py H); 7.81-7.87 (m, 2H, Py H, Ph H); 7.60-7.64 (m, 2H, Ph H); 7.44-7.51 (m, 2H, Ph H); 7.41 (d, *J* = 3.6 Hz, 1H, Ph H); 7.37 (m, 1H, *J* = 4.0 Hz, Ph H); 6.87 (d, 1H, *J* = 3.6 Hz, Ph H); 2.98 (t, 2H, *J* = 6.0 Hz, CH_2); 2.55 (t, 2H, *J* = 6.4Hz, CH_2), 1.91-1.95 (m, 2H, CH_2). ^{13}C (100 MHz, $CDCl_3$, TMS): δ 166.3, 149.1, 128.4, 127.9, 126.0, 125.9, 125.8, 125.3, 125.1, 123.9, 123.2, 113.2, 30.6, 29.4, 22.5. For the minor ligand: ^{1}H NMR (400 MHz, $CDCl_3$, TMS): δ 8.47 (d, 1H, *J* = 2.0 Hz, Py H); 8.20 (d, 1H, *J* = 3.4 Hz, Py H); 7.81-7.83 (m, 1H, Py H); 7.65 (d, 1H, *J* = 4.4 Hz, Ph H); 7.44-7.51 (m, 3H, Ph H); 7.33 (d, 1H, *J* = 1.8 Hz, Ph H); 7.16-7.19 (m, 1H, Ph H); 6.81 (d, 1H, *J* = 4.2 Hz, Ph H); 5.65 (t, 1H, *J* = 4.6 Hz, CH); 2.93 (t, 2H, *J* = 8.0 Hz, CH_2); 2.43-2.48 (m, 2H, CH_2). ^{13}C (100 MHz, $CDCl_3$, TMS): δ 150.1, 146.0, 134.9, 134.1, 128.6, 126.3, 125.9, 125.4, 124.9, 122.3, 122.2, 121.9, 120.8, 119.0, 116.5, 101.3, 27.6, 21.5.

8-(2-anthracenylimino)-5,6,7-trihydroquinoline (**L10**)**.** The yellow ligand **L10** was obtained using the same procedure as for the synthesis of **L9** with a yield 73 %. For combined isomers: FT−IR (KBr, cm^{-1}): 3049, 2941, 1690, 1630 (C=N), 1539, 1523, 1462, 1442, 1421, 1329, 1295, 1196, 1113, 883, 801, 740, 619. For the major ligand: ^{1}H NMR (400 MHz, $CDCl_3$, TMS): δ 8.72 (d, 1H, *J* = 4.6Hz, Py H); 8.32 (d, 1H, *J* = 4.6Hz, Py H); 8.24 (s, 1H, Ph); 7.94 (d, 1H, *J* = 3.8Hz, Ph H); 7.91-7.97 (m, 2H, Py, Ph H); 7.65 (d, 1H, *J* = 4.6Hz, Ph H); 7.32-7.44 (m, 5H, Ph H); 3.04 (t, 2H, *J*

= 6.4 Hz, CH_2); 2.83 (t, 2H, *J* = 6.6Hz, CH_2), 2.18-2.25 (m, 2H, CH_2). ^{13}C (100 MHz, $CDCl_3$, TMS): δ 165.5, 149.2, 145.9, 137.6, 135.0, 129.1, 128.2, 127.6, 126.9, 125.9, 125.3, 124.1, 123.7, 122.7, 122.4, 109.4, 39.7, 29.2, 22.7. For the minor ligand: ^{1}H NMR (400 MHz, $CDCl_3$, TMS): δ 8.43 (d, 1H, *J* = 3.0 Hz, Py H); 8.02 (d, 1H, *J* = 4.2 Hz, Py H); 7.81 (s, 1H, Ph H); 7.71 (d, 1H, *J* = 3.0 Hz, Py H); 7.50 (d, 1H, *J* = 3.6 Hz, Ph H); 7.32-7.44 (m, 5H, Ph H);7.15-7.17 (m, 1H, Ph H); 6.16 (t, 1H, *J* = 5.0 Hz, Ph H); 2.97 (t, 2H, *J* = 8.0 Hz, CH_2); 2.56-2.60 (m, 2H, CH_2). ^{13}C (100 MHz, $CDCl_3$, TMS): δ 160.4, 149.1, 137.4, 134.1, 129.0, 127.8, 126.2, 125.5, 125.2, 125.1, 124.8, 122.1, 122.2, 103.1, 29.4, 27.5.

8-(1-pyrenylimino)-5,6,7-trihydroquinoline (**L11**). Using the same procedure as for the synthesis of L9, yellow solid **L11** was obtained. Yield: 61 %. For combined isomers: FT−IR (KBr, cm^{-1}): 3037, 2917, 1634 (C=N), 1600, 1549, 1520, 1488, 1437, 1321, 1289, 1185, 1111, 1019, 835, 817, 798. For the major ligand: ^{1}H NMR (400 MHz, $CDCl_3$, TMS): δ 8.85 (d, *J* = 3.0 Hz, 1H, Py H); 8.18 (d, *J* = 4.2 Hz, 1H, Py H); 8.12-8.15 (m, 2H, Py H, Ph H); 8.05 (d, 1H, *J* = 4.4 Hz, Ph H); 7.98-8.00 (m, 4H, Ph H); 7.66 (d, *J* = 3.6 Hz, 1H, Ph H); 7.51 (d, 1H, *J* = 4.0 Hz, Ph H); 7.41 (t, *J* = 3.8 Hz, 1H, Ph H); 2.97-3.04 (m, 2H, CH_2), 2.53-2.57 (m, 2H, CH_2), 1.91-1.98 (m, 2H, CH_2). ^{13}C (100 MHz, $CDCl_3$, TMS): δ 166.6, 149.2, 146.0, 137.6, 137.4, 131.7, 127.4, 126.7, 126.0, 125.9, 125.7, 125.3, 125.2, 124.6, 124.4, 124.2, 123.2, 121.9, 119.9, 116.7, 31.1, 29.4, 22.4. For the minor ligand: ^{1}H NMR of the minor (400 MHz, $CDCl_3$, TMS): δ 8.72 (d, *J* = 2.2 Hz, 1H, Py H); 8.37 (d, *J* = 4.4 Hz, 1H, Py H); 8.09-8.11 (m, 2H, Py H, Ph H); 8.03-8.09 (d, 1H, *J* = 2.0 Hz, Ph H); 7.92-7.97 (m, 3H, Ph H); 7.83 (d, 1H, *J* = 4.4 Hz, Ph H); 7.53 (d, *J* = 5.2 Hz, 1H, Ph H); 7.38 (d, *J* = 2.2 Hz, 1H, Ph H); 7.20 (t, *J* = 3.8 Hz, 1H, Ph H); 5.71 (t, *J* = 4.8 Hz, 1H, C*H*); 2.81-2.84 (m, 2H, CH_2); 2.19-2.25 (m, 2H, CH_2). ^{13}C (100 MHz, $CDCl_3$, TMS): δ

166.0, 150.1, 146.5, 137.5, 134.9, 131.5, 127.6, 126.9, 126.7, 126.1, 125.9, 125.4, 125.3, 124.5, 124.2, 122.4, 121.9, 120.3, 119.9, 100.6, 29.2, 22.7.

8-(5-quinolinylimino)-5,6,7-trihydroquinoline (**L12**). ^{1}H NMR (400 MHz, $CDCl_3$, TMS): δ 8.49 (d, *J* = 2.2 Hz, 1H, Py *H*); 8.31 (d, *J* = 2.6 Hz, 1H, Py *H*); 7.59 (d, *J* = 3.8 Hz, 1H, Py *H*); 7.47 (t, *J* = 8.4 Hz, 1H, Py *H*); 7.38 (d, *J* = 4.2 Hz, 1H, Py *H*); 7.27-7.31 (m, 2H, Py *H*); 6.71 (d, *J* = 3.8 Hz, 1H, Py *H*); 6.42 (d, *J* = 2.8 Hz, 1H, Py *H*);.3.09 (t, *J* = 7.8 Hz, 2H, CH_2); 2.68 (t, *J* = 8.0 Hz, 2H, CH_2). ^{13}C NMR (100 MHz, $CDCl_3$, TMS): 152.4, 150.3, 146.9, 145.8, 142.9, 138.3, 135.8, 135.7, 132.4, 130.3, 124.1, 122.0, 116.6, 109.6, 104.9, 103.3, 26.2, 19.9. FT−IR (KBr, cm^{-1}): 2919, 1605, 1575, 1543, 1407, 1345, 1286, 1174, 1122, 1095, 862, 787, 764, 660.

8-(8-quinolinylimino)-5,6,7-trihydroquinoline (**L13**)**.**^{1}H NMR (400 MHz, $CDCl_3$, TMS): δ 8.76 (d, *J* = 2.8 Hz, 1H, Py *H*); 8.71 (d, *J* = 2.2 Hz, 1H, Py *H*); 8.07 (d, *J* = 4.8 Hz, 1H, Py *H*); 7.65 (d, *J* = 3.8 Hz, 1H, Py *H*); 7.32-7.40 (m, 3H, Py *H*); 7.15 (d, *J* = 4.0 Hz, 1H, Py *H*); 6.93 (d, *J* = 4.2 Hz, 1H, Py *H*); 3.03 (t, *J* = 6.0 Hz, 2H, CH_2); 2.81 (d, *J* = 6.6 Hz, 2H, CH_2); 2.17-2.24 (m, 2H, CH_2). ^{13}C NMR (400 MHz, $CDCl_3$, TMS): 152.8, 150.4, 149.3, 147.5, 144.3, 140.8, 137.7, 136.2, 129.2, 127.5, 127.1, 121.5, 116.2, 110.2, 106.3, 39.8, 29.3, 22.8.

4.4.2 Synthesis of the nickel complexes

All the nickel complexes were prepared using a similar procedure: $NiCl_2{\cdot}6H_2O$ was reacted with one or two equivalents of the corresponding ligand in ethanol, and was stirred at room temperature for 6 h. The precipitate was collected by filtration, washed several times with diethyl ether, and dried under reduced pressure. The desired complex was obtained as a powder in good yield. All complexes were isolated as air-stable powders and characterized by FT−IR spectroscopy and elemental

analyses.

The complex **Ni6** was isolated as a light green solid with a yield of 83 %. FT−IR (KBr, cm^{-1}): 3047, 1633, 1598, 1573, 1509, 1442, 1391, 1372, 1319, 1265, 1165, 1022, 815,781, 646. Anal. Calcd for $C_{34}H_{28}Cl_2N_4Ni$ (622.21): Calcd. C 65.63, H 4.54, N 9.00; Found C 65.33, H 4.90, N 8.79 %.

The complex **Ni7** was isolated as a brown solid with a yield of 80 %. FT−IR (KBr, cm−1): 3054, 1628, 1600, 1543, 1480, 1439, 1377, 1257, 1163, 1025, 886, 780, 752, 647. Anal. Calcd for $C_{42}H_{32}Cl_2N_4Ni$ (722.33): Calcd. C 69.84, H 4.47, N 7.76; Found 69.55, H 4.29, N 8.04 %.

The yield of the yellow solid **Ni8** was 87 %. FT−IR (KBr, cm^{-1}): 3046, 1626, 1597, 1569, 1441, 1372, 1321, 1257, 1185, 1049, 1021, 849, 784. Anal. Calcd for $C_{46}H_{32}Cl_2N_4Ni$ (770.37): Calcd. C 71.72, H 4.19, N 7.27; Found 71.36, H 3.92, N 7.52 %.

The yield of the red solid **Ni9** was 80 %. FT−IR (KBr, cm^{-1}): 3035, 1631, 1593 (C=N), 1508, 1462, 1392, 1334, 1288, 1216, 1131, 1014, 925, 784. MS-ESI: $C_{19}H_{16}Cl_2N_2Ni$ m/z 402, 403; $(C_{19}H_{16}Cl_2N_2Ni{\cdot}NH_4)^+$ m/z 420.0, 418.0; $C_{19}H_{16}Cl_2N_2NiCl{\cdot}NH_4$ m/z 384.0, 382.0; $C_{19}H_{16}Cl_2N_2Ni{\cdot}HCl$ m/z 367.0, 365.0; $(C_{19}H_{16}Cl_2N_2Ni{\cdot}NH_4)^{2+}$ m/z 347.1.

The yield of the red solid **Ni10** was 78 %. FT−IR (KBr, cm^{-1}): 3033, 2937, 1622, 1588 (C=N), 1531, 1459, 1431, 1352, 1332, 1285, 1217, 1195, 1129, 968, 893, 795, 742. MS-ESI: $C_{23}H_{18}Cl_2N_2Ni$ m/z 452, 454; $(C_{23}H_{18}Cl_2N_2Ni{\cdot}NH_4)^+$ m/z 470.1, 470.2; $(C_{23}H_{18}N_2NiCl)^+$ m/z 415.1, 417.0; $C_{23}H_{18}N_2NiCl{\cdot}NH_4$ m/z 432.0, 434.0.

The yield of the red solid **Ni11** was 71 %. FT−IR (KBr, cm^{-1}): 3036, 2952, 1625, 1587 (C=N), 1502, 1486, 1459, 1353, 1333, 1288, 1217, 1185, 1130, 1116, 932, 850, 796, 771, 713, 682. MS-ESI: $C_{25}H_{18}Cl_2N_2Ni$ m/z 476, 474; $(C_{25}H_{18}Cl_2N_2Ni{\cdot}NH_4)^+$

m/z 494.0, 488.0; $(C_{25}H_{18}N_2NiCl)^+$ m/z 437.0, 435.0.

The yield of the red solid **Ni12** was 77 %. FT−IR (KBr, cm^{-1}): 3199, 2145, 2029, 1611, 1584, 1496, 1467, 1218, 1128, 1083, 837, 801,774, 679.

The yield of the yellow solid **Ni13** was 84 %.FT−IR (KBr, cm^{-1}): 3196, 3130, 1612, 1572, 1550, 1473, 1415, 1376, 1340, 1298, 1220, 1182, 1123, 10885, 1052, 791, 761, 717, 684.

References

[1] P. Serp, M. Corrias, P. Kalck, "Carbon nanotubes and nanofibers in catalysis", *Appl. Catal. A*, 2003, 253, 337-358.

[2] B. F. Machado, P. Serp, "Graphene-based materials for catalysis", *Catal. Sci. Technol.*, 2011, 2, 54-75.

[3] R. H. Baughman, "Carbon Nanotubes-the Route Toward Applications", *Science*, 2002, 297, 787–792.

[4] S. Iijima, "Helical microtubules of graphitic carbon", *Nature*, 1991, 354, 56–58.

[5] E. T. Mickelson, C. B. Huffman, A. G. Rinzler, R. E. Smalley, R. H. Hauge, J. L. Margrave, "Fluorination of single-wall carbon nanotubes", *Chem. Phys. Lett.*, 1998, 296, 188–194.

[6] R. J. Chen, Y. Zhang, D. Wang, H. Dai, "Noncovalent Sidewall Functionalization of Single-Walled Carbon Nanotubes for Protein Immobilization", *J. Am. Chem. Soc.*, 2001, 123, 3838–3839.

[7] E. T. Mickelson, I. W. Chiang, J. L. Zimmerman, P. J. Boul, J. Lozano, J. Liu, R. E. Smalley, R. H. Haug, J. L. Margrave, "Solvation of Fluorinated Single-Wall Carbon Nanotubes in Alcohol Solvents", *J. Phys. Chem. B*, 1999, 103, 4318–4322.

[8] M. Holzinger, O. Vostrowsky, A. Hirsch, F. Hennrich, M. Kappes, R. Weiss, F. Jellen, “Sidewall Functionalization of Carbon Nanotubes”, *Angew. Chem. Int. Ed.*, 2001, 40, 4002–4005.

[9] W. Lu, N. Li, W. Chen, Y. Yao, “The role of multiwalled carbon nanotubes in enhancing the catalytic activity of cobalt tetraaminophthalocyanine for oxidation of conjugated dyes”, *Carbon*, 2009, 47, 3337–3345.

[10] P. D. Tran, A. Le Goff, J. Heidkamp, B. Jousselme, N. Guillet, S. Palacin, H. Dau, M. Fontecave, V. Artero, “Noncovalent Modification of Carbon Nanotubes with Pyrene-Functionalized Nickel Complexes: Carbon Monoxide Tolerant Catalysts for Hydrogen Evolution and Uptake”, *Angew. Chem. Int. Ed.*, 2011, 50, 1371–1374.

[11] G. Liu, B. Wu, J. Zhang, X. Wang, M. Shao, J. Wang, “Controlled Reversible Immobilization of Ru Carbene on Single-Walled Carbon Nanotubes: A New Strategy for Green Catalytic Systems Based on a Solvent Effect on π−π Interaction”, *Inorg. Chem.*, 2009, 48, 2383–2390.

[12] F. J. Gómez, R. J. Chen, D. Wang, R. M. Waymouth, H. Dai, “Ring opening metathesis polymerization on non-covalently functionalized single-walled carbon nanotubes”, *Chem. Commun.*, 2003, 2, 190–191.

[13] Y. Sánchez, C. Albano, A. Karam, R. Perera, E. Casas, “In situ Polymerization of Nanocomposites by $TpTiCl_2(Et)$ System: UHMWPE Filled with Carbon Nanotubes”, *Macromol. Symp.*, 2009, 282, 185–191.

[14] S. Bredeau, L. Boggioni, F. Bertini, I. Tritto, F. Monteverde, M. Alexandre, P. Dubois, “Ethylene–Norbornene Copolymerization by Carbon Nanotube-Supported Metallocene Catalysis: Generation of High-Performance Polyolefinic Nanocomposites”, *Macromol. Rapid Commun.*, 2007, 28, 822–827.

[15] S. Park, S. W. Yoon, H. Choi, J. S. Lee, W. K. Cho, J. Kim, H. J. Park, W. S.

Yun, C. H. Choi, Y. Do, I. S. Choi, “Pristine Multiwalled Carbon Nanotube/Polyethylene Nanocomposites by Immobilized Catalysts”, *Chem. Mater.*, 2008, 20, 4588–4594.

[16] S. Park, S. W. Yoon, K.-B. Lee, D. J. Kim, Y. H. Jung, Y. Do, H. Paik, I. S. Choi, “Carbon Nanotubes as a Ligand in Cp_2ZrCl_2-Based Ethylene Polymerization”, *Macromol. Rapid Commun.*, 2006, 27, 47–50.

[17] K. S. Novoselov, A. K. Geim, S. V. Morozov, D. Jiang, Y. Zhang, S. V. Dubonos, I. V. Grigorieva, A. A. Firsov, “Electric Field Effect in Atomically Thin Carbon Films”, *Science*, 2004, 306, 666–669.

[18] Y. Zhu, S. Murali, W. Cai, X. Li, J. W. Suk, J. R. Potts, R. S. Ruoff, “Graphene and Graphene Oxide: Synthesis, Properties, and Applications”, *Adv. Mater.*, 2010, 22, 3906–3924.

[19] K. P. Loh, Q. Bao, G. Eda, M. Chhowalla, “Graphene oxide as a chemically tunable platform for optical applications”, *Nat. Chem.*, 2010, 2, 1015–1024.

[20] H. Wang, L.-F. Cui, Y. Yang, H. Sanchez Casalongue, J. T. Robinson, Y. Liang, Y. Cui, H. Dai, “Mn_3O_4−Graphene Hybrid as a High-Capacity Anode Material for Lithium Ion Batteries”, *J. Am. Chem. Soc.*, 2010, 132, 13978–13980.

[21] S. Guo, S. Dong, “Graphene nanosheet: synthesis, molecular engineering, thin film, hybrids, and energy and analytical applications”, *Chem. Soc. Rev.*, 2011, 40, 2644–2672.

[22] L.-S. Zhang, L.-Y. Jiang, H.-J. Yan, W. D. Wang, W. Wang, W.-G. Song, Y.-G. Guo, L.-J. Wan, “Mono dispersed SnO_2 nanoparticles on both sides of single layer graphene sheets as anode materials in Li-ion batteries”, *J. Mater. Chem.*, 2010, 20, 5462–5467.

[23] D. R. Dreyer, K. A. Jarvis, P. J. Ferreira, C. W. Bielawski, “Graphite Oxide as

a Dehydrative Polymerization Catalyst: A One-Step Synthesis of Carbon-Reinforced Poly(phenylene methylene) Composites", *Macromolecules*, 2011, 44, 7659–7667.

[24] D. R. Dreyer, H.-P. Jia, C. W. Bielawski, "Graphene Oxide: A Convenient Carbocatalyst for Facilitating Oxidation and Hydration Reactions", *Angew. Chem. Int. Ed.*, 2010, 49, 6813–6816.

[25] I. V. Lightcap, T. H. Kosel, P. V. Kamat, "Anchoring Semiconductor and Metal Nanoparticles on a Two-Dimensional Catalyst Mat. Storing and Shuttling Electrons with Reduced Graphene Oxide", *Nano Lett.*, 2010, 10, 577–583.

[26] G. M. Scheuermann, L. Rumi, P. Steurer, W. Bannwarth, R. Mülhaupt, "Palladium Nanoparticles on Graphite Oxide and Its Functionalized Graphene Derivatives as Highly Active Catalysts for the Suzuki−Miyaura Coupling Reaction", *J. Am. Chem. Soc.*, 2009, 131, 8262–8270.

[27] A. A. Balandin, S. Ghosh, W. Bao, I. Calizo, D. Teweldebrhan, F. Miao, C. N. Lau, "Superior Thermal Conductivity of Single-Layer Graphene", *Nano Lett.*, 2008, 8, 902–907.

[28] S. Park, R. S. Ruoff, "Chemical methods for the production of graphenes", *Nat. Nanotechnol.*, 2009, 4, 217–224.

[29] M. Stürzel, F. Kempe, Y. Thomann, S. Mark, M. Enders, R. Mülhaupt, "Novel Graphene UHMWPE Nanocomposites Prepared by Polymerization Filling Using Single-Site Catalysts Supported on Functionalized Graphene Nanosheet Dispersions", *Macromolecules*, 2012, 45, 6878–6887.

[30] B. Choi, J. Lee, S. Lee, J.-H. Ko, K.-S. Lee, J. Oh, J. Han, Y.-H. Kim, I. S. Choi, S. Park, "Generation of Ultra-High-Molecular-Weight Polyethylene from Metallocenes Immobilized onto N-Doped Graphene Nanoplatelets", *Macromol. Rapid Commun.*, 2013, 34, 533–538.

[31] L. K. Johnson, C. M. Killian, M. Brookhart, “New Pd (II)-and Ni (II)-based catalysts for polymerization of ethylene and. alpha.-olefins”, *J. Am. Chem. Soc.*, 1995, 117, 6414–6415.

[32] S. D. Ittel, L. K. Johnson, M. Brookhart, “Late-Metal Catalysts for Ethylene Homo- and Copolymerization”, *Chem. Rev.*, 2000, 100, 1169–1204.

[33] V. C. Gibson, S. K. Spitzmesser, “Advances in Non-Metallocene Olefin Polymerization Catalysis”, 2003, 103, 283–315.

[34] L. Zhang, X. Hao, W.-H. Sun, C. Redshaw, “Synthesis, Characterization, and Ethylene Polymerization Behavior of 8-(Nitroarylamino)-5,6,7-trihydroquinolylnickel Dichlorides: Influence of the Nitro Group and Impurities on Catalytic Activity”, *ACS Catal.*, 2011, 1, 1213–1220.

[35] H. Liu, W. Zhao, X. Hao, C. Redshaw, W. Huang, W.-H. Sun, “2,6-Dibenzhydryl-N-(2-phenyliminoacenaphthylenylidene)-4-methylbenzenamine Nickel Dibromides: Synthesis, Characterization, and Ethylene Polymerization”, *Organometallics*, 2011, 30, 2418–2424.

[36] X. Hou, Z. Cai, X. Chen, L. Wang, C. Redshaw, W.-H. Sun, “N-(5,6,7-Trihydroquinolin-8-ylidene)-2-benzhydrylbenzenaminonickel halide complexes: synthesis, characterization and catalytic behavior towards ethylene polymerization”, *Dalton Trans.*, 2012, 41, 1617–1623.

[37] J. Yu, X. Hu, Y. Zeng, L. Zhang, C. Ni, X. Hao, W.-H. Sun, “Synthesis, characterisation and ethylene oligomerization behaviour of N-(2-substituted-5,6,7-trihydroquinolin-8-ylidene)arylaminonickel dichlorides”, *New J. Chem.*, 2011, 35, 178.

[38] J. Yu, Y. Zeng, W. Huang, X. Hao, W.-H. Sun, “N-(5,6,7-Trihydroquinolin-8-ylidene)arylaminonickel dichlorides as highly active

single-site pro-catalysts in ethylene polymerization", *Dalton Trans.*, 2011, 40, 8436–8443.

[39] C. Vriamont, M. Devillers, O. Riant, S. Hermans, "Catalysis with Gold Complexes Immobilised on Carbon Nanotubes by π–π Stacking Interactions: Heterogeneous Catalysis versus the Boomerang Effect", *Chem. – Eur. J.*, 2013, 19, 12009–12017.

[40] F. Li, B. Zhang, X. Li, Y. Jiang, L. Chen, Y. Li, L. Sun, "Highly Efficient Oxidation of Water by a Molecular Catalyst Immobilized on Carbon Nanotubes", *Angew. Chem. Int. Ed.*, 2011, 50, 12276–12279.

[41] F. D'Souza, A. S. D. Sandanayaka, O. Ito, "SWNT-Based Supramolecular Nanoarchitectures with Photosensitizing Donor and Acceptor Molecules", *J. Phys. Chem. Lett.*, 20110, 1, 2586–2593.

[42] A. Schaetz, M. Zeltner, W. J. Stark, "Carbon Modifications and Surfaces for Catalytic Organic Transformations", *ACS Catal.*, 2012, 2, 1267–1284.

[43] D. Didier, E. Schulz, "π-Stacking interactions at the service of [Cu]-bis(oxazoline) recycling", *Tetrahedron Asymmetry*, 2013, 24, 769–775.

[44] F. Giroud, S. D. Minteer, "Anthracene-modified pyrenes immobilized on carbon nanotubes for direct electroreduction of O_2 by laccase", *Electrochem. Commun.*, 2013, 34, 157–160.

[45] N. Nakashima, "Solubilization of single-walled carbon nanotubes with condensed aromatic compounds", *Sci. Technol. Adv. Mater.*, 2006, 7, 609.

[46] Z. Zhang, C. H. Turner, "Structural and Electronic Properties of Carbon Nanotubes and Graphenes Functionalized with Cyclopentadienyl–Transition Metal Complexes: A DFT Study", *J. Phys. Chem. C*, 2013, 117, 8758–8766.

[47] T. V. Laine, M. Klinga, M. Leskelä, "Synthesis and X-ray Structures of New

Mononuclear and Dinuclear Diimine Complexes of Late Transition Metals", *Eur. J. Inorg. Chem.*, 1999, 959–964.

[48] S. Zai, H. Gao, Z. Huang, H. Hu, H. Wu, Q. Wu, "Substituent Effects of Pyridine-amine Nickel Catalyst Precursors on Ethylene Polymerization", *ACS Catal.*, 2012, 2, 433–440.

[49] S. Zai, F. Liu, H. Gao, C. Li, G. Zhou, S. Cheng, L. Guo, L. Zhang, F. Zhu, Q. Wu, "Longstanding living polymerization of ethylene: substituent effect on bridging carbon of 2-pyridinemethanamine nickel catalysts", *Chem. Commun.*, 2010, 46, 4321–4323.

[50] T. Usami, S. Takayama, "Identification of Branches in Low-Density Polyethylenes by Fourier Transform Infrared Spectroscopy", *Polym. J.*, 1984, 16, 731–738.

[51] X. Chen, L. Zhang, J. Yu, X. Hao, H. Liu, W.-H. Sun, "Synthesis, characterization and ethylene oligomerization behavior of 2-(chloro-substituted-1H-benzoimidazol-2-yl)-6-(1-aryliminoethyl)pyridylnickel dihalides", *Inorganica Chim. Acta*, 2011, 370, 156–163.

[52] P. Hao, S. Zhang, W.-H. Sun, Q. Shi, S. Adewuyi, X. Lu, P. Li, "Synthesis, Characterization and Ethylene Oligomerization Studies of Nickel Complexes Bearing 2-Benzimidazolylpyridine Derivatives", *Organometallics*, 2007, 26, 2439–2446.

[53] M. M. Wegner, A. K. Ott, B. Rieger, "Gas Phase Polymerization of Ethylene with Supported α-Diimine Nickel(II) Catalysts", *Macromolecules*, 2010, 43, 3624–3633.

[54] G. B. Galland, R. F. de Souza, R. S. Mauler, F. F. Nunes, "^{13}C NMR Determination of the Composition of Linear Low-Density Polyethylene Obtained with [η^3-Methallyl-nickel-diimine]PF_6 Complex", *Macromolecules*, 1999, 32, 1620–

1625.

[55] T. V. Laine, K. Lappalainen, J. Liimatta, E. Aitola, B. Löfgren, M. Leskelä, “Polymerization of ethylene with new diimine complexes of late transition metals”, *Macromol. Rapid Commun.*, 1999, 20, 487–491.

[56] S. Park, I. S. Choi, “Production of Ultrahigh-Molecular-Weight Polyethylene/Pristine MWCNT Composites by Half-Titanocene Catalysts”, *Adv. Mater.*, 2009, 21, 902–905.

Chapter 5: Catalytic isoprene polymerization around iron nanoparticles confined into multi-walled carbon nanotubes

5.1 Introduction

Rubber, a kind of rugged polymer which can be obtained from rubber tree, is popular for packaging and labeling, textiles, plastic parts, stationery, car parts, laboratory equipment, and reusable containers. Interestingly, natural rubber is resistant to many chemical solvents and displays high-performance mechanical properties [1-2]. In particular, it can undergo much more elastic deformations under stress than most materials and still return to its previous size without permanent deformation. Therefore, rubber is preferred to be used in elastomer application and special industry, such as in automotive and aircraft industries for door and window profiles, hoses, belts, matting, flooring and dampeners (anti-vibration mounts). Moreover, in the last few years, the requirement of the rubber has been increased with the rapid industrial development. Polydienes, especially polyisoprene, which can be produced by polymerization of diene monomers have the same molecular structure and properties as natural rubber. It is reported that 15 billion kilograms of rubbers are produced annually and of that amount two thirds is synthetic [3]. Moreover, global revenues will rise to approximately US$56 billion in 2020 [4]. Therefore, dienes polymerization has attracted interest in both academy and industry.

Polymerization of isoprene offers several possible isomeric structures for polyisoprene, such as *trans*-1,4-polyisoprene, *cis*-1,4-polyisoprene, 3,4-polyisoprene and 1,2-polyisoprene (Scheme 5.1) [5-6]. Moreover, *cis*-1,4-polyisoprene has a structure similar to that of the rubber produced from the latex of the rubber trees and the nature of the isomers has a great influence on the properties of resulting materials [7]. Therefore, the selectivity of the polyisoprene catalysts is crucial.

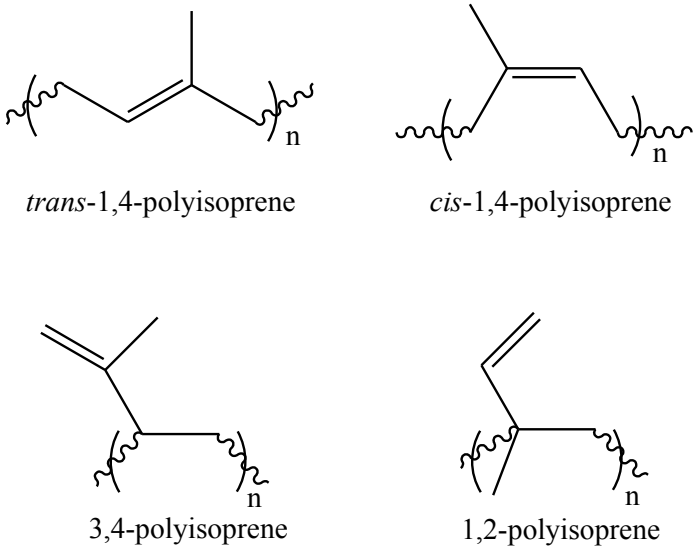

trans-1,4-polyisoprene *cis*-1,4-polyisoprene

3,4-polyisoprene 1,2-polyisoprene

Scheme 5.1 Isomers of the polyisoprene.

Dienes polymerization can be carried out in different ways, such as radical polymerization [8] and cationic polymerization [5, 9-17]. Industrial polydienes are dominated by alkyllithium-based cationic polymerization [5, 9, 18]. Polydienes can also be obtained by combing metal complexes with alkylaluminiums. Catalysts based on titanium catalyzed the butadiene or isoprene polymerization, using MAO as co-catalyst with rather low activity [19-21]. Vanadium-MAO system were reported by Ricci as catalysts for polyisoprene with high selectivity toward *trans*-1,4-polyisoprene [22-23]. Recently, rare earth metal complexes were also investigated as polydienes catalysts and the stereospecific polydienes were obtained through controlling the structure of the ligand [14-17, 24]. Living polymerization of isoprene with a high 3,4-selectivity was reported using rare earth metal complexes bearing fluorenyl N-heterocyclic carbene ligands [15]; the highly *cis*-1,4-selective polymerization of isoprene or butadiene were obtained by the rare earth metal complexes bearing imino ligands [14, 16-17, 24].

Bisiminopyridine late-transition metal complexes are of interest in polymerization since the works of Gibson and Brookhart at the end of last century

[25-27]. Immediately, those kinds of catalysts have been used and investigated in polymerization of dienes. Cobalt catalysts play a very important role in butadiene polymerization. Different microstructure of polybutadiene were produced by cobalt complexes bearing bidentate phosphorus ligands [25, 28-30] and two kinds of polybutadiene; *cis*-1,4-polybutadiene and syndiotactic 1,2-polybutadiene; have been produced on an industrial scale [31]. Iron complexes have been studied in the field of dienes polymerization [5, 10-13, 32-35]. In particular, iron complexes based on the iminopyridine ligand were used for dienes polymerization and performed high activity for 1,3-butadiene [9, 13] and isoprene [5, 9-10, 12, 34-35]. According to those investigations, it is clear that not only the nature of the ligand around the iron center but also the number of ligands present in the coordination sphere can affect both catalytic activity and stereoselectivity [32].

Carbon nanotubes (CNTs) are one of the most intensively studied class of nanomaterials due to their outstanding properties and potential use in a number of high value applications [36]. As mentioned in the previous chapters, CNTs can be considered as an excellent support [37] and can be covalently or non-covalently functionalized to immobilize a wide variety of catalysts. Especially, CNTs have been successfully used and investigated in polymerization reactions [38-42]. It was reported that the presence of CNTs can affect the activity, moreover, a "super-materials" polymer nanocomposites have been produced by this method. Due to the unique properties of CNTs, the obtained composite materials are stronger, stiffer, more thermally conductive, and more electrically conductive than anything that is used today [43-45]. This could be reached by a better control of CNT alignment in the polymer matrix [46-47]. In addition, catalysis utilizing the interior surface of CNTs has been explored recently [48-50]. The CNTs channels are anticipated to provide an

intriguing confinement environment for metal catalysts and catalytic reaction. Besides, functionalized CNTs are emerging as new tools in the field of nanobiotechnology and nanomedicine due to the fact that they can be easily manipulated and modified by encapsulation with biopolymers or by covalent or non-covalent functionalization [51]. Indeed, CNTs have optical, electronic, and mechanical properties that can be exploited in biological or biomedical applications [52]. Such as, CNTs can be used in the field of treatment of the kidney tumors [53] and CNTs are used to delivery drug chage for cancer therapeutics [54] and to bind blood proteins or DNA [55].

On the other hand, metallic magnetic nanoparticles (MMNPs) of the 3d series and their alloys are some of the most important targets in nanoscience research. The long and medium term applications targeted range from ultra-high density magnetic recording [56] to multifunctional magnetic probes and transport media for biomedicine [57], which are domains that hold promises of important innovation and therefore economic impact. Up to now, if iron based magnetic oxides are often preferred [58-60] due to their biocompatibility, MMNPs possess magnetic properties that differentiate them from oxides quantitatively as well as qualitatively: they combine a large magnetization, which guarantees a more efficient response to magnetic field stimuli, and a tunable anisotropy, which may be optimized depending on the target application. Both advantages, if properly exploited, may open new markets [61]. These unique properties, which may significantly deviate from those of their bulk counterparts, can be further tailored by interaction with CNTs in order to meet the demand of novel versatile materials [62]. A major issue in the use of MMNPs in numerous applications is their low biocompatibility coupled with their sensitivity towards oxidation. Many approaches to protect MMNPs from air and water have been reported, including: i) a controlled oxidation of the pure metal core, a

technique long known for the passivation of air sensitive supported catalysts [63]; however, it has been documented that nonmetallic surface layers negatively influence the desired magnetic properties; ii) coating of the metallic core by a noble metal as gold; however, many of the reported metallic shells do not provide sufficient protection of the magnetic core because of non-uniform coating; iii) carbon encapsulation; however this technique requires harsh reaction conditions that can affect MMNPs size; iv) the coating of the metal core with surfactants or polymer [64]; however robust synthetic routes to controllably functionalize high moment/coercivity magnetic colloids remains an important challenge or v) the formation of alloys [65]; however, controlling the composition of magnetic alloy nanoparticles can be difficult when they are produced from two or more precursors.

Recently, confinement effects coming from specific interactions of nanoparticles with the internal walls of CNTs have become the object of a research domain that makes use of CNTs as nanoreactors [49-50]. As part of our continuous effort to develop new synthesis strategies to confined metallic nanoparticles in CNTs and to study confinement effects in these nanostructures [66], we intend to produce air protected and confined iron NPs in CNTs. The CNTs will become the nanoreactors in which we will perform reactions aiming at: i) tuning the structural and magnetic properties of MMNPs, and ii) protecting them from oxidation by an air-barrier polymer coating. These two independent modifications (structure and chemical reactivity) may answer to main drawbacks of the implementation of MMNPs in biological applications such as hyperthermia or transport media for biomedicine. It should also be possible to take advantage of the magnetic properties of the MMNPs confined in CNTs in order to manipulate the CNTs. Indeed, these MMNPs can serve as magnetic “handles” for the alignment of CNTs which could facilitate their

integration in composite materials.

Polyisoprene, a kind of high crosslink material, is a widely used biopolymer in the manufacture of medical products [2] and could be applied in protection of sensitive particles. As part of this strategy, we have therefore developed iron based catalytic systems to promote polyisoprene synthesis. According to the literature reported by the Ritter group [5], iron iminopyridine complexes shown high activity for the isoprene polymerization and produced various high-performance rubbers through effectively controlled polymerization conditions. In this chapter, we report the investigation of iron complexes keeping the iminopyridine framework and introducing polyaromatic groups, which can be immobilized on the surface of particles *via* π-interactions. One of them, $[Fe(C_{17}H_{14}N_2)_2Cl_2]$ was chosen for immobilization on the surface of iron MMNPs (**Cat@NPs**) through π-π interactions. Furthermore, **Cat@NPs@MWCNT** was obtained by confining the **Cat@NPs** into the internal cavity of CNTs. The catalytic properties of **Cat@NPs** and **Cat@NPs@MWCNT** were also explored and are described below. The general synthesis strategy we have followed to produce such multifunctional hybrid nanomaterial combined both molecular and surface chemistry; and is depicted on Scheme 5.2.

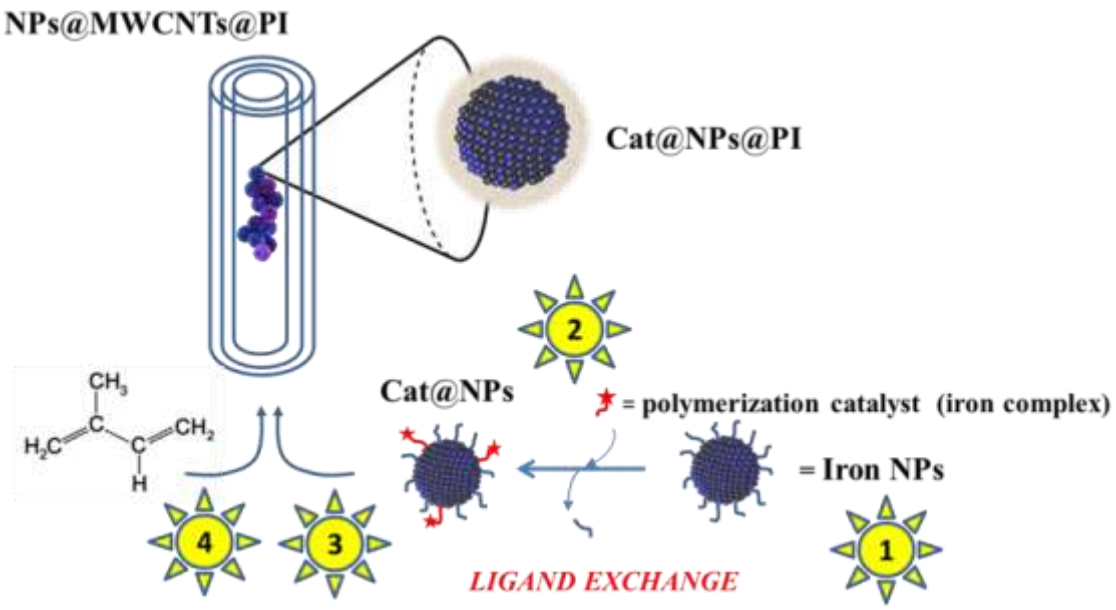

Scheme 5.2 Bottom-up approach to produce air-protected magnetic nanoparticles confined in CNTs: (1) synthesis of Fe NPs; (2) synthesis of Fe NPs modified with a Fe polymerization catalyst (**Cat@NPs**); (3) selective confinement of **Cat@NPs** in CNTs; and (4) Polymerization of isoprene in a confined space to produce **Cat@NPs@MWCNT@PI**.

5.2 Results and discussion

5.2.1 Synthesis and characterization of ligands and iron complexes

The ligands (**L6**–**L8**) in Scheme 5.3 were synthesized and prepared according to the procedure described in Chapter IV [67]. Iron complexes **Fe6**–**Fe8** (Scheme 5.3) were prepared by reacting under inert atmosphere $FeCl_2$ with two equivalents of the corresponding ligand in EtOH (Scheme 5.3). All iron complexes were isolated as air-stable solids but slowly turn from blue to yellow in solution upon air exposure, probably due to oxidation of Fe(II) to Fe (III). Compared to the IR spectra of the free ligands, the C=N stretching vibrations in complexes **Fe6**–**Fe8** are

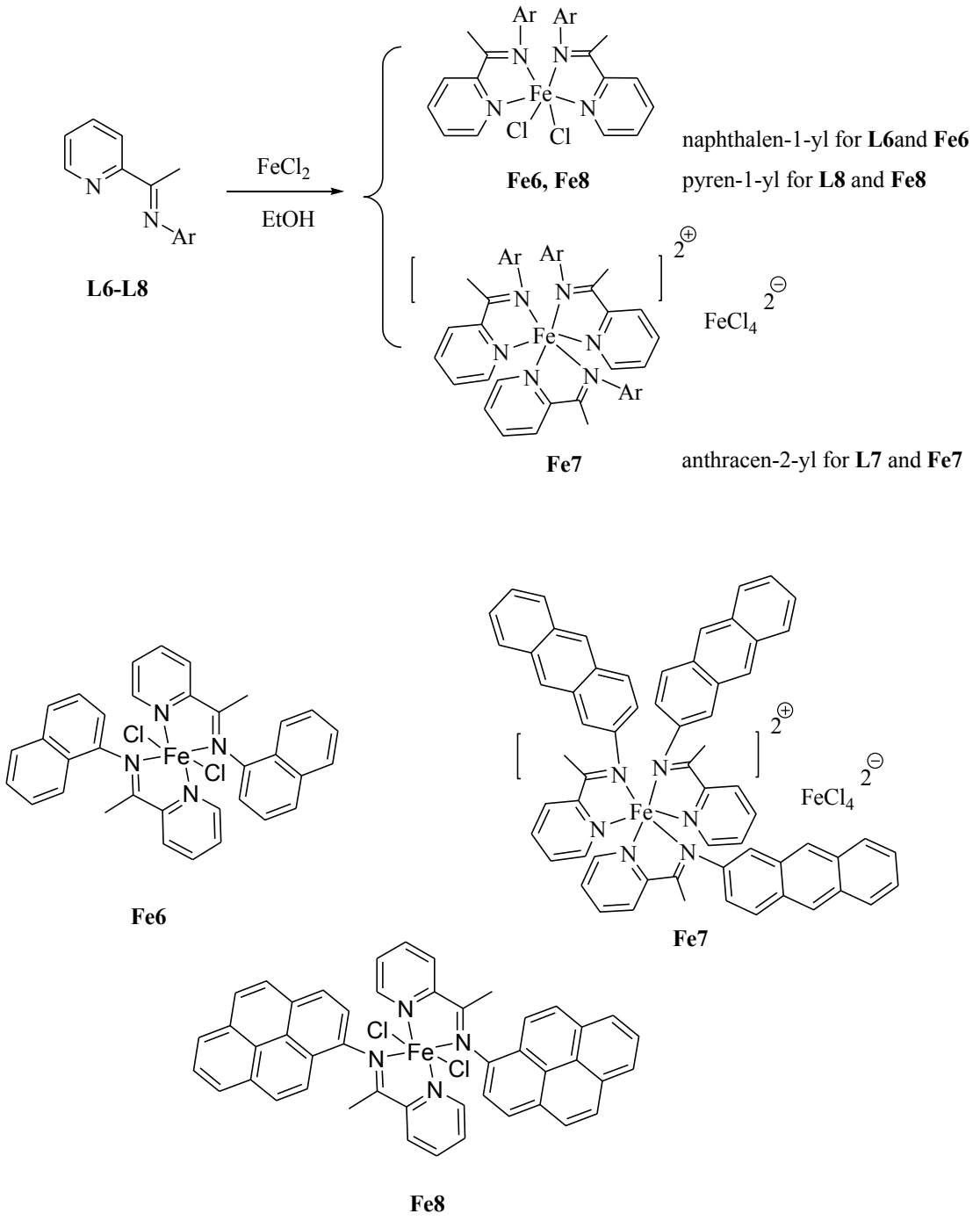

Scheme 5.3 Synthetic procedure for iron complexes **Fe6**–**Fe8** from ligands **L6**–**L8**.

shifted to lower frequencies (1596 cm^{-1}, 1597 and 1596 cm^{-1}), indicating effective coordination between the imino nitrogen atoms and the iron center. Single crystals of complexes **Fe6**–**Fe8**, grown by laying diethyl ether onto their methanol solutions at

room temperature under argon, further confirmed the complex structure through X-ray diffraction analysis.

5.2.2 X-ray crystallographic studies

As shown in Figure 5.1, similar to its analogous complex **Ni6** described in Chapter IV [67], the iron center in **Fe6** is surrounded by two bidentate **L6** and two chloride ligands to afford a distorted octahedral geometry around the metal center. The pyridine ring of one ligand is almost perpendicular to the amino-naphthalene ring belonging to the same ligand with a dihedral angle of 93.6°. However, the dihedral angle comprising the pyridine ring of one ligand and the amino-naphthalene ring of another ligand is 19.3° and the distance between them is 3.4821 Å which is shorter than in its analogous complex **Ni6** (3.5972 Å), indicating a stronger π-π interaction induced by the naphthalene ring. Concerning the bond lengths around the iron center, the Fe–Cl1 (2.3530 (7) Å) is shorter than the Fe–Cl2 (2.4681 (7) Å), whereas the bonds lengths of Fe–N showed a slight difference. The bonds lengths of Fe–N (Pyridine); Fe1−N1 2.1612(19) Å and Fe1−N3 2.157(2) Å; are shorter than the Fe–N (imino) bond length, due to the conjugation inside of the pyridine ring.

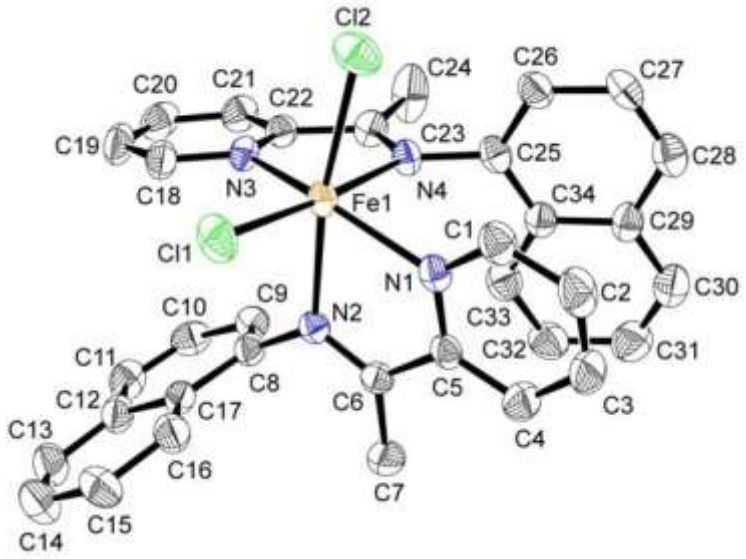

Figure 5.1 ORTEP molecular structure of **Fe6**. Thermal ellipsoids are shown at 30 % probability. Hydrogen atoms have been omitted for clarity. Selected bond lengths (Å) and angles (°): Fe(1)−N(1) = 2.1612(19); Fe(1)−N(2) = 2.272(2); Fe(1)−N(3) = 2.157(2); Fe(1)−N(4) = 2.274(2); Fe(1)−Cl(1) = 2.3530(7); Fe(1)−Cl(2) = 2.4681(7); N(1)−C(1) = 1.325(3); N(1)−C(5) = 1.360(3); N(2)−C(6) = 1.292(3); N(3)−C(18) = 1.342(3); N(3)−C(22) = 1.342(3); N(4)−C(23) = 1.271(3). N(1)−Fe(1)−N(2) = 73.40(7); N(3)−Fe(1)−N(4) = 73.11(7); N(1)−Fe(1)−N(4) = 84.77(7); N(2)−Fe(1)−N(4) = 88.76(7); N(3)−Fe(1)−Cl(1) = 102.78(6); N(1)−Fe(1)−Cl(1) = 99.75(5); N(2)−Fe(1)−Cl(1) = 93.05(5); N(4)−Fe(1)−Cl(1) = 175.45(5); N(3)−Fe(1)−Cl(2) = 97.67(6); N(1)−Fe(1)−Cl(2) = 99.05(6); N(2)−Fe(1)−Cl(2) = 171.00(5); N(4)−Fe(1)−Cl(2) = 85.63(6); Cl(1)−Fe(1)−Cl(2) = 93.08(3).

Complex **Fe7** (Figure 5.2) adopts six-coordination numbers with six N atoms belonging respectively to three ligands around the iron atom displaying an octahedral coordination environment. A free $FeCl_4^{2-}$ anion was observed away from the main cationic part FeL_3^{2+}, as counteranion. A similar structure was observed in other

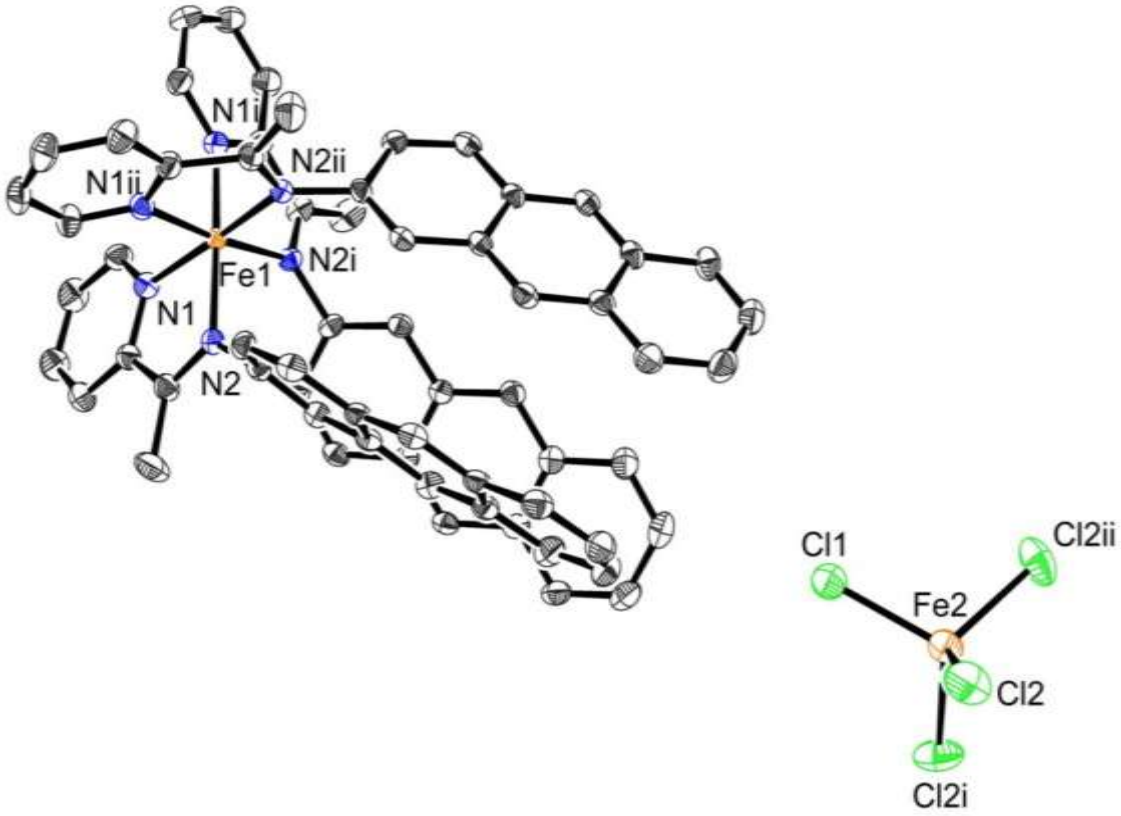

Figure 5.2 ORTEP molecular structure of **Fe7**. Thermal ellipsoids are shown at 30 % probability. Hydrogen atoms have been omitted for clarity. Selected bond lengths (Å) and angles (°): Fe(1)−N(1) = Fe(1)−N (1i) = Fe(1)−N(1ii) = 1.9697(19); Fe(1)−N(2) = Fe(1)−N (2i) = Fe(1)−N (2ii) = 1.9855(18); Fe(2)−Cl(1) = 2.3152(14); Fe(2)−Cl (2) = Fe(2)−Cl (2i) = Fe(2)−Cl (2ii) = 2.3175(8). N(1)−Fe(1)−N(1i) = N(1)−Fe(1)−N(1ii) = N(1i)−Fe(1)−N(1ii) = 94.55(8); N(1)−Fe(1)−N(2) = N(1i)−Fe(1)−N(2i) = N(1ii)−Fe(1)−N(2ii) = 80.18(8); N(1i)−Fe(1)−N(2) = N(1ii)−Fe(1)−N(2i) = N(1)−Fe(1)−N(2ii) = 174.22(8); N(2)−Fe(1)−N(2i) = N(2)−Fe(1)−N(2ii) = N(2i)−Fe(1)−N(2ii) = 97.18(7); N(1)−Fe(1)−N(2i) = N(1i)−Fe(1)−N(2ii) = N(1ii)−Fe(1)−N(2) = 88.28(8).

reported iron complexes coordinated by six nitrogen atoms from three bipyridine ligands and with a free $FeCl_4^{2-}$ anion [68]. The molecular structure of the complex **Fe7** is completely symmetrical as the iron atom is the center and the iron atom

deviates by 0.0255 Å from the equatorial plane which contains N1, N2, N1i and N2ii. Pyridine rings are nearly perpendicular to each other with the dihedral angles being: 81.5° between the ring containing N1 and the pyridine ring with the N1i, between the ring containing N1i and the pyridine ring with the N1ii ; and 85.1° between the rings containing N1 and N1ii. The dihedral angles are 120.2°, 60.2° and 60.2° between those anthracene rings in the order of C8–C21, C8i–C21i and C8ii-C21ii. A cavity is produced by the three anthracene rings held together and the $FeCl_4^{2-}$ anion is located at the extremity of this cavity.

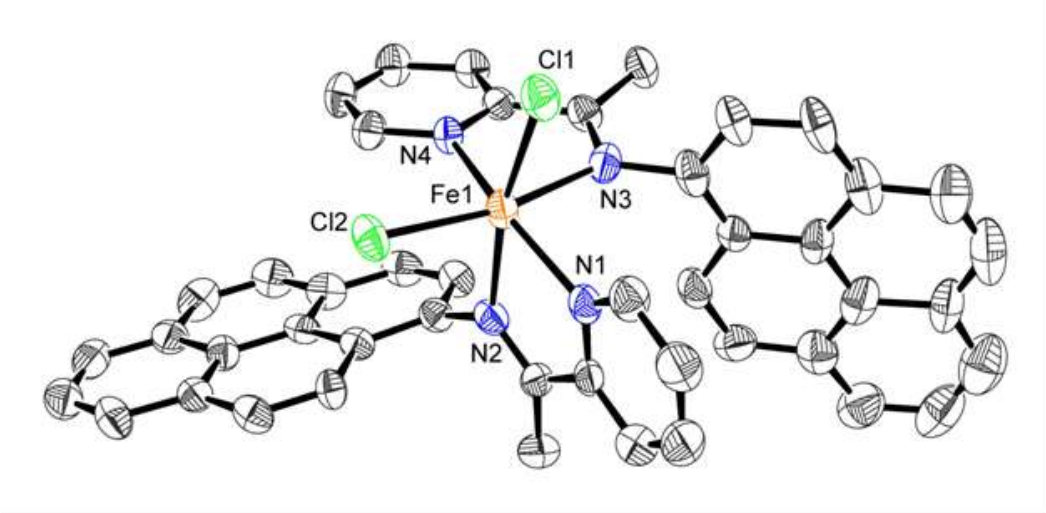

Figure 5.3 ORTEP molecular structure of **Fe8**. Thermal ellipsoids are shown at 30 % probability. Hydrogen atoms and solvent molecules have been omitted for clarity. Selected bond lengths (Å): Fe(1)−N(1) = 2.161; Fe(1)−N(2) = 2.231; Fe(1)−N(3) = 2.256; Fe(1)−N(4) = 2.178; Fe(1)−Cl(1) = 2.450; Fe(1)−Cl(2) = 2.369.

Similar with the **Fe6**, the iron center of the **Fe8** (see Figure 5.3) is coordinated with four N-atoms belong to two bidentate ligands and two chloride, possesses a distorted octahedral environment. The Fe–N bond lengths (belonging to the amino ring) of the **Fe8** are than same bonds of **Fe6**. It is probably because of more π-electron

of the pyrene rings. The pyridine ring of one ligand is almost perpendicular with the amino-pyrene ring belonging to the same ligand with dihedral angles of 92.7° and 80.9, severally. Two pyridine rings are perpendicular to each other with a dihedral angle of 89.4°, and the dihedral angle of two pyrene rings is 75.4°. The X-ray structure details for complexes **Fe6**–**Fe8** determinations and refinement are provided in Table 5.1.

Table 5.1 Crystal data and structure refinement for **Fe6**–**Fe8**

	Fe6	**Fe7**	**Fe8**
empirical formula	$C_{34}H_{28}Cl_2FeN_4$	$C_{63}H_{48}FeN_6 \cdot Cl_4Fe$	$(C_{46}H_{32}Cl_2FeN_4)_4$, $(CH_3OH)_3$
Formula weight	619.35	1142.57	3166.15
T (K)	180(2)	180(2)	180(2)
wavelength (Å)	0.71073	0.71073	0.71073
cryst syst	orthorhombic	trigonal	triclinic
space group	p 21 21 21	R^{-3}	p1
a (Å)	8.4829(2)	13.0947(3)	12.3471(10)
b (Å)	13.8918(5)	13.0947(3)	14.6278(11)
c (Å)	28.3144(9)	62.8986(19)	23.956(2)
α (°)	90	90	94.307(3)
β (°)	90	90	94.077(3)
γ (°)	90	120	112.721(2)
V (Å^3)	3336.65(18)	9340.3(6)	3961.5
Z	4	6	1
*D*calcd.	1.233	1.213	1.329

(gcm^{-3})			
μ (mm^{-1})	0.639	0.679	0.557
F(000)	1280	3528	1638
cryst size (mm)	0.6 × 0.1 × 0.1	0.16 × 0.14 × 0.04	0.26 × 0.18 × 0.04
θ range (°)	1.44–25.35	1.94–27.77	1.52–23.29
	−10 ≤ h ≤ 10	−17 ≤ h ≤ 17	−13 ≤ h ≤ 13
limiting indices	−16 ≤ k ≤ 16	−14 ≤ k ≤ 17	−15 ≤ k ≤ 16
	−34 ≤ l ≤ 31	−82≤ l ≤ 82	−26 ≤ l ≤ 26
no. of rflns collected	43381	21989	78695
no. unique rflns [R(int)]	6092 (0.0367)	4826 (0.0477)	19234(0.0378)
Comp. to θ (%)	99.8%	98.2%	94.5 %
data/restraints/params	6092 / 0 / 373	4826 / 0 / 227	19234 / 3 / 1978
Goodness of fit on F^2	1.102	0.953	1.039
Final R indices [$I>2\sigma(I)$]	R1 = 0.035	R1 = 0.0470	R1 = 0.0412,
	wR2 = 0.0855	wR2 = 0.1273	wR2 = 0.1032
R indices (all data)	R1 = 0.0365	R1 = 0.0721	R1 = 0.0483,
	wR2 = 0.0880	wR2 = 0.1347	wR2 = 0.1067
Max./min. $\Delta\rho$[a] [$eÅ^{-3}$]	0.301 and −0.271	0.577 and −0.548	0.943 and -0.534

5.2.3 Isoprene polymerization with iron complexes Fe6–Fe8

Isoprene polymerization catalyzed by iron complexes **Fe6**–**Fe8** was carried out in a glovebox under argon. As shown in Table 5.2, **Fe6** was subjected to a study under different reaction conditions by varying the temperature and the reaction time. Triisobutylaluminum was used as co-catalyst to abstract the chloride from the

dichloride iron complexes and produce the active species. In absence of this co-catalyst no polymer was formed. Moreover, trityl tetrakis(pentafluorophenyl)borate can be used as the dealkylating reagent to abstract one alkyl group in order to increase the reaction rate (Table 5.2, Entries 1–2).

Concerning the reaction temperature, low temperatures are detrimental to the polymerization (Table 5.2, Entries 2–4). More than 99% isoprene (5.1 g) is converted into polyisoprene in half an hour at room temperature. This activity is higher than that of other isoprene catalysts based on iron [5, 10] and rare-metal complexes [16-17, 24] previously reported. For comparative purpose, 1 μmol of the iron catalysts reported by Ritter can convert 0.08 g of isoprene into polyisoprene in 2 h; the molecular weight of the resulting polymer was 125 kg mol^{-1} and a 91% *trans*-1,4-polyisoprene selectivity) [5]. Lower molecular weight polymers are produced from **Fe6** which is probably due to the absence of ortho-substituted aryl groups on the ligand.

The conversion is decreased to 96% at 0 °C and 78% at -33 °C. The molecular weight (M_w) and the molecular weight distribution (M_w/M_n) are also changed with the reaction temperature. As shown in Table 5.2 (Entries 2–4), M_w of the produced polyisoprene increased from 32.7 kg mol^{-1}, 37.8 to kg mol^{-1} to 38.6 kg mol^{-1} when the reaction temperature decreased from 25 °C to 0 °C and to -33 °C. This phenomenon is just opposite to the trend observed for iron catalysts reported by Ritter [5] for which lower molecular weight obtained at lower temperature**.** In addition, lower reaction temperature resulted in the lower polydispersity M_w/M_n, partly because of the lower concentration of catalytic active sites produced by the co-catalyst at lower reaction temperature. The resulting polymers were characterized by ^{1}H and ^{13}C NMR (Figure 5.4) and DSC (Table 5.2). According to the ^{1}H NMR data, using the equations 1–3 [5, 14], the selectivity toward 1,4-polyisoprene *vs* 3,4-polyisoprene is slightly in favor of

the 1,4 motive and is not much affected by reaction temperature variations. Moreover, according to the ^{1}H NMR data and the equations 2 and 3, the *cis* 1,4-polyisoprene content is raised up to more than 99% at and below 0 °C (Table 5.2, Entries 3–4). High glass temperature polyisoprenes are produced by **Fe6** due to the high content of 3,4-motive inside the polymer [7-8]. Reduction of the reaction time evidenced that after 15 minutes an isoprene conversion of 86% is already reached (Table 2, Entry 5).

$$\textbf{eq.1}\ [\%1,4\text{−motif}] = \frac{A(\sim CH = CMe\text{−}1,4\text{−motif})}{A(\sim CH = CMe\text{−}1,4\text{−motif}) + A(CH_2 = CMe\ \text{−}3,4\ \text{−motif})/2}$$

$$\textbf{eq.2}\ [\%trans\text{−}1,4\text{−motif}] = \frac{A(CH_3\text{−}trans\text{−}1,4\text{−motif})}{A(CH_3\text{−}trans\text{−}1,4\text{−motif}) + A(CH_3\text{−}cis\text{−}1,4\text{−motif})}$$

$$\textbf{eq.3}\ [\%cis\text{−}1,4\text{−motif}] = \frac{A(CH_3\text{−}cis\text{−}1,4\text{−motif})}{A(CH_3\text{−}trans\text{−}1,4\text{−motif}) + A(CH_3\text{−}cis\text{−}1,4\text{−motif})}$$

The effect of the ligand on the polyisoprene synthesis was also investigated by studying, under the optimum conditions determined for catalyst **Fe6**, the catalytic polymerization behaviour of **Fe7** and **Fe8** bearing different aromatic groups. The conversion of the isoprene reached by **Fe7** in half an hour is 93% with a molecular weight of 59.7 kg mol^{-1} which is higher compared to the polyisoprene produced by iron complexes **Fe6** and the complexes based on rare earth metal [15-17, 24], but still lower than that of the iron complexes reported by Ritter [5] and Porri [10]. Therefore, compared to **Fe6**, **Fe7** is less active under similar conditions but leads to the formation of polymers of higher molecular weights (Table 5.2, Entries 2 and 6).

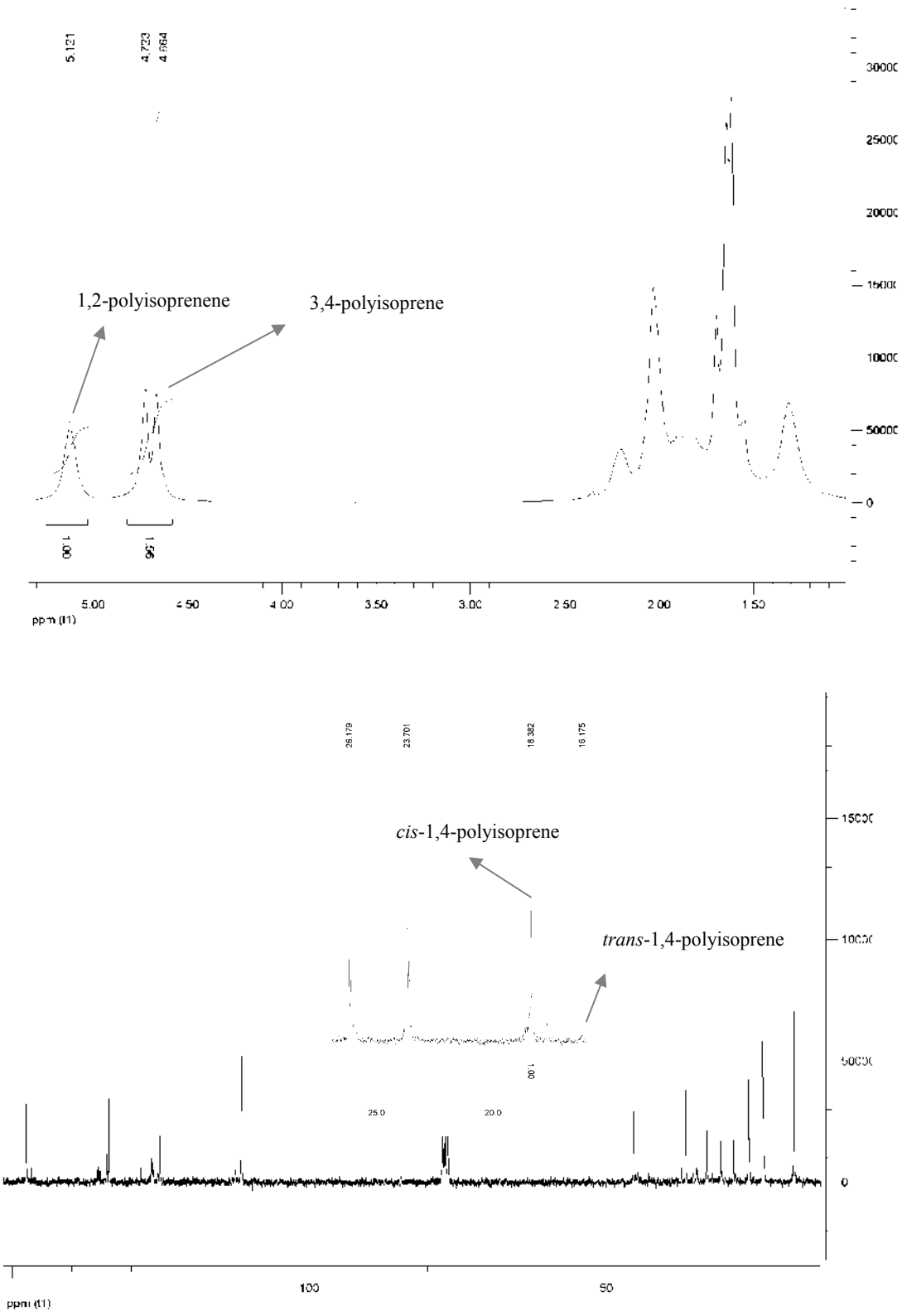

Figure 5.4 ^{1}H NMR (top) and ^{13}C NMR (bottom) spectra of polyisoprene (Table 5.2, Entry 2).

Concerning **Fe8,** 97% isoprene was converted into polymer in 30 minutes. In this

case, and unlike observed for **Fe7**, lower molecular weight and molecular weight distributions are observed for the polymer obtained.

Table 5.2 Isoprene polymerization with iron $\mathbf{Fe_n}$ / $Al(^iPr)_3$[a]

Entry	Cat.	T (°C)	t (min)	Conv. (%)	T_g[b] (°C)	M_w[c] (kg mol^{-1})	M_w/M_n[c]	1,4/3,4[d]	1,4 (%)[d] *cis*/*trans*
1	**Fe6**[e]	25	30	65	-29.3	33.0	15.9	27:23	>99
2	**Fe6**	25	30	>99	-31.8	32.7	17.5	11:9	19:1
3	**Fe6**	0	30	96	-30.8	37.8	16.7	57:43	>99
4	**Fe6**	-33	30	78	-28.8	38.6	8.6	14:11	>99
5	**Fe6**	25	15	86	-33.9	17.0	15.1	11:9	24:1
6	**Fe7**	25	30	93	-31.6	59.7	15.1	27:23	>99
7	**Fe8**	25	30	97	-31.0	21.3	10.2	57:43	23:2

[a] Reaction conditions: 3 μmol $\mathbf{Fe_n}$; 7.5 mL isoprene (M), [Al]/[Ph_3C^+]/[Fe]/[M] = 12:1:1:25000; 100 mL toluene. [b] Determined by GPC. [c] Determined by DSC. [d] Determined by ^{1}H NMR and ^{13}C NMR. [e] No Ph_3C^+.

Regarding the catalytic results of different efficiency isoprene catalysts **Fe6**–**Fe8**, **Fe6** shows higher activity than others. Therefore, catalyst **Fe6** was further used to be immobilized on the iron particles and in catalytic systems.

5.2.4 Preparation of nanoparticles supported catalysts (Cat@NPs)

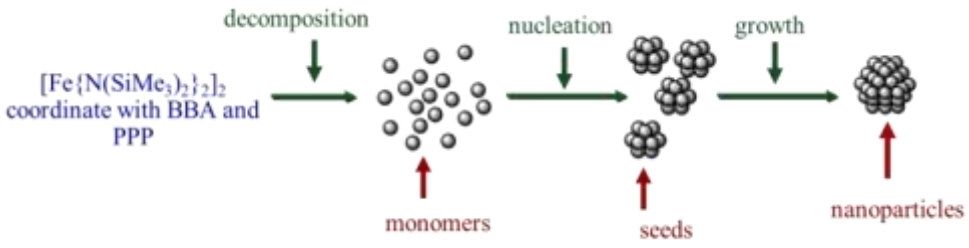

Scheme 5.4 Synthetic procedure for iron particles.

The iron particles used in this study were synthesized according to previously reported procedures [69-70] and as depicted in Scheme 5.4. The iron precursor $[Fe\{N(SiMe_3)_2\}_2]_2$ is reduced under 3 bar H_2 in the presence of an acid (2-benzylbenzonic acid) and an amine (4-(3-phenylpropyl)pyridine), which are the stabilizing ligands to control the particles size during the growth process [70]. Iron complex **Fe6**, which appeared to be the most efficient system tested in isoprene polymerization (*vide supra*) was selected to carry out the immobilization on magnetic iron nanoparticles. The naphthalene ring contained in the ligand structure was used to interact with the surface of iron-particle though π-π interactions. The anchoring of **Fe6** proceeds by exchange with stabilizing agents around the NPs as depicted in Scheme 5.2. Immobilization of the iron complex **Cat@NPs** was carried out in a glovebox by stirring a 10 mL THF solution of **Fe6** and iron particles (NPs) for 1 day. Pentane was then added into the solution; which was kept for one night until the particles deposited on the bottom of the flask. The particles were there recovered by removal of the solvent, and washed twice with toluene.

Comparison of the infra-red spectrum of the particles containing the iron complex with the one of the orignal particles (Figure 5.5) evidenced an additional vibration at 1615 cm^{-1} belonging to the C=N of the iron complex supported by the particles. The

corresponding C=N stretching vibrations of the free iron complex is observed at 1596 cm^{-1}; therefore indicating an effective interaction between the iron complex and the surface of the particles. The success of the ligand exchange was also confirmed by TEM. As shown in Figure 5.6, either before or after ligand exchange, the iron NPs and **Cat@NPs** are homogeneously dispersed. However, compared to the original NPs, the mean diameter shows a slight increase for the **Cat@NPs**, d = 4.82 ± 0.58 nm for **Cat@NPs** *vs* d = 4.44 ± 0.32 nm for NPs.

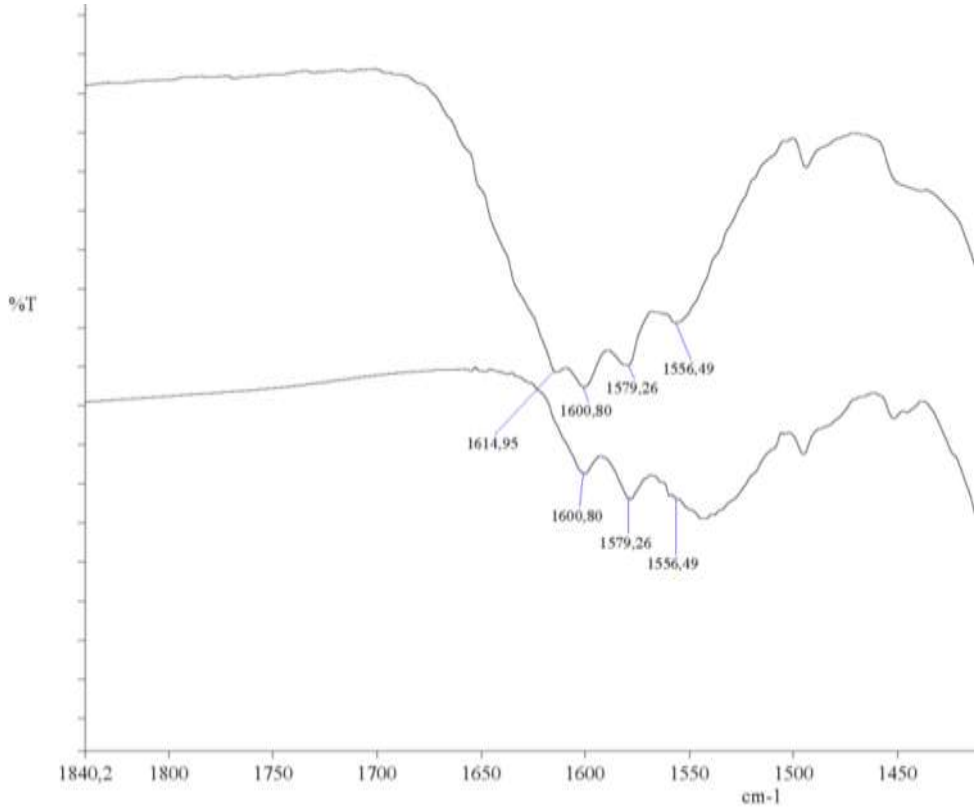

Figure 5.5 IR spectra of NPs (bottom) and **Cat@NPs** (top).

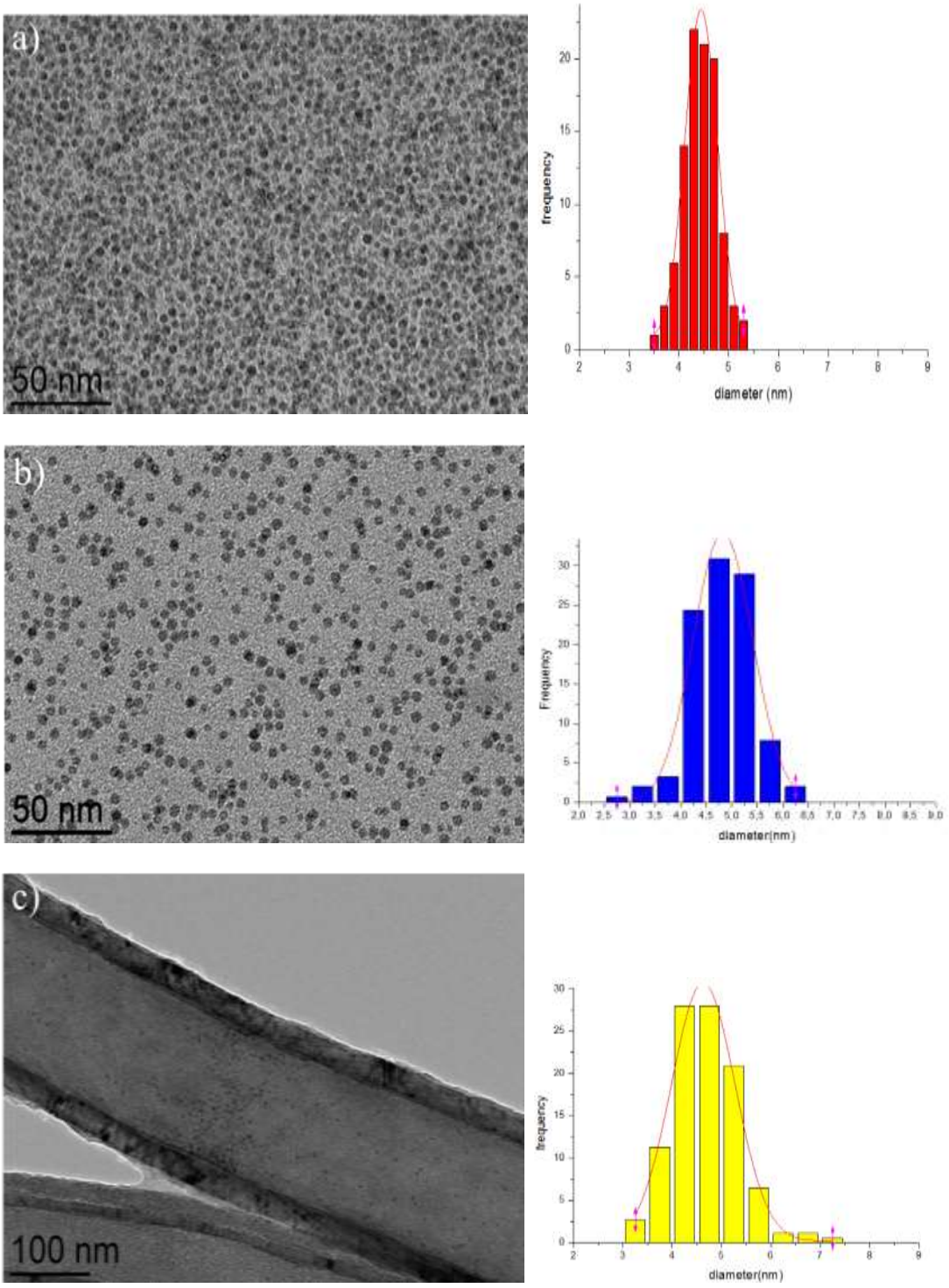

Figure 5.6 TEM images a) iron nanoparticles (NPs), b) **Cat@NPs** and c) **Cat@NPs@MWCNT**.

5.2.5 Confinement of Cat@NPs inside f-MWCNTs

Prior to confinement of **Cat@NPs** into the inner cavity of MWCNTs, a surface functionalization of MWCNTs is necessary in order to selectively drive the nanoparticles inside the MWCNTs, as previously reported in our research group [66]. This procedure was carried out in two steps (Scheme 5.5): 1) reaction of the MWCNTs with nitric acid at 120 °C for 3h to produce carboxylic acid functions; 2) formation of amide fonctionality by reaction of those carboxylic acid groups with $SOCl_2$ and long alkyl groups amines (hexadecylamine, HDA).

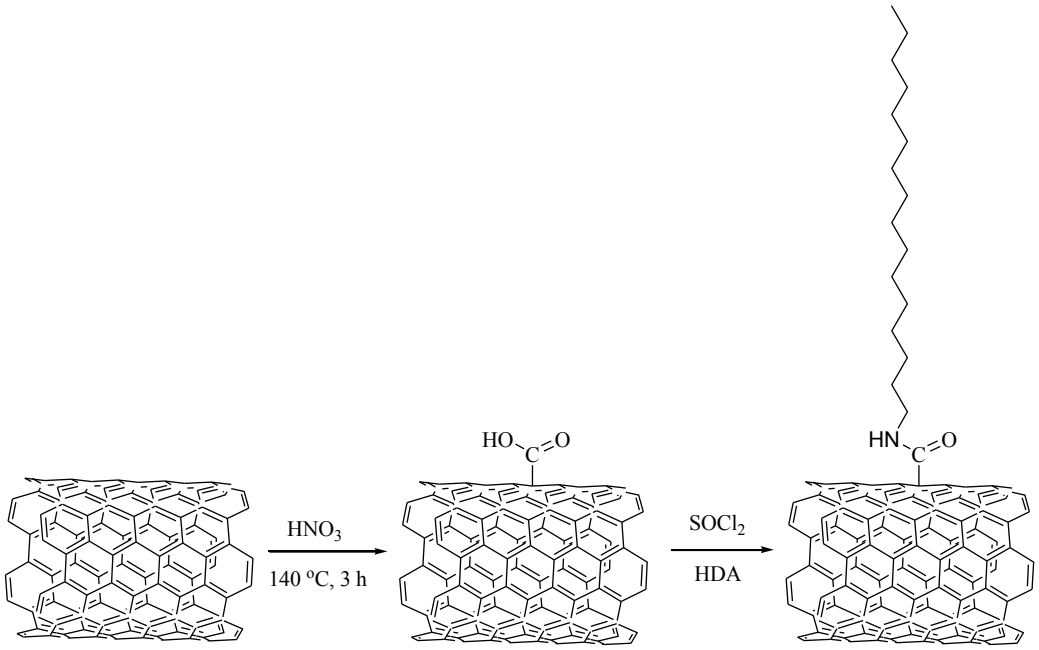

Scheme 5.5 CNTs functionalization.

Cat@NPs@MWCNT system was produced by stirring a **Cat@NPs** THF solution with the MWCNTs functionalized with the long chain alkyl groups (f-MWCNT) at room temperature for 1 day. The TEM image (Figure 5.6, c) showed that most of the **Cat@NPs** (4.63±0.64 nm) are effectively confined inside the tubes. Then **Cat@NPs@MWCNT** was used as the catalyst for isoprene polymerization (Scheme 5.2).

5.2.6 Cat@NPs and Cat@NPs@MWCNT behavior in isoprene polymerization

The catalytic polymerization of isoprene was then investigated using the above-describes **Cat@NPs** and **Cat@NPs@MWCNT** systems (Table 5.3). $Al(^{i}Pr)_3$ was used as co-catalyst for generation of the active species. Since the amount of complex **Fe6** effectively immobilized could not be determined, the isoprene polymerization activities for those immobilized catalysts could not be calculated. Moreover, the resulting polymers produced by these immobilized catalysts could not be analyzed by gel permeation chromatography (GPC) due to impossible separation of the particles from the polymer. Interestingly, the DSC analysis of the resulting polymer showed some differences with the polymer produced by the homogeneous catalysts. The glass temperature values are -37.2 °C and -40.2 °C for the polymers produced respectively by **Cat@NPs** and **Cat@NPs@MWCNT**, which are lower than that of the polyisoprene obtained by the homogeneous iron complexes (-29.3 to -33.9 °C). This means that the presence of the NPs and the confinement have an influence on the properties of the produced polymer. In order to characterize the gum coating the nanoparticles, TEM observations have been carried out (Figure 5.7). As shown in the micrographs (Figure 5.7a), the particles are dispersed homogeneously inside of the resulting polyisoprene surrounding them. Figure 5.7b shows that the resulting polyisoprene is effectively surrounding the NPs confined into the MWCNTs. This means that the iron complex **Fe6** is still grafted to the NPs after **Cat@NPs** was introduced inside of MWCNTs. On the other hand, the resulting polyisoprene coating the NPs and the MWCNTs have the functions to keep the oxygen away from those sensitive NPs.

Table 5.3 Isoprene polymerization promoted by supported iron catalysts[a]

Entry	Cat.	Isoprene (mL)	Amount of Cat. (mg)	Conv. (%)	T_g[b] (°C)
1	**Cat@NPs**	7.5	10	45	-
2	**Cat@NPs**	1.0	10	>99	-37.2
3	**Cat@NPs@MWCNT**	1.0	20	>99	-40.6

[a] Reaction conditions: 2 mL (0.02 M in toluene) $Al(^iPr)_3$; 20 mg trityl tetrakis(pentafluorophenyl)borate; 30 min; 25 °C; 100 mL toluene. [b] Determined by DSC.

The aim of the project is the use of the resulting polyisoprene to protect NPs against oxidation. Therefore, we carried out magnetic measurements on these systems (Figure 5.8). The left part of Figure 5.8 shows results for **Cat@NPs@MWCNT** and the red curve evidences a shift respected to the black curve, indicative of the formation of oxide of NPs. The right image in Figure 5.8 is the result for a sample of **Cat@NPs@MWCNT@PI** exposed to air for 10 min. The overlap of the two curves (black and red) indicates the absence of oxidation. It means that the resulting polyisoprene can effectively protect NPs against oxidation.

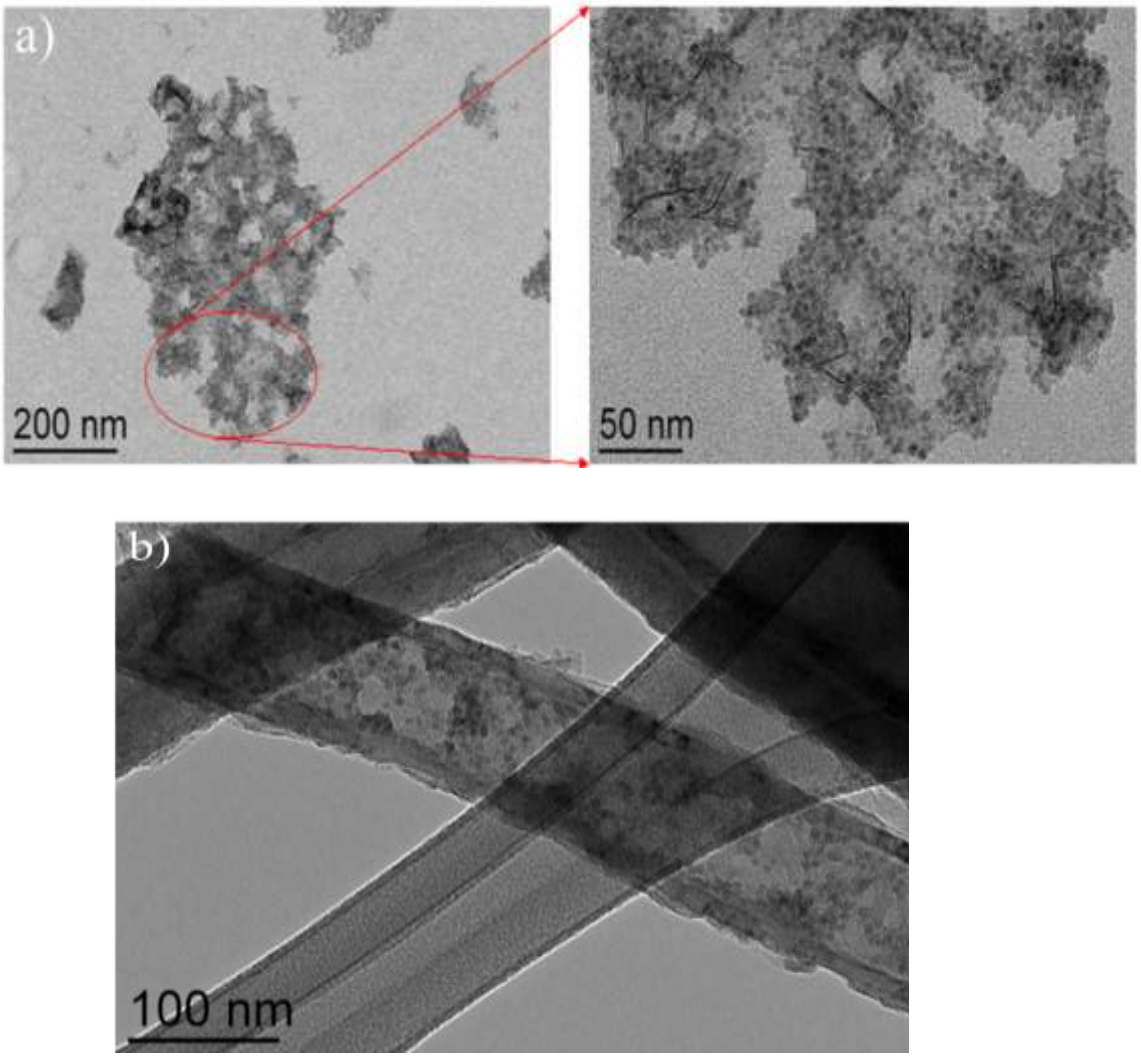

Figure 5.7 TEM images of: a) **Cat@NPs@PI** (Table 5.3, Entry 2) and b) **Cat@NPs@MWCNT@PI** (Table 5.3, Entry 3).

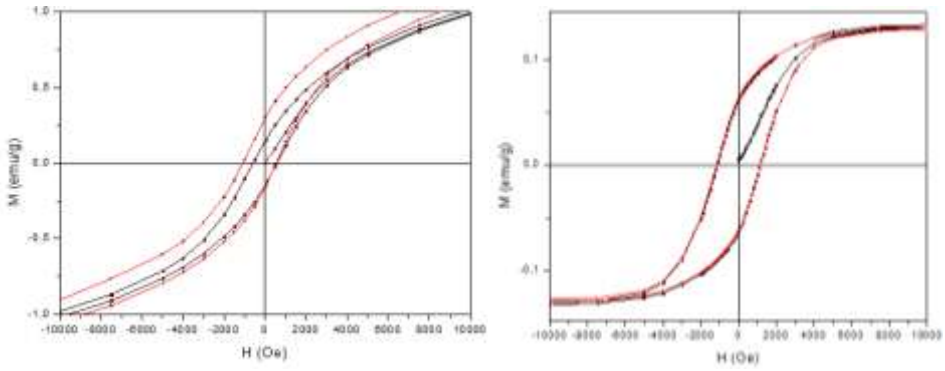

Figure 5.8 Magnetic measurement: **Cat@NPs@MWCNT** (left) and **Cat@NPs@MWCNT@PI** (right).

5.3 Conclusions

A series of iron complexes (**Fe6**–**Fe8**) bearing 1-aryliminoethylpyridine ligands have been synthesized and fully characterized. With triisopropylaluminum as co-catalyst, these iron complexes shown excellent activity for the isoprene polymerization and produced high glass temperature polyisoprene with a high *cis*-1,4-polyisoprene selectivity. Furthermore, the immobilized catalysts **Cat@NPs** and **Cat@NPs@MWCNT** were produced and used in polymerization. DSC values show that the presence of the NPs has an influence on the properties of the resulting polymer. The TEM images of the **Cat@NPs@PI** shown that NPs are surrounded by the resulting polyisoprene and homogeneously dispersed. In the case of the polyisoprene produced by the **Cat@NPs@MWCNT** system, the produced polymer is effectively located inside the MWCNTs and coated the nanoparticles. Moreover, the size of the iron particles is not changed significantly after both ligands exchanged and polymerization. The efficiency of the resulting polyisoprene to protect NPs against oxidation has been measured by Squid and the NPs showed no oxidation after air exposure.

5.4 Experimental Section

5.4.1 Synthesis of the iron complexes Fe6–Fe8

Ligands **L6-L8** were produced as reported in Chapter IV [67]. Under argon, a mixture of $FeCl_2$ (63.5 mg, 0.5 mmol) and two equivalents of the corresponding ligand (1 mmol) was stirred in ethanol (5 mL) at room temperature for 6 h. 20 mL of diethyl ether were then added into the solution and the resulting precipitate was collected by filtration, washed several times with diethyl ether, and dried under reduced pressure. The desired iron complex was obtained as a brown powder.

Fe6. Yield: 86% (266 mg). FT−IR (KBr, cm^{-1}): 3058 (w), 1629 (m), 1596 (s), 1572 (w), 1508 (m), 1474 (w), 1439 (m), 1391 (m), 1372 (m), 1316 (m), 1263 (m), 1165 (m), 1019 (m), 812 (m), 780 (s).

Fe7. Yield: 69%. FT−IR (KBr, cm^{-1}): 3057 (w), 1620 (s), 1597 (s), 1477 (w), 1436 (m), 1370 (m), 1318(m), 1259 (s), 1174 (m), 1017 (m), 895 (s), 796 (m), 749 (s), 644 (m), 470 (s).

Fe8. Yield: 74%. FT−IR (KBr, cm^{-1}): 3039 (w), 1626 (s), 1596 (s), 1502 (w), 1487 (w), 1441(m), 1371 (m), 1319(m), 1256 (s), 1184 (m), 1019 (m), 849 (s), 779 (m), 714 (m).

5.4.2 Immobilization on the surface of iron nanoparticles (Cat@NPs)

10 mg of nanoparticles are added to a THF (10 mL) solution of iron complex (3 μmol, 1.9 mg) and stirred for 1 day. 5 mL of pentane are then added into the solution. After one night, the particles deposited on the bottom of the flask were collected by removal of the solvent. They were then washed with toluene twice.

5.4.3 Confinement of Cat@NPs inside MWCNTs (Cat@NPs@MWCNT)

10 mg of the preformed **Cat@NPs** were dispersed in 5 mL of THF by ultrasonication for 5 min. 50 mg MWCNTs were then added into this suspension. The mixture was submitted to ultrasonication for 5 min. After a subsequent stirring for 1 day, the mixture was filtered and washed with 20 mL THF. The black solid was finally dried under vacuum.

References

[1] S. K. De, J. R. White, "Rubber technologist's handbook (Ed: rapra technology limited), rapra technology limited, shawbury", 2001, 49–51.

[2] S. Ouardad, M.-E. Bakleh, S. V. Kostjuk, F. Ganachaud, J. E. Puskas, A. Deffieux, F. Peruch, "Bio-inspired cationic polymerization of isoprene and analogues: state-of-the-art", *Polym. Int.*, 2012, 61, 149–156.

[3] D. Threadingham, W. Obrecht, W. Wieder, G. Wachholz, R. Engehausen, "Rubber, 3. Synthetic Rubbers, Introduction and Overview", *Ullmann's Encyclopedia of Industrial Chemistry*, 2000.

[4] Ceresana, "Market Study Synthetic Rubber", 2013.

[5] J. Raynaud, J. Y. Wu, T. Ritter, "Iron-Catalyzed Polymerization of Isoprene and Other 1,3-Dienes", *Angew. Chem. Int. Ed.*, 2012, 51, 11805–11808.

[6] G. Ricci, G. Leone, A. Boglia, A. C. Boccia, L. Zetta, "cis-1,4-alt-3,4 Polyisoprene: Synthesis and Characterization", *Macromolecules*, 2009, 42, 9263–9267.

[7] J. M. Widmaier, G. C. Meyer, "Glass transition temperature of anionic

polyisoprene", *Macromolecules*, 1981, 14, 450–452.

[8] A. kongkaew, J. Wootthikanokkhan, "Polymerization of isoprene by using benzyl diethyldithiocarbamate as an iniferter", *ScienceAsia*, 1999, 25, 35–41.

[9] G. Ricci, A. Sommazzi, F. Masi, M. Ricci, A. Boglia, G. Leone, "Well-defined transition metal complexes with phosphorus and nitrogen ligands for 1,3-dienes polymerization", *Coord. Chem. Rev.*, 2010, 254, 661–676.

[10] C. Bazzini, A. Giarrusso, L. Porri, "Diethylbis(2,2′-bipyridine)iron/MAO. A Very Active and Stereospecific Catalyst for 1,3-Diene Polymerization", *Macromol. Rapid Commun.*, 2002, 23, 922–927.

[11] B. Moreau, J. Y. Wu, T. Ritter, "Iron-Catalyzed 1,4-Addition of α-Olefins to Dienes", *Org. Lett.*, 2009, 11, 337–339.

[12] J. Y. Wu, B. N. Stanzl, T. Ritter, "A Strategy for the Synthesis of Well-Defined Iron Catalysts and Application to Regioselective Diene Hydrosilylation", *J. Am. Chem. Soc.*, 2010, 132, 13214–13216.

[13] B. Wang, J. Bi, C. Zhang, Q. Dai, C. Bai, X. Zhang, Y. Hu, L. Jiang, "Highly active and trans-1,4 specific polymerization of 1,3-butadiene catalyzed by 2-pyrazolyl substituted 1,10-phenanthroline ligated iron (II) complexes", *Polymer*, 2013, 54, 5174–5181.

[14] W. Gao, D. Cui, "Highly cis-1,4 Selective Polymerization of Dienes with Homogeneous Ziegler−Natta Catalysts Based on NCN-Pincer Rare Earth Metal Dichloride Precursors", *J. Am. Chem. Soc.*, 2008, 130, 4984–4991.

[15] B. Wang, D. Cui, K. Lv, "Highly 3,4-Selective Living Polymerization of Isoprene with Rare Earth Metal Fluorenyl N-Heterocyclic Carbene Precursors", *Macromolecules*, 2008, 41, 1983–1988.

[16] D. Li, S. Li, D. Cui, X. Zhang, "β-Diketiminato Rare-Earth Metal Complexes.

Structures, Catalysis, and Active Species for Highly cis-1,4-Selective Polymerization of Isoprene", *Organometallics*, 2010, 29, 2186–2193.

[17] L. Zhang, M. Nishiura, M. Yuki, Y. Luo, Z. Hou, "Isoprene Polymerization with Yttrium Amidinate Catalysts: Switching the Regio- and Stereoselectivity by Addition of AlMe3", *Angew. Chem. Int. Ed.*, 2008, 47, 2642–2645.

[18] C. W. Kamienski, "Lithium Catalysis in Industrial polymerization", *Ind. Eng. Chem.*, 1965, 57, 38–55.

[19] G. S. Girolami, G. Wilkinson, A. M. R. Galas, M. Thornton-Pett, M. B. Hursthouse, "Synthesis and properties of the divalent 1,2-bis(dimethylphosphino)ethane (dmpe) complexes $MCl_2(dmpe)_2$ and $MMe_2(dmpe)_2$(M = Ti, V, Cr, Mn, or Fe). X-Ray crystal structures of $MCl_2(dmpe)_2$(M = Ti, V, or Cr), $MnBr_2(dmpe)_2$, $TiMe_{1.3}Cl_{0.7}(dmpe)_2$, and $CrMe_2(dmpe)_2$", *J. Chem. Soc. Dalton Trans.*, 1985, 7, 1339–1348.

[20] F. A. Cotton, C. A. Murillo, M. A. Petrukhina, "Reactions of $TiCl_4$ with phosphines and alkylating reagents: an organometallic route to a titanium(II) cluster compound", *J. Organomet. Chem.*, 1999, 573, 78–86.

[21] J. A. Lopez-Sanchez, M. Lamberti, D. Pappalardo, C. Pellecchia, "Polymerization of Conjugated Dienes Promoted by Bis(phenoxyimino)titanium Catalysts", *Macromolecules*, 2003, 36, 9260–9263.

[22] G. Ricci, S. Italia, C. Comitani, L. Porri, "Polymerization of conjugated dialkenes with transition metal catalysts. Influence of methyl aluminoxane on catalyst activity and stereospecificity", *Polym. Comun.*, 1991, 32, 514–517.

[23] G. Ricci, S. Italia, L. Porri, "polymerization of 1,3-dienes with methylaluminoxane-triacetylacetontovanadium", *Macromol. Chem. Phys.*, 1994, 195, 1389–1397.

[24] L. Zhang, T. Suzuki, Y. Luo, M. Nishiura, Z. Hou, "Cationic Alkyl Rare-Earth Metal Complexes Bearing an Ancillary Bis(phosphinophenyl)amido Ligand: A Catalytic System for Living cis-1,4-Polymerization and Copolymerization of Isoprene and Butadiene", *Angew. Chem. Int. Ed.*, 2007, 46, 1909–1913.

[25] B. L. Small, M. Brookhart, A. M. A. Bennett, "Highly Active Iron and Cobalt Catalysts for the Polymerization of Ethylene", *J. Am. Chem. Soc.*, 1998, 120, 4049–4050.

[26] G. J. P. Britovsek, V. C. Gibson, S. J. McTavish, G. A. Solan, A. J. P. White, D. J. Williams, G. J. P. Britovsek, B. S. Kimberley, P. J. Maddox, "Novel olefin polymerization catalysts based on iron and cobalt", *Chem. Commun.*, 1998, 7, 849–850.

[27] G. J. P. Britovsek, M. Bruce, V. C. Gibson, B. S. Kimberley, P. J. Maddox, S. Mastroianni, S. J. McTavish, C. Redshaw, G. A. Solan, S. Strömberg, A. J. P. White, D. J. Williams, "Iron and Cobalt Ethylene Polymerization Catalysts Bearing 2,6-Bis(Imino)Pyridyl Ligands: Synthesis, Structures, and Polymerization Studies", *J. Am. Chem. Soc.*, 1999, 121, 8728–8740.

[28] Y. Jang, P. Kim, H. Lee, "Electronic and Steric Effects of Phosphine Ligand on the Polymerization of 1,3-Butadiene Using Co-Based Catalyst", *Macromolecules*, 2002, 35, 1477–1480.

[29] Y. Jang, P. Kim, H. Y. Jeong, H. Lee, "Effects of polarizability and electronic character of phosphine ligand on the polymerization of 1,3-butadiene using Co-based catalyst", *J. Mol. Catal. Chem.*, 2003, 206, 29–36.

[30] D. C. D. Nath, T. Shiono, T. Ikeda, "Copolymerization of 1,3-butadiene and isoprene with cobalt dichloride/methylaluminoxane in the presence of triphenylphosphine", *J. Polym. Sci. Part Polym. Chem.*, 2002, 40, 3086–3092.

[31] S. K.-H. Thiele, D. R. Wilson, “Alternate Transition Metal Complex Based Diene Polymerization”, *J. Macromol. Sci. Part C Polym. Rev.*, 2003, 43, 581–628.

[32] G. Ricci, D. Morganti, A. Sommazzi, R. Santi, F. Masi, “Polymerization of 1,3-dienes with iron complexes based catalysts: Influence of the ligand on catalyst activity and stereospecificity”, *J. Mol. Catal. Chem.*, 2003, 204–205, 287–293.

[33] B. K. Bahuleyan, J. M. Oh, D. Chandran, J. Y. Ha, A. Y. Hur, D.-W. Park, C. S. Ha, H. Suh, I. Kim, “Highly Efficient Supported Diimine Ni(II) and Iminopyridyl Fe(II) Catalysts for Ethylene Polymerizations”, *Top. Catal.*, 2010, 53, 500–509.

[34] C. Bazzini, A. Giarrusso, L. Porri, B. Pirozzi, R. Napolitano, “Synthesis and characterization of syndiotactic 3,4-polyisoprene prepared with diethylbis(2,2′-bipyridine)iron–MAO”, *Polymer*, 2004, 45, 2871–2875.

[35] B. Pirozzi, R. Napolitano, V. Petraccone, S. Esposito, “Determination of the Crystal Structure of Syndiotactic 3,4-Poly(2-methyl-1,3-butadiene) by Molecular Mechanics and X-Ray Diffraction”, *Macromol. Chem. Phys.*, 2004, 205, 1343–1350.

[36] M. Monthioux, P. Serp, E. Flahaut, M. Razafinimanana, C. Laurent, A. Peigney, W. Bacsa, J.-M. Broto,, *Springer Handb. Nanotechnol. Ed B Bhushan Springer Berl. Heidelb.*, 2007, 43–112.

[37] P. Serp, M. Corrias, P. Kalck, “Carbon nanotubes and nanofibers in catalysis”, *Appl. Catal. Gen.*, 2003, 253, 337–358.

[38] S. Park, I. S. Choi, “Production of Ultrahigh-Molecular-Weight Polyethylene/Pristine MWCNT Composites by Half-Titanocene Catalysts”, *Adv. Mater.*, 2009, 21, 902–905.

[39] S. Park, S. W. Yoon, H. Choi, J. S. Lee, W. K. Cho, J. Kim, H. J. Park, W. S. Yun, C. H. Choi, Y. Do, I. S. Choi, “Pristine Multiwalled Carbon Nanotube/Polyethylene Nanocomposites by Immobilized Catalysts”, *Chem. Mater.*,

2008, 20, 4588–4594.

[40] S. Park, S. W. Yoon, K.-B. Lee, D. J. Kim, Y. H. Jung, Y. Do, H. Paik, I. S. Choi, “Carbon Nanotubes as a Ligand in Cp_2ZrCl_2-Based Ethylene Polymerization”, *Macromol. Rapid Commun.*, 2006, 27, 47–50.

[41] F. J. Gómez, R. J. Chen, D. Wang, R. M. Waymouth, H. Dai, “Ring opening metathesis polymerization on non-covalently functionalized single-walled carbon nanotubes”, *Chem. Commun.*, 2003, 2, 190–191.

[42] S. Bredeau, L. Boggioni, F. Bertini, I. Tritto, F. Monteverde, M. Alexandre, P. Dubois, “Ethylene–Norbornene Copolymerization by Carbon Nanotube-Supported Metallocene Catalysis: Generation of High-Performance Polyolefinic Nanocomposites”, *Macromol. Rapid Commun.*, 2007, 28, 822–827.

[43] M. Alexandre, E. Martin, P. Dubois, M. G. Marti, R. Jérôme, “Polymerization-Filling Technique: An Efficient Way to Improve the Mechanical Properties of Polyethylene Composites”, *Chem. Mater.*, 2001, 13, 236–237.

[44] L. Cui, J. Yu, Y. Lv, G. Li, S. Zhou, “Doped polyaniline/multiwalled carbon nanotube composites: Preparation and characterization”, *Polym. Compos.*, 2013, 34, 1119–1125.

[45] D. Qian, E. C. Dickey, R. Andrews, T. Rantell, “Load transfer and deformation mechanisms in carbon nanotube-polystyrene composites”, *Appl. Phys. Lett.*, 2000, 76, 2868.

[46] E. J. García, A. J. Hart, B. L. Wardle, A. H. Slocum, “Fabrication and Nanocompression Testing of Aligned Carbon-Nanotube–Polymer Nanocomposites”, *Adv. Mater.*, 2007, 19, 2151–2156.

[47] P.-C. Ma, N. A. Siddiqui, G. Marom, J.-K. Kim, “Dispersion and functionalization of carbon nanotubes for polymer-based nanocomposites: A review”,

Compos. Part Appl. Sci. Manuf., 2010, 41, 1345–1367.

[48] X. Pan, X. Bao, "Reactions over catalysts confined in carbon nanotubes", *Chem. Commun.*, 2008, 47, 6271–6281.

[49] X. Pan, X. Bao, "The Effects of Confinement inside Carbon Nanotubes on Catalysis", *Acc. Chem. Res.*, 2011, 44, 553–562.

[50] P. Serp, E. Castillejos, "Catalysis in Carbon Nanotubes", *ChemCatChem*, 2010, 2, 41–47.

[51] P. Liu, "Modification Strategies for Carbon Nanotubes as a Drug Delivery System", *Ind. Eng. Chem. Res.*, 2013, 52, 13517–13527.

[52] W. Yang, P. Thordarson, J. J. Gooding, S. P. Ringer, F. Braet, "Carbon nanotubes for biological and biomedical applications", *Nanotechnology*, 2007, 18, 412001.

[53] A. Burke, X. Ding, R. Singh, R. A. Kraft, N. Levi-Polyachenko, M. N. Rylander, C. Szot, C. Buchanan, J. Whitney, J. Fisher, H. C. Hatcher, R. D'Agostino, N. D. Kock, P. M. Ajayan, D. L. Carroll, S. Akman, F. M. Torti, S. V. Torti, "Long-term survival following a single treatment of kidney tumors with multiwalled carbon nanotubes and near-infrared radiation", *Proc. Natl. Acad. Sci.*, 2009, 106, 12897–12902.

[54] Z. Liu, K. Chen, C. Davis, S. Sherlock, Q. Cao, X. Chen, H. Dai, "Drug Delivery with Carbon Nanotubes for In vivo Cancer Treatment", *Cancer Res.*, 2008, 68, 6652–6660.

[55] C. Ge, J. Du, L. Zhao, L. Wang, Y. Liu, D. Li, Y. Yang, R. Zhou, Y. Zhao, Z. Chai, C. Chen, "Binding of blood proteins to carbon nanotubes reduces cytotoxicity", *Proc. Natl. Acad. Sci.*, 2011, 108, 16968–16973.

[56] N. Weiss, T. Cren, M. Epple, S. Rusponi, G. Baudot, S. Rohart, A. Tejeda, V.

Repain, S. Rousset, P. Ohresser, F. Scheurer, P. Bencok, H. Brune, “Uniform Magnetic Properties for an Ultrahigh-Density Lattice of Noninteracting Co Nanostructures”, *Phys. Rev. Lett.*, 2005, 95, 157204.

[57] J. Gao, H. Gu, B. Xu, “Multifunctional Magnetic Nanoparticles: Design, Synthesis, and Biomedical Applications”, *Acc. Chem. Res.*, 2009, 42, 1097–1107.

[58] Y.-M. Huh, Y. Jun, H.-T. Song, S. Kim, J. Choi, J.-H. Lee, S. Yoon, K.-S. Kim, J.-S. Shin, J.-S. Suh, J. Cheon, “In Vivo Magnetic Resonance Detection of Cancer by Using Multifunctional Magnetic Nanocrystals”, *J. Am. Chem. Soc.*, 2005, 127, 12387–12391.

[59] P. Tartaj, M. del P. Morales, S. Veintemillas-Verdaguer, T. González-Carreño, C. J. Serna, “The preparation of magnetic nanoparticles for applications in biomedicine”, *J. Phys. Appl. Phys.*, 2003, 36, R182.

[60] S. Laurent, D. Forge, M. Port, A. Roch, C. Robic, L. Vander Elst, R. N. Muller, “Magnetic Iron Oxide Nanoparticles: Synthesis, Stabilization, Vectorization, Physicochemical Characterizations, and Biological Applications”, *Chem. Rev.*, 2008, 108, 2064–2110.

[61] L.-Y. Lu, L.-N. Yu, X.-G. Xu, Y. Jiang, “Monodisperse magnetic metallic nanoparticles: synthesis, performance enhancement, and advanced applications”, *Rare Met.*, 2013, 32, 323–331.

[62] L. Bogani, R. Maurand, L. Marty, C. Sangregorio, C. Altavilla, W. Wernsdorfer, “Effect of sequential grafting of magnetic nanoparticles onto metallic and semiconducting carbon-nanotube devices: towards self-assembled multi-dots”, *J. Mater. Chem.*, 2010, 20, 2099–2107.

[63] H. Bönnemann, W. Brijoux, R. Brinkmann, N. Matoussevitch, N. Waldöfner, N. Palina, H. Modrow, “A size-selective synthesis of air stable colloidal magnetic

cobalt nanoparticles", *Inorganica Chim. Acta*, 2003, 350, 617–624.

[64] J. Pyun, "Nanocomposite Materials from Functional Polymers and Magnetic Colloids", *Polym. Rev.*, 2007, 47, 231–263.

[65] I. Robinson, S. Zacchini, L. D. Tung, S. Maenosono, N. T. K. Thanh, "Synthesis and Characterization of Magnetic Nanoalloys from Bimetallic Carbonyl Clusters", *Chem. Mater.*,2009, 21, 3021–3026.

[66] E. Castillejos, P.-J. Debouttière, L. Roiban, A. Solhy, V. Martinez, Y. Kihn, O. Ersen, K. Philippot, B. Chaudret, P. Serp, "An Efficient Strategy to Drive Nanoparticles into Carbon Nanotubes and the Remarkable Effect of Confinement on Their Catalytic Performance", *Angew. Chem. Int. Ed.*, 2009, 48, 2529–2533.

[67] L. Zhang, E. Yue, B. Liu, P. Serp, C. Redshaw, W.-H. Sun, J. Durand, "Beneficial influence of nanocarbon on the aryliminopyridylnickel chloride catalyzed ethylene polymerization", *Catal. Commun.*, 2014, 43, 227–230.

[68] W. T. Eckenhoff, A. B. Biernesser, T. Pintauer, "Structural characterization and investigation of iron(III) complexes with nitrogen and phosphorus based ligands in atom transfer radical addition (ATRA)", *Inorganica Chim. Acta*, 2012, 382, 84–95.

[69] F. Dumestre, B. Chaudret, C. Amiens, P. Renaud, P. Fejes, "Superlattices of Iron Nanocubes Synthesized from [image]", *Science*, 2004, 303, 821–823.

[70] L.-M. Lacroix, S. Lachaize, A. Falqui, M. Respaud, B. Chaudret, "Iron Nanoparticle Growth in Organic Superstructures", *J. Am. Chem. Soc.*, 2009, 131, 549–557.

General conclusions and perspectives

Conclusions

Olefins, particularly ethylene and isoprene, are the basic building block of the petrochemical industry, while olefin-based polymers are by far the most important and thus the most produced synthetic polymers today. Catalysts which revolutionized the polyolefin manufacturing industry play important role in polymerization. Beside the Ziegler-Natta and Phillips catalysts which are the main catalyst successfully used in industrial, the 4 groups-based metallocene catalysts and single-site late transition metal catalysts based on imino-pyridine ligands have attracted interest in industrial and academy since the end of last century, due to either higher activity or easily controlled resulting polyolefin. Maintaining an elevated catalytic activity and the development of suitable systems for most of the industrial processes, using slurry or gas-phase reactors, require a necessary support for those homogeneous catalysts. A variety of inorganic supports, such as silica gel, $MgCl_2$, Al_2O_3, MgO etc., have been used to immobilize those homogeneous catalysts in decades. Nanocarbon materials (carbon nanotubes, CNTs and few layer graphene, FLG) were also used and investigated to support group 4-based metallocene catalysts and higher molecular weight nanometer morphology polyethylenes were obtained. However, only one family of CNTs supported late transition metal catalysts has been reported to date and was not investigated in detail. The research work of this PhD thesis intends to fill this gap: nanomaterials (CNTs, FLG and iron particles) covalently or non-covalently supported late transition metal catalysts and their use in olefin polymerization. Nanocarbons or particles, that can be considered as a bulky macro-ligand have a great influence in catalyst activities towards olefin polymerization and polymer coated polymer nanocomposites are obtained by those supported catalysts.

During this work, late transition metal catalysts based on imino-pyridine ligand and nanomaterial (CNTs, FLG and iron particles) covalently or non-covalently supported catalysts have been developed and employed in olefin polymerization.

Nickel complexes containing an $-NH_2$ function have been synthesized and supported by two kinds of functionalized multi-walled carbon nanotubes, CNT_F and CNT_C, *via* covalent bonds (O=C–N). Both those homogeneous catalysts and supported catalysts have been investigated in the ethylene polymerization reaction and shown moderate activity. Using carbon nanotubes as support, the activities of these immobilized catalysts are higher than these homogeneous catalysts. Besides that, the nature of the support has a great influence on the catalytic performances. The results of the ethylene polymerization promoted by immobilized catalysts show that the CNT_F as the support increase remarkably the homogeneous catalyst activity, and more than CNT_C. This study evidenced that not only CNTs can be beneficial to the polymerization reaction, but also that the nature of the nanomaterial used is also of importance. Moreover, the presence of the carbon nanotubes can also be efficient for increasing the molecular weight of the produced polymer.

Two iron complexes based on the 2,6-bis(imino)pyridyl framework and containing a pyrenyl moiety have been synthesized and immobilized catalysts have been produced by MWCNTs grafting of those iron complexes *via* π-π stacking interactions between the pyrene group and the surface of the support. Activated by MMAO, all of the iron homogeneous pre-catalysts promote ethylene polymerization with excellent activities and the iron complex with two pyrene groups showed higher activity and lower molecular weight distribution than the one having only one pyrene group, which evidenced a beneficial influence of the pyrene substituent introduced on the ligands. The catalytic screening of the heterogenized systems evidenced in one

case a significant increase of the productivity compared to the analogous unsupported system. Moreover, according to TEM and SEM images, the resulting materials show good dispersion of the MWCNTs into the polyethylene matrix resulting from the surface initiated polymerization reaction.

Imino-pyridine nickel complexes containing various kinds of aromatic groups (naphthalene, anthracene and pyrene) have also been synthesized and characterized. The polymerization conditions in the presence and in the absence of nanocarbon materials, such as MWCNTs or few layer graphene (FLG), were fully investigated using MAO as the co-catalyst. The microstructure of the polyethylene and the activities behavior could be controlled and tailor-made by ligand design and the presence of the nanocarbons. Without the nanocarbon materials, all of the nickel complexes are single-site catalysts which show high activity for the ethylene polymerization to afford low molecular weight and highly branched polyethylene. Furthermore, the presence of either MWCNTs or FLG in the catalytic mixture has an influence both on catalytic activity and on the properties of resulting polyethylene. Moreover, compared to the MWCNTs, the presence of FLG proved to be more beneficial for the catalytic activity. The SEM observations of the PE waxes produced in the presence of nanocarbons show a homogeneous dispersion of these carbon nanomaterials in the polymer matrix.

A series of iron complexes bearing 1-aryliminoethylpyridine ligands have been synthesized and been used as the catalysts for isoprene polymerization. With the triisopropylaluminum as the co-catalyst, those iron complexes shown excellent activity for the isoprene polymerization with the high *cis*-1,4-polyisoprene selectivity. Furthermore, the iron complex containing the naphthalene group has been immobilized on iron particles *via* π-π stacking interactions and then the immobilized

catalysts Cat@NPs were confined into the cavity of MWCNTs. The immobilized catalysts Cat@NPs and Cat@NPs@MWCNT were then used in isoprene polymerization. From the infrared spectroscopy, the iron complex are effectively immobilized at the surface of the nanoparticles, however, data concerning the amount effectively immobilized could not be determined. The TEM images of the Cat@NPs@IP shown that NPs are surrounded by the resulting polyisoprene and homogeneously dispersed inside. The polyisoprene produced by Cat@NPs@MWCNT are located inside the inner cavity of the MWCNTs. The goals of the project, which is the use of these resulting polyisoprene to protect NPs against oxidation, have been measured by Squid and the NPs showed no oxidation after air exposure.

Perspectives

For the research work of this PhD thesis, both the homogeneous late transition metal catalysts with nitrogen-donor ligands and their analogues covalently or non-covalently supported on nanomaterials (CNTs, FLG and iron particles) shown good or excellent activities for the olefin polymerization. Interestingly, the presence of the nanomaterials has a great influence on catalyst activities and properties of the resulting polymer nanocomposites. An important extension of this work would be to use these homogeneous and supported catalysts to synthesize other polymers or ethylene/olefin monomer copolymers. Late transition metal catalysts with diimine ligands were indeed also reported as the catalyst for the other monomers, such as propylene, butadiene, styrene, norbornene, …. Therefore, one of the further works could investigate the polymerization behaviour of nanocarbon material supported late

transition catalysts in those kinds of polymerization and co-polymerization.

Selection of the best nanocarbon support is also a promising issue. According to the results of the work described here, the nature of the carbon nanotubes have an influence on catalytic activity and polymer properties can be controlled by the chemical composition supported catalysts. Therefore, it is suggested that various nanocarbon materials (MWCNTs and FLG) with different size and diameters, are used to support homogeneous catalyst and investigated in polymerization procedures. The resulting polymer morphology and the properties of the resulting polymer nanocomposites (mechanical, thermal conductivity, flexibility, …) are worth to be comprehensively studied. Indeed, the efficient immobilization of single-site polymerization catalysts is a promising approach for the development of polymer nanocomposites containing a higly dispersed filler into a controlled polymeric matrix, an important issue in this research field of material science.

Concerning the polyisoprene part, polymerization conditions should be further investigated in order to improve the selectivity between *cis*-1,4-polyisoprene, *trans*-1,4-polyisoprene and 3,4-polyisoprene. Toluene was used as the solvent and other apolar solvents (heptane and methylcyclohexane) could be considered to be used in polymerization system and to study the effect of those solvent on the catalytic performances. For those immobilized catalysts, data concerning the amount of iron complexes which were effectively immobilized on the particles and their isoprene polymerization activity should be investigated.

Experimental details

1. Materials

Multi-walled nanotubes MWCNTs (98% purity, 2% iron catalyst, XRD: d_{002} = 0.3405, BET: 177 m^2/g) were synthesized by chemical vapor deposition and purified according to previously reported procedures [1]. FLG were synthesized by chemical vapor deposition according to reported procedures [2]. $FeCl_2$, $NiCl_2$, 2-acteylpridine, 2,6-diacetylpyridine 1-aminonaphthalene, 2-aminoanthracene, and 1-aminopyrene were purchased from Alfa Chemicals. 5,6,7-dihydroquinolin-8-one, 2,6-dimethylbenzene-1,3-diamine, 2,6-diethylbenzene-1,3-diamine, 2,6-diisopropylbenzene-1,3-diamine and 2,6-dimethylbenzene-1,4-diamine were purchased from AstaTech (Chengdu, China). Isoprene (99 % contains < 1000 ppm *p*-ter-butylcatechol), α-Phenyl-o-toluic acid (97%) and triisobutylaluminum ($Al(^iPr)_3$, 1.0 M solution in toluene) were purchased from Aldrich. Trityltetrakis(pentafluorophenyl)borate (97 %) was purchased from Strem chemicals.

$[Fe\{N(SiMe_3)_2\}_2]_2$ were purchased from NanoMeps. 4-(3-phenylpropyl)pyridine (98%) were purchased from Alfa Aesar. Methylaluminoxane (MAO, 1.46 M solution in toluene) and modified methylaluminoxane (MMAO, 1.93 M in heptane, 3A) were purchased from Akzo Nobel Corp. Diethylaluminum chloride (Et_2AlCl, 0.79 M in toluene) was purchased from Acros Chemicals. High-purity ethylene was obtained from Beijing Yansan Petrochemical Co. Toluene was refluxed over sodium-benzophenone and distilled under nitrogen prior to use. All other solvents were used as received from Aldrich or Acros Chemicals.

2. Experimental procedures

All manipulations of air and/or moisture sensitive compounds were carried out under a nitrogen atmosphere using standard Schlenk techniques or in glove-boxes.

2.1 Procedure for Ethylene Polymerization

2.1.1 Homogeneous polymerization

Ethylene polymerization at 10 atm ethylene pressure was carried out in a 250 mL stainless steel autoclave equipped with a mechanical stirrer and a temperature controller. Toluene, the desired amount of iron pre-catalyst and a toluene solution of the co-catalyst (for total volume of 100 mL) were added to the reactor in this order under an ethylene atmosphere. When the desired reaction temperature was reached, the ethylene pressure was increased to 10 atm, and maintained at this level by constant feeding of ethylene. After the desired reaction time, the reaction was quenched by addition of acidic ethanol. The precipitated polymer was washed with ethanol and water several times, and then dried under vacuum.

2.1.2. Polymerization using the MWCNTs supported complexes

Heterogeneous polymerizations were carried out by first adding desired amount of MWCNT-supported catalyst into the reactor. Then toluene and the desired amount of co-catalyst (total volume 100 mL) were added to the reactor under an ethylene atmosphere. The following procedure was the same as the one used for homogeneous polymerization.

2.1.3. Polymerization in the presence of MWCNTs or FLG

The desired amount of MWCNTs or FLG was placed into the reactor and the reactor was dried under vacuum. When the temperature stabilized at the required temperature, a 50 mL toluene solution of the nickel complex (5 μmol) was added to the reactor at 1 atm ethylene. The solution was stirred for 10 min at 1 atm ethylene, and then the desired mount of MAO was injected into the reactor as well as 50 mL toluene. The pressure of ethylene was immediately increased to 10 atm. After the desired duration, the reaction was quenched by addition of acidic ethanol. The precipitated polymer was washed with ethanol several times and dried under vacuum.

2.2. Procedure for isoprene polymerization

2.2.1. Homogeneous isoprene polymerization

3 μmol iron complex, 12 eq. $Al(^{i}Pr)_3$ (36 μmol) and the same eq. trityltetrakis(pentafluorophenyl)borate (3 μmol) were dissolved in 50 mL toluene. The solution was stirred for 5 min in a glove-box. When the colour of the solution turned to blue, isoprene (5.3 g, 7.5 mL) and the toluene were added into the solution, for a total volume of 100 mL. The reaction mixture was intensively stirred for the desired time under different temperature. The reaction was quenched by the addition of acidic ethanol. The precipitated polymer was washed with ethanol several times and dried under reduced pressure.

*2.1.2. Isoprene polymerization using the iron particles supported iron complexes (**Cat@NPs** and **Cat@NPs@MWCNT**)*

The procedure for heterogeneous polymerization is similar to that used for the

homogeneous iron complexes: Immobilized catalyst (10 mg **Cat@NPs** or 20 mg **Cat@NPs@MWCNT**), the desired volume of isoprene, 2 mL $Al(^{i}Pr)_3$ (0.02 M in toluene), 20 mg trityl tetrakis(pentafluorophenyl)borate and 100 mL toluene were added into a Schlenk flask. The reaction mixture was intensively stirred for 30 min at 25 °C. The toluene was removed under reduced pressure.

2.3. X-ray Crystallographic Studies

All of the crystals suitable for X-ray diffraction analysis were obtained by layering diethyl ether onto methanol at room temperature. With graphite-monochromated MoKα radiation (λ = 0.71073 Å) at 173(2) K, cell parameters were obtained by global refinement of the positions of all collected reflections. Intensities were corrected for Lorentz and polarization effects and empirical absorption. The structures were solved by direct methods and refined by full-matrix least squares on F^2. All hydrogen atoms were placed in calculated positions. Structure solution and refinement were performed by using the SHELXL-97 package [3].

3. Instruments and measurements

Transmission electron microscope (TEM) images were obtained using a JEOL JEM 2100F FEG at 200 kV or JEOL JEM-1400 at 120 kV. Samples were prepared by suspending the samples in solution (ethanol, acetone, THF or distilled water) under ultrasonic vibration. Some drops of the thus produced suspensions were deposited onto carbon-coated copper grids. Scanning electron microscope (SEM) images were obtained on a JEOL JSM 6700 Field Emission Gun scanning electron microscope. Thermogravimetric analysis (TGA) in air was conducted on a Setaram apparatus

using a temperature program of 30–800 °C, with a heating rate of 10 °C/min. The elemental analyses for C, H, O and N were performed on a Perkin Elmer 2400 series II microanalyser. The analyses of Al and Fe, were carried out by the "Service central d'analyse du CNRS" in Solaize, France. X-ray photoelectron (XPS) measurements were carried out using a K-alpha Thermo Scientific instrument operating with an Al Kα source (1486.6 eV). The binding energies were corrected with respect to the C1s core level fixed at 284.4 eV. ICP-MS measurements were carried out by Antellis. NMR spectra for the ligands were recorded on a Brucker AV 400 MHz instrument, NMR spectra for the polyethylene were recorded on a Bruker DMX 300 MHz instrument and NMR spectra for the polyisoprene were recorded on an Bruker 300 MHz instrument at ambient temperature using TMS as an internal standard. IR spectra were recorded on Perkin Elmer spectra one spectrometer using KBr salt for solid pellet analysis. Molecular weights (M_w) and molecular weight distribution (M_w/M_n) of polyethylenes were determined by a PL-GPC220 at 150 °C with 1,2,4-trichlorobenzene as the solvent and molecular weights (M_w) and molecular weight distribution (M_w/M_n) of polyisoprene were determined by performed on a size-exclusion chromatography (SEC) system equipped with a refractive index detector (RI 2000) using $CHCl_3$ as the solvent. DSC trace and melting points of polyethylene were obtained from the second scanning run on Perkin-Elmer DSC-7 at a heating rate of 10 °C min^{-1}. DSC trace and glass temperature of polyisoprene were determined by Netzsch DSC 204 with the TASC 414/4 controller scanning calorimeter under nitrogen atmosphere (flow rate = 50 ml min^{-1}).

References

[1] R. Philippe, A. Morançais, M. Corrias, B. Caussat, Y. Kihn, P. Kalck, D. Plee,

P. Gaillard, D. Bernard, P. Serp, “Catalytic Production of Carbon Nanotubes by Fluidized-Bed CVD”, *Chem. Vap. Depos.*, 2007, 13, 447–457.

[2] R. Bacsa, P. Serp, *FR Pat. 1103952*, 2011.

[3] G. M. Sheldrick, “SHELXTL-97, Program for the Refinement of Crystal Structures,”, *Univ. Gött. Ger.*, 1997.

Résumé

Le présent travail de doctorat est consacré à l'étude de l'immobilisation, covalente ou non covalente, sur différents nanomatériaux de catalyseurs moléculaires de polymérisation à base de fer et de nickel et comportant des ligands spécifiques azotés. Les polyoléfines sont à l'heure actuelle de loin les polymères le plus produits dans le monde et sont devenus indispensables à la vie quotidienne. De part un certain nombre de propriétés physico-chimiques, ils trouvent des applications dans différents domaines et l'on estime à environ 400 millions de tonnes d'ici 2050.

Parmi les polyoléfines, le polyéthylène, produit de la polymérisation de l'éthylène, représente à lui seul environ 50 % de la production industrielle. Ceci a été rendu possible grâce au développement de catalyseurs efficaces capables d'activer l'éthylène. Au niveau industriel, les catalyseurs hétérogènes de type Ziegler-Natta restent les plus utilisés pour la production de polyéthylène. Cependant, les recherches dans ce domaine ont vu l'émergence d'un certain nombre de systèmes aux propriétés catalytiques intéressantes, notamment dans l'optique de la synthèse contrôlée de polymères à polydispersité faible. Outre le catalyseur de Phillips, système hétérogène à base de chrome, différents systèmes homogènes ont également été développés et sont utilisés au niveau industriel, notamment les dérivés des métaux du groupe 4 de type métallocènes, permettant de produire différents type de polyéthylènes (Polyéthylène haute densité, polyéthylène basse densité, …).

Les composés des métaux de la droite du tableau périodique ont également attiré

l'attention comme catalyseurs de polymérisation d'oléfines depuis la fin des années 1990. En effet ces derniers présentent un certain nombre d'avantages par rapport à leurs homologues du groupe 4 comme par exemple une meilleure tolérance aux groupements fonctionnels (permettant la copolymérisation de monomères polaires), une activité catalytique élevée, une facilité de synthèse plus intéressante et une plus grande stabilité. Parmi ces derniers, citons notamment les complexes du fer et du nickel, conduisant respectivement à des polymères linéaires et branchés. Différents types de ligands, bidente ou tridente, ont été développés pour ces catalyseurs permettant l'obtention de systèmes parfois très actifs et très sélectifs, offrant ainsi de nouvelles opportunités pour l'industrie des polyoléfines. Cependant, ces systèmes catalytiques solubles dans le milieu réactionnel présentent certaines limitations à leur utilisation à un niveau industriel. Le principal problème lié à l'emploi de catalyseur homogène à grande échelle est la croissance contrôlée du polymère qui finit par se déposer sur les parois du réacteur. De plus, la plupart des sites de production industrielle utilisent des procédés en phase gaz ou « slurry ». En conséquence, pour pouvoir être utilisés dans de tels procédés, les catalyseurs moléculaires doivent être hétérogénéisés sur un support. Dans ce but, différents types de matériaux inorganiques ont été utilisés comme la silice, l'alumine ou l'oxyde de magnésium. Ces études ont montré qu'à la fois la nature du support et le procédé utilisés pour l'immobilisation du catalyseur ont un rôle crucial sur l'activité finale du système supporté. Dans la plupart des cas, l'immobilisation se traduit par une perte significative d'activité, limitant donc l'intérêt de l'utilisation des systèmes moléculaires supportés. En conséquence, la découverte de supports efficaces ne

nuisant pas aux performances initiales du site catalytique, reste toujours un enjeu de taille pour aller vers un développement industriel à grande échelle des systèmes moléculaires supportés.

D'autre part, dans la famille des polyoléfines, les polymères obtenus par polymérisation de diènes, et en particulier de l'isoprène, représentent également une part importante de l'activité industrielle dans ce domaine.

De par leurs propriétés particulières, les nanomatériaux comme les nanotubes de carbone, le graphène ou les nanoparticules métalliques nous ont alors semblé être un choix pertinent pour l'immobilisation de ces catalyseurs de polymérisation d'oléfine à base de nickel et de fer.

Quelques études récentes ont montré que, dans différents types de réactions catalytiques, l'immobilisation d'espèces moléculaires, en particulier à la surface de nanotubes de carbone, peut conduire à des performances catalytiques améliorées en termes d'activité, de sélectivité et/ou de recyclage. Dans le cas de catalyseurs de polymérisation, quelques études ont porté sur l'immobilisation sur nanotubes de carbone de catalyseurs à base de métaux de la gauche du tableau périodique, mettant en évidence une influence bénéfique de ce matériau nanocarboné sur l'activité ou la longueur des chaînes polymériques obtenues.

L'immobilisation de ces espèces moléculaires à la surface de nanomatériaux peut être effectuée selon deux grandes voies : la fonctionnalisation covalente, mettant en jeu la formation de liaisons chimiques entre le support et l'espèce immobilisée ou la fonctionnalisation non-covalente, mettant en jeu, dans le cas de matériaux

graphitiques, essentiellement des interactions π.

Dans les travaux décrits dans la littérature scientifique, un seul exemple mentionne l'utilisation de nanotubes de carbone pour l'immobilisation d'un complexe d'un métal de la droite du tableau périodique et son utilisation en catalyse de polymérisation d'oléfine.

Nous nous sommes donc intéressés au cours des travaux décrits dans ce manuscrit, à l'étude de l'influence de l'immobilisation de complexes du fer et du nickel sur des nanotubes de carbone, du graphène et des nanoparticules de fer. Nous avons ensuite testé leur activité catalytique dans la polymérisation d'oléfines (éthylène et isoprène) afin de développer des systèmes catalytiques physiquement hétérogènes mais possédant une réactivité de type homogène, en nous efforçant de rationaliser l'influence du support et de la méthode d'immobilisation sur les performances catalytiques.

Le chapitre I de ce manuscrit décrit l'état de l'art de la polymérisation d'oléfines à l'aide de catalyseurs contenant un métal de la droite du tableau périodique ainsi que les avancées concernant leur immobilisation sur différents supports. Nous y décrivons également les récents travaux portant sur l'utilisation de matériaux nanocarbonés (graphène et nanotubes de carbone) comme support de catalyseurs moléculaires ainsi que l'apport parfois bénéfique de ce type de support dans les différentes réactions catalytiques où ils ont été utilisés. Les différentes méthodes possibles d'immobilisation, et le type d'interactions mises en jeu au cours de ces processus d'immobilisation, sont également décrits. Enfin, l'analyse de ces travaux antérieurs,

nous conduit à conclure sur les différentes propriétés des nanosupports en termes de modifications des performances catalytiques et sur leurs potentiels apports à la catalyse de polymérisation d'oléfines.

Le chapitre II est consacré à l'étude d'une famille de composés du nickel, spécifiquement préparés et modifiés en vue de leur immobilisation covalente sur des nanotubes de carbones fonctionnalisés (Figure 1). Tous ces composés moléculaires ont été caractérisés et la structure de deux d'entre eux confirmée par diffraction des rayons X. Tous ces dérivés contiennent sur la structure de leur ligand un groupement fonctionnel amino $–NH_2$ ayant permis la formation d'un lien covalent de type amide avec des groupements carboxyliques préalablement introduits à la surface des nanotubes de carbone par un traitement à l'acide nitrique. Cette approche covalente, complémentaire de la fonctionnalisation non-covalente, a été largement étudiée pour le greffage de différents types d'espèces moléculaires ou macromoléculaires à la surface de matériaux nanocarbonés, en particulier de nanotubes de carbone. La formation d'une liaison covalente de type amide, comme dans les travaux décrits ici, reste à ce jour de loin la plus utilisée. La caractérisation des systèmes hybrides ainsi obtenus a ensuite été effectuée à l'aide de différentes techniques analytiques. La spectroscopie infra-rouge a permis de mettre en évidence la diminution de l'intensité de la vibration caractéristique des fonctions carboxyliques et la formation d'un lien amide a été confirmée grâce à l'apparition d'une bande caractéristique dans les systèmes où le catalyseur homogène a été greffé sur le nanotube. La spectroscopie Raman montre également une modification du système suite à cette fonctionnalisation. Enfin, les analyses par spectroscopie de photoélectrons XPS ont montré la présence

de signaux caractéristiques des atomes contenus dans le ligand, azote notamment, ainsi que du nickel à la surface des nanotubes de carbone fonctionnalisés. Du fait des faibles taux de fonctionnalisation, l'analyse semi-quantitative par XPS est relativement difficile à effectuer, c'est pourquoi la quantification précise de métal catalytiquement actif a été effectuée par dosage ICP-MS. Différents types de nanotubes de carbone ont été utilisés dans cette étude, mettant en évidence une très nette influence de la nature du support (porosité, diamètre et surtout pureté) à la fois sur l'efficacité de l'immobilisation (taux de fonctionnalisation de la surface) et sur les performances catalytiques des systèmes supportés dans la réaction de polymérisation de l'éthylène.

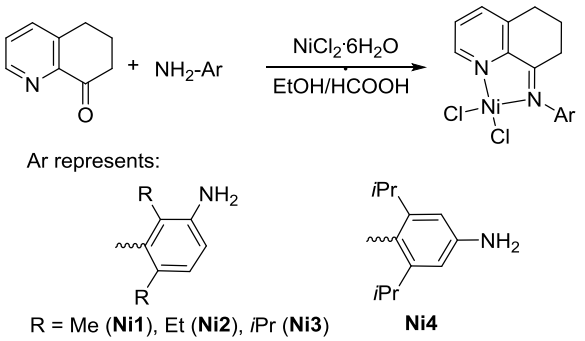

Figure 1. Catalyseurs à base de nickel synthétisés en vue d'une immobilisation covalente sur nanotubes de carbone

Dans un premier temps, les précatalyseurs **Ni1**-**Ni4** (Figure 1) ont fait l'objet d'un screening catalytique afin d'évaluer leurs performances pour la polymérisation de l'éthylène et d'optimiser les conditions de réactions. Ainsi l'influence de la nature de l'activateur, ainsi que des quantités introduites, celle de la température, du temps de

réaction ont été étudiés. Comme pour ceux décrits dans les chapitres suivants, tous les polymères obtenus ont ensuite été également analysés par chromatographie d'exclusion stérique, par calorimétrie différentielle à balayage et par spectroscopie de résonance magnétique nucléaire (RMN) afin d'étudier l'influence des conditions de réactions non seulement sur l'activité du système catalytique mais également sur les propriétés des polyéthylènes obtenus, notamment le poids moléculaire (longueur de la chaîne), la polydispersité, la température de fusion et le degré de branchement de la chaîne.

Cette étude a ainsi permis d'identifier le méthylaluminoxane (MAO) comme le meilleur activateur pour ces systèmes, les performances catalytiques en terme d'activité étant maximales pour un rapport Al/Ni de 1500. Une légère élévation de la température de réaction, de 20 à 50 °C, a montré une très nette diminution de l'activité catalytique.

Les précatalyseurs de nickel ainsi préparés présentent, dans des conditions de catalyse homogène, des activités raisonnables, comparés à celles d'autres composés analogues décrits dans la littérature. Les systèmes étudiés présentent différentes activités catalytiques et il a été possible de mettre en évidence l'ordre suivant : **Ni3** > **Ni2** > **Ni1** >> **Ni4**. La comparaison avec des systèmes analogues met en évidence une influence négative de la présence du groupement fonctionnel $-NH_2$ sur l'activité catalytique, probablement pour des raisons électroniques plus que stériques et/ou la possibilité de réactions secondaires au niveau de ce groupement. Les mauvaises performances du système **Ni4** montrent également que la position de ce groupement amino joue un rôle important dans la catalyse de polymérisation de l'éthylène.

En revanche, l'optimisation du choix du support et des conditions de réactions a conduit à l'amélioration des performances catalytiques pour les systèmes immobilisés de manière covalente sur des nanotubes de carbone multi-paroi.

Activés à l'aide du MAO, les systèmes comprenant les composés **Ni1**-**Ni3** supportés de manière covalente sur les nanotubes de carbone sont tous plus actifs que leurs analogues non supportés. Ces améliorations incluent non seulement une influence positive sur l'activité catalytique, mais se traduisent également par des modifications au niveau des polymères obtenus. Ainsi les polyéthylènes formés à l'aide des systèmes supportés sur nanotube de carbone sont de poids moléculaire plus élevés que ceux obtenus dans des conditions homogènes. Concernant le taux de branchement de la chaîne polymérique, on note également à ce niveau une influence du support puisque les polymères obtenus avec les systèmes immobilisés contiennent tous un nombre de branches plus élevés. Enfin, notons également que la polydispersité des polymères est aussi plus élevée dans le cas des systèmes contenant le support carboné, ce qui pourrait indiquer la formation dans ce cas de plusieurs types d'espèces catalytiquement actives, contrairement à ce qui est observé pour les systèmes homogènes qui conduisent à des polyéthylènes de polydispersité plus faible et plus proche de 2. Toutes ces observations mettent donc en évidence le rôle important joué par le support carboné sur différents facteurs influençant l'activité et la sélectivité de l'espèce catalytique comme la stabilité de l'espèce active, le nombre de sites activés, les vitesses relatives de propagation de chaîne, d'isomérisation et de terminaison. En effet la proximité du nanotube de carbone et du site catalytiquement actif dans les systèmes décrits ici, ainsi que l'interaction covalente mise en jeu,

conduit à une influence importante du support sur les performances catalytiques du système pour lequel le support joue le rôle de « macro-ligand » et influence donc sa réactivité à la fois de manière stérique et électronique. D'autre part la synthèse d'un dérivé moléculaire analogue aux systèmes supportés, contenant un lien amide et un groupement aromatique, a permis de montrer, lors de l'étude de son comportement catalytique, que l'amélioration observée était bien due à la présence du nanotube de carbone et non à la formation du lien amide et/ou la disparition du groupement amine sur le ligand. Notons que dans la plupart des cas, l'utilisation d'un support pour l'immobilisation d'une espèce moléculaire conduit généralement, et pour différentes raisons liées à des paramètres physico-chimiques comme décrit dans le chapitre I, à une diminution de l'activité catalytique. En revanche, il existe plusieurs cas où les études ont permis de montrer que cette tendance n'est pas généralisable à tous les systèmes et en particulier, quelques catalyseurs supportés contenant des métaux de la gauche du tableau périodique ont montré des améliorations notoires, aussi bien en termes d'activité que de poids moléculaire des polymères formés, dans les réactions de polymérisations d'oléfines comme l'éthylène ou le propylène. L'origine de cette amélioration n'est certes pas encore très claire. Nous pouvons évoquer la nature et les propriétés du nanotube utilisé comme support. En particulier la conductivité thermique de ce dernier pourrait conduire à une évacuation efficace de la chaleur dégagée par la réaction de polymérisation exothermique et donc éviter la formation de points chauds, conduisant à une meilleure stabilité de l'espèce active. Nous avons montré que l'utilisation de tubes contenant plus de défauts au niveau de leur structure, et donc une moins bonne conductivité, augmentait également les performances du

système mais dans une bien moindre mesure.

Enfin, la caractérisation par microscopie électronique à balayage des matériaux polymériques obtenus a mis en évidence une très bonne dispersion des nanotubes de carbone au sein de la matrice polymérique. Tous les nanotubes sont complétement recouverts d'une couche de polyéthylène. Ainsi, l'approche décrite dans ce travail peut également ouvrir la voie à la préparation de matériaux nanocomposites polyéthylène/nanotubes de carbone aux propriétés contrôlées. En effet, l'immobilisation d'un catalyseur moléculaire permet à la fois, du fait que la polymérisation est initiée depuis la surface du nanotube, de casser les agrégats et l'espèce catalytique permet un contrôle précis de la morphologie du polymère obtenu, de manière beaucoup plus efficace que pour un polymère obtenue par une voie non contrôlée comme la polymérisation radicalaire ou anionique, fréquemment utilisée pour la préparation de nanomatériaux composites de ce type.

Dans le chapitre III, différents complexes de fer, basés sur des ligands à squelette de type bis-iminopyridine, et contenant un ou deux groupement(s) polyaromatique(s) de type pyréniques ont été synthétisés (Figure 2), en vue cette fois-ci de leur immobilisation non covalente sur des nanomatériaux carbonés (nanotubes de carbone et graphène). Dans cette approche, l'interaction entre l'espèce immobilisée et le support est moins forte qu'une liaison covalente mais présente l'avantage de pouvoir être effectuée sans modification chimique préalable de la surface. Les ligands correspondants ainsi que leurs complexes de fer ont été caractérisés en utilisant la spectroscopie infra-rouge, RMN, ainsi que par analyse élémentaire. La structure

moléculaire du complexe **Fe1** a également pu être confirmée grâce à une analyse par diffraction des rayons X sur monocristal. Le processus d'immobilisation met en jeu des interactions faibles entre le groupe polyaromatique porté par le catalyseur moléculaire et la surface graphitique du nanomatériau, ces dernières sont grandement dépendante des conditions dans lesquelles est réalisée cette immobilisation. L'analyse de ces systèmes supportée par différentes techniques a permis de mettre en évidence son efficacité lors qu'elle est effectuée à température ambiante dans le dichlorométhane. Les données obtenues par spectroscopie XPS mettent en évidence la présence de fer au degré d'oxydation II et l'absence de Fe métallique au degré d'oxydation 0, montrant ainsi la stabilité du complexe au cours du processus d'immobilisation. Comme précédemment décrit, les quantités de complexes immobilisés étant relativement faibles, l'analyse semi-quantitative par XPS n'a pas été possible. La détermination quantitative de la quantité de complexes effectivement adsorbés à la surface a donc été effectuée par ICP-MS.

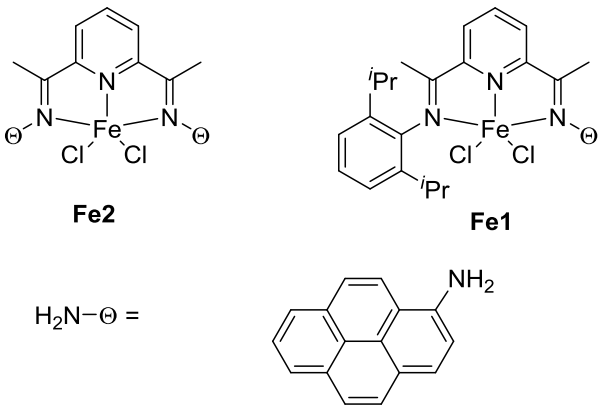

Figure 2. Catalyseurs moléculaires à base de fer synthétisés en vue d'une immobilisation non covalente sur nanotubes de carbone

Pour les deux complexes **Fe1** et **Fe2**, une étude préalable de leur comportement catalytique dans ces conditions homogènes, a permis de mettre en évidence le rôle bénéfique du groupement pyrénique introduit dans la structure du ligand. Dans un premier temps, nous avons conduit une étude paramétrique afin d'optimiser les conditions de réactions pour ces systèmes. Il a ainsi été possible d'identifier le meilleur activateur, le rapport Fe/Al le plus efficace pour cet activateur, ainsi que la meilleure température de réaction. Une fois activés par le MMAO (méthylaluminoxane modifié), ces complexes catalysent la polymérisation de l'éthylène avec des activités particulièrement élevées, comparables à celles des meilleurs systèmes décrits dans la littérature. Cette influence bénéfique du groupement pyrénique est également confirmée par la comparaison des activités de **Fe1** et **Fe2**, ce dernier étant encore plus actif que son homologue ne contenant qu'un seul fragment pyrénique. De plus, une étude cinétique a permis de montrer que pour **Fe2** la réaction est pratiquement terminée au bout de 15 minutes environ contre 30 pour **Fe1**. L'influence du nombre de groupements pyréniques portés par le complexe est également observée au niveau de la nature des polymères formés. Ainsi le complexe **Fe2** conduit à des polyéthylènes de plus faible poids moléculaire ainsi qu'à une polydispersité plus faible, probablement due à la nature symétrique de l'espèce catalytique, contrairement au cas du complexe **Fe1**.

Notons également que pour les deux systèmes une augmentation de la température conduit à une baisse significative de l'activité catalytique mais à une

augmentation de la longueur des chaînes de polyéthylène formées ainsi que de la polydispersité.

L'immobilisation de ces systèmes sur nanotubes de carbone multi-paroi a conduit également dans un cas (**Fe1**) au développement d'un système encore plus actif que son analogue non supportée, mettant en évidence le rôle non innocent du support carboné dans la catalyse de polymérisation. Dans le cas de **Fe2**, l'influence bénéfique du support se traduit par une diminution significative de la polydispersité des polyéthylènes formés, probablement due à la formation d'un nombre moindre d'espèces actives et/ou à un encombrement stérique beaucoup trop important dans ce cas, le complexe possédant deux groupements pyréniques susceptibles d'interagir avec la surface des nanotubes pouvant en effet réduire de manière importante l'accessibilité du site actif. De manière surprenante, l'étude catalytique a montré une influence différente de la température selon le système considéré. En effet, pour le systèmes **Fe1** supporté sur nanotubes de carbone, comme pour les systèmes homogènes, une augmentation de la température conduit à une augmentation importante du poids moléculaire des polymères obtenus alors que pour **Fe2**, cette même élévation de la température de réaction conduit à une diminution des longueurs de chaînes.

L'analyse par microscopie électronique à balayage a montré que dans les échantillons polyethylène/nanotube de carbone formés, ces derniers sont individuellement séparés, montrant l'efficacité de cette approche d'immobilisation non covalente pour obtenir des nanocomposites où le matériau nanocarboné est dispersé au sein de la matrice polymérique. Ces résultats montrent également qu'au

cours de la réaction catalytique, l'espèce active reste en contact intime avec la surface du support et que le processus de désorption est limitée voire inexistant.

Le chapitre IV décrit la synthèse et la caractérisation de deux familles de complexes de nickel. Ces complexes comportent tous un ligand bidente de type imino-pyridine et un substituent polyaromatique dérivé soit de l'anthracène, du naphtalène ou du pyrène. L'objectif de cette partie est d'étendre à des composés du nickel les résultats obtenus précédemment avec les complexes de fer décrits dans le chapitre III concernant l'immobilisation non covalente. Ainsi, il a été possible de développer des systèmes actifs en polymérisation de l'éthylène (fragment nickel-iminopyridine) et capables d'interagir (partie polyaromatique) de manière non-covalente avec la surface graphitique de nanomatériaux carbonés (graphène et nanotubes de carbone). La première famille de complexes (**Ni6**-**Ni8**) est basée sur des ligands à squelette imino-pyridine, la seconde famille de complexes décrit (**Ni9**-**Ni13**) est basée sur le squelette 5,6,7-trihydroquinoline (Figure 3). Au sein de ces deux familles, différents types de substituants polyaromatiques, capables de former des interactions avec la surface de nanomatériaux carbonés, ont été introduits afin de déterminer leur influence à la fois sur le processus d'immobilisation et dans la réaction catalytique de polymérisation de l'éthylène.

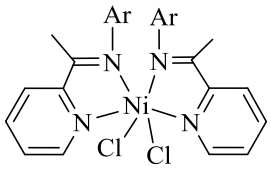

Ni6-Ni8

Ar :

naphthalen-1-yl **Ni6**

anthracen-2-yl **Ni7**

pyren-1-yl **Ni8**

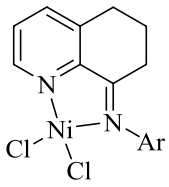

Ni9-Ni13

Ar:

naphthalen-1-yl **Ni9**

anthracen-2-yl **Ni10**

pyren-1-yl **Ni11**

quinolin-5-yl for **Ni12**

quinolin-8-yl **Ni13**

Figure 3. Catalyseurs moléculaires à base de nickel synthétisés en vue d'une immobilisation non covalente sur nanotubes de carbone et graphène

La structure moléculaire de deux de ces complexes a été confirmée par diffraction des rayons X, mettant en évidence que, selon la nature du ligand utilisé, les structures des complexes formés peuvent exister sous forme monomérique ou dimérique. Dans ce dernier cas, les ligands chlorures sont pontants entre deux atomes de nickel.

L'étude du comportement catalytique en conditions homogènes de ces précurseurs de nickel a montré une activité modérée pour la polymérisation de l'éthylène, conduisant à la formation de polyéthylènes branchés de faible poids moléculaire. Une étude détaillée de ces systèmes homogènes a été menée, permettant d'optimiser les conditions de réactions. Ainsi il a été montré que pour ces dérivés, le méthylaluminoxane (MAO) est le meilleur activateur, conduisant à la meilleur activité pour un rapport Al/Ni de 1000 ou 1500 selon les systèmes considérés. Contrairement à ce qui a été décrit pour d'autres systèmes catalytiques à base de nickel, ce rapport correspond également à un maximum pour le poids moléculaire des polyéthylènes

formés. De plus, et comme décrit pour les systèmes étudiés au cours des chapitres précédents, une augmentation de la température de réaction conduit généralement à une baisse significative de l'activité catalytique. Notons que généralement, les précatalyseurs de la première famille sont globalement plus actifs que ceux appartenant à la seconde.

Les réactions de polymérisation ont ensuite été testées en ajoutant au sein du réacteur différentes quantités de matériau nanocarboné (graphène ou nanotubes de carbone multi-parois). Ces études ont permis de montrer que l'effet de l'addition de nanotubes de carbone produit un effet contrasté sur les performances catalytiques du système. En effet, de faibles quantités ne modifient pas significativement l'activité du système alors que l'augmentation de la quantité de nanotubes conduit à une diminution des performances catalytiques pour la première famille de catalyseurs. De plus, l'augmentation des quantités de nanotubes ajoutées conduit également à une diminution du poids moléculaire des polymères formés ainsi qu'à une augmentation importante du nombre de branches présentes au sein de ces chaînes polymériques. La tendance est légèrement différente pour les catalyseurs de la seconde famille pour lesquels il a été observé généralement une légère augmentation de l'activité catalytique en présence de faibles quantités de nanotubes de carbone. Dans ce cas, une augmentation des longueurs de chaînes des polymères, obtenus en présence de nanotubes de carbone, a également été observée. En revanche, l'addition de petites quantités de graphène s'est avérée plus bénéfique, conduisant à une augmentation significative de l'activité ainsi qu'à la formation de polymères dont le poids moléculaire est plus élevé par rapport à celui des polyéthylènes obtenus à partir des

catalyseurs analogues non supportés, et ce pour les deux familles de catalyseurs étudiées.

L'analyse thermogravimétrique des matériaux hybrides (polymère/nanocarbone) ainsi obtenus a montré une diminution significative de la température de décomposition due à la présence du support, graphène ou nanotubes.

Les analyses microscopiques (microscopie électronique en transmission et microscopie électronique à balayage) ont montré, comme pour les systèmes décrits précédemment, un bon taux de dispersion des nanotubes de carbone au sein des matrices polymériques, mettant en évidence une probable interaction entre les espèces catalytiques et la surface des tubes au sein du milieu réactionnel. Cette interaction engendrant la croissance de la chaîne polymérique depuis la surface du nanotube, conduisant ainsi à leur séparation individuelle. Dans le cas des échantillons contenant le graphène, ce dernier est difficilement observable sur les clichés de microscopie mais l'absence de ségrégation semble suggérer dans ce cas également une dispersion effective du support carboné au sein du polymère formé.

Dans le chapitre V, les ligands décrits précédemment dans le chapitre IV ont été utilisés pour préparer de nouveaux composés de fer pour la polymérisation de l'isoprène (Figure 4). Cette partie s'inscrit dans le cadre d'un projet plus vaste, visant au confinement de nanoparticules magnétiques métalliques de fer à l'intérieur de la cavité de nanotubes de carbone. Afin de préserver intactes les propriétés magnétiques de ces particules, particulièrement sensibles à l'oxydation au contact de l'oxygène, il est indispensable de pouvoir les protéger de l'air. C'est pourquoi nous avons

développé les composés décrits dans ce chapitre (Figure 4) dont la partie polyaromatique portée par le ligand peut interagir efficacement avec la surface des nanoparticules métalliques. Cette interaction nous a alors permis d'envisager la formation catalytique de polyisoprène directement depuis la surface de la particule métallique à protéger de l'oxydation. La stratégie générale utilisée est représentée schématiquement dans la Figure 5.

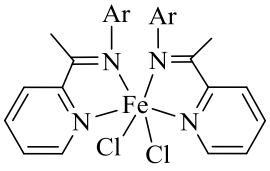

Fe6, Fe8

Ar:
naphthalen-1-yl **Fe6**
pyren-1-yl **Fe8**

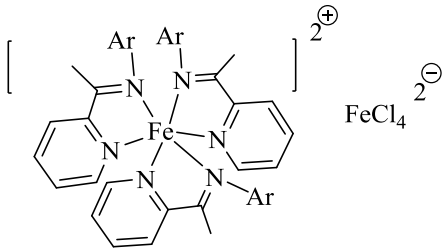

Fe7

Ar :
anthracen-2-yl **Fe7**

Figure 4. Catalyseurs moléculaires à base de fer synthétisés en vue d'une immobilisation non covalente à la surface de nanoparticules magnétiques

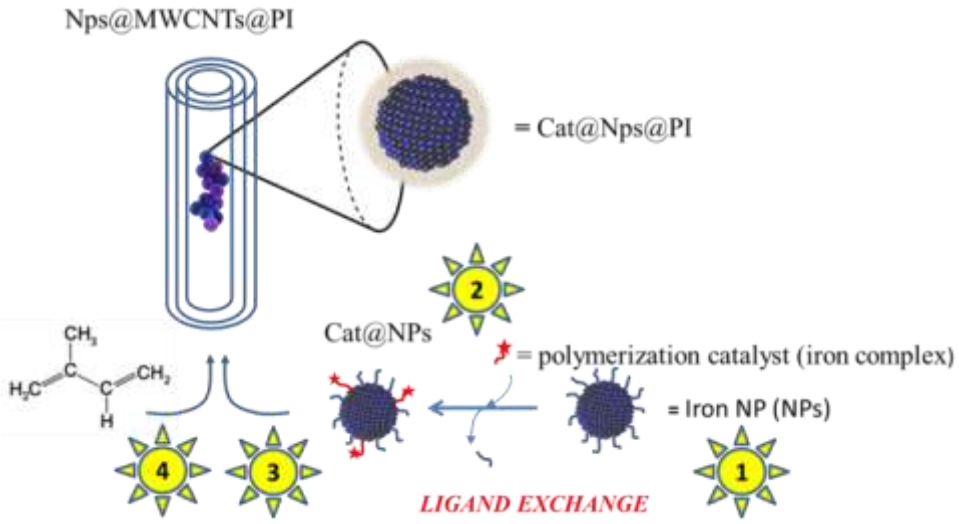

Figure 5. Approche "Bottom-up" pour la production de nanoparticules magnétiques confinées dans des nanotubes de carbone multi-parois et protégées de l'air. (1) synthèse de nanoparticules de fer; (2) synthèse de nanoparticules de fer modifies par un catalyseur de polymérisation; (3) confinement sélectif dans des nanotubes de carbone et (4) polymérisation de l'isoprène en milieu confiné

Tous ces complexes ont été caractérisés par spectroscopie et analyse élémentaire. De plus, les composés **Fe6-Fe8** (Figure 4) synthétisés ont pu tous être caractérisés également par diffractions des rayons X sur monocristaux. Cette étude a permis de mettre en évidence deux types de structures différentes pour ces composés. En effet, si dans deux cas la structure est bien celle attendue, à savoir un centre métallique portant deux ligands chlorures et deux ligands bidentes azotés, dans le cas du ligand contenant le fragment anthracényl, la structure révèle un cation du fer(II) comportant trois ligands bidente et un contre-anion $FeCl_4^{2-}$ (Figure 4). Au sein de cette structure, les trois groupements aromatiques anthracényles sont orientés du même côté de la

molécule formant une structure particulière présentant une cavité tubulaire au bout de laquelle est placée le contre-anion.

Avant d'effectuer leur incorporation à la surface des nanoparticules métalliques, ces composés ont tous été testés dans des conditions homogènes en tant que catalyseurs de la polymérisation de l'isoprène. Ce screening catalytique a permis, une fois encore, de montrer l'effet bénéfique du substituant polyaromatique porté par le ligand sur l'activité catalytique. En effet, activés par le triisopropylaluminum, tous les systèmes décrits se sont révélés être particulièrement actifs, rivalisant avec les meilleurs systèmes décrits jusqu'à présent dans la littérature. D'autre part, une analyse complète des polymères obtenus, notamment par calorimétrie différentielle à balayage et spectroscopie RMN, a montré la formation de polyisoprènes à température de transition vitreuse élevée ainsi que la formation majoritaire du motif *cis*-1,4 (jusqu'à plus de 99 %) au sein de la chaîne polymérique. Au cours de cette étude, nous avons également étudié l'influence de la température et de la présence ou non d'activateur sur les performances des systèmes. Ceci nous a permis d'identifier le complexe **Fe6** comme étant le plus actif. Il a donc ensuite été sélectionné pour être immobilisé à la surface de nanoparticules de fer par échange de ligand. Ces particules ont ensuite été introduites sélectivement dans la cavité interne de nanotubes de carbone, selon une procédure développée précédemment au sein du laboratoire. Cette étape nécessite un fonctionnalisation préalable de la surface des nanotubes de carbone par une fonction amide portant une longue chaîne carbonée. L'efficacité de cette méthodologie a pu être confirmée, y compris dans le cas des systèmes décrits dans ce travail, par microscopie électronique qui montre bien que la grande majorité des particules

formées se situent à l'intérieur de la cavité des nanotubes de carbone. Ces deux systèmes hybrides ont ensuite été testés comme catalyseurs pour la polymérisation de l'isoprène. Dans les deux cas, la formation de polymère est observée, montrant l'échange efficace du catalyseur **Fe6** à la surface des nanoparticules et leur maintien sur cette surface au cours du confinement dans les nanotubes. Les analyses microscopiques ont également montré que ces systèmes permettent la formation d'une couche de polyisoprène autour des nanoparticules, y compris pour le système où ces dernières sont confinées à l'intérieur de la cavité du nanotube de carbone. D'autre part, l'observation de ces systèmes par microscopie électronique en transmission a montré qu'au cours du processus les particules initiales restent bien dispersées et l'analyse de la distribution de taille n'a pas montré de modifications significatives. Enfin, des mesures magnétiques sur ces systèmes nanocomposites (nanoparticules de fer entourées de polyisoprène) après exposition à l'air ont été effectuées et ont montré un maintien des propriétés magnétiques de particules, mettant en évidence la validité de notre approche et l'efficacité de la couche de polyisoprène pour protéger de l'oxydation les particules magnétiques.

En conclusion, au cours de ce travail, différents complexes des métaux de la droite du tableau périodique, nickel et fer, basés sur des ligands à squelette imino-pyridine ont été préparés et immobilisés, de manière covalente ou non, sur différents types de nanomatériaux comme des nanotubes de carbone multi-parois, du graphène ou encore des nanoparticules magnétiques. Ces systèmes ont ensuite été étudiés en détail pour leur comportement catalytique dans la polymérisation d'oléfines

comme l'éthylène ou l'isoprène. Dans tous les cas, une étude préalable des performances des systèmes a été menée dans des conditions homogènes (systèmes non supportés) afin d'une part, d'optimiser les paramètres de la réaction catalytique et de pouvoir ainsi identifier les meilleures conditions de réactions et d'autre part de pouvoir essayer au mieux de comparer les performances des systèmes immobilisés et donc l'influence du support sur le comportement catalytique de ces systèmes. Ces performances ont été évaluées non seulement en termes d'activité catalytique mais également en nous intéressant aux caractéristiques de polymères obtenus comme leur poids moléculaire, la polydispersité, leur température de fusion ou de transition vitreuse, ou encore le taux de branchement de la chaîne.

Les différents systèmes moléculaires étudiés ont été spécifiquement modifiés en introduisant différentes fonctionnalités chimiques en vue d'une interaction avec les supports considérés. Ainsi, des groupements amino ont été introduits sur le squelette des ligands pour une interaction covalente par formation de liaison de type amide avec le support. D'autre part, différents groupes polyaromatiques ont été introduits afin de favoriser les interactions faibles avec la surface graphitique des supports.

Nous avons ainsi pu mettre en évidence la validité des deux approches, covalente ou non, pour favoriser les performances du système. Dans différents cas, il a été possible de développer des systèmes dont l'activité est plus élevée à la suite de l'immobilisation. Cette dernière pouvant également conduire à des modifications structurale notables des polymères formés (longueur de chaînes, taux de branchement, etc…). Nous avons également pu mettre en évidence le rôle important joué par la nature du support. Ainsi par exemple, différents types de nanotubes multi-parois

conduisent à des comportements catalytiques notablement différents. De la même manière, l'influence du graphène s'est avérée être plus bénéfique dans les cas où elle a été comparée à celle des nanotubes de carbone. Ces résultats offrent des perspectives intéressantes dans le domaine du développement de systèmes catalytiques qui peuvent potentiellement être utilisés dans des procédés industriels de polymérisation nécessitant l'emploi de catalyseurs hétérogénéisés. En effet, la plupart du temps les processus d'immobilisation conduisent à une réduction non négligeable et non souhaitée de l'activité catalytique, inconvénient qui peut être contourné grâce aux systèmes décrits dans ce travail. D'autre part, comme nous l'avons montré, un choix judicieux de combinaison support/catalyseurs ainsi que des conditions opératoires optimisées permettent également un contrôle de la morphologie des polyéthylènes obtenus et donc de leurs propriétés physiques.

Enfin, dans tous les cas étudiés, ces systèmes supportés sur nanomatériaux carbonés ont conduit à la formation de nanocomposites de polyéthylène pour lesquels le support initial se retrouve au sein de la matrice polymérique avec un taux de dispersion important, ouvrant ainsi la voie à de nouvelles méthodes de préparation de polymères à structure contrôlée et modifiés par de petites quantités de nanotubes de carbone ou de graphène.

Enfin, nous avons également pu développer des systèmes qui peuvent permettre la formation d'une couche protectrice autour de nanoparticules magnétiques confinées au sein de la cavité de nanotubes de carbone et sensibles à l'oxydation par l'air. Ces travaux devraient pouvoir permettre l'utilisation de ces nouveaux systèmes hybrides dans différents domaines.

Abstract

This present thesis deals with the development of active olefin polymerization catalysts based on late transition metal (nickel and iron) imino-pyridine complexes supported on nanomaterial. Chapter I gives a comprehensive literature review of unsupported and supported ethylene polymerization catalyst. In Chapter II we report the ethylene polymerization studies using nickel complexes containing an $–NH_2$ group for covalent immobilization on multi-walled carbon nanotubes (MWCNTs) of the corresponding precatalysts. Comparison of the homogeneous catalysts with their supported counterparts evidenced higher catalytic activity and higher molecular weights for the polymers produced. In Chapter III, iron complexes containing a pyrene group have been synthesized and immobilized on MWCNTs through non-covalent π-π interactions between pyrene group and surface of MWCNTs. Activated by MMAO, both the iron complexes and immobilized catalysts show high activities for ethylene polymerization. It was possible to evidence that MWCNTs have a great influence on the catalytic activity and on the structure of the resulting polyethylenes. Imino-pyridine nickel complexes containing various kinds of aromatic groups have been synthesized in Chapter IV and polymerization conditions in the presence and in the absence of nanocarbon materials, such as MWCNTs or few layer graphene (FLG), are discussed. For those nickel catalysts bearing 1-aryliminoethylpyridine ligands, the presence of MWCNTs in the catalytic mixture allows the formation of waxes of lower molecular weight and polydispersity, whereas the presence of FLG proved to be beneficial for the catalytic activity. In Chapter V, isoprene polymerization catalyzed by iron complexes containing polyaromatic groups and non-covalently supported on nanoparticles and confined into the inner cavity of MWCNTs (Cat@NPs and Cat@NPs@MWCNTs) are investigated. Iron complexes show excellent activity for the isoprene polymerization and produced high glass temperature polyisoprene with a high *cis*-1,4-polyisoprene selectivity. Polymer nanocomposites are produced by supported catalysts and, transmission electron microscopy (TEM) evidenced efficient coating of the resulting polyisoprene around the oxygen sensitive $iron^0$ nanoparticles.

Résumé

Le présent travail de thèse décrit le développement de systèmes actifs de polymérisation d'oléfines basés sur des métaux de fin de transition (nickel et fer) supportés sur des nanomatériaux. Le chapitre I décrit l'état de l'art des systèmes catalytiques supportés ou non pour la polymérisation d'oléfines. Dans le chapitre II, nous décrivons la polymérisation de l'éthylène en utilisant des catalyseurs de nickel contenant un groupement $–NH_2$ pour leur immobilisation covalente sur nanotubes de carbone ; montrant l'influence positive de l'immobilisation : les catalyseurs ainsi supportés sont en effet à la fois plus actifs et conduisant à des polymères de plus haut poids moléculaire. Dans le chapitre III, des complexes de fer contenant un groupement pyrène sont décrits et immobilisés sur nanotubes de carbone par interaction non covalente π-π. Dans ce cas, à la fois les systèmes homogènes et leurs analogues supportés catalysent la réaction de polymérisation de l'éthylène avec des activités particulièrement élevées. Il a également pu être mis en évidence l'importante influence du support carboné sur les performances du système catalytique ainsi que sur la structure des polymères obtenus. Différents types de complexes de nickel contenant un ligand imino-pyridine et différents groupes polyaromatiques ont été synthétisés et leur utilisation en polymérisation de l'éthylène est décrite dans le chapitre IV. L'influence de l'addition de faibles quantités de matériaux nanocarbonés (nanotubes de carbone ou graphène) au milieu réactionnel a ainsi été étudiée. Le graphène s'est dans ce cas révélé particulièrement bénéfique sur les performances du catalyseur. Enfin, le chapitre V décrit la polymérisation de l'isoprène à l'aide de catalyseurs de fer contenant des groupements polyaromatiques permettant leur immobilisation à la surface de nanoparticules de fer. Ces systèmes ont ensuite pu être confinés dans des nanotubes de carbone. Les systèmes catalytiques décrits sont particulièrement actifs produisant des polyisoprènes à température de transition vitreuse élevée et avec une haute sélectivité *cis*-1,4-polyisoprène.